

# Sheffield Hallam University

*Heat and mass transfer from endogenous combustion processes in packed beds.*

FENNER, Markus.

Available from the Sheffield Hallam University Research Archive (SHURA) at:

<http://shura.shu.ac.uk/19644/>

## A Sheffield Hallam University thesis

This thesis is protected by copyright which belongs to the author.

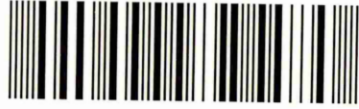
The content must not be changed in any way or sold commercially in any format or medium without the formal permission of the author.

When referring to this work, full bibliographic details including the author, title, awarding institution and date of the thesis must be given.

Please visit <http://shura.shu.ac.uk/19644/> and <http://shura.shu.ac.uk/information.html> for further details about copyright and re-use permissions.

SHEFFIELD S1 1WB

101 624 180 1



**REFERENCE**

ProQuest Number: 10694525

All rights reserved

INFORMATION TO ALL USERS

The quality of this reproduction is dependent upon the quality of the copy submitted.

In the unlikely event that the author did not send a complete manuscript and there are missing pages, these will be noted. Also, if material had to be removed, a note will indicate the deletion.



ProQuest 10694525

Published by ProQuest LLC (2017). Copyright of the Dissertation is held by the Author.

All rights reserved.

This work is protected against unauthorized copying under Title 17, United States Code  
Microform Edition © ProQuest LLC.

ProQuest LLC.  
789 East Eisenhower Parkway  
P.O. Box 1346  
Ann Arbor, MI 48106 – 1346

**HEAT AND MASS TRANSFER FROM  
ENDOGENOUS COMBUSTION PROCESSES IN PACKED BEDS**

Dipl.-Ing. Markus Fenner

A thesis submitted in partial fulfilment of the requirements of  
Sheffield Hallam University  
for the degree of Doctor of Philosophy

July 2002

Collaborating Organisation: Fachhochschule Gelsenkirchen, Germany



## ABSTRACT

Since fires can develop from endogenous smouldering combustion processes deep inside packed beds, especially domestic refuse beds, it is a major task in early fire detection to detect the indications of such combustions as early as possible. Since it is believed that the surface temperature distribution of the bed is affected by the heat and mass transfer from a source of endogenous combustion deep within the bed, the measurement of the surface temperature using IR-Thermography (IRT) has been supposed to be the most promising technique in early combustion detection.

The present work thus deals with the heat and mass transfer from endogenous sources of combustion in packed beds, particularly domestic refuse beds, in order to predict the temperature distribution inside and at the surface of these beds and thus, to allow for an assessment of IRT based early combustion detection systems. An IR-thermographically measurable surface temperature increase will only be achieved by sufficient heat transfer from the source of combustion. Experimental procedures and mathematical modelling have shown that the heat transfer by conduction and radiation is ineffective and therefore, no indication will be obtainable from the surface temperature distribution. A more satisfactory increase in the surface temperature is given as soon as additional heat is transferred by the diffusion of gaseous combustion products. As a result, the heat transfer by convection from the hot combustion gases is theoretically analysed, in particular the way in which the gases flow from the combustion to the surface of the bed. The results obtained show that the gas flow is initiated and maintained by buoyancy and thus the gas tends to flow vertically towards the surface with minimal collateral diffusion. It was also shown that heterogeneous polydispersed beds can be treated as homogeneous monodispersed beds as long as average values for the characteristic bed properties can be obtained. Based upon that, a mathematical continuum model was derived by which the temperature distribution inside and at the surface of the bed could be predicted.

The theoretically obtained results and their implications were then experimentally verified, confirming that heat is predominantly vertically transferred by the gaseous combustion products. The two final sets of experiments were undertaken in a 27 m<sup>3</sup> batch of a representative sample of domestic refuse and a batch of wood chips. Comparing the experimental results with the mathematical predictions, a certain deviation becomes apparent, which is attributed to the not exactly one-dimensional condition inside the bed and especially to the effect of condensation and re-evaporation of the water content of the combustion gas, which has not been included in the model. The temperature of hot spots at the surface, that have the size of only a few square-centimetres, increased to the dew point temperature of the combustion gas, i.e. 65 °C to 85 °C, within the first hour after ignition but remained almost constant at this level for several hours. About 30 minutes before the combustion proceeded to the surface, their temperature increased rapidly but not their size. The rapid temperature increase was attributed to the condensation and re-evaporation ceasing because the entire bed had heated up to a temperature at which these effects no longer occur.

All results obtained, especially for the surface temperature development, allow for an assessment of IRT based early combustion detection systems. Whilst, on one hand, sources of endogenous combustion are principally detectable from the surface temperature distribution, on the other hand, the reliable detection of the very small hot spots requires a spatial resolution of the system, which is up to ten times higher than recent state-of-the-art systems can provide.

## PREFACE

The work presented in this thesis was carried out between March 1997 and June 2002 in the School of Engineering, Sheffield Hallam University and at the Institut für rationelle Energieverwendung at Fachhochschule Gelsenkirchen.

The work described in this thesis is, to the best of my knowledge, original except where reference has been made to others, and no part of it has been submitted for an award at any other College or University.

During the course of work, the following conferences were attended:

- VDI Seminar 43-08-02 "Brand- und Explosionsschutzmaßnahmen in Feuerungs- und Verbrennungsanlagen", Düsseldorf, Germany, 15<sup>th</sup> –16<sup>th</sup> October 1998
- 4<sup>th</sup> International Conference on Quality, Reliability, and Maintenance, St. Edmund Hall, University of Oxford, UK, 21<sup>st</sup> – 22<sup>nd</sup> March 2002

The following papers relating to this work have been published, copies of which may be found in Appendix E of this thesis.

- Braun, R.; Fenner, M.; Weidener, H.: Prüfkriterien zur Beurteilung unterschiedlicher IR- Thermographie-Brandfrüherkennungssysteme. VDI Seminar 43-08-02 "Brand- und Explosionsschutzmaßnahmen in Feuerungs- und Verbrennungsanlagen", Düsseldorf, Germany, 15<sup>th</sup> –16<sup>th</sup> October 1998
- Fenner, M.; Braun, R.; Acheson, R.; Garbett, E. S.: Fire prevention in refuse storage facilities using IR-Thermography. Proceedings of the 4<sup>th</sup> International Conference on Quality, Reliability, and Maintenance. St. Edmund Hall University of Oxford, UK, March 2002, Professional Engineering Publishing Limited, London UK 2002
- Fenner, M.; Acheson, R.; Garbett, E. S., Braun, R.: Heat transfer and combustion detection in refuse beds. VGB PowerTech, Volume 82/2002, VGB Verlag, Essen 2002

## ACKNOWLEDGEMENTS

First of all, I would like to thank my supervisors Dr. Robin Acheson and Dr. Eric Garbett for giving all the support I needed to write this thesis. Both aided me patiently to solve every theoretical and organisational problem I was confronted with during this project. The same applies to Prof. Dr.-Ing. Rainer Braun, Fachhochschule Gelsenkirchen, who willingly helped in all theoretical manners, particularly thermodynamics.

I would also like to thank Dipl.-Ing. Martin Sukowski, Fachhochschule Gelsenkirchen, who supported me in solving the technical problems I was confronted with during the experimental work.

I appreciated furthermore the endeavour of Prof. Dr. Uwe Kron, Fachhochschule Gelsenkirchen, who kindly assisted me in the solution of the mathematical model derived for this thesis.

My acknowledgements are also due to David Croft who kindly supported me in solving organisational problems.

Additionally, I would like to thank Dr. Axel Werner and the entire team of the refuse incineration plant "RZR Herten", Germany, for providing me with the possibility to carry out the large-scale experiment conducted in a bed of authentic domestic refuse. This essential experiment was required to undertake the comparison of the mathematical prediction with actual measurements.

# CONTENTS

NOMENCLATURE	vii
1 INTRODUCTION	2
2 LITERATURE REVIEW	5
2.1 Packed bed storage and properties of domestic refuse in Germany	5
2.2 Fire hazards from endogenously initiated smouldering combustion processes in domestic refuse beds	8
2.2.1 External sources of ignition in domestic refuse beds	9
2.2.2 Internal sources of ignition in domestic refuse beds	10
2.2.3 Fire events at German refuse storage facilities	11
2.3 The application of IR-Thermography systems in early detection of combustion processes	14
2.4 Mathematical modelling of heat transfer inside heterogeneous packed beds, in particular domestic refuse beds	18
2.4.1 Model types	18
2.4.2 Heat transfer characteristics of packed beds	21
2.4.2.1 Void fraction	21
2.4.2.2 Thermal conductivity	23
2.4.3 Heat transfer in packed beds where the fluid flow arises from endogenous combustion processes	25
3 EXPERIMENTAL PROCEDURES	30
3.1 Selection of a substitute bed material	31
3.1.1 Heat transfer characteristics of domestic refuse	31
3.1.2 Heat transfer characteristics of the wood shavings	32
3.2 Temperature profiles in a shavings bed undergoing self-ignition – Experiment 1	33
3.3 Temperature profiles in a shavings bed subjected to an electrical heat source – Experiment 2	37
3.4 Comparison of the heat transfer by conduction with that by convection – Experiment 3	39
3.5 The flow of hot combustion gases through a small-scale domestic refuse bed – Experiment 4	41
3.6 Large-scale experiment conducted in a 27 m <sup>3</sup> batch of domestic refuse – Experiment 5	45
3.7 Intermediate-scale experiments using wood chips – Experiment 6	52

4	EXPERIMENTAL RESULTS	56
4.1	Temperature profiles in a shavings bed undergoing self-ignition – Experiment 1	56
4.2	Temperature profiles in a shavings bed subjected to an electrical heat source – Experiment 2	60
4.3	Comparison of the heat transfer by conduction with that by convection – Experiment 3	63
4.4	The flow of hot combustion gases through a small-scale domestic refuse bed – Experiment 4	67
4.5	Large-scale experiment conducted in a 27 m <sup>3</sup> batch of domestic refuse – Experiment 5	71
4.6	Intermediate-scale experiments using wood chips – Experiment 6	77
5	DISCUSSION	93
5.1	Experimental procedures	93
5.1.1	The substitution of domestic refuse and combustion gases	93
5.1.2	Temperature measurements	99
5.2	Mathematical modelling of heat transfer inside heterogeneous packed beds	102
5.2.1	Simplifying assumptions	103
5.2.2	Derivation of the mathematical model	104
5.2.3	The sensitivity of the model towards parameter variations	107
5.3	Comparison of the model prediction against the experimentally obtained data	111
5.4	Applicability of IR-Thermography systems to the early detection of combustion processes inside domestic refuse beds	121
5.4.1	Required spatial resolution the early detection of a combustion process	121
5.4.2	Importance of the spectral band for IR thermographic temperature measurement	126
5.4.3	Can IRT systems be applied to early detection of combustion?	126
6	CONCLUSIONS AND RECOMMENDATIONS FOR FURTHER WORK	130
	REFERENCES AND BIBLIOGRAPHY	133
	APPENDICES	143
	Appendix A Standard equipment and custom built apparatus	144
	Appendix B Reports on fires at German refuse storage facilities	153
	Appendix C Solution of the system of partial differential equations	163
	Appendix D Combustion temperature, excess air and dew point	169
	Appendix E Publications	172

## NOMENCLATURE

a		structural parameter
$A_s$	$m^2/m^3$	volume specific surface area
A	$m^2$	area
C	m/s	velocity
$c_p$	J/(kg K)	specific heat capacity at constant pressure
d	m	diameter
$\dot{E}$	$W/m^2$	energy flux density
g	$m/s^2$	gravitational acceleration
h	J/(kg K)	mass specific enthalpy
H	m	height
$H_u$	J/kg	net calorific value
j	J	dissipation energy
k	$W/(m^3 K)$	parameter
L	m	length
$L_{min}$	$m^3/kg_{Fuel}$	minimum quantity of specific air required for stoichometric combustion of a solid fuel
m	kg	mass
$\dot{m}$	kg/s	mass flow rate
p	Pa	pressure
q	J	change in heat energy
$\dot{q}$	$W/m^2$	heat flux density
$\dot{Q}$	W	heat flux
r	m	radial space co-ordinate
s	J/kg	mass specific entropy
t	s	time
T	K	absolute temperature
u	$J/(m^3 K)$	parameter

$v$	$m^3/kg$	specific volume
$V$	$m^3$	volume
$\dot{V}$	$m^3/s$	volume flow rate
$w_t$	J	technical work
$w$	$J/(m^3 K)$	parameter
$x, y, z$	m	space co-ordinates
$z$	m	geodetic height

### Greek Symbols

$\alpha$	$W/(m^2 K)$	heat transfer coefficient
$\delta$	$m^2/s$	diffusion coefficient
$\Delta$		prefix for a value change in a parameter
$\varepsilon$		emissivity
$\vartheta$	$^{\circ}C$	temperature
$\lambda$	$\mu m$	wavelength
$\lambda$	$W/m K$	thermal conductivity
$\lambda$		excess air value
$\mu$	$m^{-1}$	parameter
$\nu$	$m^{-1}$	parameter
$\rho$	$kg/m^3$	density
$\sigma$	$5.67 \cdot 10^{-8} W/(m^2 K^4)$	Stefan-Boltzmann constant
$\sigma$		integration variable
$\tau$		dimensionless time
$\xi$		dimensionless length; mass percentage
$\psi$		void fraction
$\zeta$		velocity independent friction loss parameter; volumetric percentage

## Subscripts

0	starting point of fluid flow inside a packed bed
1	at location 1
2	at location 2
A	ash at adiabatic combustion temperature
ad	adiabatic
air	air
Air	air at ambient temperature
amb	ambient
Bed	bed
B	bulk material
C	gas flow channel
combination	combination of parallel and series connection
E	exhaust gas at adiabatic combustion temperature
Fluid	fluid
F	fuel at ambient temperature
G	gas
i	general variable
l	interstitial
in	inlet
HS	heat source
min	minimum
n	general variable
n	standard conditions: 1013,15 hPa, 0 °C
NH <sub>3</sub>	ammonia gas
out	outlet
parallel	parallel connection
R	residues at adiabatic combustion temperature

# 1 INTRODUCTION

One of the major problems of collecting domestic refuse and then storing it in a bunker on an incineration plant is that it is liable to become a fire hazard [1]. The combustion process can be initiated in many ways and once a fire has started there are two undesirable effects:

1. The structural damage to the plant caused by the fire and
2. the environmental damage caused by the uncontrolled combustion and the method by which the fire is extinguished.

Following a number of disastrous fires in the storage bunkers of domestic refuse incineration plants, legislation requiring the installation of automatic combustion detection systems was introduced in Germany in 1991 [2, 3, 4, 5]. Although there is no specification as to which kind of system should be used, it has been proposed that such systems should use IR-Thermography for the measurement of the surface temperature of the refuse bed. It was believed that a source of endogenous combustion deep within the refuse would be detectable from so-called hot spots within the surface temperature distribution [6], thereby providing the means for automatic warning of a potential fire using an appropriate alarm threshold surface temperature [6, 7].

As yet, not all plants in Germany are equipped with such systems but of the more than twenty existing plants that have been, the equipment used and their installation and operating practices are not yet standardised. This situation has arisen because opinion varies as to the effectiveness of such systems and how best to apply and interpret the results they give [8, 9], in particular because fire events took place [10, 11, 12, 13, 14], even in plants that have been equipped with early combustion detection systems. Additionally, quantitative understanding of the effect of an endogenous combustion source on the surface temperature distribution of the refuse bed has, until now, not been investigated.

Therefore, the objective of this thesis is to analyse the heat and mass transfer inside refuse beds in order to predict the temperature distribution inside and at the surface of these beds. The aims of this work are twofold:

- To investigate the heat and mass transfer phenomena which occur inside the body of refuse material from an experimental and analytic viewpoint. In this way, the origin and propagation of the combustion may be explained and the associated bed and surface temperatures of the material may be predicted.
- To develop and test on-site a method of early combustion detection, in particular assess the potential for using IR-thermographic techniques for surface temperature measurement.

Starting with a review of published material covering the origins of combustion in packed beds together with the heat and mass transfer processes involved, the thesis proceeds with a review of the various techniques which are available for the early detection of combustion processes. Thereafter, mathematical models for predicting the temperature distribution inside and at the surface of the bed are reviewed. It then follows a detailed account of experiments undertaken to analyse the nature of the start-up processes of self-ignition, the general development of endogenous combustion processes and the corresponding temperature distribution inside and at the surface of the bed. Thereafter, the thesis proceeds with a presentation of the experimentally obtained results. This is then followed by a critical discussion of the experimental work, the derivation of an appropriate mathematical model and the analytical interpretation of the heat and mass transfer in comparison to the experimental results. Finally, an opinion on state-of-the-art IR-Thermography systems for the early detection of combustion processes inside refuse bunkers is given and potential improvements are presented before conclusions are drawn and recommendations are given for further work.

# CHAPTER 2

## LITERATURE REVIEW

## 2 LITERATURE REVIEW

### 2.1 Packed bed storage and properties of domestic refuse in Germany

At present, two thirds of German domestic refuse is stored in disposal sites and the remaining third is thermally treated in more than 50 incineration plants with an overall annual capacity of more than 14 million tonnes [15]. Dust carts deliver the refuse from the households to the incineration plants, where the bulky parts are reduced in size using shears or grinders. The refuse is then stored inside a bunker, as shown in **Figure 2.1**, until required for incineration.



**Figure 2.1** Photograph of part of a refuse bunker with the refuse delivery at the bottom left.

The refuse is built up to a wall to keep the delivery clear.

Although the bunkers are designed to be a short-term storage facility only, the refuse is sometimes stored for several days before it is incinerated, depending on the combustion capacity and the magnitude of delivery. Generally, the crane operators mix the refuse during storage and in particular before incineration, in an attempt to achieve a more uniform calorific value, because of the very heterogeneous composition of domestic refuse.

In order to analyse the heat and mass transfer in domestic refuse beds, the composition and properties of the refuse must be determined. Since the refuse varies even regionally, individual compositions can neither be taken into account nor will they be representative. Thus, average data on domestic refuse must be used. The most recent and comprehensive statistical data on domestic refuse in Germany is based on an analysis in 1993 [16], of the refuse inside the household bins at the time of collection. Bulky refuse was thus not taken into account.

Since 1993 the refuse composition will have undergoing changes due to the introduction by "Duales System Deutschland AG" (DS) of a new refuse bin for all recyclable material, except for glass and paper. 51.6 % of sold packages of any kind were collected by the DS refuse bins in 1993, which increased to 86 % in 1997 [17]. A third refuse bin has been regionally introduced that is to be used for organic refuse. As a consequence, the refuse composition has changed over the last 10 years. Since more comprehensive data on the refuse composition is not available and bearing in mind that the composition is not uniform at all, the data presented in reference [16] will be used for the analysis of domestic refuse. **Table 2.1** lists the mass percentages of the principal components given by [16], and their properties taken from various literature, such as [18].

**Table 2.1** Average properties of the collected domestic refuse in Germany (1993) [16, 18]

Component	% by mass	Density kg/m <sup>3</sup>	% by volume	Thermal conductivity W/(m K)	Specific heat capacity kJ/(kg K)
<b>Paper/Cardboard</b>	<b>18.0</b>	<b>820</b>	<b>15</b>	<b>0.140</b>	<b>1.4</b>
Cardboard	2.1	800			
Paper and Magazines	6.4	800			
Mixed paper	4.8	800			
Kitchen tissues	2.5	870			
Other	2.2	800			
<b>Plastics</b>	<b>5.9</b>	<b>1020</b>	<b>5</b>	<b>0.297</b>	<b>1.4<sup>a)</sup></b>
Bulky parts	2.6	1120			
Plastic bags (HDPE)	0.9	950			
Foils (LDPE)	2.2	920			
Polystyrene	0.1	1070			
Disposable cutlery	0.1	1100			
<b>Glass</b>	<b>7.2</b>	<b>2500</b>	<b>2</b>	<b>0.810</b>	<b>0.84</b>
<b>Fabrics</b>	<b>2.0</b>	<b>340</b>	<b>5</b>	<b>0.042</b>	<b>0.85<sup>a)</sup></b>
<b>Wood (average)</b>	<b>1.1</b>	<b>720</b>	<b>1</b>	<b>0.166</b>	<b>1.74</b>
<b>Metals</b>	<b>3.3</b>	<b>7380</b>	<b>1</b>	<b>92.182</b>	<b>0.26</b>
Tins (tinplate)	1.8	7850			
Tins (Aluminium)	0.1	2700			
Drinks cans (tinplate)	0.7	7850			
Aluminium packages	0.1	2700			
Other (tinplate)	0.4	7850			
Other (aluminium)	0.1	2700			
Aerosol cans (tinplate)	0.1	7850			
<b>Organic refuse</b>	<b>27.7</b>	<b>1100</b>	<b>31</b>	<b>0.45</b>	<b>3.13<sup>a)</sup></b>
<b>Composite materials</b>	<b>6.2</b>	<b>960</b>	<b>5</b>	<b>0.269</b>	<b>1.25<sup>a)</sup></b>
Composite paper	0.1	800			
Drinks composite packages	1.0	800			
Composite packages	1.3	1000			
Other	3.8	1000			
<b>Inert matter<sup>a)</sup></b>	<b>1.5</b>	<b>1500</b>	<b>1</b>	<b>2.0</b>	<b>0.8</b>
<b>Unsorted fraction &lt;40 mm</b>	<b>22.3</b>	<b>943<sup>b)</sup></b>	<b>29</b>	<b>1.82<sup>b)</sup></b>	<b>1.92<sup>b)</sup></b>
<b>Unspecified<sup>b)</sup></b>	<b>4.8</b>	<b>943</b>	<b>5</b>	<b>1.82</b>	<b>1.92</b>
<b>Total without any voids</b>	<b>100</b>	<b>943<sup>c)</sup></b>	<b>100</b>	<b>See section 3.1.1</b>	<b>1.92<sup>d)</sup></b>
<b>Measured density of the refuse collected from the household bins, incl. voids</b>		<b>167 [16]</b>			

a) Estimated value

b) Since no specific data is available, the average values of all known components have been used

c) Average values calculated from the individual density values and volume fractions

d) Average values calculated from the individual specific heat capacity values and mass fractions

## **2.2 Fire hazards from endogenously initiated smouldering combustion processes in domestic refuse beds**

Smouldering is a slow, flameless combustion processes without the emission of light [19], that can take place inside all areas with limited ventilation [20]. Usually, little smoke is emitted but does contain harmful substances due to the non-stoichiometric combustion. When temperatures increase within the matter, glowing combustion takes place, which is the combustion of solid matter without flames but with light emission [19]. Both, smouldering and glowing combustion can lead to pyrolysis of adjacent material. Pyrolysis is an irreversible endothermic chemical decomposition caused by rising temperature but without oxidation. Since the chemical reactions during thermal decomposition are very complex and oxygen availability usually cannot be excluded, oxidative processes mostly take place, leading to so-called oxidative pyrolysis [19]. Smouldering, glowing and pyrolysis mostly occur simultaneously, which makes it almost impossible to differentiate between these processes. Therefore, the combination of these processes is referred to as smouldering combustion. In contrast to flaming combustion that can be detected easily by vision, smouldering combustion is more difficult to discover and thus always bears the risk of proceeding to an open fire without being noticed [20]. In particular, this applies to domestic refuse beds [4, 5].

There are various sources that can initiate smouldering combustion processes in domestic refuse beds, e.g. small hot particles [21] or fermentation of biological material [22]. Refuse, stored in large quantities, is hence always liable to become a fire hazard from endogenously initiated smouldering combustion processes. Generally, the sources that initiate these combustion processes can be divided into external and internal sources. External sources have their origin outside the refuse bed and hence, they transfer heat energy into the bed. Internal sources have their origin inside the refuse bed without any transfer of heat energy into it. Due to the composition of the refuse, these sources of ignition usually cannot be entirely avoided.

### **2.2.1 External sources of ignition in domestic refuse beds**

External sources transfer heat into the refuse bed from the environment. Flames, sparks and other glowing materials as the most important external sources.

Flames, having temperatures in the range of 640 °C to 900 °C [21], transmit heat mostly by radiation which can be split into 20 % light and 80 % heat emission [23]. The transferred energy may lead to self-accelerating oxidation [24] and hence ignition of adjacent materials. More detailed information is given in [25, 26].

Sparks are usually produced by friction when kinetic energy is converted into heat energy and small particles of material become separated. Particles of low energy usually cool down quickly so that ignition of other solid materials can be virtually excluded, whereas particles of high energy are likely to react exothermically. Whilst in contact with atmospheric oxygen, the amount of the heat increases usually about 1000 %. The heat of a spark is transferred by conduction (70 %) and radiation (30 %) [27]. The ignition of solids is only possible if the mass of the spark is sufficient or the enthalpy of the spark increases during oxidation. Gases and vapours can be ignited more easily if the energy of the spark reaches only 10 % of the necessary ignition energy and the spark temperature is above the gas ignition temperature [28].

Wood and cellulose are the most common examples of glowing materials. The glowing process can be split into three zones that differ regarding the chemical reactions [29, 30], the temperature and heat balance, the gas exchange, the pyrolysis products and the dependence on the airflow. Other bed materials can be easily ignited by already glowing material [31, 32].

Ignition by a hot surface can be distinguished into two types, that is direct or instantaneous ignition and ignition caused by a build-up of heat. The first is characterised by the temperature of the hot surface being higher than the ignition

temperature of the material subject to ignition. Heat can be transferred by conduction, convection or radiation and the material is set on fire instantly or with very little delay [33]. In contrast, ignition caused by build-up of heat is characterised by the temperature of the hot surface being equal to or below the ignition temperature of the adjacent material. Usually, the heat is transferred by conduction or, in very few cases, by radiation if the distance is very small [34]. Ignition is only possible if the received amount of energy is higher than that passed on to the environment. This might result in an increase of temperature, thermal processing or the acceleration of auto-oxidative processes within the adjacent material, possibly leading to ignition.

### **2.2.2 Internal sources of ignition in domestic refuse beds**

Internal sources may spontaneously generate heat inside a bed of combustible matter, e.g. auto-oxidation processes. If a substance produces enough heat, it might ignite itself or adjacent material with a lower ignition temperature. Catalytic effects may support or accelerate these reactions [35].

Generally, two spontaneous heating processes can be distinguished, namely the classic spontaneous heating and the temperature controlled exothermic reaction [35]. The classic spontaneous heating is characterised by the process being initialised at ambient temperature and the internal generation of heat within the system itself. The most common examples are thermal effects of mesophilic and thermophilic micro-organisms inside hay [22] and the auto-oxidation of coal stored in large piles [36]. In contrast to these reactions, exothermically initiated reactions require a higher temperature level for initiation, e.g. the exothermic combustion of wood caused by a hot surface that starts at 80 °C to 110 °C [37].

All spontaneous combustion processes, except special gas explosions, require a certain time for development, referred to as the spontaneous heating phase [40]. Within this phase, the exothermic chemical, micro-biological or biochemical processes taking

place initially heat up the matter above ambient temperature. In many cases, spontaneous heating takes place in cellulose containing substances [38]. Following auto-oxidative processes, the substance becomes carbonised and very reactive surface layers of charcoal develop that have a high specific surface area. Oxygen can be taken up within these areas and an autonomous exothermic reaction begins that might succeed to smouldering combustion [39]. Whether or not spontaneous heating eventually leads to ignition depends on several conditions [40]:

- The rate at which heat is generated and removed from the material being oxidised. This becomes more complex if the heat is removed from the oxidised material but is directly transferred to adjacent material. In this case, a material different than the oxidising material may undergo ignition, possibly accelerated by catalytic reactions.
- The ignition temperature of a fibrous combustible material, hydrocarbon or any gases liberated by oxidation.
- The specific surface area of the hydrocarbon exposed to an oxidiser.
- The moisture content of the atmosphere present and of the material itself.

Both, the chemical and the biological initiation of self-ignition are very complex and not yet fully understood. More information on the chemical processes can be found in reference [41, 42, 43] and detailed information on the biological processes is given for example in reference [22, 44, 45, 46].

### **2.2.3 Fire events at German refuse storage facilities**

In the past, several fire events inside refuse storage bunkers resulted in such immense impairments to the plant that the damage and the disposal of the water contaminated refuse lead to an economic write-off of the plant [47]. In order to avoid these fires or at least to minimise the future risks by means of early detection, the fires of the past should be analysed in terms of initiation and propagation. The major difficulty in analysing such fires is that official statistics concerning quantities, extents and causes [47], are generally not available to the public. The plant authorities in Germany do not

provide any information but try to play down the fires and their consequences because every fire is a potential environmental hazard. A disastrous fire inside the refuse bunker of the incineration plant in Darmstadt, Germany in 1995 is a good example of this.

Detailed information was not given by the authorities, even though the fire devastated the entire bunker and surrounding parts of the plant. The only officially released information about fires at domestic refuse storage facilities [10, 11, 12, 13, 14] has been analysed and a summary of the results will now be presented. The detailed analysis is given in Appendix B.1. An interview with the crane drivers of the domestic refuse incineration plant in Essen, Germany is presented in Appendix B.2.

Fire events have often been reported that emerged from areas of the refuse bed that have been accessed by the crane a very short time before the flashover took place. These fires can be put down to either the ignition of combustible gases and/or to smouldering combustion underneath the surface. Combustible gases, accumulated inside the heap and ignited by for example a spark from the crane grab, may have been solvent vapours or methane gas from fermentation processes. An already developed endogenous smouldering combustion might have produced combustible pyrolysis gases as well, which ignited on exposure on atmospheric oxygen when the grab picked up the refuse matter and uncovered it. The flashover might then occur due to the rapid temperature increase by the accelerated oxidation.

A self-ignition process inside the refuse material has been assumed to be the cause of another fire. The authorities confirmed that “these processes occur from time to time” [13].

Another fire started near one of the refuse delivery locations of a bunker [14], leading to the conclusion that already smouldering refuse has been delivered to the bunker by a dust cart. When such a refuse is charged into the bunker, the higher oxygen availability

might lead to a temperature increase and flashover. Usually, the delivery locations are frequently accessed and therefore it can be assumed that there has not been a long-term process of fermentation or smouldering within the refuse bed.

Generally, a fire is likely to spread rapidly once the combustion has reached the surface, because of the high flammability and the high net calorific value of the refuse of 8000 to 11000 kJ/kg [18]. Once flashover took place, black smoke will be emitted from the combustion area. This is due to the high carbon content of the refuse of more than 20% by mass [11].

From an interview of four of the crane operators of the “Müllheizkraftwerk Essen-Karnap” plant in Germany [48], details of which can be found in Appendix B, the following information was obtained:

- In all cases of flashover, refuse had just previously been picked up from the area where the fire had started.
- No evidence could be found of biological processes initiating a smouldering combustion.
- Whenever an endogenous combustion occurs, light blue smoke is emitted from the bed that accumulates underneath the ceiling of the bunker.
- During the cold season, risk of fire increases due to the delivery of live coals or hot ashes from households. There are records of cases where the refuse inside the dust cart was already smouldering when the cart entered the plant area.

The above information is all that is available to the public, but it is well known that there have been many more fire events inside refuse storage facilities in the past. Therefore, legislation requiring the installation of automatic combustion detection systems was introduced in Germany in 1991.

### **2.3 The application of IR-Thermography systems in early detection of combustion processes**

Avoiding ignition is the best way to prevent a fire but the previous sections have shown that the ignition sources for domestic refuse are too many to be entirely avoided.

Consequently, the extent of a fire must be minimised by means of the early detection of combustion processes inside the refuse matter before flashover occurs. It has been suggested that automatic combustion detection systems can achieve the desired time between detection and flashover, the so-called advance warning time, of at least 10 minutes which it has been estimated will be required [49]. During this time counter measures can be implemented to extinguish the combustion [50]. Therefore, early combustion detection systems have been demanded for [2, 28, 49] that work independent of staff and ambient conditions. Such systems are based on the detection of different effects of combustion and can be split into five main types:

1. Smoke detection systems
2. Carbon monoxide gas detection systems
3. Heat detection systems
4. Flame detection systems
5. IR-Thermography systems

For a packed bed the size of a refuse bunker, smoke detectors will not operate properly since there are too many influences such as airborne particles and the rarefaction of the smoke inside the large bunker space. The same applies to carbon monoxide detectors. Additionally, there might occur false alerts due to the natural production of carbon monoxide gas by biochemical reactions. The utilisation of heat detection systems is inappropriate as well because the increase in air temperature caused by a smouldering combustion is too low and hence not detectable. Flame detectors do not have any advantage because when a flame appears, flashover has already taken place and thus there is no advance warning time.

Since all other combustion detection systems would not successfully work, the application of IR-Thermography (IRT) is the only promising technique, which can provide long distance, non-contact measurements of surface temperatures. The measurement of the surface temperature of a refuse bed has been suggested because it was believed that a source of endogenous combustion deep within the bed would be detectable from so-called hot spots within the surface temperature distribution. Thereby, IRT systems would provide the means for automatic warning of a potential fire using an appropriate alarm threshold surface temperature. BRAUN and WEIDENER [7] and BRAUN ET AL. [8] suggested an alarm threshold temperature of 70 °C because this is the lowest possible threshold that would be reached by biological activity inside the bed, such as fermentation. The more than twenty IRT systems employed on refuse incineration plants in Germany commonly employ this surface temperature alarm threshold. Nevertheless, the equipment used and their installation and operating practices are not yet standardised. This situation has arisen because opinion varies as to the effectiveness of such systems and how best to apply and interpret the results they give [4-9, 47-49, 51].

The application of IRT is characterised by the possibility of non-contact surface temperature measurements [52]. A general restriction is that measurements should not be impaired by extinction, i.e. absorption and scattering, of thermal radiation within the intermediate medium, which usually is air in most technical applications. This would reduce the temperature displayed by the IRT system below the actual temperature of the measured object. H<sub>2</sub>O, CO<sub>2</sub>, smoke, mist and dust are the main absorbing and scattering components. Their appearance is random and thus the IRT systems cannot be calibrated to compensate for their presence. However, in the wavelength ranges 2 to 5 µm and 7 to 14 µm, the so-called atmospheric windows, the absorption is least, especially at the longer wavelength. This has been proved by extensive experiments conducted by BRAUN and WEIDENER [9]. In addition to reduced extinction, the wavelength range between 7 to 14 µm is favourable for a second reason: For the

purpose of early combustion detection, the temperature range from 0 to 100 °C is most important [4-9]. The wavelength of maximum thermal radiation of black or grey bodies within this temperature range is 10.62 μm at 0 °C and 7.77 μm at 100 °C, respectively. This can be obtained from PLANCK's radiation law [53]. Considering the above, IRT systems should preferably work in the longer wavelength range.

Another limitation of IRT is the spatial resolution of the system [54]. The spatial resolution defines the smallest resolvable isothermal area from a given distance, the so called instantaneous field-of-view (IFOV). When utilised in early combustion detection, IRT systems must provide a very high spatial resolution, and thus a small IFOV to detect changes in temperature of very small surface areas. The successful detection of an isothermal area of 5 cm x 10 cm at 70 °C has been initially suggested as the criterion for refuse bunker IRT applications [4, 5]. This isothermal area had to be detected from the worst case distance inside a refuse bunker, which can be up to 40 m. The most recent IRT systems employ a 320 x 240 pixels micro-bolometer chip and 40° x 30° lenses and thus have, in theory, an IFOV of 0.25 cm x 0.25 cm from a distance of 1 m. From 40 m, the theoretical IFOV then is 9 cm x 9 cm. BRAUN and WEIDENER [9] did extensive experiments from which they concluded that even the best contemporary systems provide an IFOV of not less than 30 cm x 30 cm in a practical application from a distance of 40 m.

Another important restriction is the often not known emissivity  $\varepsilon$  of the object. The emissivity is the ratio of the thermal radiation of a non-black body to a black body within the same wavelength range and thus a correction must be applied to the IRT system to obtain an accurate computation of the actual temperature of the object from the received thermal radiation.  $\varepsilon$  is a property of a material and depends on its chemical composition, surface structure and temperature. The literature also mentions a dependence on the direction of view [53] but this effect is minimal if the angle between

the direction of viewing and the normal of the surface being measured is less than  $45^\circ$  [9]. The determination of an appropriate emissivity value will be complex in refuse bunker applications due to the large variety of materials involved. Experiments by BRAUN and WEIDENER [7] have shown that omnipresent dust inside a refuse bunker quickly covers the stored material with a thin layer. A layer thickness of only 0.25 mm produces an almost uniform emissivity  $\geq 0.95$  [7]. Due to the dust layer, the ambient radiation, such as from sunlight or lamps, is not reflected at the surface and thus does not influence the measurement of the natural thermal radiation of the body.

IRT systems are claimed to offer an additional and unique feature, that of monitoring during fire fighting [3], i.e. the visualisation of the fire and its location through heavy smoke and mist. However, this can only be achieved by IRT systems working in the longer wavelength range [7, 8, 9].

The scanning of the entire surface of the refuse bed should be fast enough to allow detection of a hot spot as early as possible. It should not take longer than 2 minutes [4] but not all recent systems can comply with this and some systems need up to 4 minutes [5]. More information can be found in [4-9, 50, 54, 55].

## 2.4 Mathematical modelling of heat transfer inside heterogeneous packed beds, in particular domestic refuse beds

Bearing in mind that IRT is unable to penetrate the refuse, endogenous combustion processes can only be successfully detected when hot spots appear within the surface temperature distribution of the bed. These hot spots will appear only if there is sufficient heat transfer from the source of combustion to the surface. This particular form of heat transfer has as yet neither been theoretically analysed nor mathematically modelled.

Heat can be transferred by two basic mechanisms: By contact or radiation. Heat transfer by contact can occur by conduction or convection. Conduction takes place between two bodies having contact and being at rest relative to each other. Convection takes places when the bodies are in relative motion. Both processes transfer heat on a molecular basis and can be described by FOURIER'S law of contact heat transfer

$$\dot{q} = -\lambda \left( \frac{\partial \vartheta}{\partial y} \right)_{\text{contact area}}, \quad (2.1)$$

wherein  $\dot{q}$  represents the heat flux density,  $\vartheta$  the temperature,  $\lambda$  the thermal conductivity and  $y$  denotes the space co-ordinate.

Heat transfer by radiation, as defined by the STEFAN-BOLTZMANN law [56], can be described by the energy flux density  $\dot{E}$  that is emitted by every body whose temperature is above absolute zero in the form of

$$\dot{E} = \varepsilon \sigma T^4, \quad (2.2)$$

wherein  $\varepsilon$  is the emissivity value of the emitting surface,  $\sigma$  is the Stefan-Boltzmann constant and  $T$  denotes the absolute temperature of the emitting surface.

### 2.4.1 Model types

The models, proposed in the literature and introduced in the following sections, can be split into two groups: viz. cell models and continuum models. The attempt to simulate a bed using a cell model is characterised by a combination of simpler systems, which

represent the heat transfer behaviour of the bed, whereas a continuum model regards the entire bed or a part of it as a continuous medium, giving differentiable temperature and composition functions of space co-ordinates. These functions can be determined from balances and kinetic equations for heat and mass transfer that can be derived from FOURIER's and FICK's laws, containing transport coefficients, i.e. effective thermal conductivity and dispersion coefficients. Usually, homogeneous cell models are adopted unless large differences in temperature between the fluid and the particles or transient conditions occur. The primary parameters to describe the heat transfer characteristics inside packed beds are the void fraction and the thermal conductivity of the bed material and the fluid, respectively [57]. In addition to the primary parameters, there are secondary parameters, introduced by TSOTSAS and MARTIN [58]. The so-called effective thermal conductivity of a packed bed is then given by the influences of the primary and the secondary parameters. More detailed information is given in reference [59, 60, 61].

TSOTSAS and MARTIN [58] reviewed 50 different models for predicting the thermal conductivity of packed beds permeated by a gaseous phase. No conclusions could be drawn as to the "best model", since within the range of experimental accuracy, different models were shown to produce very similar results in individual applications [57]. The development of an appropriate model thus cannot be completed until it has been investigated to what extent the individual heat transfer mechanisms conduction, convection and radiation contribute to the overall heat transfer inside domestic refuse beds. Generally, models can be divided into three categories:

**Type I models** are based on the exact determination of the temperature field. The temperature field derived by these models is calculated analytically [62] or numerically [63] by solving the LAPLACE equation for heat transfer in and around the particles. The first analytical solution has been given by MAXWELL [62] in 1873. This solution is only suitable for dilute suspensions and emulsions because it presupposes that the particles

do not mutually interfere. To do away with the assumption of infinite dilution, a geometrically arranged structure must be assumed. This leads to extremely complicated analytical calculations. WAKAO ET AL. [64, 65] calculated the thermal conductivity of different beds using this model. Nevertheless, calculations of this nature are very time-consuming and are not very suitable for practical use. More information can be found in reference [66, 67, 68, 69].

**Type II models** use a completely different approach by substituting the bed properties using connections of thermal resistances. The simplest schemes for the substitution consist of two basic means of connection, that is the series circuit and the parallel circuit. By analogy to electrical resistances and for given thermal conductivities of the gas and the solid  $\lambda_G$  and  $\lambda_S$ , respectively and void fraction  $\psi$ , the series circuit has the highest and the parallel circuit has the lowest thermal resistance. A theoretical determination of the extent to which series or parallel circuits occur in an existing packed bed is hardly possible. More information can be found in reference [70, 71, 72, 73].

**Type III models** are based on the assumption that a unit cell represents the entire bed. This approach to determine the thermal conductivity might result in less consumptive calculations as it represents a compromise between the realistic but complicated Type I models and the simple but rather inaccurate Type II models. Either parallel heat flux streamlines (Type IIIa) or parallel isotherms (Type IIIb) are assumed for simplification, although both assumptions do not apply exactly, except for the trivial case of equal thermal conductivities for the gaseous phase  $\lambda_G$  and the solid particles  $\lambda_S$ .  $\lambda_S$ ,  $\lambda_G$  and  $\psi$  [58] are the so-called primary parameters to describe the thermal conductivity of a packed bed  $\lambda_{Bed}$ . Good agreement between model predictions and measured conductivities must be achieved and thus, every predictive model should correctly describe a series of limiting cases concerning the primary parameters involved [74]:

1.  $\psi = 0 \quad \Rightarrow \lambda_{\text{Bed}} = \lambda_{\text{S}}$
2.  $\psi = 1 \quad \Rightarrow \lambda_{\text{Bed}} = \lambda_{\text{G}}$
3.  $\lambda_{\text{S}} = \lambda_{\text{G}} \quad \Rightarrow \lambda_{\text{Bed}} = \lambda_{\text{S}} = \lambda_{\text{G}}$
4.  $\lambda_{\text{G}} \rightarrow \infty \quad \Rightarrow \lambda_{\text{Bed}} \rightarrow \infty$
5.  $\lambda_{\text{S}} \rightarrow \infty \quad \Rightarrow \lambda_{\text{Bed}} \rightarrow \infty$
6.  $\lambda_{\text{G}} \rightarrow 0 \quad \Rightarrow \lambda_{\text{Bed}} \rightarrow 0$
7.  $\lambda_{\text{S}} \rightarrow 0 \quad \Rightarrow \lambda_{\text{Bed}}/\lambda_{\text{G}} = \delta_{\text{Bed}}/\delta$

Relations No. 1 to No. 4 are axiomatic. Relation No. 5 presupposes resistanceless contact between particles, while relation No. 6 is based on non-contacting particles.

Relation No. 7 states that the ratio of the thermal conductivity of a bed of non-conductive particles to that of the fluid is equal to the ratio of the diffusion coefficient for the bed  $\delta_{\text{Bed}}$  and that for the free space  $\delta$ . The quotient  $\delta_{\text{Bed}}/\delta$  has been measured by CURRIE [75] for packed beds, including polydispersed beds and angular particles. More information can be found in reference [76, 77, 78, 79],

## 2.4.2 Heat transfer characteristics of packed beds

All heat transfer models commonly employ the void fraction of the bed and the thermal conductivity of the bed material as the main parameter characterising the packed beds.

### 2.4.2.1 Void fraction

The ratio of the interstitial volume  $V_I$  to the bulk volume  $V_B$  of a porous medium is called the void fraction  $\psi$  and is defined by [57]

$$\psi = \frac{V_I}{V_B}. \quad (2.3)$$

Inside most packed beds, the interstitial volumes are filled with gaseous fluids, i.e. either filled with air or, in the case of combustion, filled with a mixture of air and gaseous combustion products. Since, the density of the gas is far less than the density

of the solid particles, the void fraction can readily be calculated from the bulk density and the densities of the gas and solid involved. From Eqn. (2.3) and with

$$V_I = V_B - V_S$$

it follows that

$$\psi = \frac{V_B - V_S}{V_B} = 1 - \frac{V_S}{V_B}, \quad (2.4)$$

wherein

$$V_S = \frac{m_S}{\rho_S} \text{ and } V_B = \frac{m_B}{\rho_B} = \frac{m_S + m_G}{\rho_B}.$$

Since  $m_G$  can be neglected compared to  $m_S$ ,

$$V_B = \frac{m_S}{\rho_B}$$

can be assumed and hence the void fraction is given by

$$\psi = 1 - \frac{\rho_B}{\rho_S}. \quad (2.5)$$

From Eqn. (2.5), the void fraction of a monodispersed packed bed can be calculated with high accuracy if the values of the corresponding densities and the particles dimensions are known. For polydispersed beds, the volume-based average density  $\bar{\rho}_S$  must be used, which can be obtained from the individual densities  $\rho_i$  and mass percentages  $\xi_i$  of all components of the bed by

$$\bar{\rho}_S = \left( \sum_{i=1}^n \frac{\xi_i}{\rho_{i_{\psi=0}}} \right)^{-1},$$

giving an average value  $\bar{\psi}$  for the void fraction of

$$\bar{\psi} = 1 - \frac{\rho_B}{\bar{\rho}_S}. \quad (2.6)$$

The exact determination of the local void fraction of a polydispersed heterogeneous packed bed is very complex because it cannot be measured and thus, only an average

void fraction value can be obtained. In addition to the local natural fluctuation of the void fraction inside the bed, the void fraction near the boundary wall of a bed may be different from the void fraction distant from the walls [80]. Fluctuations of the void fraction only appear close to boundary walls, which disturb the arrangement of the particles. They can be neglected when the distance from the wall is more than  $5d$ , where  $d$  is the particle diameter, see **Figure 2.2** and large variation in particle dimensions occur.

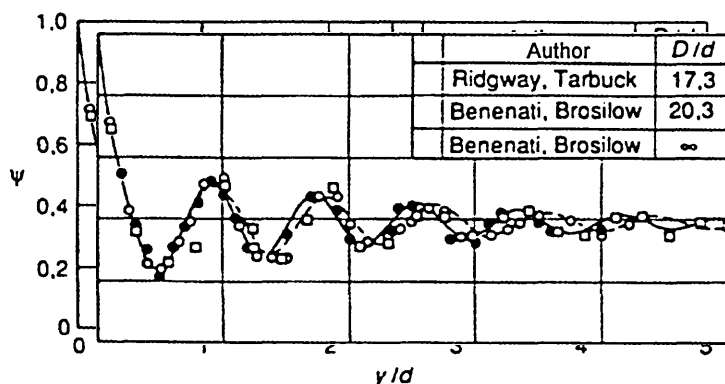


**Figure 2.2** Local void fraction of packed beds consisting of equally sized, smooth spheres (diameter  $d$ ) versus distance  $y$  from the boundary of the bed [80]

In contrast to the situation inside a homogenous monodispersed bed, heterogeneous polydispersed refuse matter is more likely to fill up the voids because of the wide range of particle sizes. Nevertheless, the local void fraction varies throughout the entire bed due to the varying particle dimensions. When employed in mathematical models, the average void fraction, which can be obtained from Eqn. (2.6), is commonly assumed to be constant and independent of location, since local variations in void fraction cannot be determined and hence cannot be adequately quantified.

#### 2.4.2.2 Thermal conductivity

KRISCHER [81] proposed a Type II model representing the thermal conductivity of a packed bed by parallel and series connections of the thermal conductivities of the materials involved. By analogy to an electric circuit, it uses the combination of both, series and parallel circuits, introducing a structural parameter 'a' that gives the relative

proportion of series to parallel connections, see **Figure 2.3**. This parameter 'a' has been determined experimentally and a value of 0.20 is recommended for packed beds [81]. For 'a = 1' a combination of maximal resistance is obtained and a respective scheme for minimal resistance is hence obtained for 'a = 0'.

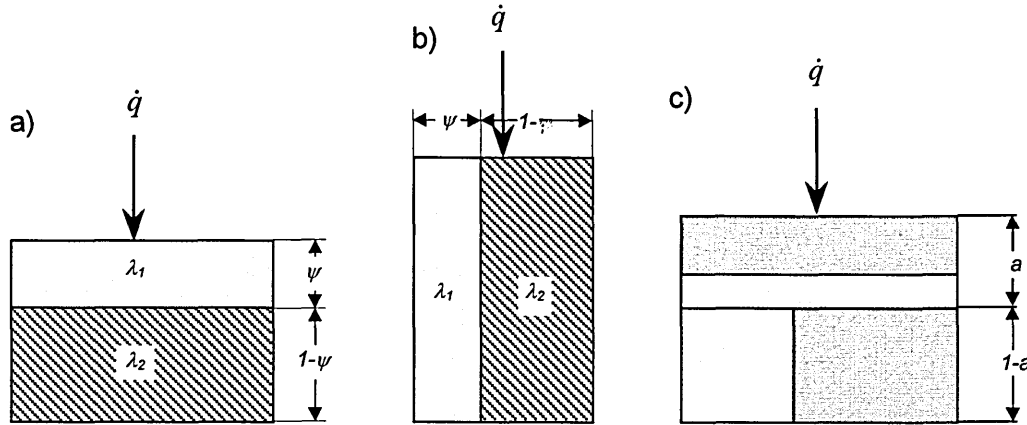


**Figure 2.3** KRISCHER [81] plate model for the determination of the thermal conductivity of dispersed fluid-solid systems.

The structural parameter *a* gives the relative proportion of series to parallel connections and can be used in order to distinguish between systems having the same void fraction but different arrangements of particles. a) series connection; b) parallel connection, c) combination of both

The equation for the thermal conductivity of a series connection can be written as

$$\frac{\lambda_{\text{series}}}{\lambda_1} = \left( \psi + \frac{1-\psi}{\frac{\lambda_2}{\lambda_1}} \right)^{-1}, \quad (2.7)$$

wherein  $\lambda_1$  and  $\lambda_2$  are the thermal conductivities of the individual materials involved.

Although this model has been developed to describe the thermodynamic behaviour of a porous bed [81] it is still applicable if the fluid inside the bed is substituted by a solid.

The void fraction  $\psi$  can be substituted by the volumetric content  $\xi$  of all individual solids and the model can be extended to a number of  $n$  solids if all individual volumetric contents  $\xi_n$  and individual thermal conductivities  $\lambda_n$  are known. For two solids, Eqn.

(2.7) can be written as

$$\frac{\lambda_{series}}{\lambda_1} = \left( \xi_1 + \frac{\xi_2}{\lambda_2} \right)^{-1},$$

which when extended to  $n$  solids gives

$$\lambda_{series} = \left( \sum_{i=1}^n \frac{\xi_i}{\lambda_i} \right)^{-1}. \quad (2.8)$$

The thermal conductivity of the analogous parallel connections can be written as

$$\lambda_{parallel} = \sum_{i=1}^n \xi_i \lambda_i. \quad (2.9)$$

Introducing the structural parameter 'a' required for the combination of both connections results in the equation:

$$\lambda_{combination} = \left( \frac{a}{\lambda_{series}} + \frac{1-a}{\lambda_{parallel}} \right)^{-1}. \quad (2.10)$$

Eqn. (2.10) does not give the thermal conductivity of a packed bed but the thermal conductivity of the bed material because the void fraction has been assumed to be zero.

### 2.4.3 Heat transfer in packed beds where the fluid flow arises from endogenous combustion processes

In addition to heat transfer by conduction and radiation that develops when only a heat source is present inside the bed, when the production of combustion gases occur, forced convection must also be considered. Whenever a combustion zone develops inside a packed bed of any shape, hot combustion gases arise and two-dimensional or three-dimensional flow fields develop as a result of changes in channel cross-sections, blockages, etc. [82]. These flow fields affect the temperature distribution inside and at the surface of the bed [4, 5, 83, 84]. Thus, the temperature and the mass flow rate of the gas, the void fraction of the bed and the thermal conductivity of the gas and the solid, may have an influence on the heat and mass transfer.

Several experiments to observe the heat transfer by combustion gases inside refuse beds and the corresponding development of the surface temperature distribution have been undertaken by EUTENEUER [85]. The combustion gas was substituted by warm air at 50 °C - 70 °C that had been blown into the bed through a nozzle at a certain depth. These experiments presupposed that the flow of the combustion gases was initiated and maintained by an excess pressure around the combustion area. However, every exothermic combustion process also requires oxygen. Inside a packed bed, this oxygen can only get to the combustion zone if fresh air is sucked into this area, similar to a chimney fire. Therefore, the fluid flow must be induced and maintained by buoyancy and an excess pressure cannot occur around the combustion as it would obstruct the flow of air towards the combustion. In EUTENEUER's experiments, the air was blown into the bed, i.e. the flow was induced by the pressure difference between the pressure at the air nozzle and the ambient air pressure, and thus the induction of heat and mass transfer by buoyancy has been entirely disregarded. Furthermore, the air was not warm enough for sufficient buoyancy to arise. The result of these experiments was a quite homogeneous warming of a large surface area that could be expected by a fluid flow initiated by an artificial pressure difference. In contrast to that, minimal collateral gas diffusion could be expected from a buoyancy induced fluid flow as it is assumed to occur inside a refuse bed subjected to an endogenous combustion.

Another way in which the surface temperature distribution is affected by the combustions gases flowing through channels to the surface of a refuse bed has been proposed in reference [6], and is illustrated in **Figure 2.4**. This model is again based on the assumption of flow induced by a pressure increase inside the bed. Whenever gases are produced inside cavities with small exits, the pressure inside the cavity is supposed to increase, thus initiating gas flow in any possible direction and consequently transferring heat in any direction. The individual areas of local surface warming spread over an area that is much larger than the combustion zone itself. Hence, it would become difficult to draw any conclusions from these hot spots at the

surface on the actual location of the combustion inside the bed. Again the restraining effect on the combustion itself by a pressure increase has been disregarded. Despite the oxygen flow governed by the partial pressure difference, a pressure increase will obstruct the flow of necessary oxygen towards the combustion.

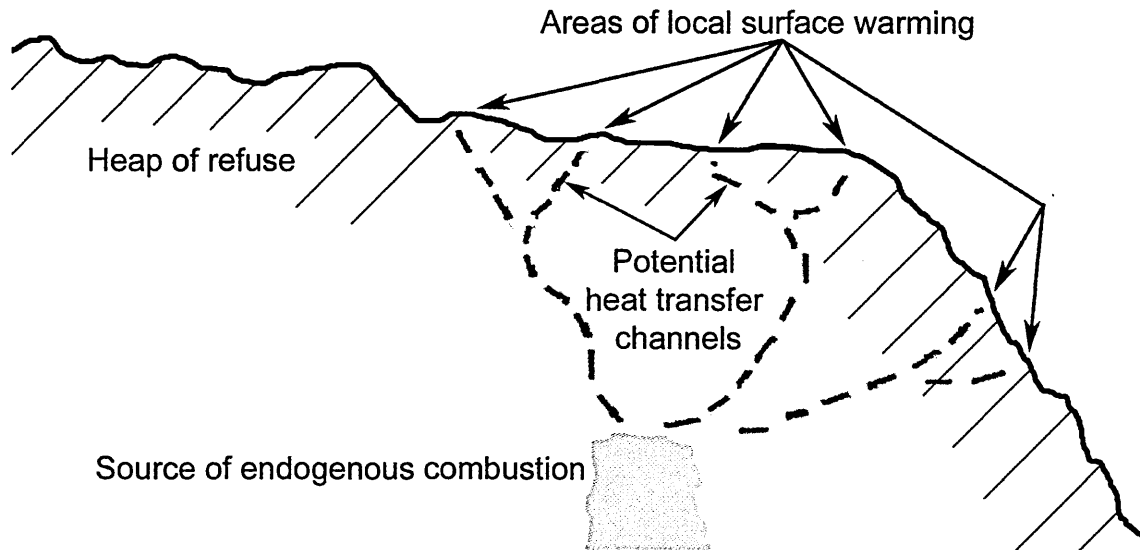


**Figure 2.4** Assumed heat transfer by hot combustion gases flowing through a refuse bed [6].

It is suggested that the areas of local surface warming spread over a large surface area and thus conclusions cannot be drawn from the surface temperature distribution on the source of endogenous combustion.

Both, the experimental approach and the theoretical considerations disregard the fact that natural flow of a hot gaseous fluid is always induced by buoyancy that occurs due to the density of the hot combustion gas being lower than the density of the ambient air.

At this point, it must be assumed that the buoyancy force induces and maintains a vertical gas flow through the voids towards the surface of the bed, similar to the buoyancy induced draught flow inside a stack. Buoyancy depends on the density difference and the effective height of the stack and according to ARCHIMEDES' theory, the buoyancy induced draught pressure difference is given by

$$\Delta p = (\rho_{amb} - \rho_G) g H, \quad (2.11)$$

wherein  $\rho_{amb}$  is the density of the ambient air,  $\rho_G$  is the density of the gas,  $g$  is the gravitational acceleration and  $H$  is the effective height of the stack, i.e. the vertical distance between the gas source and the surface of the bed.

Methods for calculating the heat transfer by hot gases are presented in reference [57] but these are mainly used for the calculations of drying processes and are based on steady-state conditions with uniform gas flow through the entire bed that is initiated by a pressure difference between inlet and outlet of the gas. Hence, their applicability for gas flow predictions from small sources of combustion inside particulate beds is questionable because there will be transient conditions and the gas source is part of the bed. Therefore, information on the initiation of combustion processes and the corresponding heat transfer must be obtained from experimental procedures.

# CHAPTER 3

## EXPERIMENTAL PROCEDURES

### **3 EXPERIMENTAL PROCEDURES**

The heat transfer from endogenous smouldering combustion processes deep within a packed bed is believed to influence the surface temperature of the bed in a way that the combustion is detectable by IRT from local hot spots. A major aim of this work was the investigation of the temperature development inside and at the surface of such packed beds. The foregoing literature review has shown that virtually no information is available about the initiation and propagation of endogenous combustion processes in domestic refuse beds. Therefore, information on the initiation of combustion processes and the corresponding heat transfer had to be obtained from experimental procedures.

Because these experimental procedures had to deal with endogenous combustion processes, the usage of domestic refuse for laboratory experiments was problematic for two reasons: On the one hand, when large quantities are used, the combustion could get out of control and release harmful fumes and on the other hand, when smaller quantities are used, representative results might not be obtainable. Thus, a substitute for the refuse, a test material, had to be found, which was less hazardous but still allowed for representative results using small quantities.

### 3.1 Selection of a substitute bed material

The void fraction, the density and the thermal conductivity of the bed material have been shown to influence heat transfer characteristics of the bed and thus, the test material had to provide similarities in terms of these properties. Hence, these properties must be determined for domestic refuse.

#### 3.1.1 Heat transfer characteristics of domestic refuse

The average density of domestic refuse without void fraction is 943 kg/m<sup>3</sup>, which can be obtained from Table 2.1. A void fraction value of 0.82 was obtained by applying Eqn. (2.6), using the density value of the refuse without void fraction and the measured density of the uncompressed refuse inside the household refuse bins of 167 kg/m<sup>3</sup> [16]. Since the refuse usually becomes compressed during transport and storage, the void fraction of 0.82 can be taken as the highest practical value. In an actual storage situation this value can only be obtained at the surface of the bed and the void fraction will decrease with increasing depth of the bed. For the refuse a void fraction range of 0.55 to 0.82 was assumed.

To determine the thermal conductivity of domestic refuse, the previously introduced KRISCHER plate model was used. With the corresponding values from Table 2.1 and applying Eqns. (2.8), (2.9) and (2.10), it follows that

$$\lambda_{series} = \left( \sum_{i=1}^n \frac{\xi_i}{\lambda_i} \right)^{-1} = 0.20 \frac{W}{m K},$$

$$\lambda_{parallel} = \sum_{i=1}^n \xi_i \lambda_i = 1.01 \frac{W}{m K}$$

and hence, with the structural parameter  $a = 0.2$  [81].

$$\lambda_{combination} = \left( \frac{0.20}{\lambda_{series}} + \frac{0.80}{\lambda_{parallel}} \right)^{-1} = 0.55 \frac{W}{m K}.$$

This is the thermal conductivity of the bed material without any voids and presupposing resistanceless conduction and can thus be taken as the highest possible value. The following example calculation shows that there is very little heat transfer by conduction: A source of combustion as constant heat source is assumed at  $\vartheta_{HS} = 800 \text{ }^\circ\text{C}$  in a depth of  $H = 2 \text{ m}$ . From there, with an infinite heat transfer coefficient, heat is transferred into the bed at the surface of which is no heat transfer. The time required for the surface temperature to increase from  $\vartheta_{amb} = 20 \text{ }^\circ\text{C}$  to threshold temperature of  $\vartheta = 70 \text{ }^\circ\text{C}$  can be obtained from [76, 86]

$$t = \frac{H^2 \cdot c_p \cdot \rho}{\lambda \cdot \mu^2} \left( \ln C - \ln \left( \frac{\vartheta - \vartheta_{HS}}{\vartheta_{amb} - \vartheta_{HS}} \right) \right)$$

Values for  $C$  and  $\mu$  are given in reference [86]. With  $c_p = 1.92 \text{ kJ/(kg K)}$ ,  $\rho = 943 \text{ kg/m}^3$ , given in Table 2.1, and  $\lambda = 0.55 \text{ W/(m K)}$ , the required time is 456 hours!

### 3.1.2 Heat transfer characteristics of the wood shavings

Wood shavings have been used as a refuse substitute in this work. Using wood shavings, only a homogeneous monodispersed bed could be produced. Nevertheless, this provides a good substitute because the characteristics of a homogeneous monodispersed bed of wood shavings are similar to the characteristics of the heterogeneous polydispersed bed of domestic refuse. A comparison of both bed materials can be seen from **Table 3.1**.

**Table 3.1** Comparison of the heat transfer characteristics of domestic refuse with wood shavings

Characteristic of the bed	Domestic refuse	Wood shavings
Density without voids	943 kg/m <sup>3</sup>	approx. 700 kg/m <sup>3</sup> <sup>1)</sup>
Void fraction	0.55 – 0.82	0.58, 0.71, 0.81 <sup>2)</sup>
Thermal conductivity <sup>3)</sup>	0.55 W/(m K)	0.18 W/(m K)

- <sup>1)</sup> Average density value of the shavings mixture containing beech, oak, spruce and pine.
- <sup>2)</sup> The void fractions indicated were achieved by sieving the shavings to different size fractions, namely smaller than 0.5 mm, 0.5 – 1.0 mm and 1.0 – 2.0 mm giving void fractions of 0.58, 0.71 and 0.81, respectively.
- <sup>3)</sup> Thermal conductivity of the material without voids and contact resistances

### 3.2 Temperature profiles in a shavings bed undergoing self-ignition – Experiment 1

The objective of the first set of experiments was the measurement of the temperature distribution inside a heap of wood shavings undergoing self-ignition. A core of shavings, soaked in linseed oil and covered by non-soaked shavings, was used to achieve an endogenous combustion process, initiated by auto-oxidative self-heating of the soaked shavings.

The first step was to determine the conditions under which self-ignition of shavings soaked in linseed oil would occur. Six different mixtures of shavings and linseed oil, summarised in **Table 3.2**, were tested. As shown in **Figure 3.1**, 50 g of each of the individual mixtures were embedded in oil free 2.0 – 8.0 mm shavings contained in a 22 cm x 22 cm x 10 cm steel box. This particle size was supposed to allow for both, a sufficient build up of heat and a sufficient availability of oxygen necessary for the oxidation process.

**Table 3.2** Details of the test mixtures used to determine the conditions under which self-ignition of shavings soaked in linseed oil will occur

Test	Particle size mm	Mass ratio: linseed oil/shavings
1	1.0 - 2.0	30 g / 50 g
2	1.0 - 2.0	50 g / 50 g
3	1.0 - 2.0	80 g / 50 g
4	0.5 – 1	30 g / 50 g
5	0.5 – 1	50 g / 50 g
6	0.5 – 1	80 g / 50 g

After the oil soaked shavings had been embedded in the box of coarse shavings, the system was left without any further disturbance. The temperatures in the centre and at the top surface of the oil-soaked shavings were measured and recorded continuously using thermocouples. Thermocoax TKA 10/25/DIN stainless steel sheath type K thermocouples were used, connected via a Philips PM9877K/2 thermocouple lineariser

with automatic cold junction compensation to a Philips PM 8252A two line chart recorder.

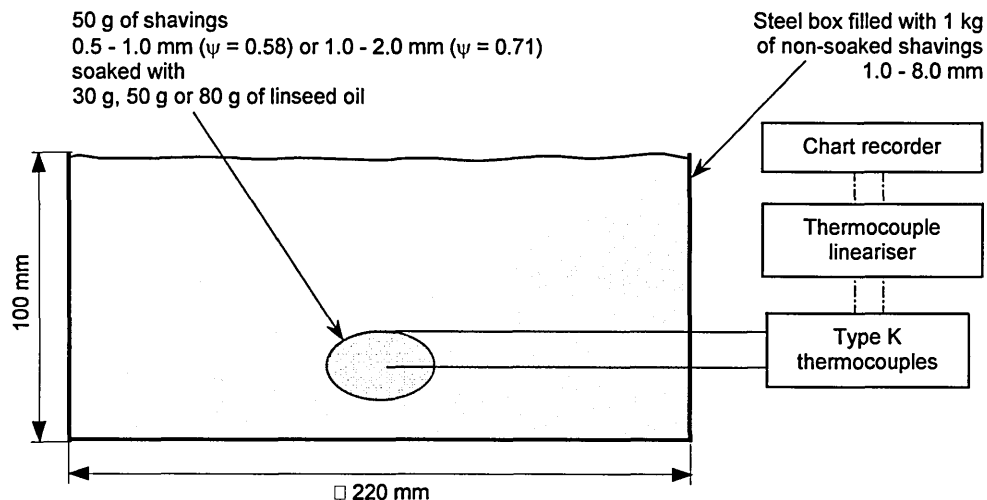


**Figure 3.1** Cross sectional schematic diagram of the experiment to determine the conditions under which self-ignition of linseed oil soaked shavings occurs

The only mixture that successfully lead to self-ignition consisted of 80 grams of linseed oil mixed with 50 g of the 0.5 – 1.0 mm shavings. All other mixtures only exhibited self-heating. The detailed results of these experiments can be found in section 4.1 of this thesis.

The experiments proceeded to the measurement of the temperature distribution inside and at the surface of a heap of shavings undergoing self-ignition. 800 g of shavings with a particle size of 1.0 - 2.0 mm were placed in a hemispherical heap over a mixture of 80 g of linseed oil with 50 g shavings with a particle size of 0.5 to 1.0 mm, as shown in **Figure 3.2**. The entire heap was constructed on a 25 cm x 25 cm steel sheet that could withstand the high temperatures. The heap was than left undisturbed to allow heating and self-ignition to occur.

All temperatures inside the heap were measured using five Thermocoax TKA 10/15/DIN stainless steel sheath type K thermocouples. This type of thermocouple allowed for precise temperature measurements to be made along the vertical radial

axis of the heap, as shown in **Figure 3.2** and **Figure 3.3**. The first thermocouple was placed at the top surface of the soaked core, 45 mm from the bottom of the heap, and the other thermocouples were placed equidistant at 15 mm intervals. They were connected to a Hewlett Packard HP 34970A data logger and PC-System with HP BenchLink data logger software.

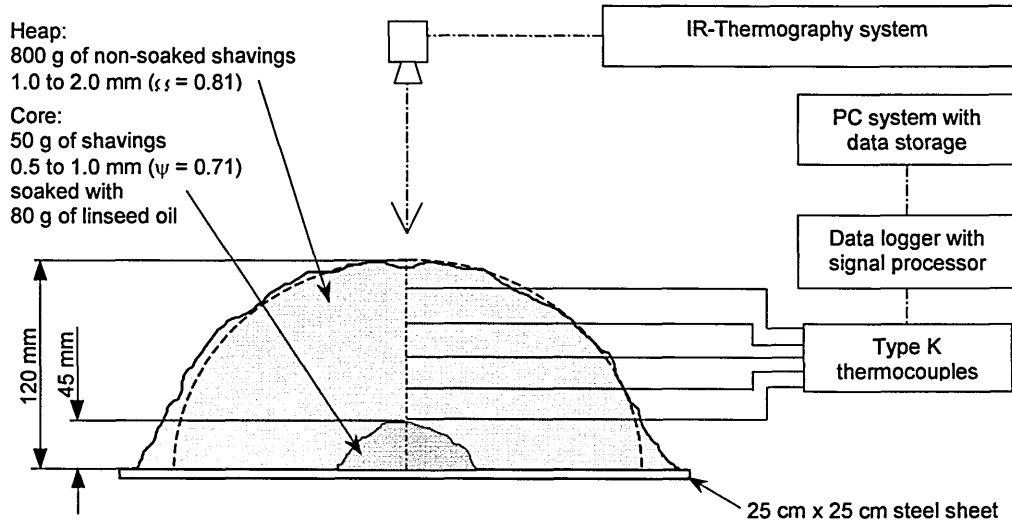


**Figure 3.2** Cross-sectional schematic diagram of the experiment on the measurement of the temperature distribution inside and at the surface of a heap of shavings undergoing self-ignition initiated by the linseed oil-soaked heap core

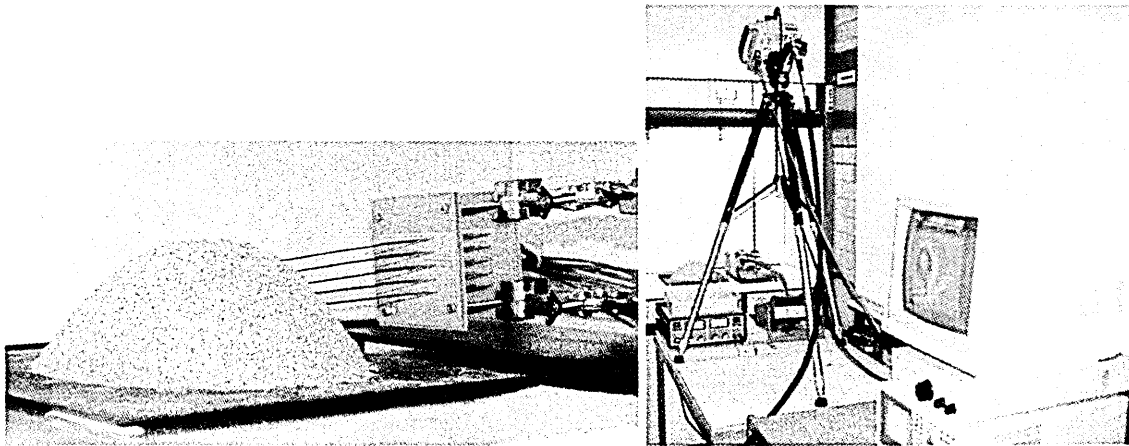


**Figure 3.3** Photographs of the actual apparatus shown diagrammatically in Figure 3.2. On the left, the thermocouple placement can be seen and on the right, the IRT system can be seen.

In order to minimise their effect on the thermal processes taking place, the thermocouples were placed horizontally into the heap so that the temperature sensitive tips were located parallel to the expected isotherms. In this way, the temperature gradient tending to conduct heat away from the core of the heap was insignificantly small. The thermocouples used were of a type that, even if a temperature gradient had occurred, they would have conducted very little heat due to the low thermal conductivity of the stainless steel sheath of  $15 \text{ W/(m K)}$  and its small diameter of 1 mm.

The thermal radiation emitted from the surface of the heap was monitored by an AVIO Compact Thermo TVS 220 IR-Thermography System from a distance of 1.5 m. The accuracy of the temperature displayed by the IRT system depended on the exact value of the emissivity of the wood shavings surface. A value of 0.95 could be obtained from reference [8].

Following successful self-ignition, the combustion progressed up to the surface of the heap where finally flashover took place. The results obtained will be presented in detail in section 4.1.

During this experiment, smoke emission from the heap was observed after ignition had been achieved, thus clearly showing that there was production of combustion gases. The fact that combustion product gases occurred suggest that the heat transfer inside the bed might be affected by convection. The next experimental step was thus to focus on a qualitative comparison of the heat transfer inside a shavings heap containing an endogenous heat source with and without the production of combustion gases.

### 3.3 Temperature profiles in a shavings bed subjected to an electrical heat source – Experiment 2

An electric heating element,  $\varnothing$  30 mm, height 10 mm (see appendix for further detail) was placed at the bottom of a heap of shavings, having a diameter of 20 cm. This is illustrated in **Figure 3.4**. The three different particle sizes, and hence porosities, as explained in section 3.1 were used to achieve comparability to domestic refuse beds. For each bed of shavings, a set of three experiments was carried out. During the first two, the heater was set at 100 °C and 250 °C, respectively. Both temperatures were too low for combustion to take place. For the third experiment, the temperature was set at 350 °C to achieve endogenous smouldering combustion. The heater always achieved the desired temperatures within 10 minutes.

Twenty thermocouples were arranged in a 10 mm grid inside the heap as shown in **Figure 3.4**. Presupposing an axis-symmetric temperature field, this arrangement allowed for the determination of a three-dimensional temperature profile within the heap. The distance between the heating element and the first thermocouple was 20 mm.

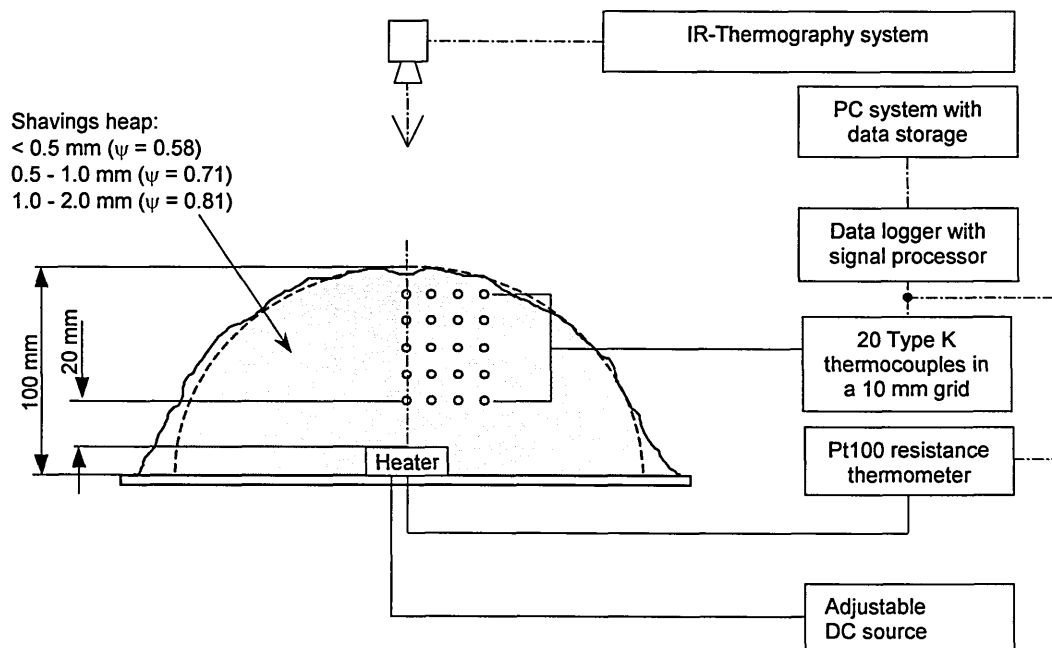


**Figure 3.4** Cross-sectional schematic diagram of the experimental set-up for the determination of the temperature distribution inside and at the surface of a homogeneous packed bed and the corresponding heat transfer caused by an endogenous heat source

The surface temperature was measured using the same IRT System employed in section 3.2, from a distance of 1.5 m. All temperatures were recorded every 30 seconds using the data logger/PC-system. The experiments were repeated four times and since the measured results did not significantly fluctuate, random deviation could be assumed to be very small. The results will be presented in section 4.2.

During this set of experiments, a large difference between the temperature distribution with and without endogenous combustion process was noted. The next experimental step was thus to examine the extent of the difference in heat transfer and the resulting surface temperature.

### 3.4 Comparison of the heat transfer by conduction with that by convection – Experiment 3

The basic idea of this experiment was to compare the heat transfer in a bed from a localised heat source emitting hot combustion gases with that produced when only a heat source was present. For the gas emitting heat source, a smouldering combustion of wood shavings was used. In order to only combust a pre-defined amount of shavings, fine glasswool was used to simulate the packed bed. The high void fraction of 0.98 of the glasswool permitted nearly undisturbed fluid flow with regard to both, air and combustion gases. Glasswool has a low thermal conductivity but high speed of response to a change in temperature.

The heater was insulated, except for its upper surface, by embedding it in a layer of Rockwool®, as shown in **Figure 3.5**. For the first stage of the experiment, the upper surface of the heater was covered with 6.3 g of beech wood shavings. This was covered by a layer of fine glasswool, 80 mm deep immediately above the heater. The heater achieved a temperature of approximately 450 °C within 5 minutes of being switched on, producing rapid ignition of the shavings. As soon as smoke was emanating from the bed, the heater was switched off. The temperature of the shavings was measured using only one thermocouple directly under the top surface of the shavings as shown in Figure 3.5. The variation of temperature versus time of both the heater and the shavings was recorded by the data logger/PC-system. The upper surface temperature of a representative 2 cm x 2 cm area of the glasswool surface was measured by the IRT System used in the previous work from a distance of 2 metres. The entire procedure was then repeated with a glasswool layer of 160 mm thickness above the heater.

The second stage of the experiment was carried out as above but without combusting shavings and with the heater as the sole heat source. Again fine glasswool layers of 80 mm and 160 mm thickness, respectively were used as the covering material. In

order to have the upper surface of the heater in the same position as the upper surface of the shavings during the previous experiment, additional Rockwool<sup>®</sup> was placed underneath the heater.

These experiments allowed a direct assessment to be made of the influence of the gaseous combustion products on the surface temperature distribution of the bed. All results will be presented in section 4.3.

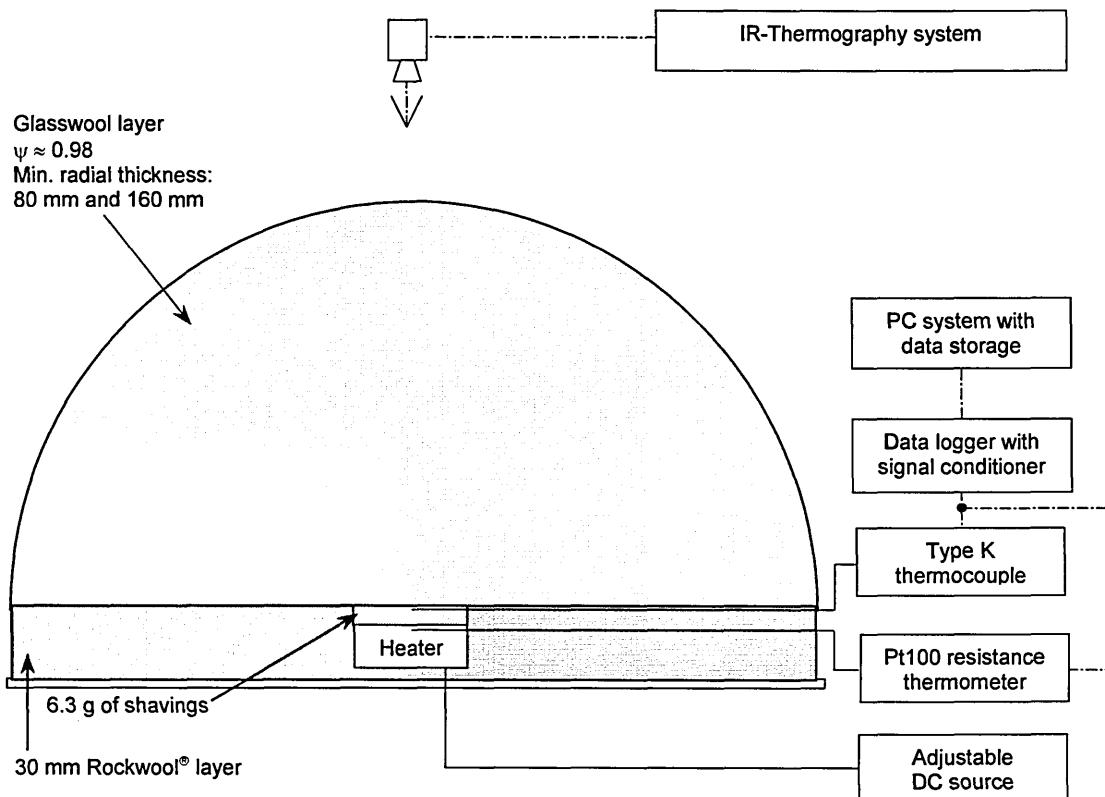


**Figure 3.5** Cross-sectional schematic diagram of the experiment set-up to compare the influence of exclusive heat transfer or a combination of heat and mass transfer on the surface temperature distribution of a hemispherical shaped, homogenous “packed” bed of fine glasswool ( $\psi \approx 0.98$ )

The IR-Thermograms of the glasswool surface showed that the hottest areas were always to be found almost vertically above the heat source. This suggested a buoyancy induced fluid flow of the hot gases. The determination of to what extent buoyancy takes place in a bed of domestic refuse is the objective of the next experiment that was conducted.

### 3.5 The flow of hot combustion gases through a small-scale domestic refuse bed – Experiment 4

The objective of this experiment was to simulate the natural flow of combustion gases through a small-scale domestic refuse bed in order to further confirm the assumption of a buoyancy induced gas flow. Since the handling of hot gases always bears the risk of igniting the bed of combustible matter, the hot gas had to be substituted by a gas having a comparable flow behaviour with regard to buoyancy.

According to ARCHIMEDES' law, the buoyancy induced draught pressure difference is given by  $\Delta p = (\rho_{amb} - \rho_G) g h$ . This shows that any gas whose density is lower than the density of the ambient air can be used to simulate hot combustion gases in terms of buoyancy induced mass flow. Since the exact composition of the combustion gases arising from smouldering refuse was not known, the combustion gas was treated, in a first approach, as air that enters the bed at 450 °C and leaves the bed at 20 °C, which gives a mean temperature between inlet and outlet of 235 °C. The density of air at ambient pressure and 235 °C is 0.69 kg/m<sup>3</sup> [57]. This is the density an appropriate substitute would be required to have, preferably at ambient temperature and thus ammonia gas was considered as a possible substitute having a density of 0.71 kg/m<sup>3</sup> at ambient pressure and 20 °C [57].

In order to observe the ammonia gas when exiting the bed, Backscatter Absorption Gas Imaging (BAGI) was used. The system used was an IR-Laser based LIS GasVue MG-30 Laser Imaging System (see appendix for further information) operating with a CO<sub>2</sub>-Laser that emitted radiation at 25 individual wavelengths in the range from 9.25 µm to 10.83 µm. The radiation was backscattered from a reflecting background and then received by an IRT system. Laser emission and reception of the backscattered radiation ran through the same optics, and thus the laser always pointed at the location from which the IRT system received the radiation. The functional principle of this gas visualisation system (GVS) is represented in **Figure 3.6**. In the

case where there is an absorbing gas plume, the laser radiation is impaired and the gas plume could be seen as a darker area on the IRT screen. Different gases absorb radiation at different wavelengths and since the laser wavelength could be triggered in the range from  $9.25 \mu\text{m}$  to  $10.83 \mu\text{m}$  a total of 77 gases could be visualised. One of the gases that can be visualised by the GVS is ammonia ( $\text{NH}_3$ ) gas. Experiments have shown that even a very small mass flow of only 2 kg/year can be visualised.

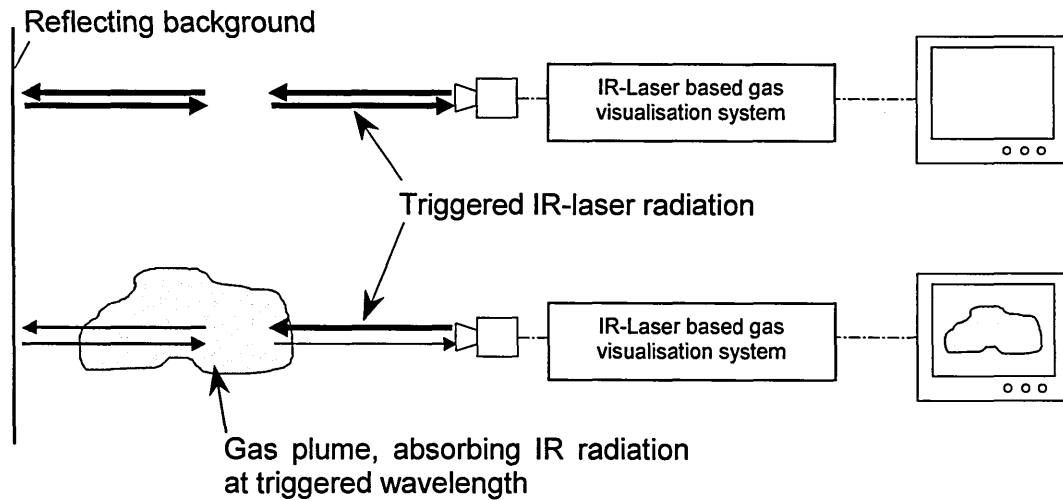


**Figure 3.6** Functional principle of the IR-Laser based gas visualisation system

A wire frame box with a wooden bottom plate, as shown in **Figure 3.7** and **Figure 3.8**, was built to hold domestic refuse and thus simulate a refuse bed. The refuse used for this experiment was collected from the refuse bins of Fachhochschule Gelsenkirchen thus providing for a mixture of compounds that might also be found in household refuse bins. The dimensions of the bed were  $0.6 \text{ m} \times 0.8 \text{ m}$  with a variable height  $H$  to simulate depth variations. The refuse matter could be manually compressed to simulate density variations. At the centre of the bottom plate a  $50 \text{ mm}$  diameter hole was drilled as the inlet for the ammonia gas. The ammonia gas was supplied from a bottle of  $32\% \text{ NH}_3\text{-H}_2\text{O}$  solution through a hose into the bottom of the bed. The flow of the ammonia gas was not controlled and the content of water vapour in the ammonia

gas could be neglected because ammonia at 20 °C vaporises at a pressure below  $8.5 \cdot 10^5$  Pa [87] and water vaporises at a pressure below  $2.3 \cdot 10^3$  Pa.

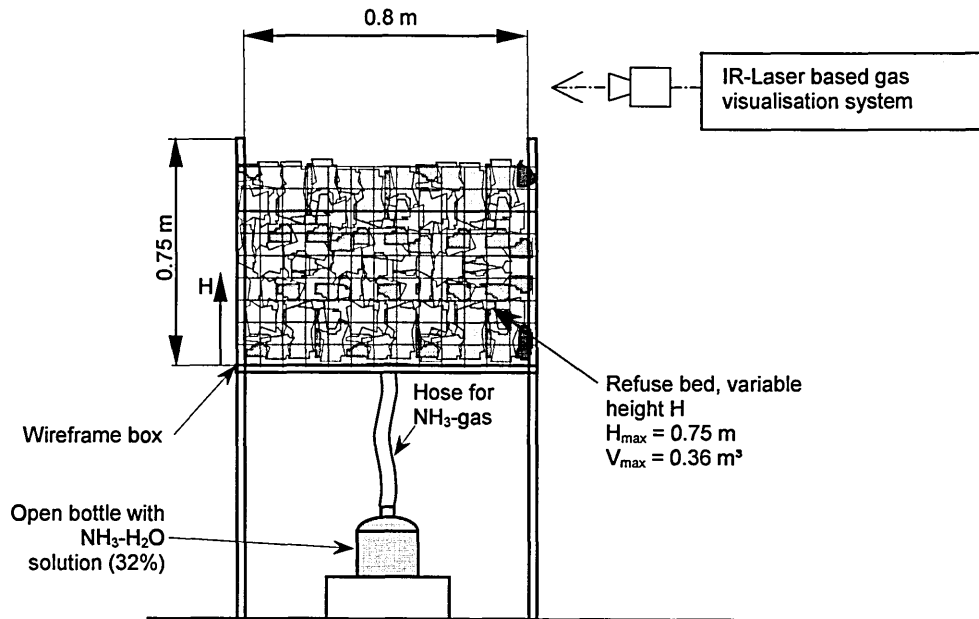


**Figure 3.7** Schematic diagram for the simulation of the flow of hot combustion gases through a domestic refuse bed with variable height H. The hot combustion gases are substituted by NH<sub>3</sub>-gas.

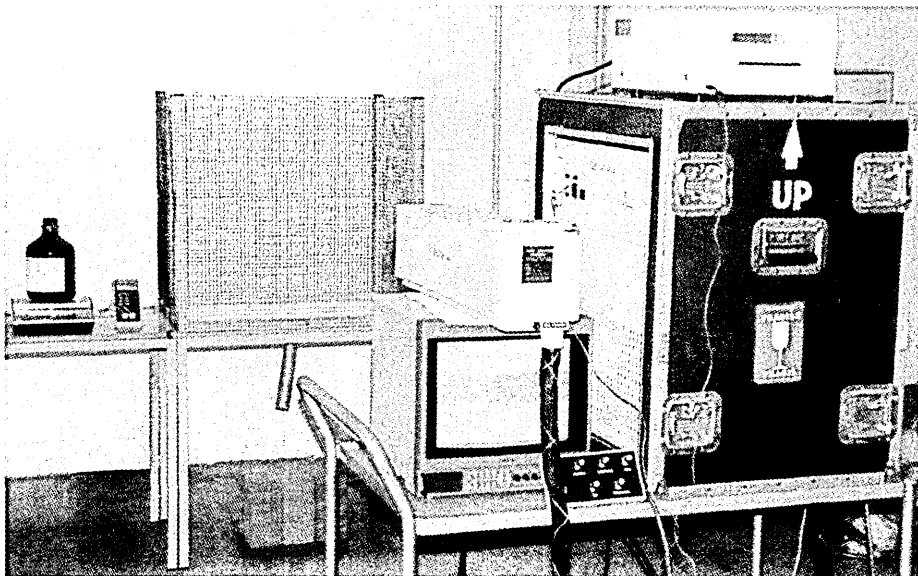


**Figure 3.8** Photograph of the experimental set-up. In the foreground, the GVS can be seen.

All sides of the bed were scanned with the GVS to ensure that there was no hidden exit of the NH<sub>3</sub>-gas. The experimental conditions are summarised in **Table 3.3** and the results will be presented in section 4.4.

**Table 3.3** Properties for the simulation of the fluid flow behaviour of hot combustion gases through a domestic refuse bed

	Refuse height	Refuse volume	Refuse density
Step 1	0.25 m	0.12 m <sup>3</sup>	79 kg/m <sup>3</sup> <sup>1)</sup>
Step 2	0.50 m	0.24 m <sup>3</sup>	79 kg/m <sup>3</sup> <sup>1)</sup>
Step 3	0.75 m	0.36 m <sup>3</sup>	79 kg/m <sup>3</sup> <sup>1)</sup>
Step 4	0.35 m	0.17 m <sup>3</sup>	169 kg/m <sup>3</sup> <sup>2)</sup>
Ambient temperature $\vartheta_{amb}$ , NH <sub>3</sub> -gas temperature			20 °C
Calculated mass flow rate of the NH <sub>3</sub> -gas $\dot{m}_{NH_3}$			7.6 kg/year <sup>3)</sup>
Calculated volume flow rate of the NH <sub>3</sub> -gas $\dot{V}_{NH_3}$			12 m <sup>3</sup> /year <sup>4)</sup>

- 1) Measured value of uncompressed refuse.
- 2) Measured value of compressed refuse. This density value corresponds to the average density of the German domestic refuse inside the household refuse bins [16].
- 3) This value was obtained by weighing the bottle with the NH<sub>3</sub>-H<sub>2</sub>O solution before and after the experiment.
- 4) Volume flow rate at ambient pressure and temperature. Calculated from the measured mass flow rate.

This experiment demonstrated that the substitute for the hot combustion gases tended to flow vertically upwards in small-scale domestic refuse beds. The next experiment was to extend this work to a large-scale domestic refuse bed. Whether or not the similarity to the buoyancy induced stack flow applies to an actual situation inside a refuse bed could now be evaluated by proceeding with the experiment.

### 3.6 Large-scale experiment conducted in a 27 m<sup>3</sup> batch of domestic refuse – Experiment 5

As will be discussed later, the following assumptions, made within the previous chapter were confirmed by the foregoing experiments:

- Conduction did not significantly contribute to the heat transfer.
- Convection by the combustion gases was the only relevant heat transfer mechanism.
- The mass transfer of the combustion gases took place as a buoyancy forced vertical plug-flow.

The aim was now to show that the assumptions could be applied just as well to a large-scale batch of domestic refuse. Therefore, the temperature development inside and at the surface of a domestic refuse bed subjected to an endogenous combustion at the bottom was measured. In order to achieve most authentic conditions, average refuse in terms that described in section 2.1, was used for this experiment.

The refuse was provided by the authorities of the domestic refuse incineration plant “RZR Herten”, Germany. A 2 m x 2.3 m x 6.5 m container, as shown in **Figure 3.9** and **Figure 3.10** was used to store the refuse during the experiment. The container depth of 2 m allowed for an artificial smouldering combustion at a realistic depth.

At the centre of the container bottom, a hole of approximately 20 cm x 20 cm had been cut. The hole was covered by a metal sheet containing approximately 225 small holes (Ø 6 mm) as shown in **Figure 3.12**. Through these holes, the necessary ignition could be applied to the bed by using a standard propane gas ring burner with a maximum heat output of 20 kW. The burner was turned off immediately after ignition was achieved. Figure 3.9 presents a photograph and Figure 3.10 a sketch of the entire set-up.

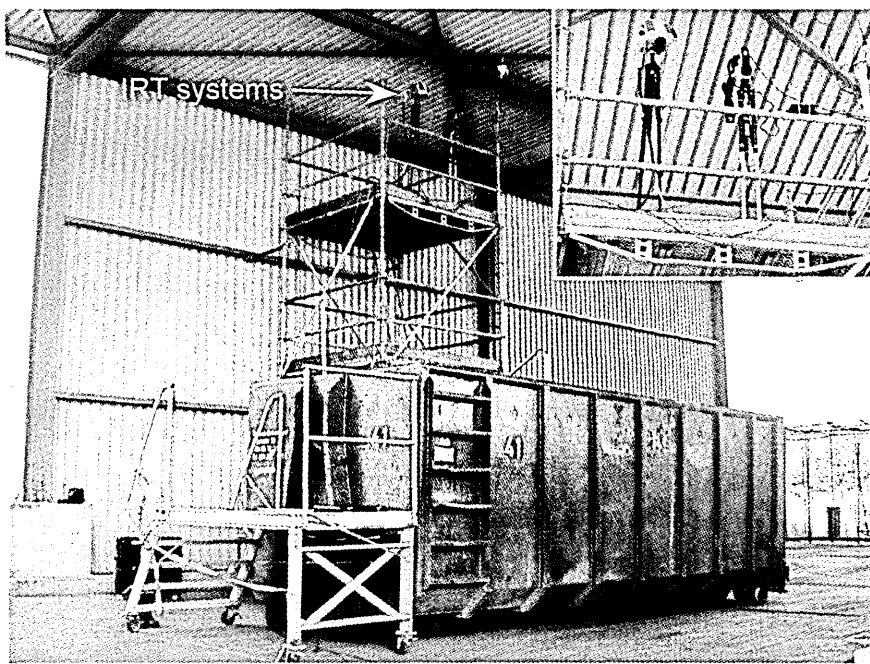


**Figure 3.9** Set-up of the refuse experiment

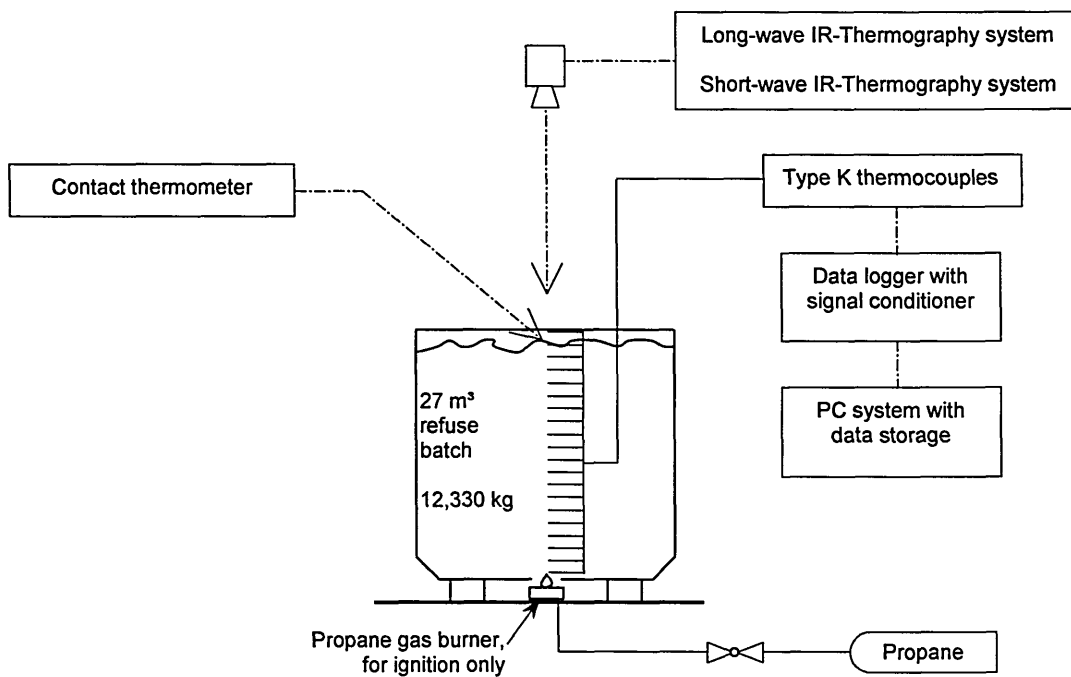


**Figure 3.10** Schematic diagram of the refuse experiment

Temperature measurement inside the refuse bed was achieved by twenty Thermocoax 2ABI30/4000/TI/D/2AB35/6m stainless steel sheath type K thermocouples supported by a stainless steel beam (see appendix for further detail). A detail of a thermocouple and the fixture to the beam is shown in **Figure 3.11**. The beam was welded to the

container bottom, as shown in **Figure 3.12**. The temperature sensitive tips of the thermocouples were vertically aligned above the perforated ignition plate. Thus, the temperature distribution inside the bed was measured one-dimensionally in the direction in which the combustion was expected to proceed, i.e. vertically upwards.

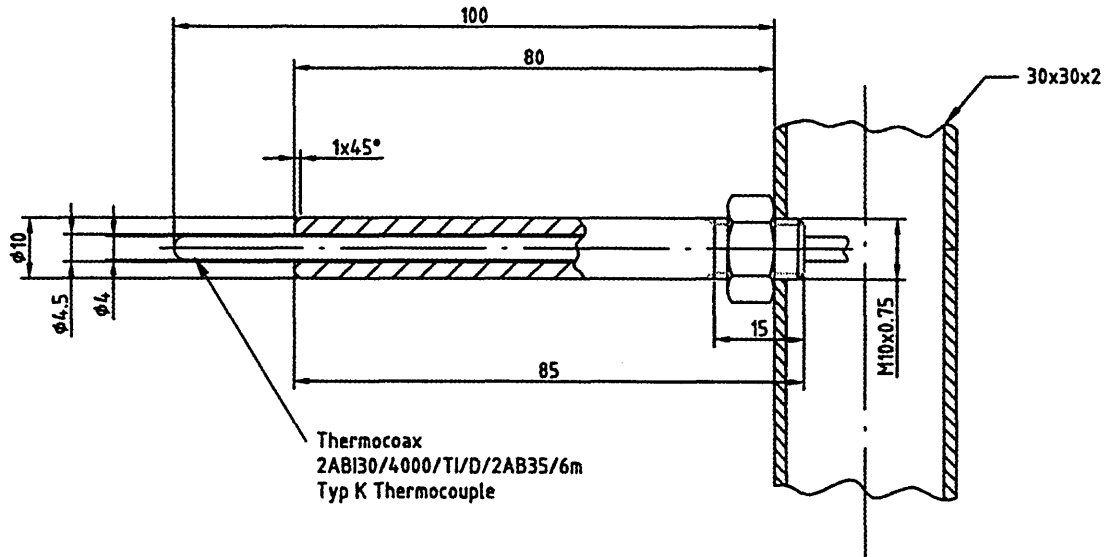


**Figure 3.11** Detail of a thermocouple and its fixture to the stainless steel beam

To keep the risk of thermal damage to a minimum, the stainless steel sheath of these thermocouples had a length of 400 cm. In order to safeguard against mechanical damage, thermocouples with a diameter of 4 mm were used which were additionally protected by placing them inside a stainless steel tube. Only the temperature sensitive tip was not covered. All thermocouples were connected to the data logger/PC-system.

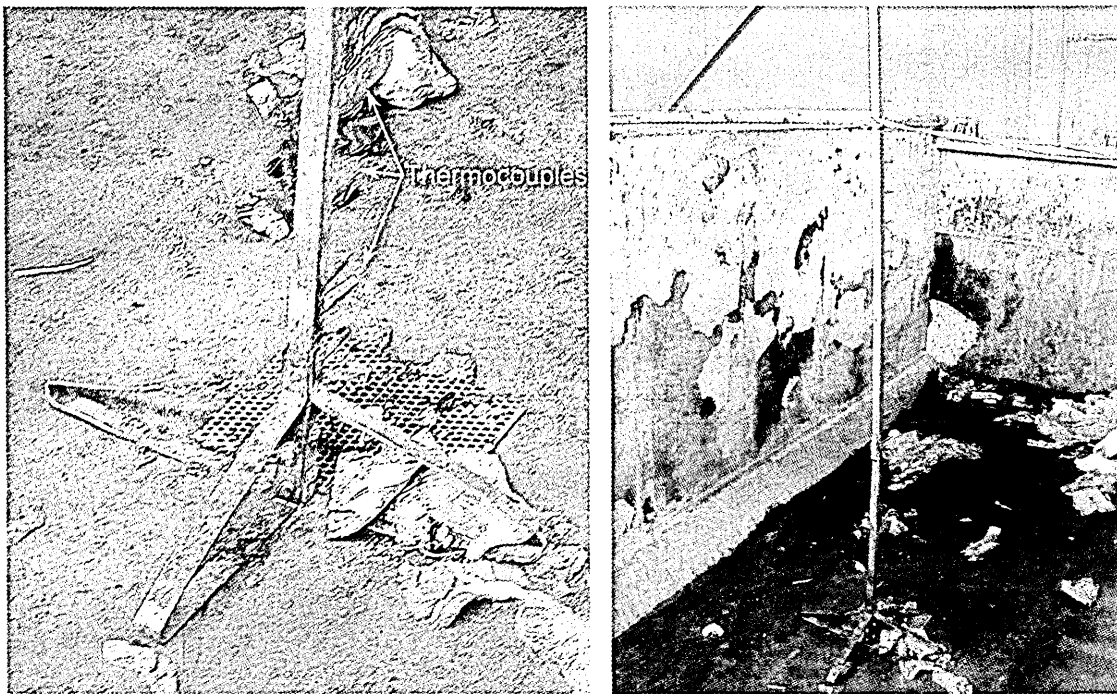


**Figure 3.12** Photographs of the perforated plate at the container bottom and the stainless steel beam, supporting the 20 thermocouples, welded to the container bottom

The refuse batch was prepared from a mix of several deliveries of the day so as to avoid any accumulation of a single type of material. According to the authorities of the plant that provided the refuse [51], the refuse had an average net calorific value of 11 MJ/kg and a water content of approximately 15 %. Using a mobile crane, 12,330 kg of refuse were loaded into the container, as presented by the sequence in **Figure 3.13**. Due to the presence of the thermocouple beam, the void fraction distribution may have been affected in this area. In order to keep this effect to a minimum, the refuse was carefully arranged around the beam and between the thermocouples, see Figure 3.13.

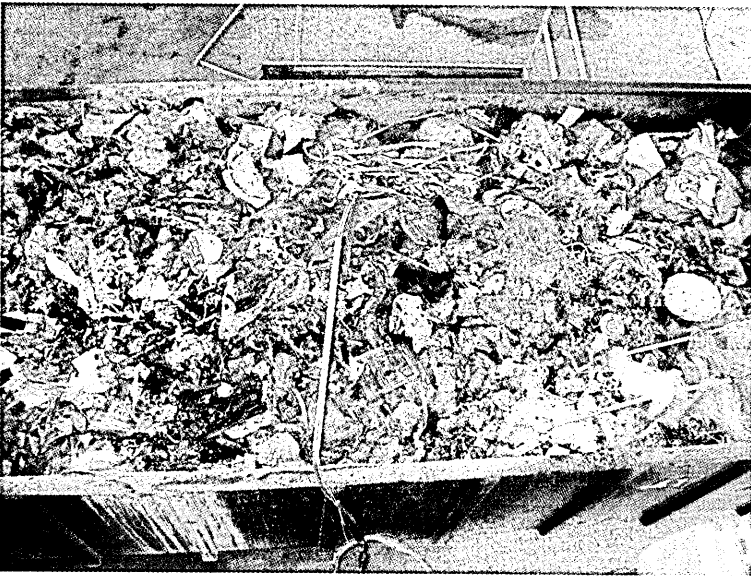
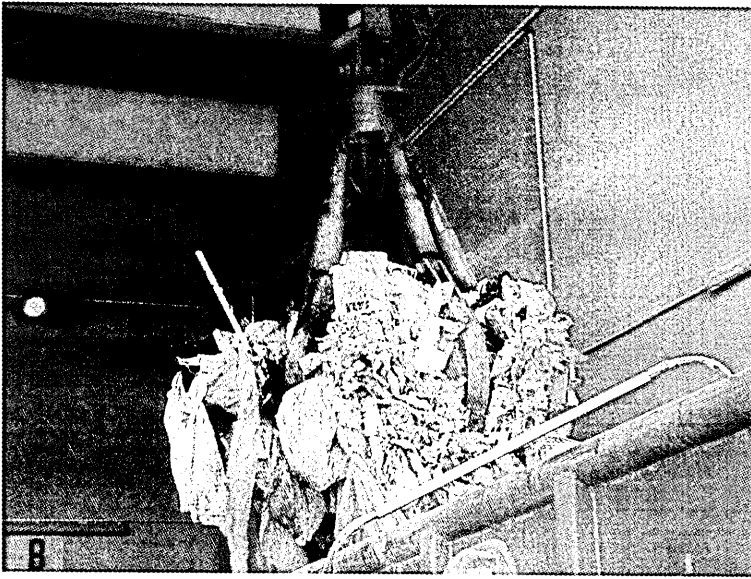


**Figure 3.13** Filling of the refuse container

After the container has been filled to a depth of 2.05 m, it was transported from the refuse delivery locations to where the experiment was to take place. Due to the transport, the refuse became compressed and the height of the bed decreased from 2.05 m to 1.85 m, representing in a volume decrease of approximately 3 m<sup>3</sup>. The refuse batch then had a calculated overall density inside the container of approximately 446 kg/m<sup>3</sup>. Following section 2.4 and Table 2.1, the calculated void fraction value then is  $\psi = 0.53$ , which corresponds to the lowest void fraction value of the shavings used during the previous experiments.

During this experiment, two different IRT systems were used. In addition to the IRT system described in section 3.2, measuring in the short-wave range from 3  $\mu\text{m}$  to 5.4  $\mu\text{m}$ , another IRT system, measuring in the long-wave range from 7.5  $\mu\text{m}$  to 13  $\mu\text{m}$  was also used. Both systems were placed on top of a scaffolding next to the refuse container, resulting in a measuring distance of 5 m, as shown in Figure 3.9. Whether or not the temperature measurement of this specific surface spot is accurate depends on the emissivity of the measured particle. A compromise had to be found due to the large variety of materials involved. Comparative measurements using an Ahlborn THERM 2285-2 contact thermometer have shown that a representative emissivity of 0.95 could be used.

At the beginning of the experiment, the bed was ignited via the perforated bottom plate using a propane gas burner that supplied a 7.5 kW flame. The burner was turned off immediately after ignition of the refuse, which took about three minutes, when light blue smoke exited the surface of the bed. After that, the entire system was left to itself and the combustion proceeded. The holes in the perforated plate were not covered after ignition, creating a natural chimney effect that will be discussed later. The temperatures inside and at the surface of the bed were recorded every two minutes. After 72 minutes, the experiment had to be aborted due to heavy smoke emission, see **Figure**

3.14, when combustion had proceeded to within approximately 140 cm of the surface of the bed. The results will be presented in section 4.5.

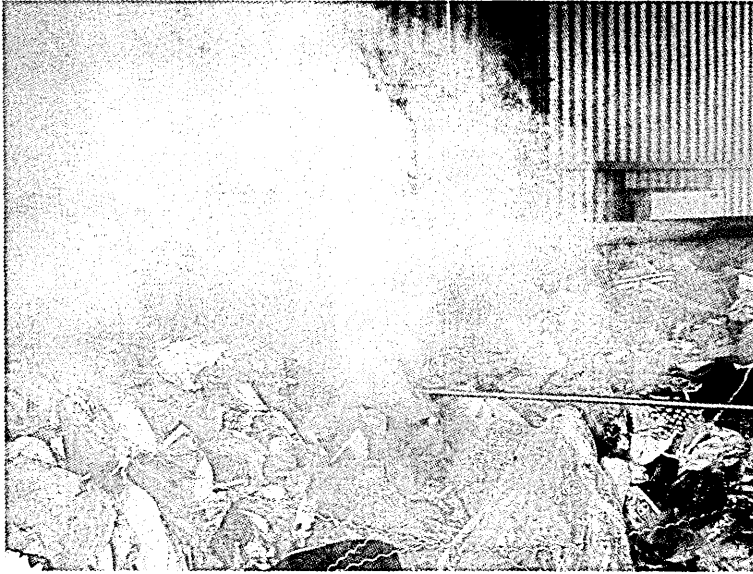


**Figure 3.14** Heavy smoke and mist emission from the refuse surface after 70 minutes. The experiment had to be aborted two minutes later.

Since during this experiment the combustion could not proceed up to the surface, a set of three additional experiments were conducted in beds of wood chips that could be combusted until flashover occurred, without the problem of harmful smoke being generated.

### 3.7 Intermediate-scale experiments using wood chips – Experiment 6

The objective of this final set of experiments was to observe the temperature distribution inside and at the surface of a packed bed, from the beginning of the smouldering combustion to the flashover at the surface at the end. In order to produce a combustion but without generating harmful smoke, wood chips were used to substitute for the refuse. The wood chips were stored inside a barrel during the combustion process instead of the larger refuse container but the general set-up corresponds to that of the previous experiment, as can be seen in **Figure 3.15** and **Figure 3.16**.

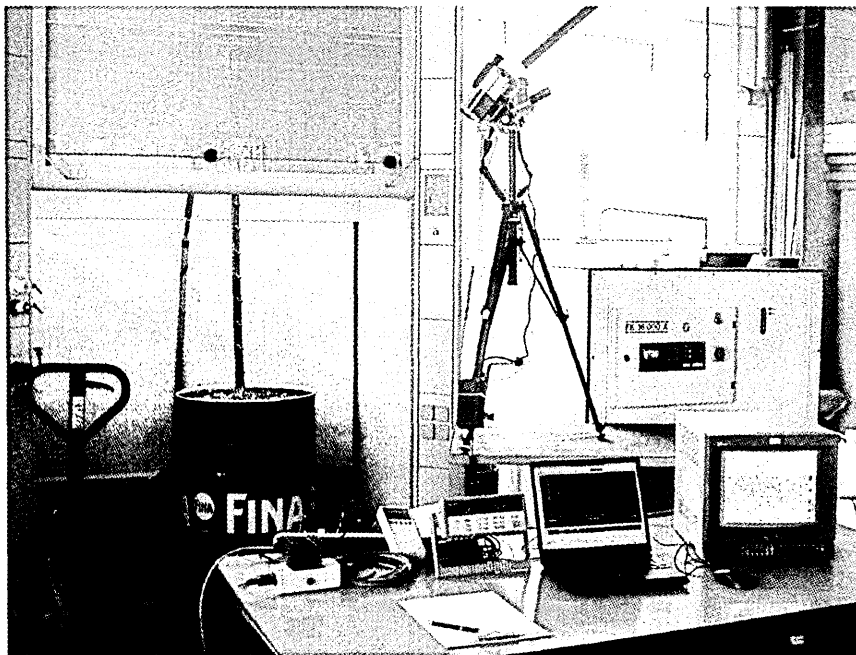


**Figure 3.15** Set-up of the wood chips experiments

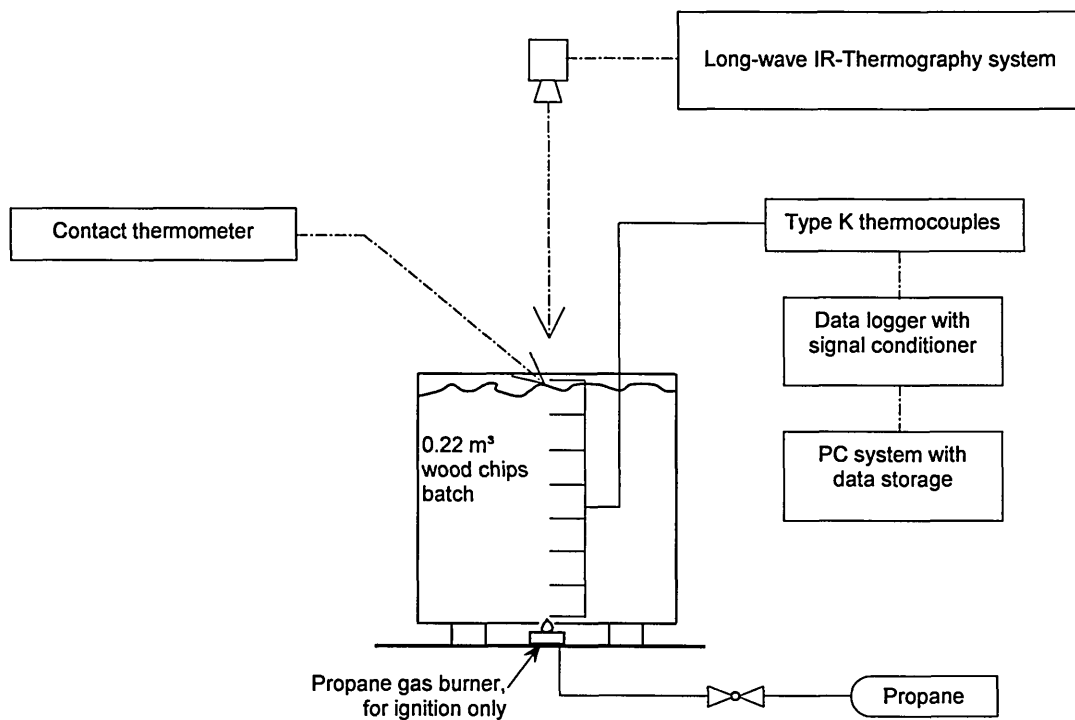


**Figure 3.16** Schematic diagram of the wood chips experiments

The barrel was filled with  $\leq 100$  mm particles of sieved wood chips. Such a bed had nearly the same void fraction ( $\psi = 0.64$ ), particle density ( $\rho \approx 700 \text{ kg/m}^3$ ) and water content ( $w = 0.15$ ) as domestic refuse and could thus be used as a substitute in terms of heat transfer parameters. To minimise the influence on the void fraction distribution of the thermocouple beam, the wood chips were carefully arranged around the beam and between the thermocouples.

At the centre of the bottom of the  $0.22 \text{ m}^3$  ( $\varnothing 58 \text{ cm} \times 85 \text{ cm}$ ) barrel,  $25 \varnothing 4 \text{ mm}$  holes were drilled in a  $15 \text{ cm} \times 15 \text{ cm}$  area. Through these holes, the necessary ignition energy could be transferred to the bed of wood chips by the propane gas burner placed underneath the barrel. The ignition phase with the gas burner required approximately 10 minutes. After that, the self-propagating endogenous smouldering combustion could proceed towards the surface. For the temperature measurements inside the bed, the thermocouple beam from the previous experiment was used. The temperature sensitive tips of the thermocouples were again placed vertically above the holes in the

bottom of the barrel. The thermocouple beam was attached to the barrel. Thus, the temperature distribution inside the bed was measured one-dimensionally in the direction in which the combustion was expected to proceed, i.e. vertically upwards. All bed temperatures were recorded every 2 minutes by the data logger/PC-System.

Since during the previous experiment, the long-wave IRT system proved to achieve more accurate measurements during the phase of smoke and mist emission at the surface of the bed, only the long-wave IRT system was used for the measurements of the surface temperature. The measuring distance was 1.2 m. Comparative measurements with a contact thermometer showed an emissivity of 0.95.

Flashover took place at the surface of the bed 390 to 417 minutes after first ignition had been achieved. In contrast to the refuse experiment, where the flashover could not be achieved, this set of experiments allowed for the observation of the surface temperature distribution and the flashover. The results of these experiments will be described in section 4.6.

# CHAPTER 4

## EXPERIMENTAL RESULTS

## 4 EXPERIMENTAL RESULTS

The experiments are detailed in the same sequence as in the previous chapter.

### 4.1 Temperature profiles in a shavings bed undergoing self-ignition – Experiment 1

The objective of the first set of experiments was to determine the conditions under which self-ignition of shavings soaked in linseed oil – as an example for an endogenous combustion - would occur. The results of the six individual experiments, as previously explained in section 3.2, are summarised in **Table 4.1**.

**Table 4.1** Results of the experiments to determine the conditions under which self-ignition of shavings soaked in linseed oil occurs

Test	Particle size mm	Mass ratio: linseed oil/shavings	Time after maximum temperature was achieved	Maximum temperature of the oil soaked nest	
				in the middle	at the top surface
1	1.0 - 2.0	30 g / 50 g	255 minutes	105 °C	155 °C
2	1.0 - 2.0	50 g / 50 g	225 minutes	110 °C	162 °C
3	1.0 - 2.0	80 g / 50 g	375 minutes	140 °C	190 °C
4	0.5 – 1	30 g / 50 g	228 minutes	110 °C	170 °C
5	0.5 – 1	50 g / 50 g	228 minutes	130 °C	195 °C
6	0.5 – 1	80 g / 50 g	555 minutes	380 °C <sup>1)</sup>	280 °C <sup>1)</sup>

<sup>1)</sup> for test 6, data acquisition was stopped due to combustion

During tests 1 to 5, only self-heating was observed. These tests were characterised by start-up times of 150 to 200 minutes, followed by an exponential temperature increase as auto-oxidation developed inside the linseed oil soaked nest of shavings. The maximum temperatures achieved during these tests were in the range from 150 to 200 °C and thus insufficient for ignition. As an example, the temperature development in time of test 2 is presented in **Figure 4.1**. Because insufficient production of heat had occurred, the temperature rise was too small for ignition to occur. This can be put down to either a lack of oxidator (linseed oil) or a lack of oxidant (atmospheric oxygen). For tests 1 to 3 this can be explained by the specific surface area of the 1.0 to 2.0 mm

shavings being too low . During the tests 4 and 5, the specific surface area had been increased by using shavings of 0.5 to 1.0 mm, but the amount of linseed oil of max. 50 g did not seem to be sufficient.

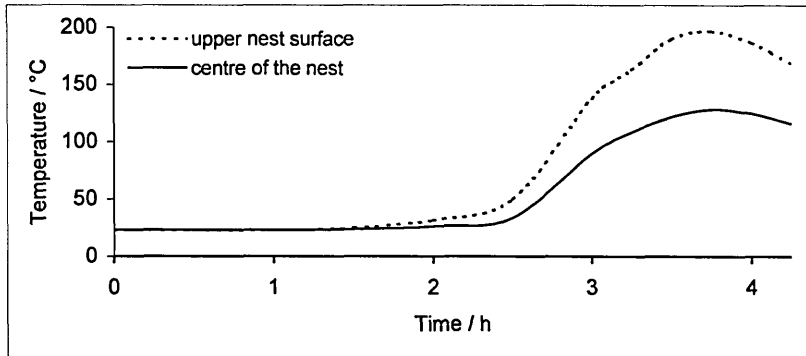


**Figure 4.1** Temperature curves of a self-ignition process of 50 g linseed oil mixed with 50 g shavings with a particle size of 1.0 - 2.0 mm, test 2. The mixture is covered with shavings of 1.0 - 8.0 mm particle size.

For test 6, during which ignition was achieved, the smaller shavings had been mixed with 80 g of linseed oil. In this case, both oxidant and oxidator were present in sufficient proportions for an appropriate production of heat that led to ignition of the shavings, as shown in **Figure 4.2**. This mixture of 80 g of linseed oil with 50 g of 0.5 to 1 mm size wood shavings was used as an endogenous ignition source in a bed of 1000 g of 1.0 to 2.0 mm wood shavings as described in section 3.2.

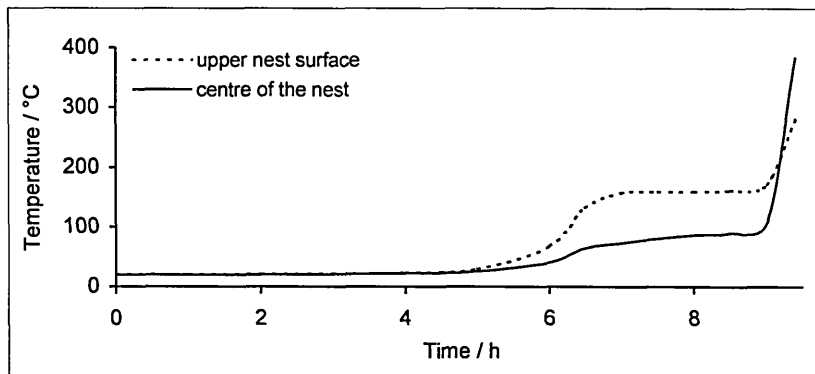


**Figure 4.2** Temperature curves of a self-ignition process of 80 g linseed oil mixed with 50 g shavings with a particle size of 0.5 - 1.0 mm. The mixture is covered with shavings of 1.0 - 8.0 mm particle size.

The variation of temperature with time at various positions inside the heap of shavings undergoing self-ignition, as illustrated in Figure 3.2, is presented in **Figure 4.3**. The ignition temperature of 350 °C was reached after 360 minutes at the top of the linseed oil soaked core. At this time, the temperature difference between the top of the linseed oil soaked core at 45 mm and the surface of the entire heap at 120 mm reached its maximum value of 200 K. This suggests that up to this point, heat transfer was principally by conduction but to a very low extent. After ignition had been achieved, the surface temperature increased more rapidly and the temperature differences between that position and the top of the core became less. This showed that the thermal resistance had decreased, which can only be explained by convection, i.e. more effective heat transfer, resulting from the combustion gases. After 390 minutes the entire heap underwent smouldering combustion and the core temperature, where the material had been almost totally combusted away, fell below the surface temperature.

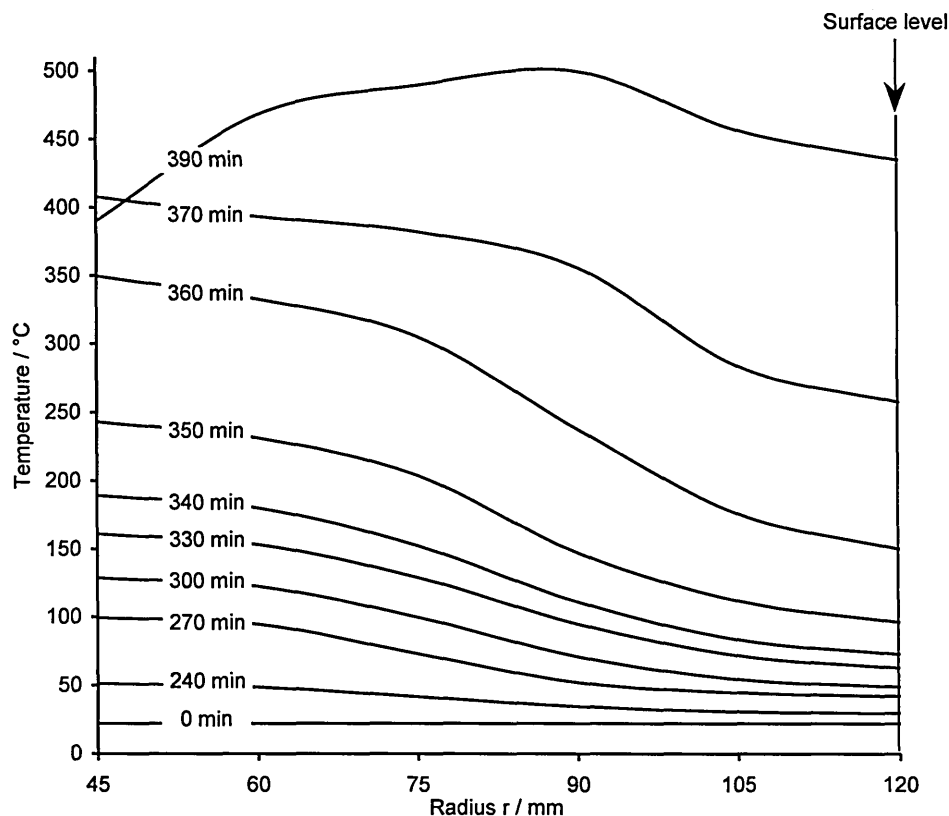


**Figure 4.3** Measured temperature distribution with time along the radial axis  $r$  at the surface and inside the hemispherical shaped heap of shavings illustrated in Figure 3.2 and Figure 3.3 with endogenous self-ignition inside the core of the heap

The hemispherical shape of the heap would be expected to exhibit a quite uniform temperature field inside and at the surface as long as conduction and radiation accounted for the heat transfer. At the surface, where the temperature distribution was measured using the IRT system, such a uniform distribution was observed as long as combustion did not take place. Since the temperatures inside the heap have been measured only vertically along the vertical radial axis, no direct conclusions on the internal temperature distribution could be made. When combustion arose, the maximum surface temperature always occurred vertically above the oil soaked core where the exiting combustion gases became apparent due to the associated light smoke. This situation suggested that, at least inside almost homogeneous packed beds, the combustion gases tend to flow directly upwards and indicates a buoyancy forced gas flow.

#### 4.2 Temperature profiles in a shavings bed subjected to an electrical heat source – Experiment 2

The results of Experiment 1 described in section 4.1 suggested that inside packed beds heat is more effectively transferred by convection, at least when combustion occurs. In order to qualitatively confirm this suggestion, this second set of experiments was conducted. Heaps of shavings with different void fractions were subjected to heating by an electrical heat source, as described in section 3.3. The temperature of the heat source was set in different experiments to individual temperatures of approximately 100 °C and 250 °C so as not to exceed the ignition temperature of the shavings, and to 350 °C when combustion was achieved. The experimental results are summarised in **Table 4.2**.

**Table 4.2** The surface temperature of heaps of wood shavings subjected to an internal heat source at the bottom

Void fraction of the shavings	Particle size mm	Heat source temperature	Maximum surface temperature
0.58	≤ 0.5	100 °C	23.6 °C
0.58	≤ 0.5	258 °C	30.8 °C
0.58	≤ 0.5	350 °C	Combustion
0.71	0.5 – 1	105 °C	23.5 °C
0.71	0.5 – 1	251 °C	29.6 °C
0.71	0.5 – 1	350 °C	Combustion
0.81	1 – 2	104 °C	23.3 °C
0.81	1 – 2	253 °C	28.3 °C
0.81	1 - 2	350 °C	Combustion

**Figure 4.4** shows the development of the surface temperatures of the heaps versus time. At a heat source temperature of  $\vartheta_{HS} = 100$  °C, the surface temperature distribution was uniform and had the same values for all void fractions. At a heat source temperature of  $\vartheta_{HS} = 250$  °C, the surface temperature was uniform as well, but increased with decreasing void fraction. This suggested that below ignition temperature, the heat was exclusively transferred by conduction, which became more effective with decreasing void fraction. At a heat source temperature of  $\vartheta_{HS} = 350$  °C the shavings ignited after 30 minutes. During the first 30 minutes, the surface temperature development suggested heat transfer by conduction. After 30 minutes, the

surface temperature distribution behaved in a different way with small areas of higher surface temperatures apparent. This can be attributed to a small degree to the growing combustion area with time, but more importantly to the convection produced by the combustion gases produced. This effect increases with increasing void fraction.

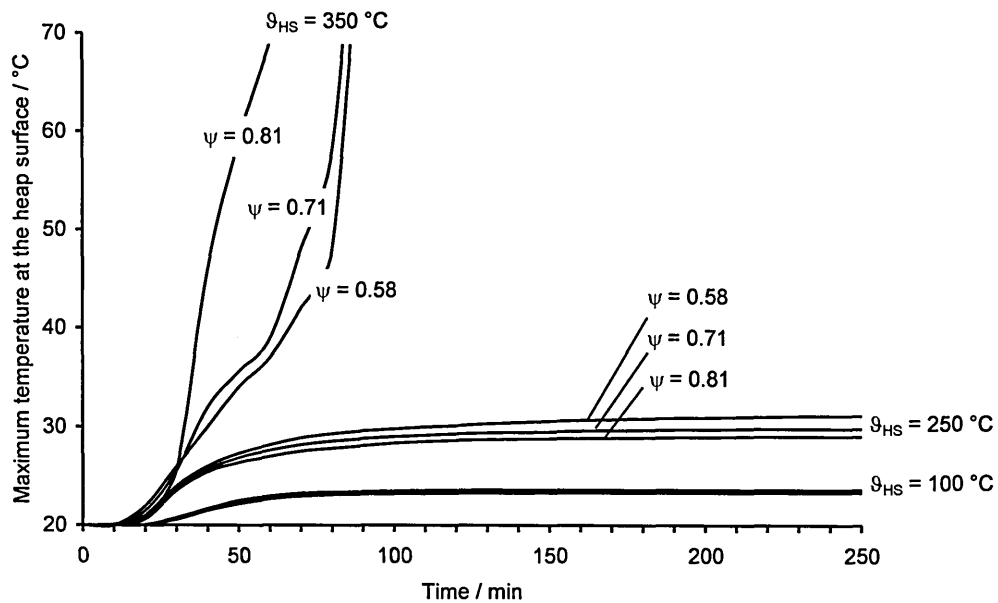


**Figure 4.4** Measured maximum surface temperatures versus time of a hemispherical shaped shavings bed of different porosities  $\psi$ . The bed covers an internal electrical heat source at different temperatures  $\vartheta_{HS}$ . The heat source temperature is constant after a start-up time of 10 minutes.

The results suggest that a low void fraction is favourable for heat transfer by conduction, whereas a better heat transfer by convection can be achieved with a higher void fraction. Conduction hardly has any influence on the surface temperature distribution but convection does in a considerable way. The same must consequently apply to the temperature distribution inside the bed. An example of the temperature variation throughout the bed is presented in **Figure 4.5** for a heat source temperature of  $\vartheta_{HS} = 200$  °C. Here, steady state conditions have been achieved after 240 minutes of heating. The determined isotherms ran almost equidistant to the heat source, showing that heat transfer was due to conduction.

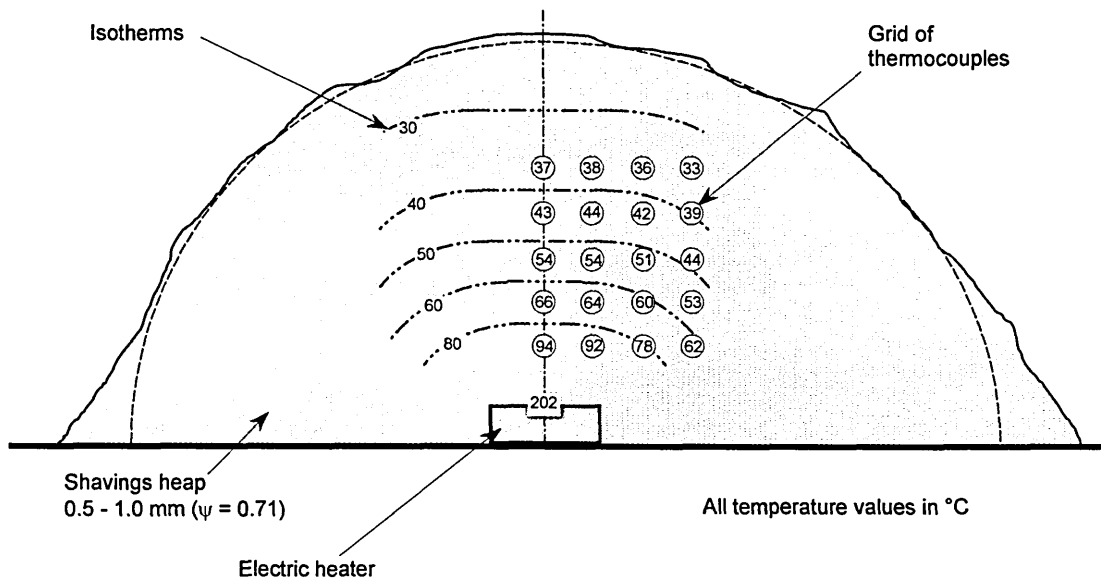


**Figure 4.5** Measured temperature distribution inside a hemispherical heap of shavings (0.5 - 1.0 mm,  $\psi = 0.71$ ) subjected to an internal heat source (202 °C) at the bottom under steady state conditions after 240 minutes

At a heat source temperature of  $\vartheta_{HS} = 350$  °C, when combustion occurred, a different situation was observed. **Figure 4.6** shows the situation 25 minutes after ignition. The isotherms do not run equidistant to the heat source. Their more elliptical form suggests that there is convection by combustion gases, which transfer heat vertically through the heap towards its surface.

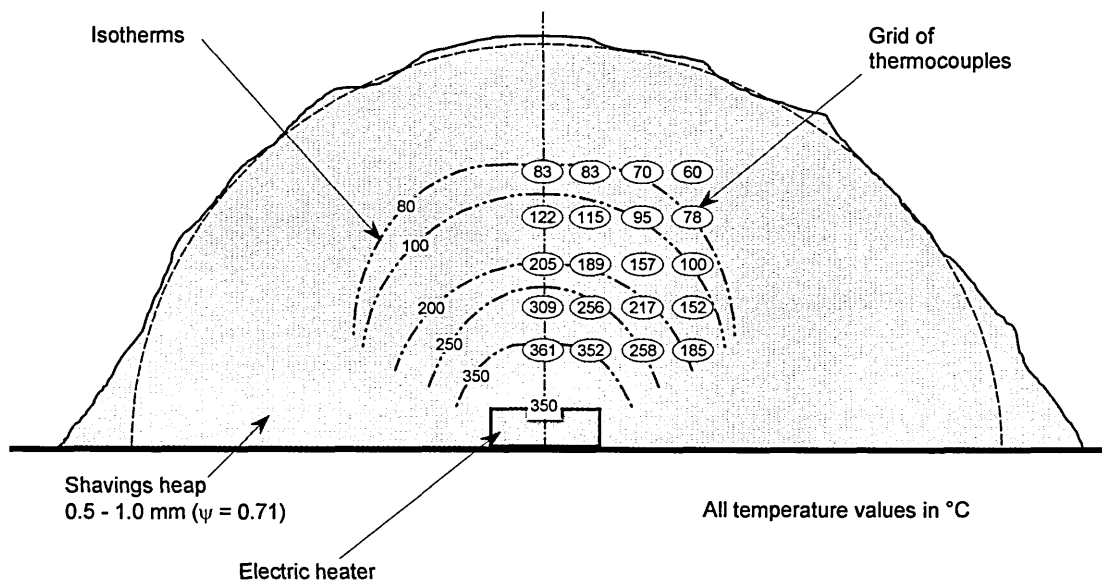


**Figure 4.6** Measured temperature distribution inside a hemispherical heap of shavings (0.5 - 1.0 mm,  $\psi = 0.71$ ) subjected to an endogenous combustion at the bottom approximately 25 minutes after ignition was achieved

### 4.3 Comparison of the heat transfer by conduction with that by convection – Experiment 3

All experimental results so far indicated that the gaseous combustion products augmented the heat transfer inside packed beds very effectively. To further confirm this, another experiment was conducted. The heat transfer from a heat source emitting hot combustion gases – for which smouldering wood shavings were used – was compared to that of a electrically heated source not emitting hot gases. Both of these localised heat sources were covered by fine glasswool that simulated the packed bed without participating in the combustion.

Figure 4.7 shows the variation with time of the temperature of the heat source and the surface temperature of the covering layer of 8 cm of glasswool. With only electrical heating, the measured temperature within a 2 cm x 2 cm surface area vertical above the heat source increased up to an average value of 72 °C and a maximum value of 79 °C.

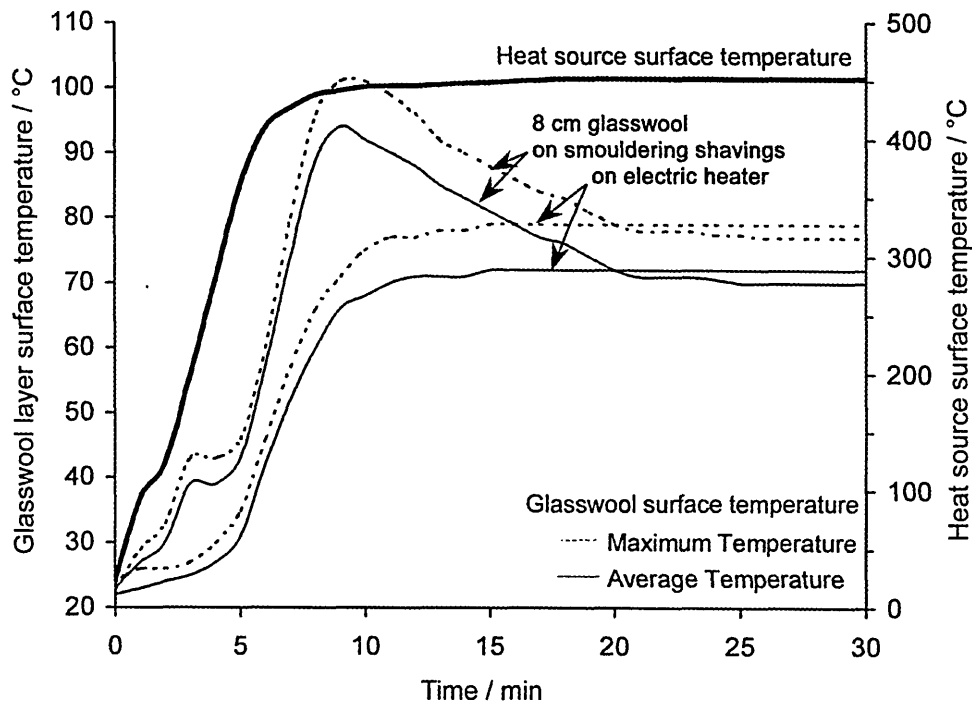
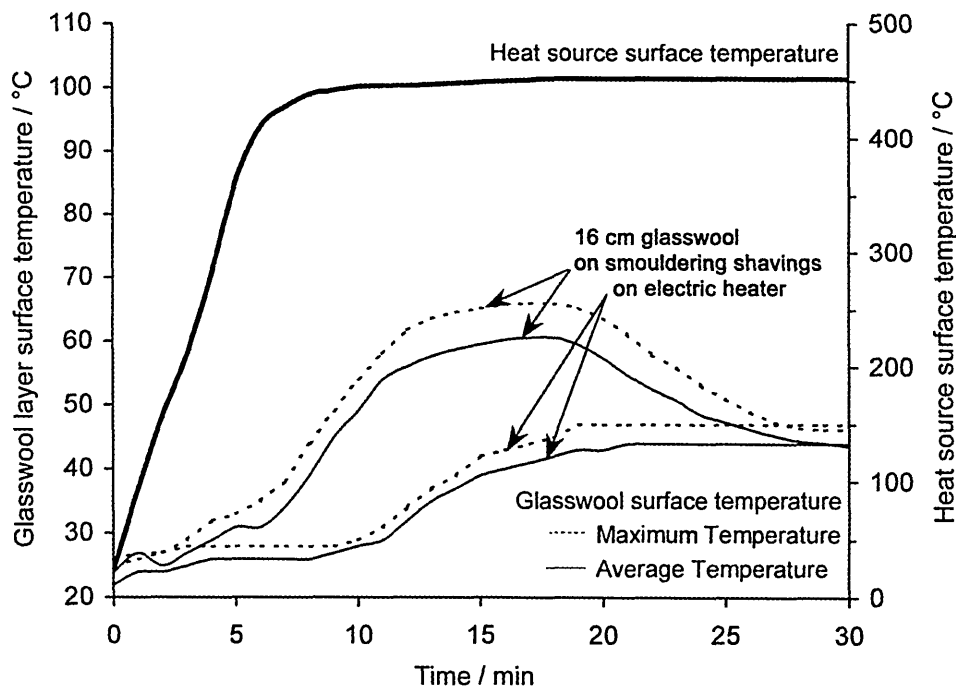


Figure 4.7 Measured temperature distribution with time for a representative surface area (2 x 2 cm<sup>2</sup>) of an 8 cm thick layer of fine glasswool ( $\psi \cong 0.98$ ) covering a heat source which is either an electric heater or smouldering shavings

When heating was produced by the combustion of wood shavings, the surface temperature increased more rapidly and reached an average value of 94 °C and a maximum value of 102 °C. Since the development of the heat source temperature was the same for both experiments, the more rapid temperature response and the higher temperatures can only be explained by convective heat transfer. After 10 minutes, most of the shavings had burnt away and the production of combustion gases ceased. The temperatures then dropped to the steady-state temperature level of the experiment without shavings. The indicated temperature difference of 2 K may be attributed to residues of the shavings remaining on the heating element as an insulating layer.

The experiment was repeated using a 16 cm glasswool layer. The results are shown in **Figure 4.8**. Again, when shaving were combusted, the speed of response was increased by the contribution of convection of the combustion gas to the overall heat



**Figure 4.8** Measured temperature distribution with time for a representative surface area ( $2 \times 2 \text{ cm}^2$ ) of an 16 cm thick layer of fine glasswool ( $\psi \cong 0.98$ ) covering a heat source which is either an electric heater or smouldering shavings

transfer under otherwise similar conditions. Compared to the previous experiment, the speed of response and the surface temperatures were lower. This must be attributed to the doubled thickness of the glasswool layer. However, the overall result corresponds to that of the previous experiment with the thinner layer of glasswool.

IR-Thermograms of the glasswool surface were also obtained. **Figure 4.9** shows a corresponding temperature distribution at the surface of the 8 cm glasswool layer with the electrical heater as heat source at 450 °C, 10 minutes after it had been switched on. A uniform temperature distribution can be seen. A different situation can be seen in **Figure 4.10** which is the IR-Thermogram when smouldering shavings were used as the heat source. The IR-Thermogram had again been taken 10 minutes after the beginning of the experiment, when the heater had already been switched off. The shavings had been ignited by then and had reached the above mentioned temperature of 450 °C. The observed surface temperature was higher and the temperature distribution was less uniform compared with the experiment using only an electrical heat source. The clearly distinguishable hot spot at 101.2 °C in Figure 4.10 appeared vertically above the smouldering shavings. This was due to the hot combustion gases, which produced a yellow discoloured area where they exited the glasswool layer.

With regard to the temperature distribution of the glasswool layer surface, the same results were obtained from the experiments using the 16 cm glasswool layer.

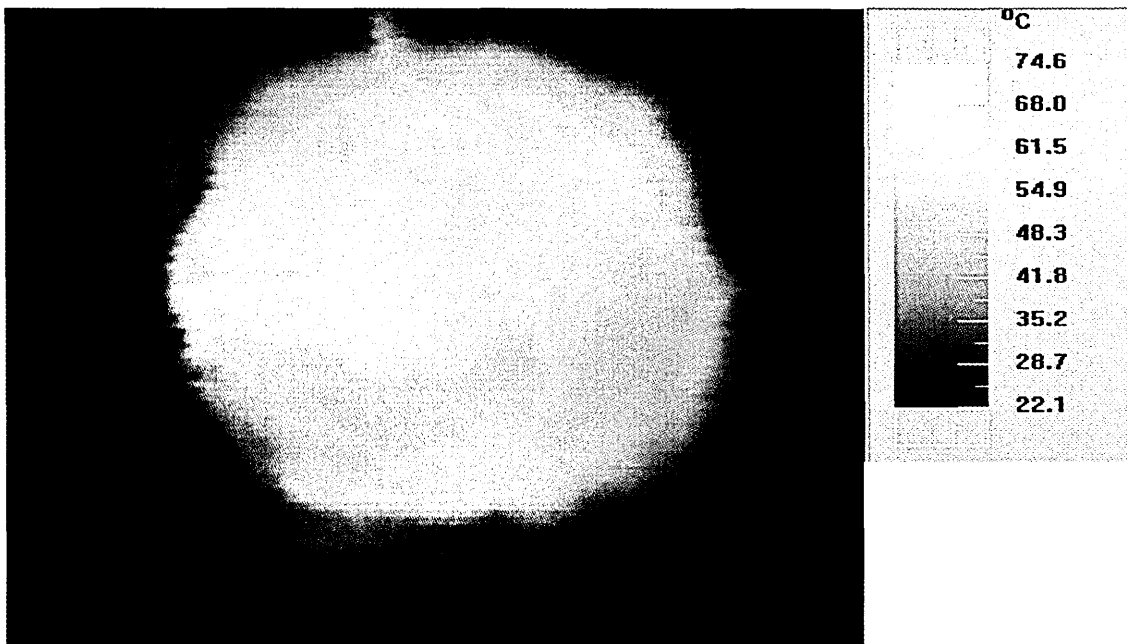


**Figure 4.9** IR-Thermogram of the surface of a hemispherical shaped glasswool layer ( $r = 8$  cm) with electric heater at 450 °C

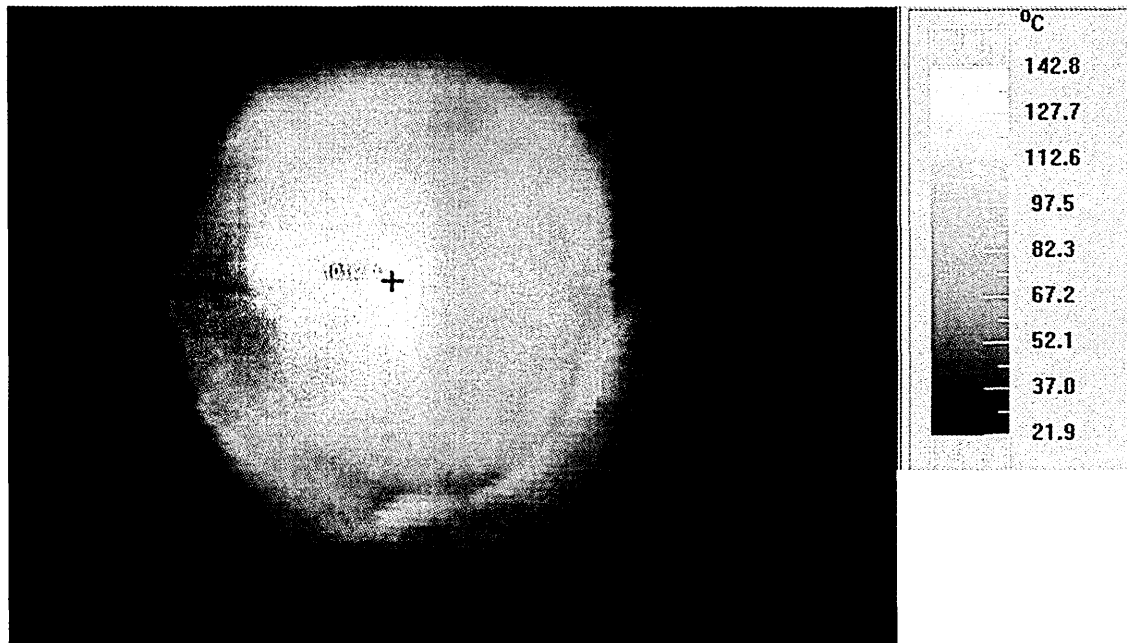


**Figure 4.10** IR-Thermogram of the surface of a hemispherical shaped glasswool layer ( $r = 8$  cm) with smouldering shavings at 450 °C

#### 4.4 The flow of hot combustion gases through a small-scale domestic refuse bed – Experiment 4

The results of Experiments 2 and 3, described in section 4.2 and 4.3, suggest that the surface temperature of a packed bed in which there is an embedded combustion source will not be significantly influenced by conduction, but much more by buoyancy induced convection from the hot combustion gases. To further confirm this belief, the fourth experiment was carried out in a small-scale domestic refuse bed with ammonia gas as the substitute for the gaseous combustion products.

The experimental results take the form of images, presented in **Figures 4.11 to 4.14**, obtained from the IR-Laser based gas visualisation system (GVS) described in section 3.5. In all experiments the ammonia gas exited the bed directly vertical above the gas inlet, irrespectively of depth or density of the individual beds, as given in Table 3.3. The GVS used was very sensitive and able to detect very small mass flow rates down to only 2 kg/year. It was thus able to confirm that no gas exited the bed other than vertically above the inlet and thus collateral gas diffusion was negligible.

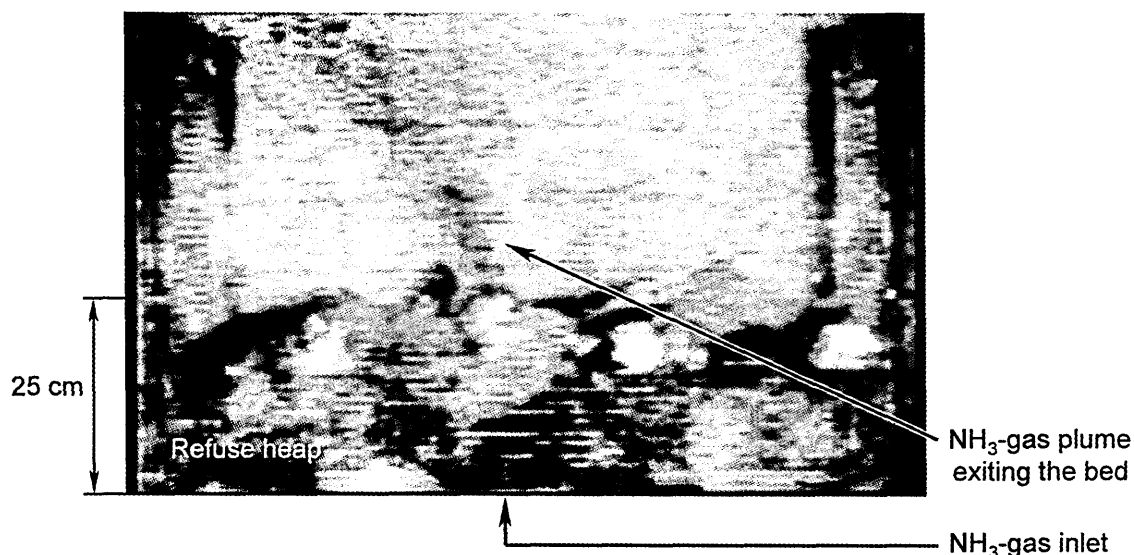


**Figure 4.11** Visualisation of  $\text{NH}_3$ -gas exiting a loosely filled ( $\rho \cong 79 \text{ kg/m}^3$ ) domestic refuse bed of 25 cm depth. The gas plume can be seen against the light background as it exits the bed directly above the gas inlet.

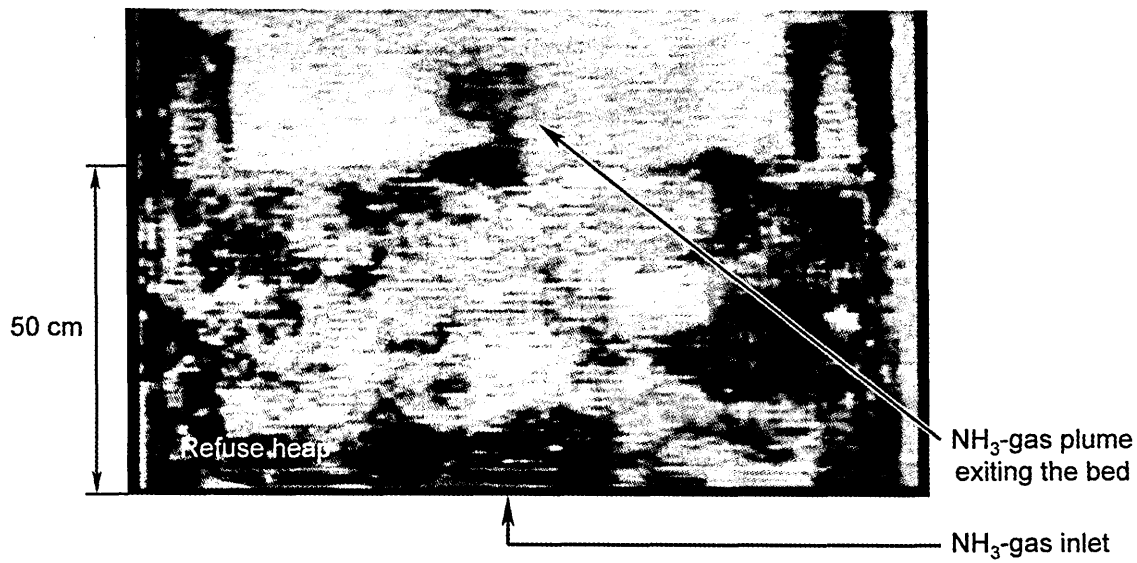


**Figure 4.12** Visualisation of NH<sub>3</sub>-gas exiting a loosely filled ( $\rho \cong 79 \text{ kg/m}^3$ ) domestic refuse bed of 50 cm depth

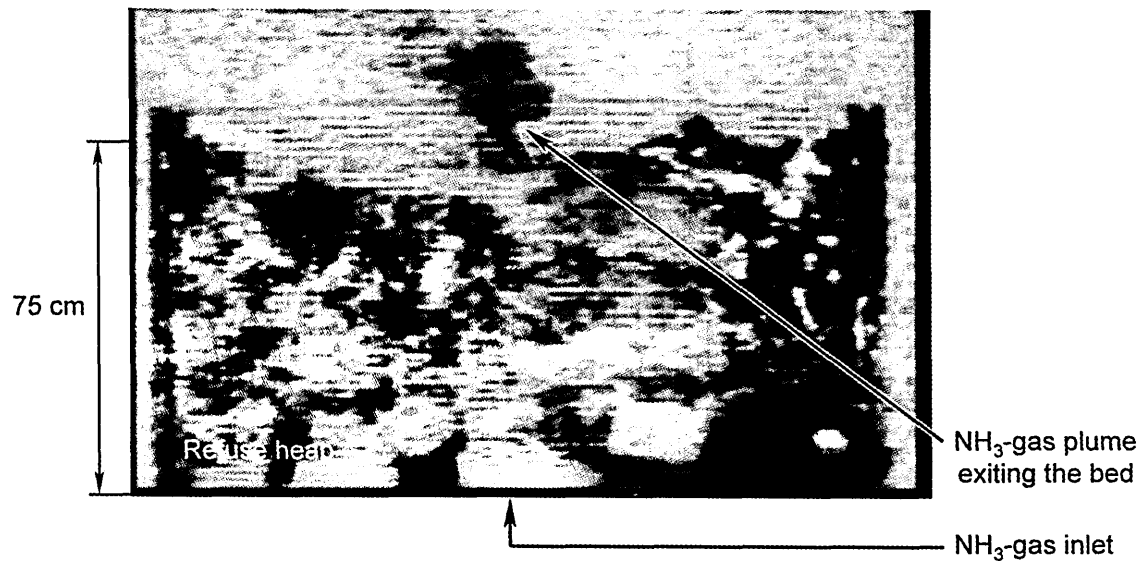


**Figure 4.13** Visualisation of NH<sub>3</sub>-gas exiting a loosely filled ( $\rho \cong 79 \text{ kg/m}^3$ ) domestic refuse bed of 75 cm depth

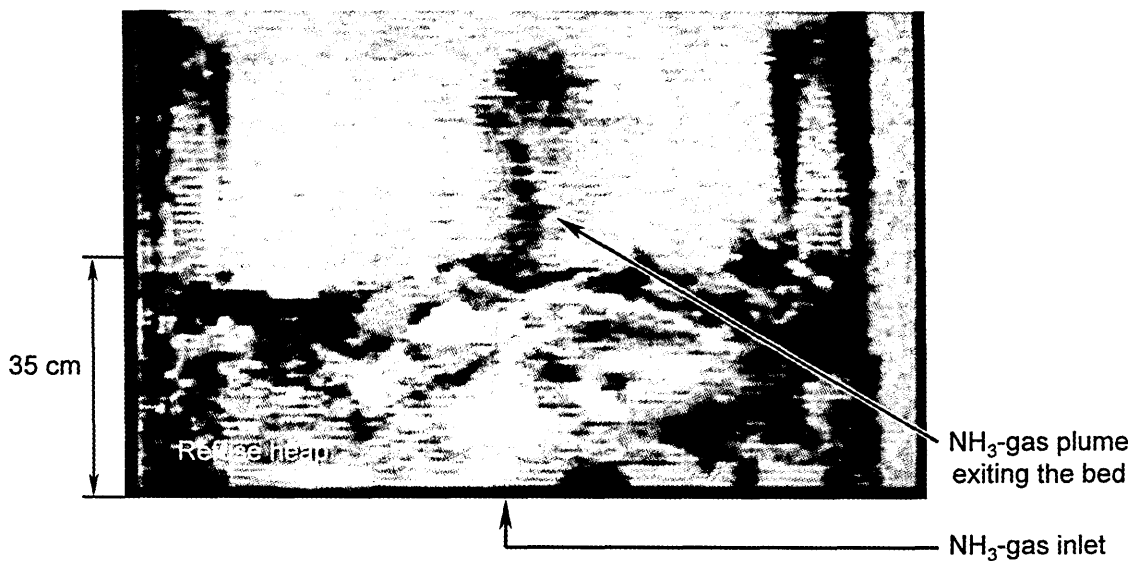


**Figure 4.14** Visualisation of  $\text{NH}_3$ -gas exiting a compressed ( $\rho \cong 169 \text{ kg/m}^3$ ) domestic refuse bed of 35 cm thickness

The results of these experiments further support the belief that the flow of a hot gas through a heterogeneous packed bed is induced and maintained by buoyancy, in clear contrast to the assertions made in the literature, see section 2.4.3. This flow behaviour can be compared to the up draught through a chimney stack and validates the initial assumption of the fluid flow made in section 3.5.

The experimentally observed minimal collateral gas diffusion can be explained as follows:

The pressure difference  $\Delta p$ , that is imposed by buoyancy, induces a mass flow.

Analogous to Ohms law, the mass flow rate is proportional to  $\Delta p$  and the reciprocal flow resistance  $R_c$  inside the individual flow channel.

$$\dot{m} \propto \frac{\Delta p}{R_c}$$

If all possible flow channels have equal cross-sectional area, their flow resistances are linearly proportional to their length  $L_c$ . With a constant pressure difference  $\Delta p$ , the mass flow rate through the individual channels then decreases hyperbolically with increasing length of the channels.

$$\dot{m} \propto \frac{\Delta p}{L_c}$$

If hot combustion gases instead of ammonia had been rising through the refuse bed, it must be supposed that the temperature increase over a certain surface area would be proportional to the mass flow rate density of the gas within this area. An increasing channel length would thus not only entail a lower mass flow rate but the hot gases would be cooled down more whilst flowing through the longer channel. The potential surface warming would thus in practice decrease even more than hyperbolically with increasing channel length. Hence, no significant hot spots would occur at the surface when the gas flows further aside from the ideal vertical way. A possible mass flow rate distribution at the surface of a packed bed is presented in **Figure 4.15**

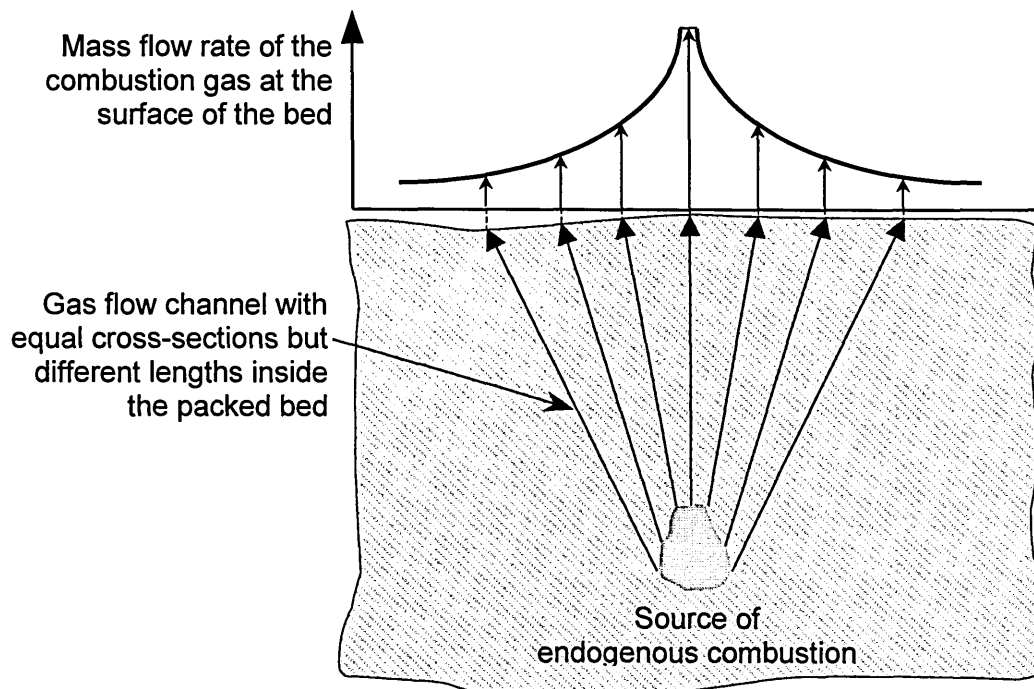


**Figure 4.15** Mass flow rate and temperature distribution at the surface of a packed bed subjected to an endogenous smouldering combustion depending on the flow of the combustion gas

It must be concluded from this experiment that if a hot spot is detected at the surface of a packed bed, the corresponding source of endogenous combustion must be almost vertically underneath.

#### 4.5 Large-scale experiment conducted in a 27 m<sup>3</sup> batch of domestic refuse – Experiment 5

All previous experiments had been, for good reason, on a small scale. To finally verify the previous observations, two experiments were conducted on a large-scale basis.

Firstly, a bed of domestic refuse inside a 30 m<sup>3</sup> container was observed, see section 3.6. **Figure 4.16** presents measured temperatures versus time inside the bed of refuse.

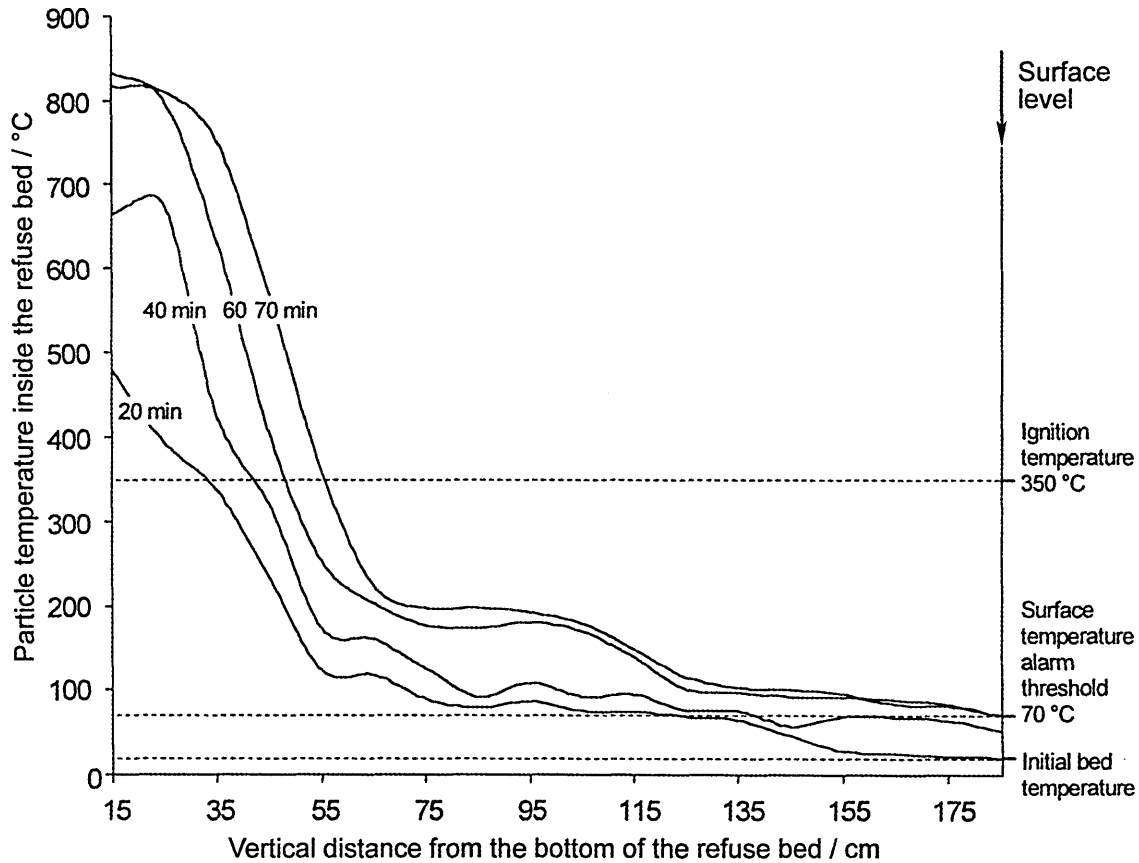


**Figure 4.16** Temperature distribution, measured by thermocouples, in time vertically above the self-preserving endogenous smouldering combustion at the bottom of the 27 m<sup>3</sup> domestic refuse bed

The refuse temperatures decreased rapidly up to 60 cm from the locally limited combustion source at the bottom of the bed. In the rest of the bed up to the surface, the temperature gradient is low, especially, in the layer between 65 cm and 105 cm at around 200 °C and in the layer between 135 cm and 185 cm at around 70 to 100 °C.

Naturally, the curves do not run smooth because the bed was very heterogeneous and the thermocouples were not equally exposed to the flowing combustion gas. With

increasing time, a higher temperature plateau and progress growth of the fire pocket was observed.

During the experiment, mist was emitted from the bed surface. This indicated condensation of the water vapour content of the combustion product gases. This would be expected to influence the temperature distribution in the upper layers of the bed and consequently the surface temperature distribution. The surface alarm temperature threshold of 70 °C was reached after 60 minutes.

In addition to the temperatures inside the bed, the surface temperature distribution was measured. A series of IR-Thermograms, showing the development of the surface temperature distribution with time, is presented in **Figure 4.17**. This clearly shows that the increase in surface temperature was locally limited to the area vertically above the combustion source. The collateral diffusion of the combustion product gases was so small that hot spots outside this area did not occur. The hot spot temperature was in the range of 65 °C to 85 °C from 40 to 70 minutes after first ignition. The fact that the temperature was in this range for such a long time also indicates the condensation of water vapour.

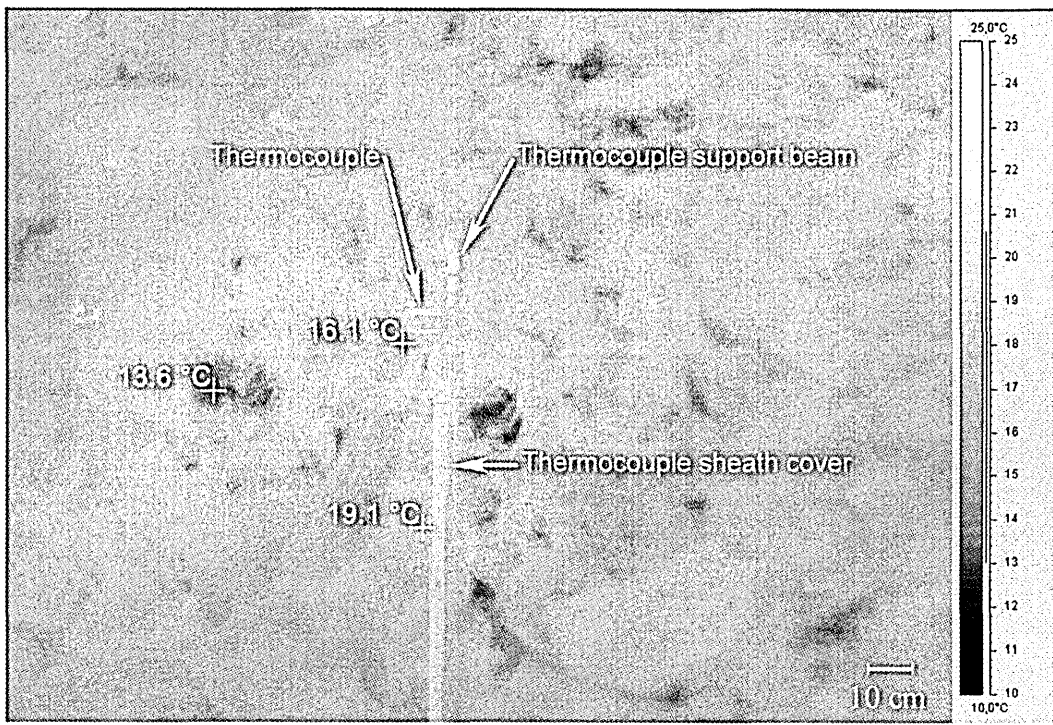


**Figure 4.17a** IR-Thermogram, spectral range 7.5 to 13  $\mu\text{m}$ , of the refuse surface, emissivity 0.95, 20 minutes after ignition

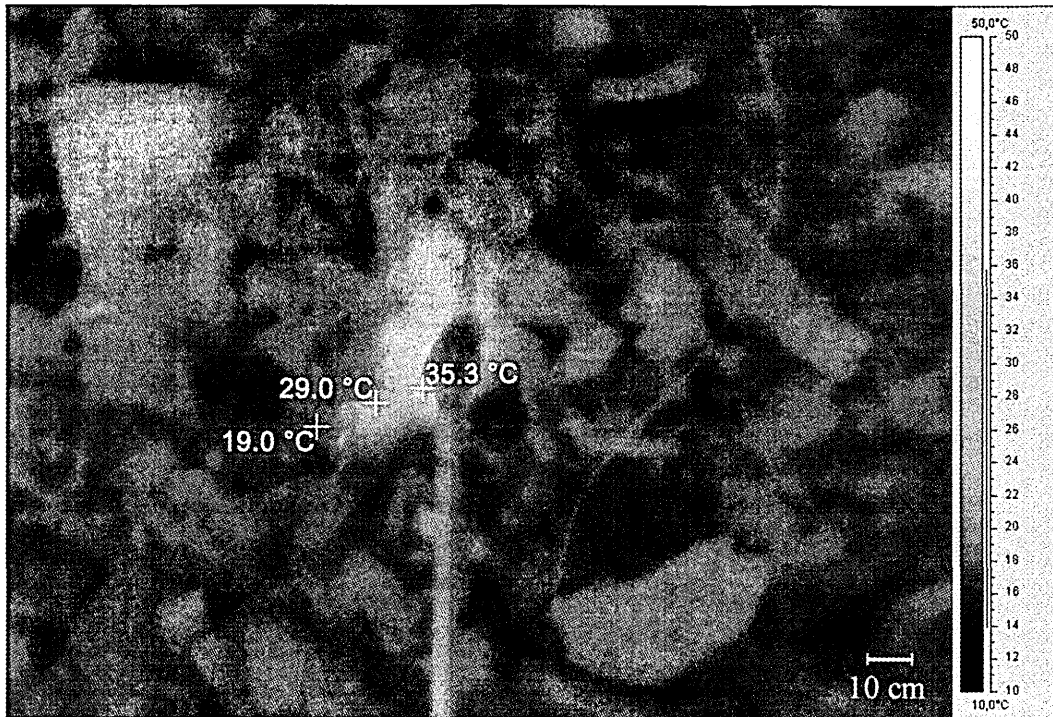


**Figure 4.17b** IR-Thermogram of the refuse surface 30 minutes after ignition

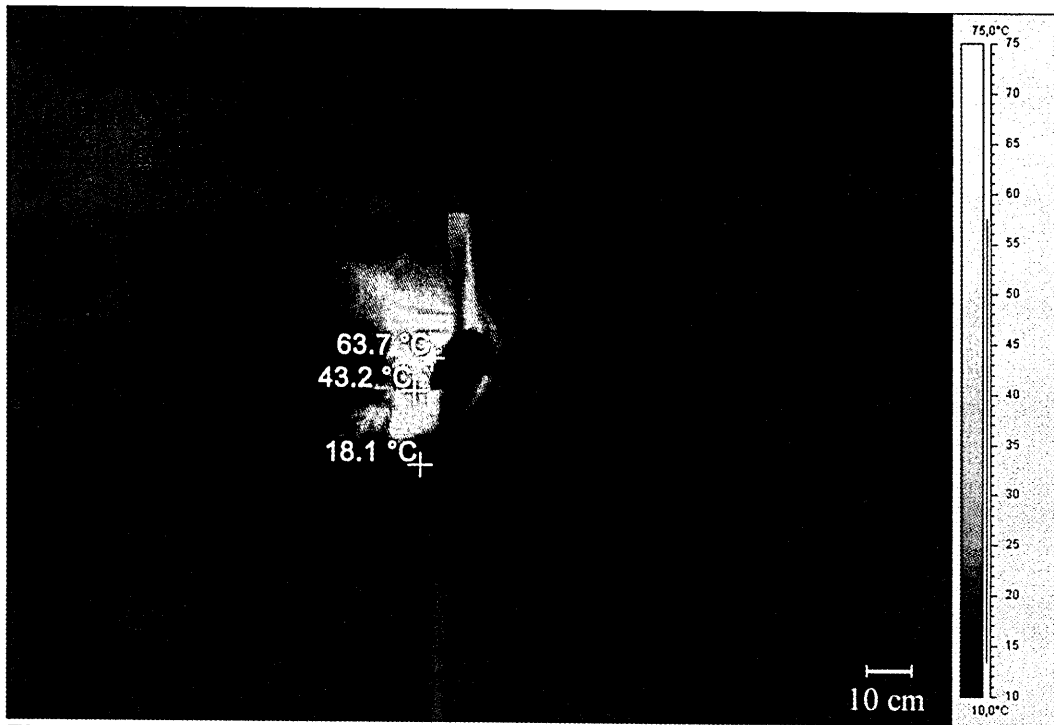


Figure 4.17c IR-Thermogram of the refuse surface 40 minutes after ignition

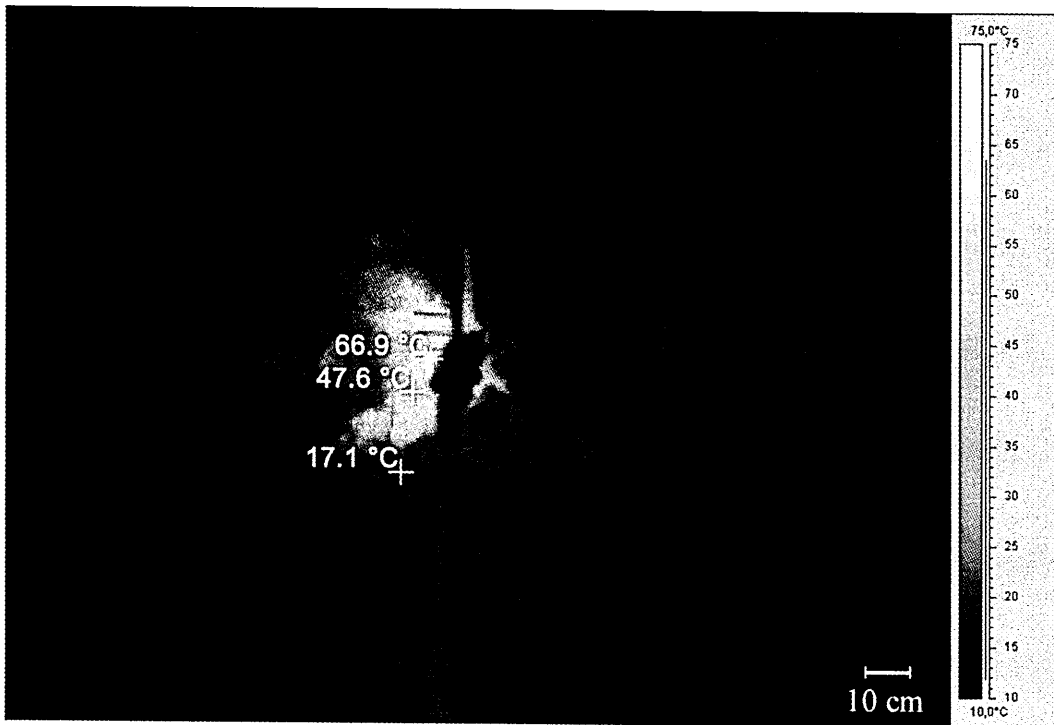
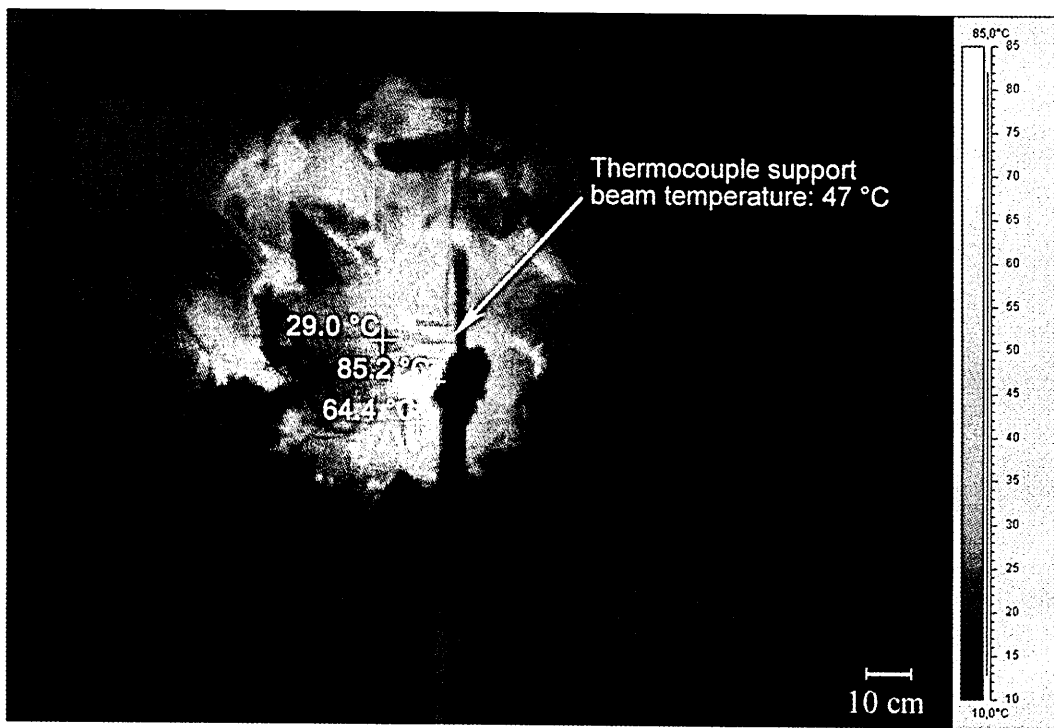
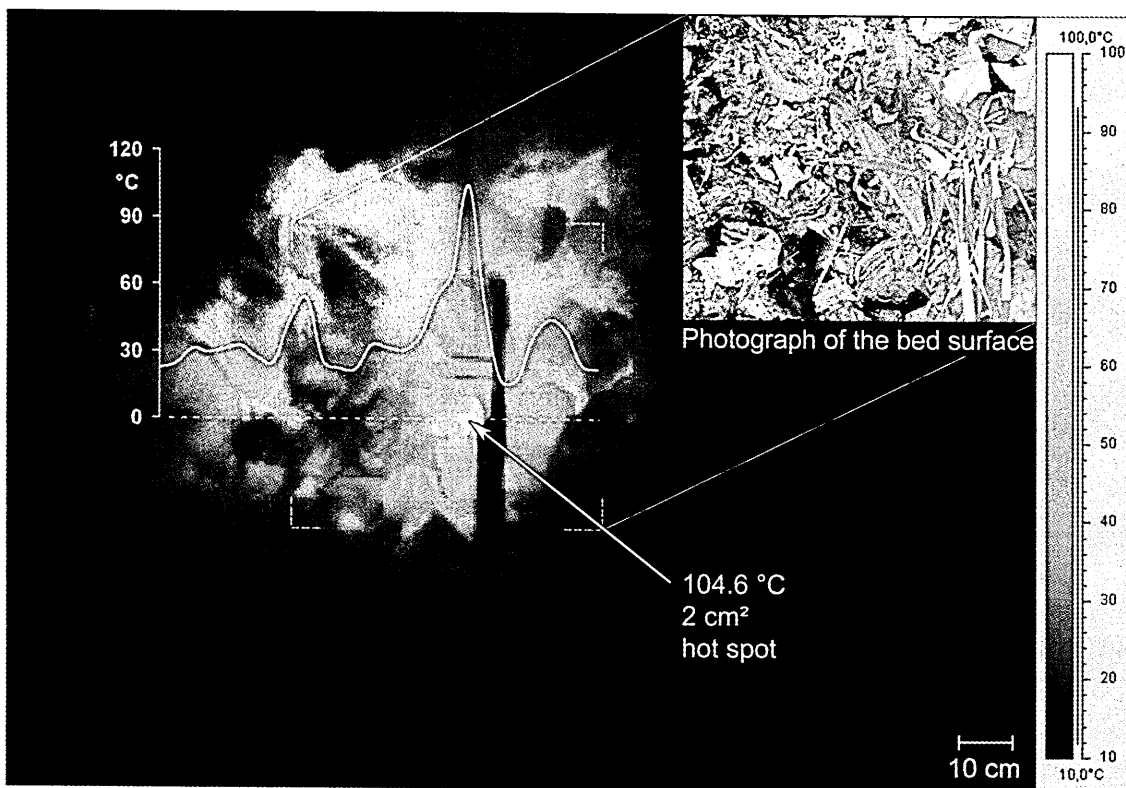


Figure 4.17d IR-Thermogram of the refuse surface 50 minutes after ignition



**Figure 4.17e** IR-Thermogram of the refuse surface 60 minutes after ignition



**Figure 4.18** IR-Thermogram, spectral range 7.5  $\mu\text{m}$  to 13  $\mu\text{m}$ , of the refuse surface, emissivity 0.95, 72 minutes after ignition, showing a single, very small hot spot at 104.6 °C

After 72 minutes, the experiment had to be aborted due to massive smoke emission. The last IR-Thermogram is presented in **Figure 4.18**. The surface temperature profile along the broken line indicates a primary hot spot, positioned vertically above the combustion source. Two additional peaks - locally very limited - can be observed that have lower maximum temperatures but equal high temperature gradients of more than 10 K/m away from them. This minor deviation from the ideal vertical gas flow is probably due to the heterogeneous nature of the bed. The highest mass flow rate through the channel apertures must have occurred at the primary hot spot with a lower mass flow through the collateral channels, as explained in the previous section. This again shows the strong influence of the length of the gas flow channels on the surface temperature increase.

#### 4.6 Intermediate-scale experiments using wood chips – Experiment 6

Since the previous experiment could not be conducted until flashover occurred, a final experiment had to be conducted in a bed of wood chips that could be combusted without generating harmful smoke. The experiment was conducted three times under identical conditions, producing similar results, which further supported the results obtained in the refuse experiment. The results of the three experiments are presented in **Figure 4.19** to **Figure 4.21**. The parameter, indicated on the curves, is the time after first ignition has been achieved.

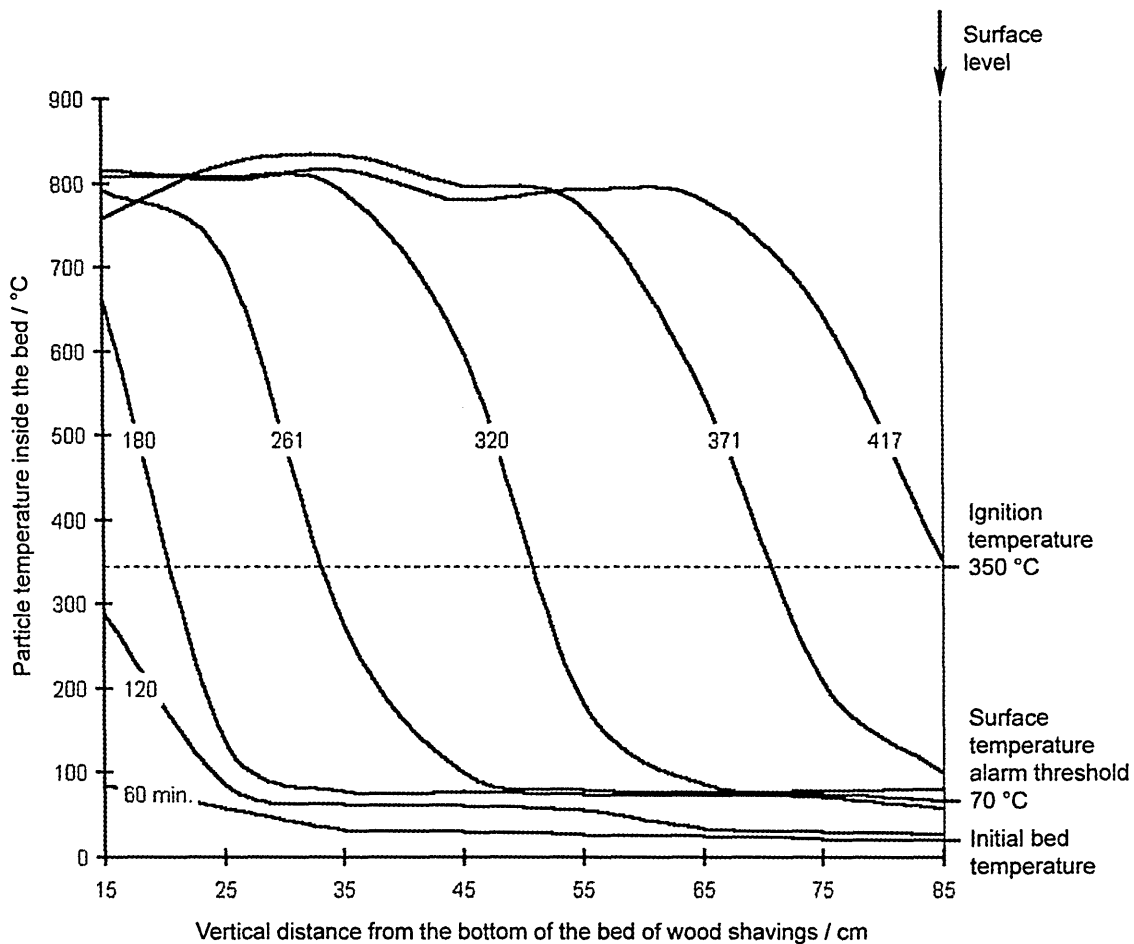


**Figure 4.19** Temperature distribution vertically above the self-propagating endogenous smouldering combustion source at the bottom of a 0.22 m<sup>3</sup> bed of wood particles. The parameter indicates the time after first ignition.

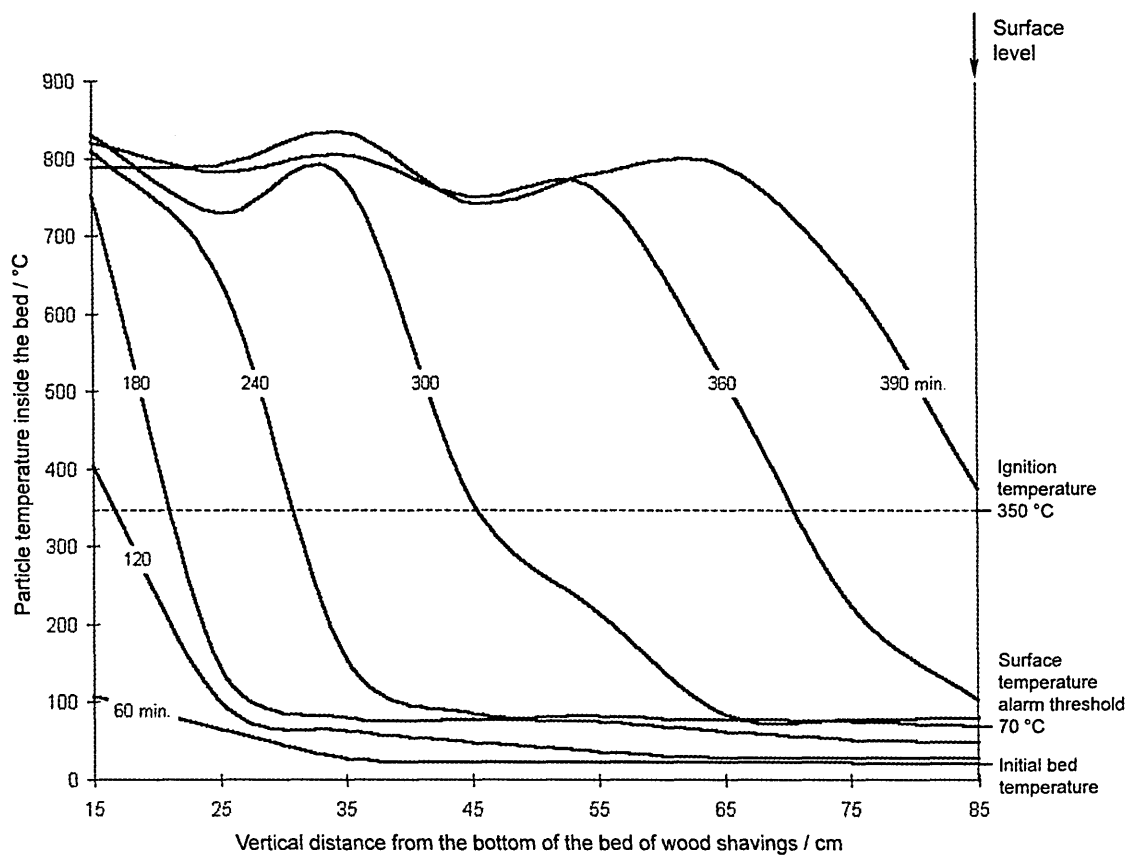


**Figure 4.20** Temperature distribution vertically above the self-propagating endogenous smouldering combustion source at the bottom of a 0.22 m<sup>3</sup> bed of wood particles

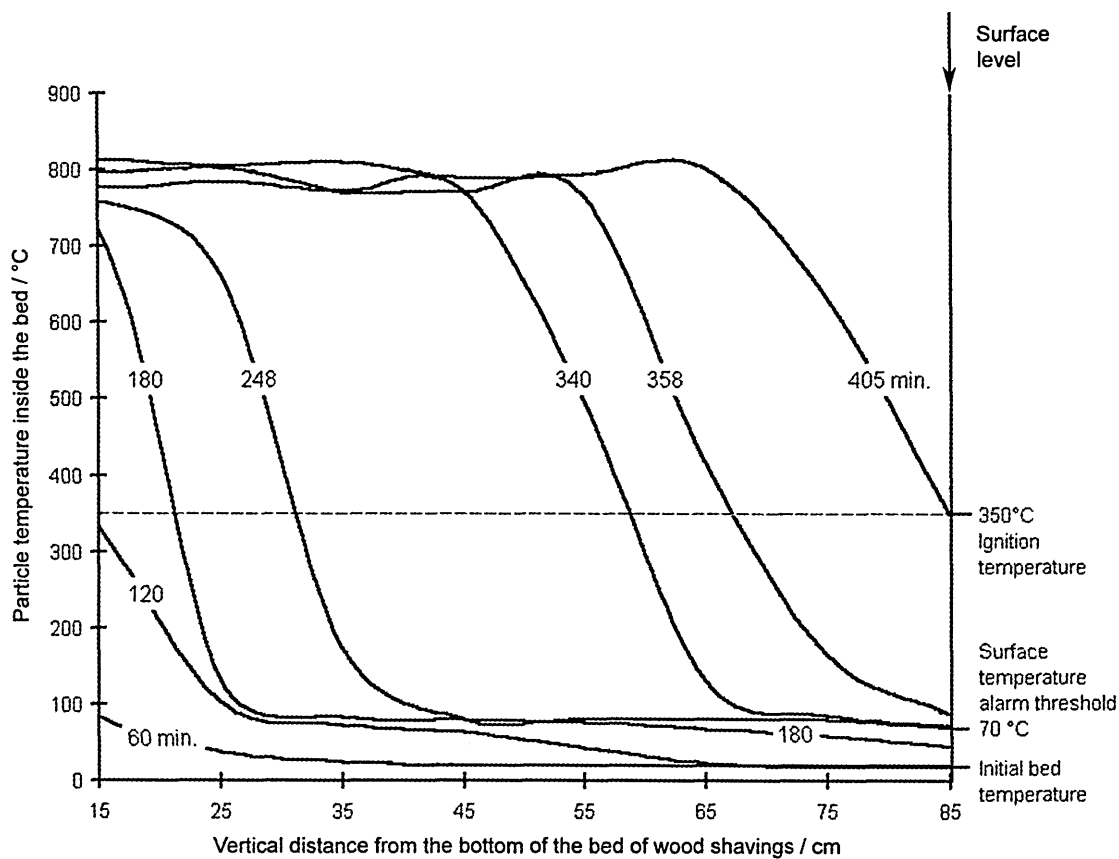


**Figure 4.21** Temperature distribution vertically above the self-propagating endogenous smouldering combustion source at the bottom of a 0.22 m<sup>3</sup> bed of wood particles

The temperature curves in Figure 4.19 to Figure 4.21 are smoother than those obtained from the refuse experiment and the plateau around 65 °C to 85 °C is even more prominent than from the results obtained in the refuse experiment. As the plateau is below 100 °C, it is believed that the plateau is due to the condensation of water vapour contained in the gaseous combustion products. The combustion products contain water which exits the gaseous state at devoted temperatures, depending on the partial pressure of the water vapour. As the combustion products cool below 85 °C the water component condenses, releasing heat of condensation. This is believed to have the effect of arresting the fall in temperature and producing a plateau in the temperature profile, which can in particular be observed on the 180 minutes curves in Figures 4.19 to 4.21. At this time the thermal effects of condensation produced a temperature level of 85 °C in the lower layers of the beds. In Figure 4.19 in the layer between 30 cm and 70 cm and in Figures 4.20 and 4.21 in the layers between 30 cm

and 55 cm. Within all these layers the bed temperature gradually changes in the range of what is believed to be the dew point temperature. Once the major part of the water vapour has condensed in the lower parts of the bed, the water vapour content and simultaneously the dew point temperature decreases and the temperature of the remaining gases and hence that of the solid can continue to fall as the surface is approached. The calculation and discussion of the dew point temperature will be done in detail in section 5.3.

As the combustion front propagates towards the surface, condensed moisture will re-vaporise, requiring heat of evaporation. The condensation zone is consequently moved progressively closer to the surface and with it the temperature plateau. This phenomenon thus has an important effect on the surface temperature of the bed and the attainment of the critical temperature of 70 °C for the IRT systems.

After 240 to 260 minutes, the condensation zones had reached the surface and there allowed the temperature to rise high enough for the IRT alarm temperature to be exceeded. The lower limit of the condensation zone also shifts towards the surface due to the re-evaporation inside the bottom layers of the bed. Not all the water vapour condensed inside the bed and the remaining vapour tended to condense on exiting the bed, leaving traces of mist – a further indicator of an endogenous combustion process below the surface of the bed. The condensing water vapour and a partly soaked wood chip at the surface of the bed is presented in **Figure 4.22**, showing that these effects at the surface are very localised.

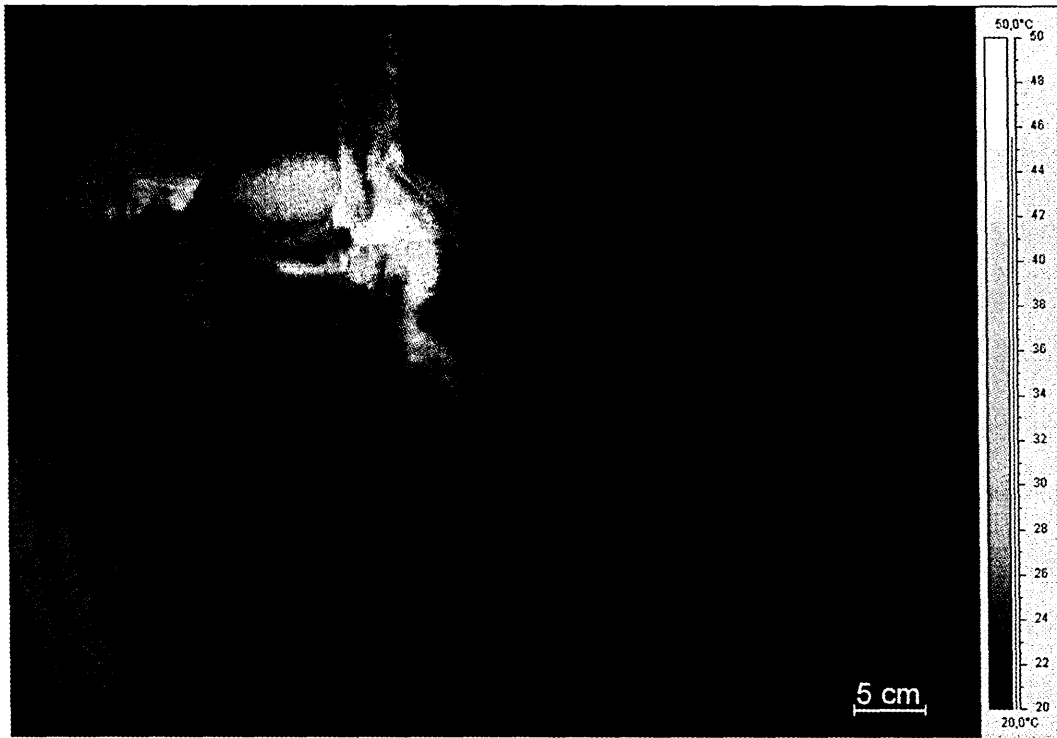


**Figure 4.22** Partly soaked particle and mist emission from the surface of the bed of wood chips

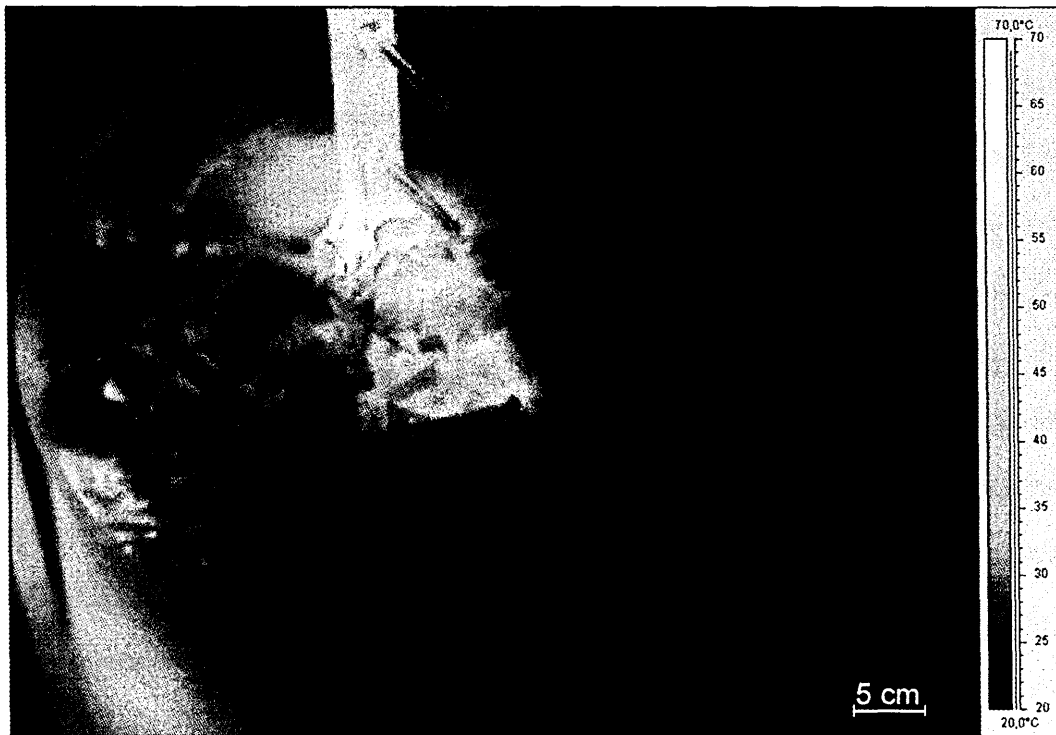
After 344 to 371 minutes, all points within the bed above the combustion source were above 100 °C and hence water only existed in the vapour phase. The restraining effects on the development of the temperature profile, caused by phase-changes involving water, were thus removed beyond this point in time. Heat transfer thus took place without phase-changes as though only a permanent gas was present. It could also be observed that beyond this point in time the mist emission ceased at the surface of the bed. The surface temperature then increased rapidly and after 390 to 417 minutes flashover took place, which had not been achieved during the refuse experiment.

As the combustion burnt away the wood chips in the bottom part of the beds, the wood chips levels inside the barrel decreased with time. In order to keep all eight thermocouples covered, wood chips were filled into the barrel during the conduction of the first experiment. Unfortunately, this resulted in IR-Thermograms that were not representative because the additional wood chips, repetitively added to the surface of the bed, had ambient temperature and did thus cover the warm bed surface with a cooler layer. During the second and third experiment, wood chips were not added and thus the surface level of the bed decreased in time. This can be observed from the

series of IR-Thermograms from the second and third experiment presented in **Figure 4.23** and **Figure 4.24**, respectively, together with the development of the temperature distribution at the surface of the beds.



**Figure 4.23a** IR-Thermogram, spectral range 7.5  $\mu\text{m}$  to 13  $\mu\text{m}$ , of the wood particle surface, emissivity 0.95, 120 minutes after ignition at the bottom. This series of IR-Thermogram was taken during the second experiment.



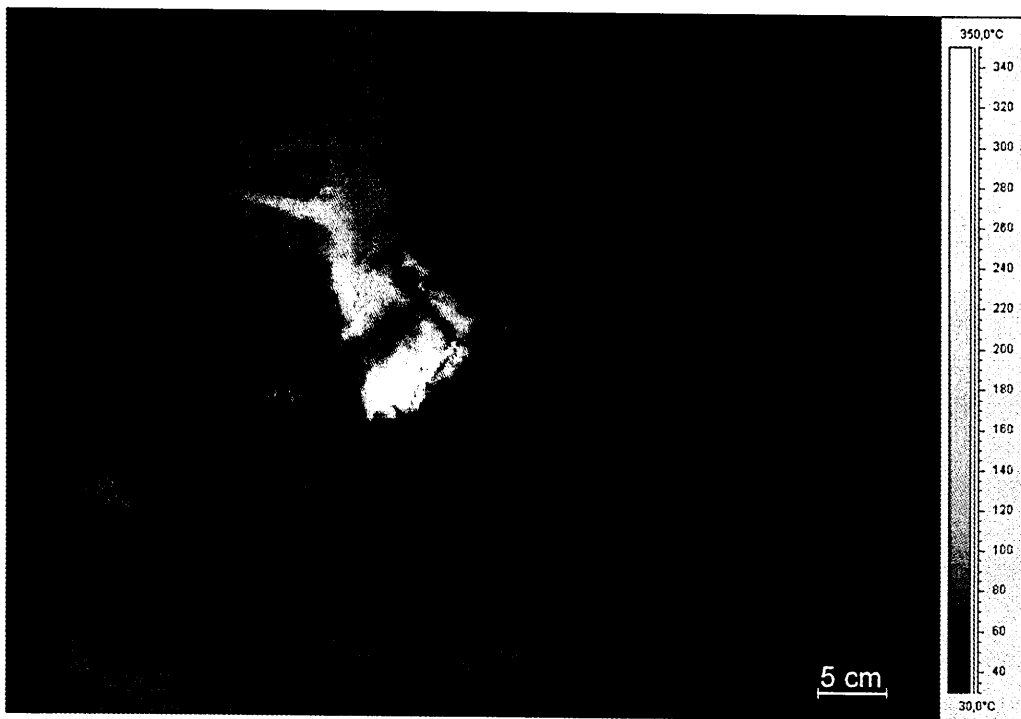
**Figure 4.23b** IR-Thermogram of the wood particle surface 180 minutes after ignition



Figure 4.23c IR-Thermogram of the wood particle surface 240 minutes after ignition



Figure 4.23d IR-Thermogram of the wood particle surface 300 minutes after ignition



**Figure 4.23e** IR-Thermogram of the wood particle surface 360 minutes after ignition



**Figure 4.23f** IR-Thermogram of the wood particle surface 390 minutes after ignition. This was the moment when the flashover took place.

A series of IR-Thermograms of the third experiment is presented in **Figure 4.24**. The same time steps have been used as for the previous series.

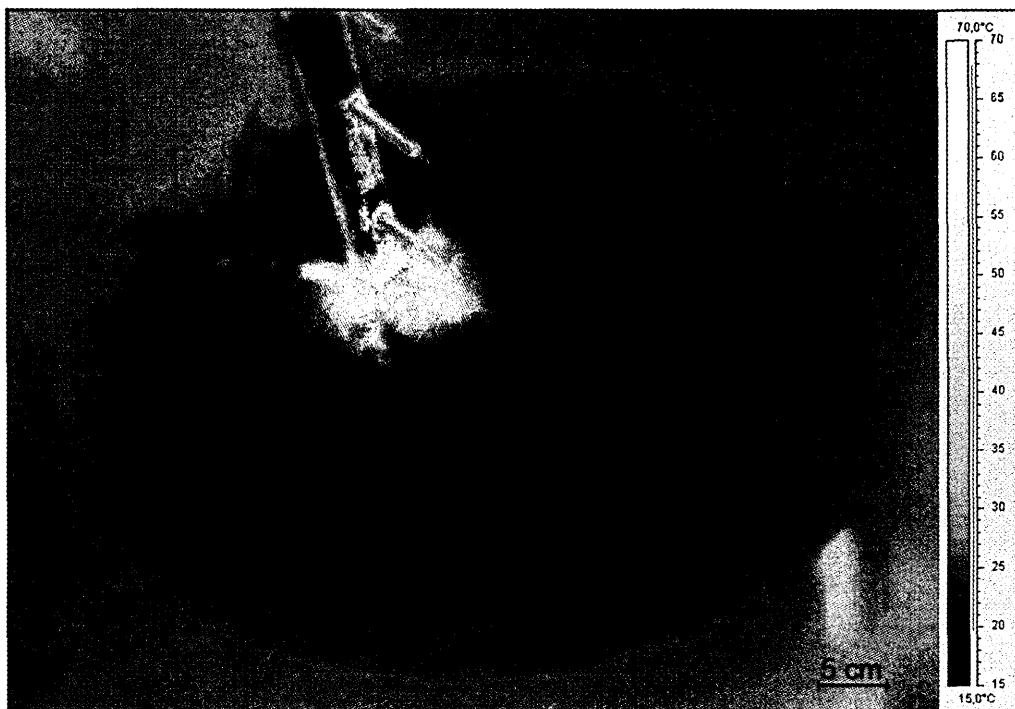


**Figure 4.24a** IR-Thermogram, spectral range  $7.5\ \mu\text{m}$  to  $13\ \mu\text{m}$ , of the wood particle surface, emissivity 0.95, 120 minutes after ignition at the bottom. This series of IR-Thermogram was taken during the third experiment.



**Figure 4.24b** IR-Thermogram of the wood particle surface 180 minutes after ignition



Figure 4.24c IR-Thermogram of the wood particle surface 240 minutes after ignition

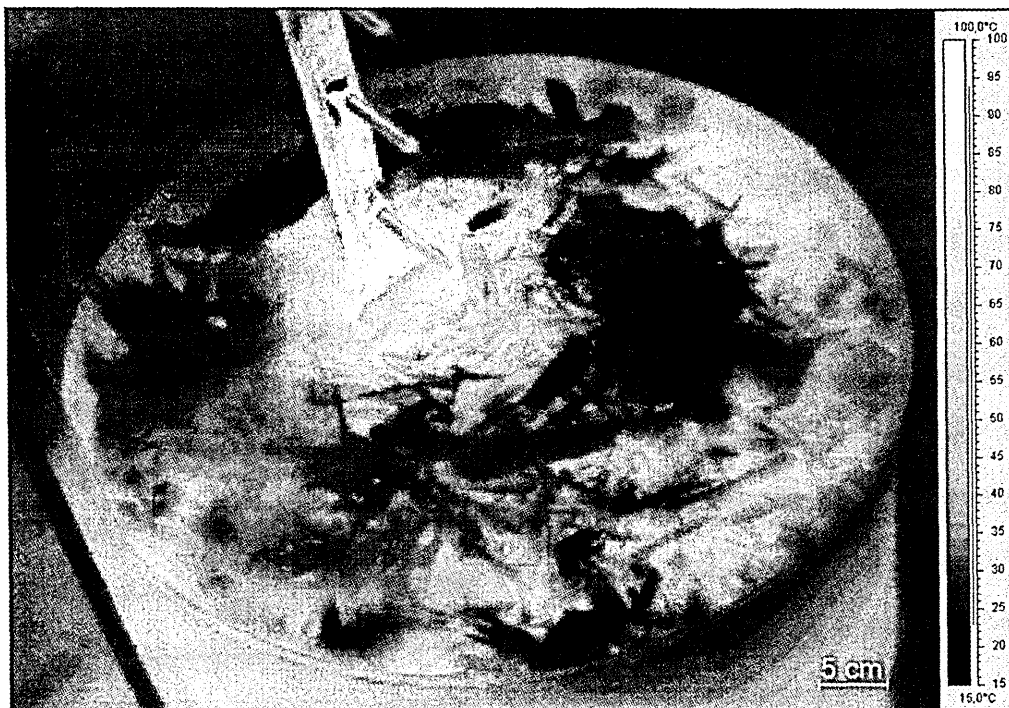


Figure 4.24d IR-Thermogram of the wood particle surface 300 minutes after ignition



**Figure 4.24e** IR-Thermogram of the wood particle surface 360 minutes after ignition

Both series of IR-Thermograms, presented in Figure 4.23 and Figure 4.24, suggest that the surface temperature distribution of both beds is affected 120 minutes after ignition at the bottom of the bed was achieved. It can also be observed that the outer radial zones of the bed are affected by heat transfer as well. This is due to the distortion of the void fraction distribution near to the boundaries of the beds, as explained in section 2.4.2.1.

Nevertheless, the developments of the surface temperature distributions were not uniform and the highest temperatures could always be observed vertically above the combustion source, suggesting that the main heat transfer took place by buoyancy forced convection of the gaseous combustion products.

The series of IR-Thermograms also show that there was a restraining effect by condensation and re-evaporation on the development of the surface temperatures which becomes apparent from **Figure 4.25** as well, which shows the measured maximum surface temperature of the wood particles bed versus time of the third

experiment. A similar result was also obtained from the second experiment. From 200 minutes to 355 minutes after ignition, the phase-changes kept the surface temperature within the range of 65 °C to 85 °C and thus in the range of the 70 °C IRT alarm threshold. 55 minutes before flashover, the zone of water condensation/evaporation had moved through the bed and from this time on, the surface temperature increased rapidly until flashover took place.

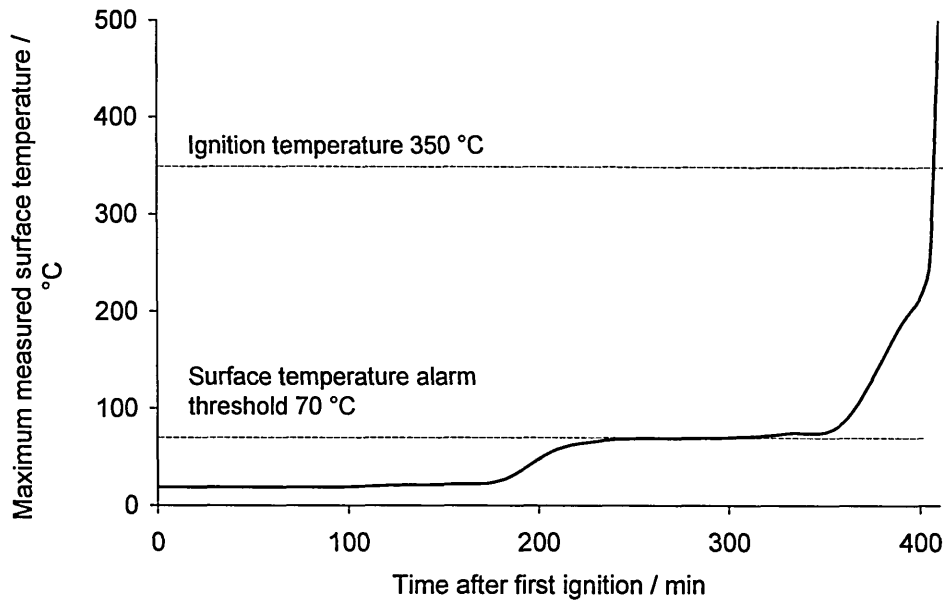


**Figure 4.25** Maximum measured surface temperature of the bed versus time. Condensation and re-evaporation keep the surface temperature in the range of 65 °C to 85 °C from 200 to 355 minutes. Beyond the point the bed becomes dried, the temperature increases rapidly and the flashover occurs at 410 minutes.

The rapid temperature increase at the surface as the point of flashover approached can be seen in the series of IR-Thermograms taken during the last ten minutes of the third experiment, presented in **Figure 4.26**. The size of the hot spot does not appear to significantly increase until the flashover took place.



**Figure 4.26a** IR-Thermogram, spectral range  $7.5 \mu\text{m}$  to  $13 \mu\text{m}$ , of the wood particle surface, emissivity 0.95, 400 minutes after ignition at the bottom. This series of IR-Thermograms was taken during the third experiment.



**Figure 4.26b** IR-Thermogram of the wood particle surface 405 minutes after ignition

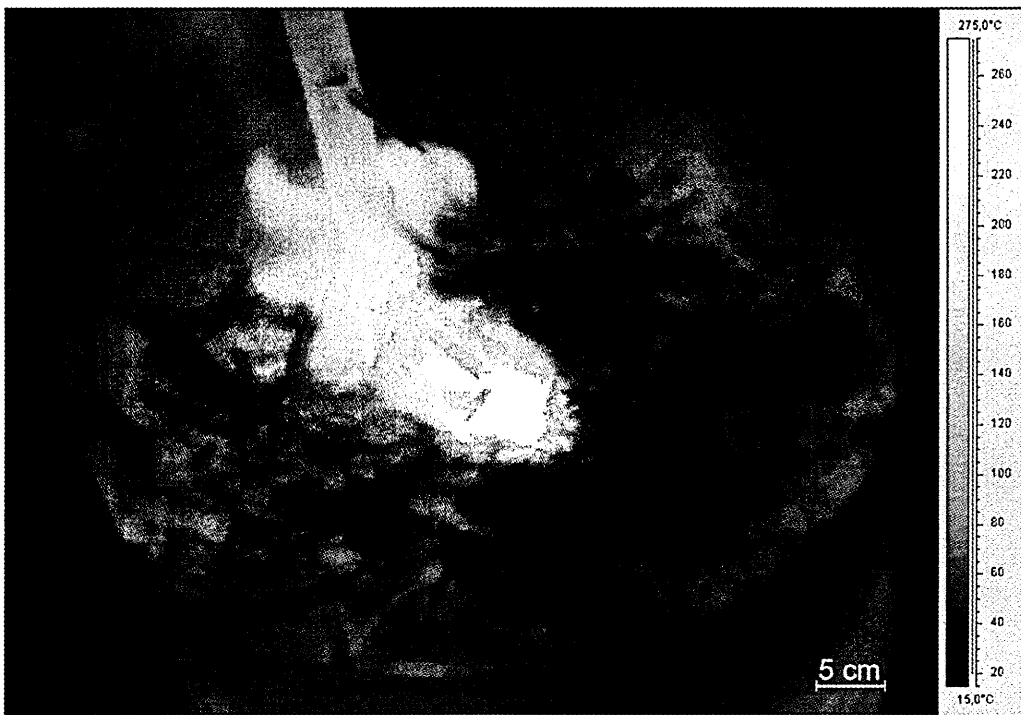


**Figure 4.26c** IR-Thermogram of the wood particle surface 410 minutes after ignition. At this time the flashover at the surface has already taken place.

**Figure 4.27** presents an IR-Thermogram of the third experiment, taken 390 minutes after ignition, i.e. 20 minutes before flashover. From this, a 0.5 cm<sup>2</sup> hot spot at 186.5 °C is evident directly above the smouldering combustion. The indicated temperature profile exhibits that the hot spot is very small with steep temperature gradients away from it. It also indicates that the temperature level of the surface has already exceeded ambient temperature and was in a range of 45 °C to 75 °C where no hot spots appeared. The secondary peaks on the temperature profile suggest minimal collateral gas diffusion. The very small primary hot spot and its appearance vertically above the endogenous source of combustion further support the results obtained from the refuse experiment. A similar result could also be obtained from the hot spot in the IR-Thermogram presented in **Figure 4.23e** which was taken 30 minutes before flashover.

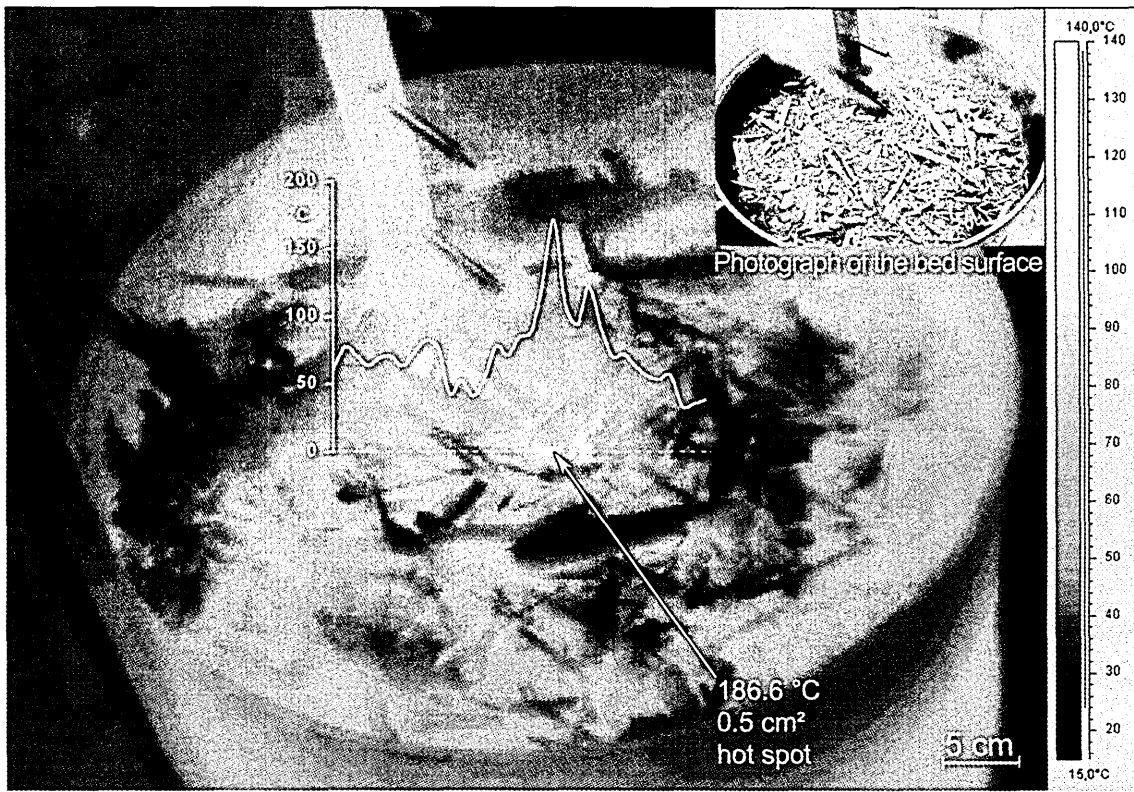


**Figure 4.27** IR-Thermogram, spectral range 7.5  $\mu\text{m}$  to 13  $\mu\text{m}$ , of the wood particles surface, emissivity 0.95, 390 minutes after ignition. The thermogram shows a single, very small hot spot and the temperature profile along the dotted line shows surface temperature gradients of more than 10 K/cm.

## 5 DISCUSSION

### 5.1 Experimental procedures

Two main problems had to be overcome in designing the experimental procedures:

1. The primary sets of laboratory experiments had to be chosen not to be conducted in domestic refuse beds for safety reasons, hence either
  - a) the refuse had to be substituted by wooden particles when the experiments involved combustion or
  - b) the combustion product gases had to be substituted when refuse was used as the bed material.
2. When the large bed of refuse and the smaller beds of wood particles were combusted, the correct measurement of the temperature distribution inside and at the surface of these beds was problematic.

#### 5.1.1 The substitution of domestic refuse and combustion gases

The results obtained from Experiment 2, sections 3.3 and 4.2, suggested that heat transfer in packed beds subjected to only an endogenous heat source is much less effective compared to the heat transfer in such beds involving an endogenous source of combustion. Along with the higher temperatures that occur when combustion is involved, the main contribution to the more effective heat transfer must be attributed to convection arising from combustion product gases.

In Experiment 4, described in section 3.5, the buoyancy driven flow of hot gaseous combustion products through a bed consisting of domestic refuse was investigated. Since the buoyancy induced pressure difference of a gaseous component rising through a packed bed only depends on density differences and not on temperatures, the experiment was conducted using ammonia gas at ambient temperature as a substitute for the hot combustion product gases. In a first approach the combustion gas was treated as air that enters the bed at 450 °C and leaves the bed at 20 °C. The

density value of air at the arithmetic mean temperature of 235 °C was 0.69 kg/m<sup>3</sup> [57] and the ammonia gas had a density of 0.71 kg/m<sup>3</sup> [57] at ambient temperature.

In order to validate the use of ammonia gas as a substitute for combustion product gases, the individual buoyancy induced draught pressure differences  $\Delta p$  must be determined. Applying ARCHIMEDES' law,  $\Delta p = (\rho_{amb} - \rho_{Fluid}) g H$ , the ratio of the buoyancy induced draught pressure differences of two different fluids can be obtained. Comparing hot air with ammonia gas at ambient temperature, flowing under otherwise identical conditions, i.e. equal densities of the ambient air  $\rho_{amb}$ , and equal height  $H$ , the ratio is given by

$$\frac{\Delta p_{NH_3}}{\Delta p_{air}} = \frac{(\rho_{amb} - \rho_{NH_3})}{(\rho_{amb} - \rho_{air})}$$

Employing  $\rho_{amb} = 1.188 \text{ kg/m}^3$ ,  $\rho_{NH_3} = 0.71 \text{ kg/m}^3$  and  $\rho_{air} = 0.69 \text{ kg/m}^3$ , the ratio of the buoyancy induced draught pressure differences of ammonia gas and hot air is 0.94.

The buoyancy induced draught pressure differences of ammonia gas was 6% lower than that of the combustion gas/air. During an actual combustion process, the combustion gas would thus even more tend to flow vertically upwards than the ammonia gas during the experiment. In addition, the combustion gas will exit the bed with increasing temperature as time goes by, which is clearly shown by the results of the wood chips experiment as described in section 4.6. Thus,  $\Delta p$  will increase with time for combustion in a refuse bed, whereas  $\Delta p$  of the ammonia gas during the experiment was constant. By this, the use of ammonia gas as a substitute for the hot combustion product gases could be justified because, if the buoyancy effects occurred using ammonia gas, they certainly occur with hot combustion gases.

In order to compare the mass flow rates of ammonia gas and combustion gas/air when flowing through a packed bed under similar conditions, the buoyancy induced draught

pressure difference must be further investigated. The buoyancy is entirely used to overcome all pressure losses during the flow, which can initially be derived from the first law of thermodynamics for the steady-state flow of a fluid through an open system between condition 1 and condition 2:

$$q_{12} + w_{t12} = h_2 - h_1 + \frac{1}{2}(C_2^2 - C_1^2) + g(z_2 - z_1) \quad (5.1)$$

Therein  $q_{12}$  is the heat transfer into or away from the system,  $w_{t12}$  is the technical work applied to or leaving the system,  $h$  is the mass specific enthalpy,  $C$  the fluid velocity and  $z$  the geodetic height.

Combining the first and second law of thermodynamics, changes in mass specific entropy  $s$  can be related to the heat energy and the dissipation energy  $j$ . The following equation applies to a process for a one-component system in which a fluid flow is assumed to take place between condition 1 and condition 2.

$$\int_1^2 T ds = q_{12} + j_{12} = h_2 - h_1 - \int_1^2 v dp \quad (5.2)$$

Inserting (5.1) in (5.2) gives

$$w_{t12} = \int_1^2 v dp + \frac{1}{2}(C_2^2 - C_1^2) + g(z_2 - z_1) + j_{12} \quad (5.3)$$

and after integration

$$w_{t12} = \frac{1}{\rho_{Fluid}}(p_2 - p_1) + \frac{1}{2}(C_2^2 - C_1^2) + g(z_2 - z_1) + j_{12} \quad (5.4)$$

Assuming  $w_{t12} = 0$ , Eqn. (5.4) can be written in the form of the BERNOULLI equation with friction losses

$$\frac{p_1}{\rho_{Fluid}} + \frac{1}{2}C_1^2 + gz_1 = \frac{p_2}{\rho_{Fluid}} + \frac{1}{2}C_2^2 + gz_2 + j_{12}. \quad (5.5)$$

Figure 5.1 shows a fluid flow between the conditions "0" and "amb", representing a buoyancy induced fluid flow through a packed bed based on the assumption that the fluid flows through a virtual stack inside the packed bed.

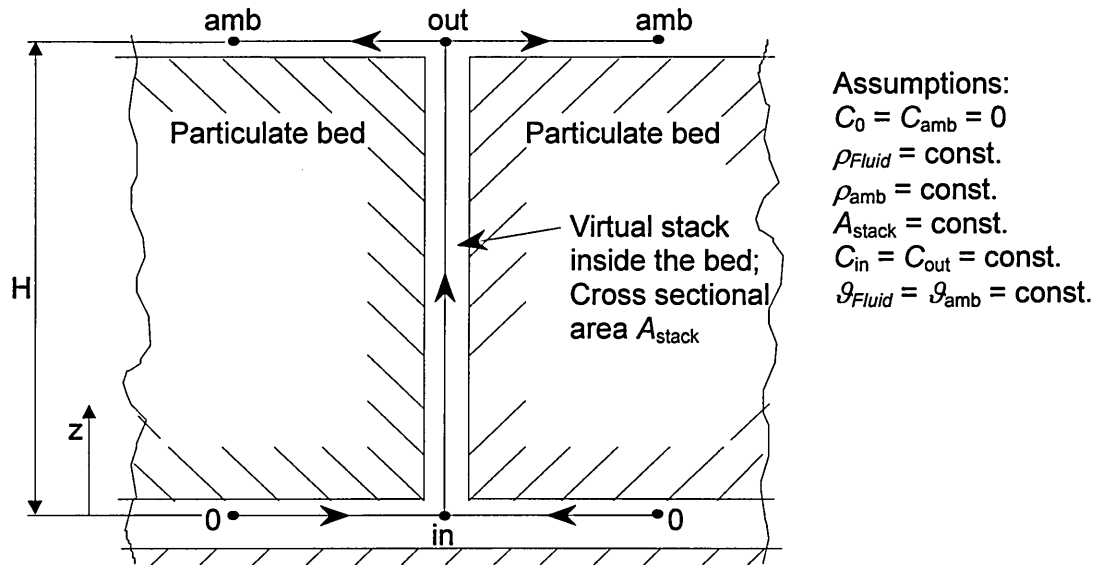


Figure 5.1 Assumed buoyancy induced fluid flow through a particulate bed, starting at "0" and ending at "amb".  
 The gas is assumed to flow with constant properties through a virtual stack inside the particulate bed.

Based on Figure 5.1, Eqn. (5.5) from "0" to "amb" gives

$$\frac{p_0}{\rho_{Fluid}} + \frac{1}{2}C_0^2 + gz_0 = \frac{p_{amb}}{\rho_{Fluid}} + \frac{1}{2}C_{amb}^2 + gz_{amb} + j_{0-amb} \cdot \quad (5.6)$$

The pressure at  $z = 0$  is given by

$$p_0 = p_{amb} + \rho_{amb} g H \quad (5.7)$$

and consideration of the above assumptions, (5.7) can be written as

$$\frac{p_{amb}}{\rho_{Fluid}} + \frac{\rho_{amb}}{\rho_{Fluid}} g H = \frac{p_{amb}}{\rho_{Fluid}} + g H + j_{0-amb}$$

$$(\rho_{amb} - \rho_{Fluid}) g H = \rho_{Fluid} j_{0-amb} \quad (5.8)$$

The first term of Eqn. (5.8) is the buoyancy induced pressure difference and the second term represents the pressure losses due to friction between condition "0" and "amb".

Thus, the entire pressure difference is used to overcome the friction losses, which is valid for all buoyancy induced stack flows. The friction losses can also be described in the form of

$$\rho_{Fluid} j_{0-amb} = \rho_{Fluid} \sum j = \frac{\rho_{Fluid}}{2} \left( \bar{C}_{0-in}^2 \zeta_{0-in} + \bar{C}_{in-out}^2 \zeta_{in-out} + \bar{C}_{out-amb}^2 \zeta_{out-amb} \right),$$

wherein  $\bar{C}_{x-y}$  is the average fluid flow velocity between the individual conditions "x" and "y" on the way of the fluid from "0" to "amb".  $\zeta$  denotes the velocity independent friction loss parameter.

Assuming that the flow starts at "0" with  $C_0 = 0$  and ends at "amb" with  $C_{amb} = 0$  and further assumption of linear fluid acceleration from "0" to "in" and from "out" to "amb", it follows that

$$\bar{C}_{0-in} = \frac{1}{2}(C_0 + C_{in}) = \frac{1}{2}C_{in},$$

analogously

$$\bar{C}_{out-amb} = \frac{1}{2}(C_{out} + C_{amb}) = \frac{1}{2}C_{out} = \frac{1}{2}C_{in}$$

and finally

$$\rho_{Fluid} j_{0-amb} = \rho_{Fluid} \sum j = \frac{\rho_{Fluid}}{2} C_{in}^2 \left( \frac{1}{4} \zeta_{0-in} + \zeta_{in-out} + \frac{1}{4} \zeta_{out-amb} \right). \quad (5.9)$$

Combining (5.8) and (5.9) gives

$$(\rho_{amb} - \rho_{Fluid}) g H = \frac{\rho_{Fluid}}{2} C_{in}^2 \left( \frac{1}{4} \zeta_{0-in} + \zeta_{in-out} + \frac{1}{4} \zeta_{out-amb} \right). \quad (5.10)$$

The mass flow rate then can be derived using

$$C_{in} = \sqrt{\frac{(\rho_{amb} - \rho_{Fluid}) g H}{\frac{\rho_{Fluid}}{2} \left( \frac{1}{4} \zeta_{0-in} + \zeta_{in-out} + \frac{1}{4} \zeta_{out-amb} \right)}} \quad (5.11)$$

and

$$\dot{m}_{Fluid} = C_{in} \rho_{Fluid} A_{stack},$$

that gives

$$\dot{m}_{in} = \sqrt{\frac{(\rho_{amb} - \rho_{Fluid}) g H}{\frac{\rho_{Fluid}}{2} \left( \frac{1}{4} \zeta_{0-in} + \zeta_{in-out} + \frac{1}{4} \zeta_{out-amb} \right)}} \rho_{Fluid} A_{stack} \quad (5.12)$$

This shows that the mass flow rate through a stack is entirely controlled by buoyancy and friction losses. Using Eqn. (5.12), the ratio of the mass flow rates of the combustion gas/air and ammonia gas can be obtained. When flowing under otherwise equal conditions, the mass flow ratio of the ammonia gas and the combustion gas is given by

$$\frac{\dot{m}_{in_{NH_3}}}{\dot{m}_{in_{air}}} = \frac{\sqrt{\frac{(\rho_{amb} - \rho_{NH_3})}{\rho_{NH_3}} \rho_{NH_3}}}{\sqrt{\frac{(\rho_{amb} - \rho_{air})}{\rho_{air}} \rho_{air}}}$$

Employing  $\rho_{amb} = 1.188 \text{ kg/m}^3$ ,  $\rho_{NH_3} = 0.71 \text{ kg/m}^3$  and  $\rho_{air} = 0.69 \text{ kg/m}^3$ , the ratio of the mass flow rates of ammonia gas and combustion gas/air is 0.99. The ratios of both, the buoyancy induced draught pressure difference and the mass flow rates of ammonia gas and combustion gas are close to a value of 1, showing that during Experiment 4 the ammonia gas could be assumed to behave like the combustion product gases.

To use wood particles to substitute domestic refuse was initially suggested in section 3.1, where it was shown that the main characteristics, i.e. void fraction, particle density and thermal conductivity, of beds of refuse correspond to that of beds of wood chips. The results obtained from Experiments 5 and 6, as presented in sections 4.5 and 4.6, show qualitatively good agreement. Although the speed in which the temperature distribution of the bed is affected by the combustion product gases during Experiment 5 differs from that of Experiment 6, there is still good agreement of the way in which the temperature distribution is affected. In particular, the temperature of the source of combustion and thus the initial temperature of the combustion product gases corresponded at a level of approximately 810 °C during the refuse experiment and

approximately 800 °C during the wood chips experiment. The differences that occurred during the development of the bed temperatures below 200 °C can, as explained in sections 4.5 and 4.6, be attributed to the less varying particle size distribution in the wood chips experiment. All in all, the results of Experiments 5 and 6 suggested that the substitution of the refuse by wood particles was appropriate.

### **5.1.2 Temperature measurements**

In Experiments 5 and 6 a number of problems had to be overcome in order to ensure the validity of the temperature measurements made. Concerns about the experimental conditions and design were

- a) the influence of the thermocouple support beam on the void fraction distribution inside the beds of refuse and wood chips,
- b) the conduction of heat along the thermocouples,
- c) the emissivity value of the bed surface and
- d) the ignition of the bed material by the propane gas burner.

A regular void fraction distribution was achieved by careful arrangement of the refuse and the wood chips around the thermocouple support beam and between the thermocouples. That this effort has been successful and the major part of the combustion gas had thus flowed through the bed and not along the beam can be seen from the location of the hot spot indicated on Figure 4.18. This appears not directly at the beam which would have occurred if the flow of gases had been affected by its presence, but instead a few centimetres to one side, vertically above the combustion source. Convection along the beam could thus be excluded.

Conduction along the beam was minimised by constructing it using stainless steel, having a relatively low thermal conductivity and a cross-sectional area of only 116 mm<sup>2</sup>. Figure 4.17e shows that the indicated beam temperature of 47 °C was far below the hot spot temperature and even below the IRT surface alarm threshold temperature of

70 °C. Even if the beam had been heated to a higher temperature, the influence on the measurement of the bed temperatures by heat transfer from the beam to the bed would have been very small due to the very low thermal conductivity of the refuse and the sensitive tips of the thermocouples being 10 cm away from the beam.

Ignition by the propane gas burner through the holes in the bottom of both the refuse container and the wood chips barrel took place very rapidly. This might not correspond to the initiation of a real combustion process, see section 2.2, but was still appropriate because there is no “standard” endogenous combustion inside a refuse bed [49]. The holes in the container and barrel bottom certainly allowed a better air-flow towards the combustion zone but only at the very beginning of each experiment. Within a few minutes the combustion residues obstructed the holes and consequently the additional air-flow. As far as the refuse experiment is concerned, the oxygen availability could hence be regarded as similar to that inside a refuse bed in a bunker. There, the combustion will not take place at the bottom of the bed but anywhere in a depth of up to three metres, allowing for a comparable oxygen availability from the remaining bed below and the surrounding volume.

The major concern regarding temperature measurement was that the influence of the measuring device should be as little as possible. Using IRT systems for surface temperature measurements, influences can be obviously excluded. A different situation arose when temperature measurement had to be done inside the body of refuse using contact thermometers. To minimise any influence, the thermocouples were aligned parallel to the expected isotherms. In addition, thermocouples with a stainless steel sheath were used that had a small diameter and a low thermal conductivity and thus conducted very little heat away from the measuring location. The smaller the diameter of a contact thermometer, the more precise and localised the temperature measurement, which is usually advantageous. During Experiment 5, a very localised measurement was disadvantageous because not all thermocouples have been equally

exposed to the combustion gas. An exactly equal exposure of the thermocouples to the combustion gases can only be achieved by a one-dimensional flow-field of the combustion gases and thus by a one-dimensional temperature field. Obviously, a one-dimensional temperature field could not be achieved because of the heterogeneous composition and the not consistent particle sizes of the refuse. The results obtained from Experiment 5 are shown in Figure 4.16. It would have been advantageous to use multiple horizontal grids of thermocouples but such an arrangement was practically impossible to apply due to the massive distortion of the void fraction distribution inside the refuse bed which would have resulted.

The measurement of the surface temperature distribution was another problem, since a representative emissivity had to be determined for the bed. This could only be done during the experiment. As long as the refuse matter was in thermal equilibrium with the ambient conditions above the bed, the IRT system would always display temperatures near ambient, no matter what emissivity value was used. The previously assumed value of 0.95 could not be confirmed until parts of the surface had been heated up by the combustion gas but it was then found that the assumption of 0.95 was to a large degree representative.

Most of the above mentioned problems did not occur during the final experiments conducted in the beds of wood chips – Experiment 6, sections 3.7 and 4.6. On the one hand this was due to the monodispersed composition of the bed and hence its constant emissivity and on the other hand this was due to the more regular particle size distribution. The latter allowed for flow fields, which could be described as one-dimensional. This is well demonstrated by the results of Experiment 6, shown in Figure 4.19 to 4.21.

## 5.2 Mathematical modelling of heat transfer inside heterogeneous packed beds

It was a major aim of the present work to mathematically model the heat and mass transfer inside packed beds to extend the experimentally obtained results to a more general level. The fact that the temperature inside and at the surface of the bed remained in the range of what was assumed to be the water vapour dew point temperature, i.e. 65 °C to 85 °C, for a long time was an important observation from the experimental results. The temperature development at the surface of the bed, as presented in Figure 4.25, shows that the surface temperature alarm threshold of IRT systems of 70 °C, as proposed by BRAUN and WEIDENER [7, 9], was a very suitable choice, although BRAUN and WEIDENER had no knowledge about the thermal effects of condensation and re-evaporation on the temperature distribution inside the refuse bed. It could also be observed from the results of experiments 5 and 6 that, once the surface temperature started to significantly increase, a level of 70 °C is reached within less than an hour. Bed surface temperatures of more than 70 °C can hence be believed to be an early sign of an endogenous combustion detectable by IRT systems. Such a surface temperature is high enough for the alarm being raised and occur early enough before flashover for counter measures to be implemented.

A presupposition for the realisation of an effective early combustion detection system is that very small hot spots, in the temperature range of 65 °C to 85 °C can be detected. This imposes the highest technical requirements on IRT systems to be fulfilled, as will be discussed in detail later. The questions to be addressed are: How does the temperature distribution develop within the bed leading up to the formation of early hot spots and what advance warning time can be achieved? Since the employment of the phase-changes in the model calculation would on one hand not provide essentially new results but would on the other hand make the model much more complex, the time after the zone of phase-changes involving water has left the bed will be the object of the following investigation.

### 5.2.1 Simplifying assumptions

To avoid the mathematical model becoming too complex, the following simplifying assumptions were initially made:

1. The bed was assumed to be homogeneous and monodispersed, consisting of equally sized spheres in a cubical arrangement [60].
2. The density and specific heat capacity of the particles was assumed to be constant and independent of location. The same applies to the void fraction.
3. The properties of the gaseous phase were assumed to be constant, no phase-changes occur and the flow of hot combustion gases took place as a result of buoyancy induced vertical flow.
4. Both fluid flow and heat transfer were assumed to be one-dimensional [59], which means there is neither fluid flow or a temperature gradient perpendicular to the vertical direction.
5. The fluid flow velocity was assumed to be uniformly distributed over the cross-section considered and did not vary in the vertical direction. This implies that a plug-flow flow can be assumed.

As far as the water, being a component of the combustion gas, is concerned, the effects of condensation and subsequent re-evaporation are not relevant. The gas can be taken to behave as a permanent gas not undergoing any phase-changes since overall, such a gas transfers the same amount of heat to the bed and reaches the same final state. Such a permanent gas has therefore been taken as the basis for the mathematical model and the thermal effects of condensation and re-evaporation have not been included.

The consequences of the above simplifying assumptions can be ultimately evaluated from the comparison of the theoretical predictions and the experimental results.

Nevertheless, some variation of the characteristic properties of the bed and the fluid must be allowed. By that, the model can be applied to a wider range of beds.

### 5.2.2 Derivation of the mathematical model

For the derivation of the model, an energy balance has been undertaken for an arbitrary volume element of the bed with an average void fraction  $\psi$ , as presented in

**Figure 5.2.**

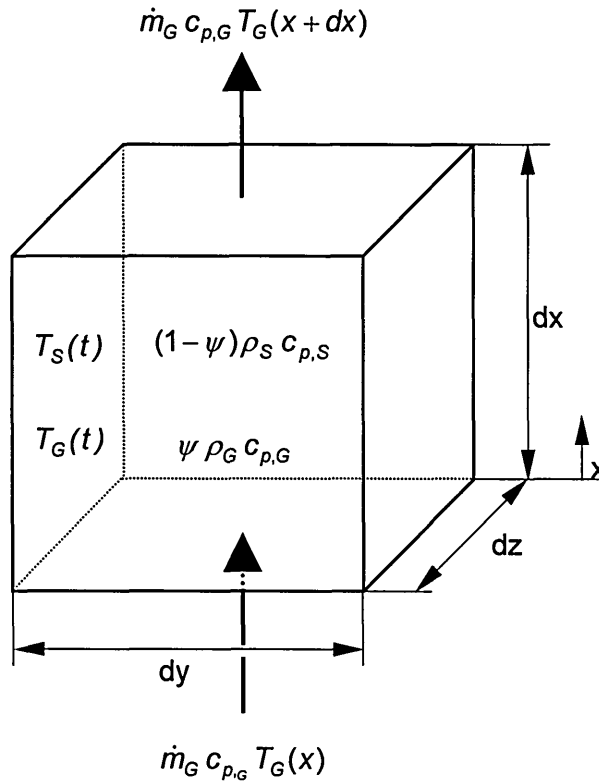


**Figure 5.2** Volume element of a gas filled packed bed, void fraction  $\psi$ .  
The gas enters the element with a heat energy of  $\dot{m}_G c_{p,G} T_G(x)$  and leaves the element with a heat energy of  $\dot{m}_G c_{p,G} T_G(x + dx)$ .

Fluid fills the voids,  $\psi dx dy dz$ , and the particles fill the remaining space,  $(1-\psi) dx dy dz$ . Fluid flows in the  $x$ -direction through the element. Since the fluid inlet temperature,  $T_G$ , is higher than the temperature of the solid particles,  $T_S$ , heat transfers to the particles inside the element during the time of contact,  $dt$ . Consequently, the particles are heated up, which can be described by

$$(1-\psi)\rho_S c_{p,S} \frac{\partial T_S}{\partial t} = \alpha A_S (T_G - T_S), \quad (5.13)$$

wherein  $\rho_S$  is the average density of the solid particles and  $\alpha$  is the heat transfer coefficient between the gas and the solid.  $A_S$  denotes the specific surface area of the solid per unit volume and  $c_{p_s}$  the specific heat capacity of the solid.

Since a part of the heat energy of the gas is transferred to the solid, the gas is consequently cooled down. This can be expressed by

$$-\psi \rho_G c_{p_g} \frac{\partial T_G}{\partial t} - \frac{\dot{m}_G c_{p_g}}{A\psi} \frac{\partial T_G}{\partial x} = \alpha A_S (T_G - T_S), \quad (5.14)$$

wherein  $\rho_G$  is the density,  $\dot{m}_G$  is the mass flow rate and  $c_{p_g}$  the specific heat capacity of the gas.  $A$  is the constant cross-sectional area of the element. The change in temperature of the fluid inside the element with time is thus given by  $-\psi \rho_G c_{p_g} \frac{\partial T_G}{\partial t}$  and  $\alpha A_S (T_G - T_S)$  denotes the heat transfer to the particles.

The constant mass flow rate density of the gas  $\frac{\dot{m}_G}{A\psi}$  equals  $\psi \rho_G C_G$ . If  $\psi$  and  $\rho_G$  are constant, the gas flow velocity  $C_G$  is constant as well. If the following parameters are defined [88]:  $k = \alpha A_S$ ,  $u = (1 - \psi) \rho_S c_{p_s}$  and  $w = \psi \rho_G c_{p_g}$ , Eqn. (5.15) and (5.16) then give the system of partial differential equations for the particle and fluid temperatures, respectively:

$$u \frac{\partial T_S}{\partial t} = k(T_G - T_S) \quad (5.15)$$

$$w \left( \frac{\partial T_G}{\partial t} + C_G \frac{\partial T_G}{\partial x} \right) = k(T_S - T_G) \quad (5.16)$$

Following solution by variable transformation and substitution [88, 89], described in Appendix C, an approximate solution for the gaseous fluid phase temperature,  $T_G(x,t)$ , and the solid particulate phase temperature,  $T_S(x,t)$ , is given by

$$T_G(x,t) = T_{G_0} - (T_{G_0} - T_{S_0}) \frac{2}{\sqrt{2\pi}(2\mu)^2} \int_0^{2\mu v} \frac{e^{-\frac{\sigma^2}{(4\mu)^2 + \sigma} - \mu^2}}{\sqrt{\sigma}^{-1}} d\sigma \quad (5.17)$$

$$T_S(x,t) = T_{S_0} + (T_{G_0} - T_{S_0}) \frac{2}{\sqrt{2\pi}(2v)^2} \int_0^{2\mu v} \frac{e^{-\frac{\sigma^2}{(4v)^2 + \sigma} - v^2}}{\sqrt{\sigma}^{-1}} d\sigma . \quad (5.18)$$

Therein,  $T_{S_0}$  is the initial solid temperature and  $T_{G_0}$  is the constant gas inlet temperature. The individual properties of the gaseous fluid phase and of the solid particulate phase, as given in Eqns. (5.17) and (5.18), as well as the location and time

are contained within the parameters  $v = \sqrt{\frac{\alpha A_S}{v_G \psi \rho_G c_{P_G}}} x$  and

$\mu = \sqrt{\frac{\alpha A_S}{v_G (1-\psi) \rho_S c_{P_S}}} (v_G t - x)$ .  $\sigma$  denotes the integration variable.

Eqns. (5.17) and (5.18) describe a model for the fluid and solid temperatures, both in time and location. For  $t \rightarrow \infty$ , the second term on the right hand side of Eqn. (5.17) becomes 0. This means that  $T_G(x,\infty) = T_{G_0}$ . From Eqn. (5.18) it can be seen, that for  $t \rightarrow \infty$ ,  $T_S$  converges to  $T_{G_0}$  and consequently it follows that  $T_G(x,\infty) = T_S(x,\infty) = T_{G_0}$ .

**Figure 5.3** displays a qualitative representation of the solution to the approximated model equations for the solid particle temperature distribution of a packed bed. It can be seen that the particle temperatures increase vertically along the bed with increasing time. The advance warning time, identified in section 2.3, during which time remedial action can be taken to avoid a full scale fire, is represented by the time difference

between the surface temperature alarm threshold being first exceeded and the point of flashover when the ignition temperature is reached at the surface.

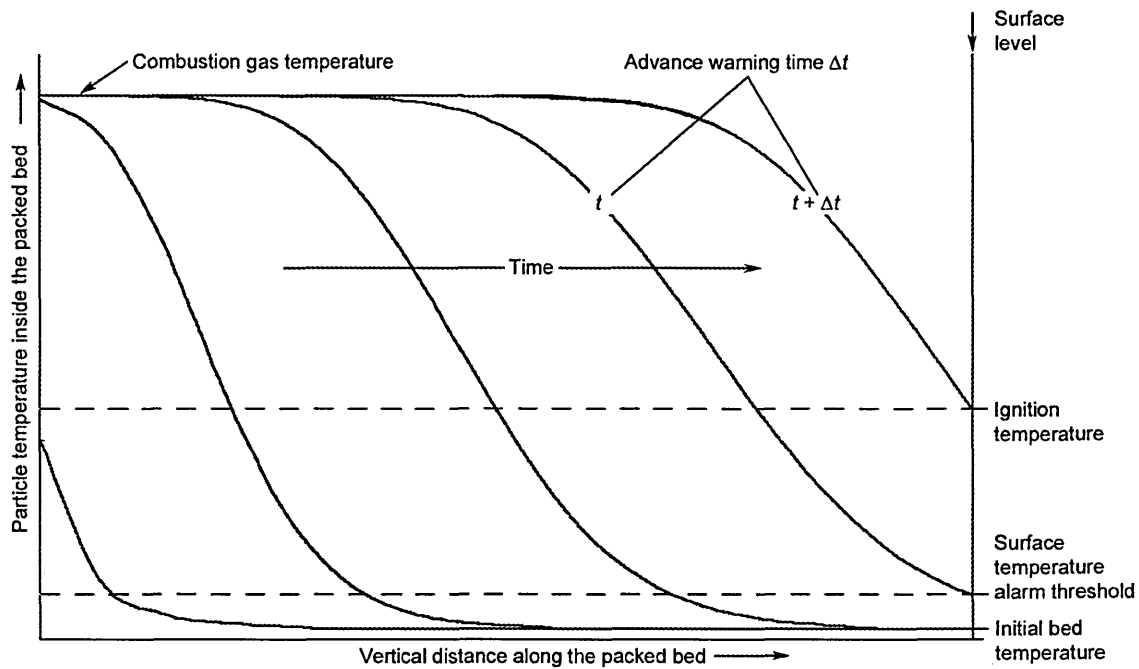


**Figure 5.3** Qualitative solution of the model equation (5.18) for the particle temperatures inside a packed bed

### 5.2.3 The sensitivity of the model towards parameter variations

To what extent a variation of the individual model parameters will affect the solution of Eqns (5.17) and (5.18) must be analysed. The parameters to be considered within the model calculations are given by the variables

$$v = \sqrt{a \cdot x} \quad \text{with} \quad a = \frac{\alpha \cdot A_S}{C_G \cdot \psi \cdot \rho_G \cdot c_{P_G}}$$

and

$$\mu = \sqrt{b \cdot (C_G \cdot t - x)} \quad \text{with} \quad b = \frac{\alpha \cdot A_S}{C_G \cdot (1 - \psi) \cdot \rho_S \cdot c_{P_S}}$$

This shows that, ignoring  $x$  and  $t$ , any change of an individual parameter can be put down to a change of either  $a$ ,  $b$  or  $C_G$ .

Any change of  $\alpha$  or  $A_S$  affects both,  $a$  and  $b$  to the same magnitude. During transient conditions, any in-/decrease of these, in-/decreases the heat transfer from the gas to the solid. This changes the steepness of the temperature curves while their point of inflection stays constant.

An in-/decrease of  $\rho_G$  or  $c_{p_g}$  affects the variable  $a$  only and results in an in-/decreasing heat transfer from gas to solid. A changing value of  $\psi$  will also influence  $a$  only, since  $b$  is independent of void fraction if  $A_S$  is related to the particle diameter by

$$A_S = 6 \frac{(1-\psi)}{d_S} \text{ [57]}. \text{ The heat transfer from gas to solid in-/decreases with de-/increasing}$$

void fraction. In contrast, an in-/decrease of  $\rho_S$  or  $c_{p_s}$  affects  $b$  only, resulting in a de-/increasing temperature rise of the solid.

Consideration of the influence of the individual parameters on the model prediction shows that the assumption of the combustion gas having the same properties as air without water vapour was appropriate. Water vapour within the combustion products would lower the average density of the gas, raising the value for  $a$ . However, simultaneously, the water vapour raises the specific heat of the combustion gas and hence lowers  $a$ . Therefore, the effects of water vapour within the combustion gas counteract each other in terms of heat transfer.

The gas velocity  $C_G$  has a twofold effect: Firstly by affecting the value of  $b$  itself and secondly by affecting the product  $b(C_G t - x)$ . An in-/decreased gas velocity de-/increases the heat transfer to the particles.

Since all parameter changes could be put down to changes of  $a$ ,  $b$  and  $C_G$ , the parameter study took only changes of these variables into account. The effects of the variations of the parameters are presented in **Figure 5.4**, which shows an arbitrary

example of the solution for the particle temperatures after a time of 9,000 seconds. The properties of air and wood were chosen for the gas and solid properties, respectively.

They are:

$$T_{G_0} = 1073 \text{ K}, T_{S_0} = 293 \text{ K}, a_s = 210 \text{ m}^2/\text{m}^3 (d_s = 0.01 \text{ m}), \alpha = 10 \text{ W}/(\text{m}^2 \text{ K}), \psi = 0.65$$

$$c_{p_s} = 1.6 \text{ kJ}/(\text{kg K}), \rho_s = 700 \text{ kg}/\text{m}^3, c_{p_g}|_{20^\circ\text{C}}^{800^\circ\text{C}} = 1.08 \text{ kJ}/(\text{kg K}), \rho_g|_{20^\circ\text{C}}^{800^\circ\text{C}} = 0.52 \text{ kg}/\text{m}^3,$$

$$C_G = 0.10 \text{ m/s}, t = 9000 \text{ s}, x = 0 \text{ to } 2 \text{ m}.$$

Hence, the following basic values for the parameters  $a$  and  $b$  can be obtained:

$a = 39.33 \text{ m}^{-1}$ ,  $b = 0.05 \text{ m}^{-1}$ . A magnitude of  $\pm 25\%$  was chosen for the variation and the individual parameter values are listed in **Table 5.1**.

**Table 5.1** Parameter variation for the mathematical model

Parameter variation	a, b			a		b		C <sub>G</sub>	
	basic	+25 %	-25 %	+25 %	-25 %	+25 %	-25 %	+25 %	-25 %
Parameter									
a in m <sup>-1</sup>	39.32	49.16	29.49	49.16	29.49	39.33	39.33	31.46	52.43
b in m <sup>-1</sup>	0.05	0.068	0.041	0.05	0.05	0.068	0.041	0.043	0.071
C <sub>G</sub> in m/s	0.1	0.1	0.1	0.1	0.1	0.1	0.1	0.125	0.075

Figure 5.4 shows that, as long as  $\alpha$  or  $A_s$  are modified, the resulting variation in temperature distribution is quite low, even with parameter modifications of  $\pm 25\%$ . In contrast, the model is much more sensitive towards a variation of any other physical properties of the gas or the solids or the gas flow velocity  $C_G$ . For these reasons, the individual properties of the gas and particles must be carefully measured or estimated. Only in doing so, a realistic comparison of the experimentally obtained results with that of the mathematical modelling can be achieved.

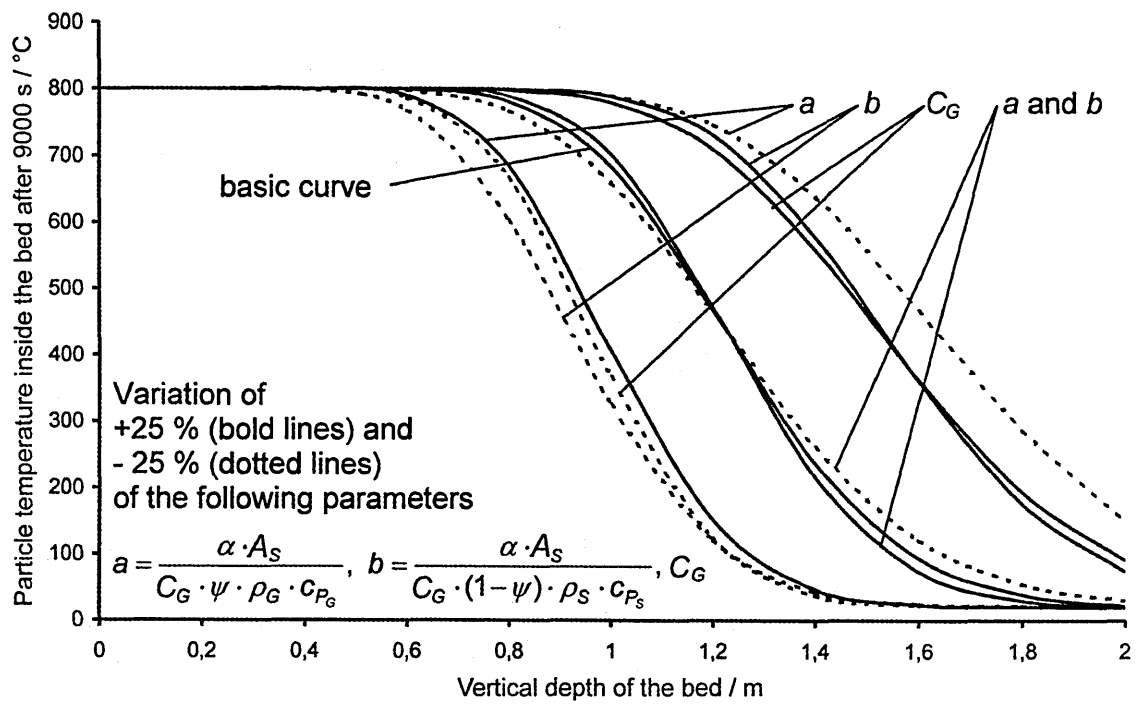


**Figure 5.4** Particle temperatures inside the bed after an assumed combustion duration of 9000 seconds with presupposed and varied ( $\pm 25\%$ ) parameters  $a$ ,  $b$  and  $C_G$ .  
For individual parameter variations see Table 5.1 above.

### 5.3 Comparison of the model prediction against the experimentally obtained data

During combustion inside the refuse and wood chips beds, transient heat transfer conditions occur. The combustion gas has a higher temperature than the solid particles. Although the particles at a particular level of the bed do not have equal temperatures due to their varying sizes, shapes and materials, it can nevertheless be assumed that no large temperature differences occur between gas and particles. If only a short period of time is considered, the conditions may then be regarded as quasi steady-state. The contact thermometers used for the temperature measurement represent solid particles and act as such in terms of heat transfer. The measured temperatures will thus be regarded as particle temperatures and the test of the model against the data will therefore focus on the particle temperatures only.

All values of the physical parameters employed in the modelling of the heat transfer inside the refuse and wood chips beds are listed in **Table 5.2**.

**Table 5.2** Parameters for the mathematical modelling of the heat transfer inside beds of domestic refuse and wood chips

Parameter	Domestic refuse	Wood chips
Average particle diameter <sup>a)</sup>	0.01 m	0.005 m
Heat transfer coefficient <sup>b)</sup>	10 W/(m <sup>2</sup> K)	10 W/(m <sup>2</sup> K)
Specific surface area <sup>c)</sup>	282 m <sup>2</sup> /m <sup>3</sup>	432 m <sup>2</sup> /m <sup>3</sup>
Gas flow velocity <sup>d)</sup>	0.37 m/s	0.26 m/s
Average void fraction <sup>e)</sup>	0.53	0.64
Gas density <sup>f)</sup>	0.52 kg/m <sup>3</sup>	0.52 kg/m <sup>3</sup>
Specific heat capacity of the gas <sup>f)</sup>	1.08 kJ/(kg K)	1.08 kJ/(kg K)
Particle density <sup>g)</sup>	943 kg/m <sup>3</sup>	700 kg/m <sup>3</sup>
Specific heat capacity of the particles <sup>g)</sup>	1.92 kJ/(kg K)	1.76 kJ/(kg K)

<sup>a)</sup> Equally sized spherical particles were assumed [90].

<sup>b)</sup> Assumed value.

<sup>c)</sup> Calculated from  $A_s = 6 \frac{(1-\psi)}{d_s}$  [90]

<sup>d)</sup> Calculated from Eqn. (5.11) with friction loss parameters obtainable from reference [90].

<sup>e)</sup> Measured value.

<sup>f)</sup> Density and specific heat capacity value of air at the arithmetic mean temperature  $((20 + 800) \text{ }^\circ\text{C})/2 = 410 \text{ }^\circ\text{C}$ .

<sup>g)</sup> Taken from Table 2.1 for the refuse and from reference [91] for the wood chips.

The gas velocity is proportional to the quotient of buoyancy induced pressure difference and friction losses. It was previously assumed that the gas properties are constant. Thus  $\Delta\rho$  is constant and consequently  $\Delta p$  depends only on the height  $H$  of the bed. It then follows that

$$C_G \sim \frac{H}{\zeta}.$$

During an actual combustion process, the fire pocket progresses towards the surface. Thus  $H$  decreases but simultaneously, the friction losses decrease by the same factor. The resulting gas velocity is thus constant unless  $H \rightarrow 0$ . By this, the initial assumption of a constant gas velocity is verified.

A comparison of the mathematical prediction with the experimentally achieved results of the refuse experiment is presented in **Figure 5.5**. It shows that basically there is

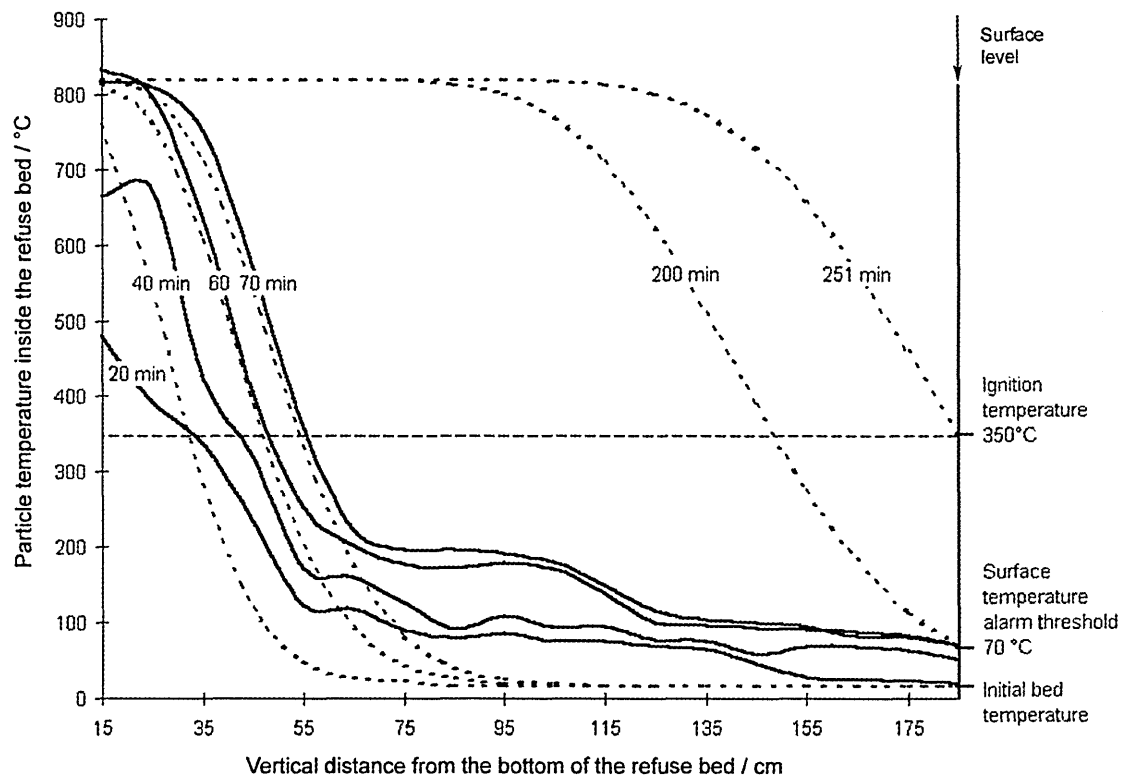


**Figure 5.5** Temperature distribution vertically above an endogenous smouldering combustion, initiated at the bottom of the 27 m<sup>3</sup> domestic refuse bed.  
**Bold curves:** measured particle temperatures along the thermocouples row  
**Dotted curves:** calculated particle temperatures

good agreement between the measured temperature curves and the results predicted by the model. At higher temperatures the curves agree, but less so at lower temperatures, especially, in the layer between 65 cm and 105 cm at around 200 °C and in the layer between 135 cm and 185 cm at around 70 °C to 100 °C. In these zones, the measured temperatures are clearly higher than the model predicts. This must in part be attributed to the one-dimensional conditions assumed in the model, compared with the real situation inside a heterogeneous refuse bed which will be non one-dimensional, together with the effect of condensation of the water content of the combustion product gases in the cooler part of the bed.

The non one-dimensional conditions that occur inside the heterogeneous refuse matter can result in different gas-flow channels inside the bed, depending on how far the combustion has proceeded within the bed. Especially, when bulkier refuse particles obstruct a certain channel, this channel might become available for gas-flow after the obstructing particles have been burnt. Thus, the thermocouples were not equally exposed to the flow of the combustion gas. This can in particular be observed from the 20 minutes and 40 minutes curves that even indicate an increase in temperature between 55 cm to 65 cm and 85 cm to 95 cm, which is impossible without any additional heat source.

Even allowing for the non one-dimensional conditions, the heat of condensation of water seems to clearly influence the development of the temperature profile in Figure 5.5. This can be observed on the 20 minutes and 40 minutes curves in the layer from 85 cm upwards and on the 60 minutes and 70 minutes curves in the layer from 125 cm upwards to the surface of the bed. In these layers, all curves show a restrain in temperature decrease at a temperature level between 70 °C and 100 °C. This can only be attributed to condensation of the water vapour, arising from the oxidation of hydrogen within the refuse compounds and from the evaporation of the free moisture in the refuse at higher temperatures inside the bed. On condensing, the water vapour

released heat in proportion to the condensation enthalpy, thereby producing a local heating effect at almost constant temperature in the upper layers of the bed. This has not been accounted for in the theoretical model. The condensation enthalpy is given by the difference between the gross and the net calorific value of the refuse. Deriving these values from an average elementary analysis of domestic refuse, see **Table 5.3** [11], the difference is 1050 kJ/kg, which is 13 % of the net calorific value. This additional 13 % of heat was released within the cooler part of the bed and, due to the large local heat transfer coefficients during condensation of more than 1,000 W/(m<sup>2</sup> K) [92], arrested the temperature drop throughout the bed in the range of the saturation dew point temperature of the water vapour.

**Table 5.3** Elementary analysis and calorific values of domestic refuse and wood chips [11]

		Domestic refuse mass fraction	Wood chips mass fraction
Carbon	c	0.22	0.38
Oxygen	o	0.08	0.32
Hydrogen	h	0.02	0.05
Nitrogen	n	0.008	0.001
Ash	a	0.35	0.003
Water	w	0.25	0.25
Sulphur	s	0.001	0.001
Net calorific value <sup>a)</sup>		8,060 kJ/kg	13,500 kJ/kg
Gross calorific value <sup>b)</sup>		9,110 kJ/kg	15,200 kJ/kg

a) Calculated from:  $NCV = 33.9 \cdot c + 121.4(h - \frac{o}{8}) + 10.5 \cdot s - 2.44 \cdot w$  [93]

b) Calculated from:  $GCV = NCV + (8.94 \cdot h + w)r$ , with r being the mass specific evaporation enthalpy of water at 25 °C of 2442 kJ/kg [93]

If the experiment had been allowed to progress, the temperature profile throughout the bed would eventually be sufficiently high that no liquid water would remain. Heat transfer would therefore be between the solid refuse and what was effectively a permanent gas, which is the basis for the theoretical model. The results for the model and experiment should thus converge under these conditions at a surface temperature level above the dew point temperature. The results from the theoretical model, indicated on Figure 5.5, suggest that this condition would have occurred after about

200 minutes and that ignition and flashover at the surface would have occurred after about 251 minutes.

In terms of early combustion detection and possible implementation of counter measures, the effect of the condensation is advantageous, since not only does it influence the temperature distribution inside the bed but also the temperature distribution at the surface. The results of the experiment suggest that it would be advantageous to choose a surface temperature alarm threshold in the range of the dew point temperature. In doing so, the advance warning time could be maximised compared to the predictions of the model based on a permanent gas. From Figure 5.5 it is evident that the advance warning time predicted by the model would be  $(251 - 200)$  minutes = 51 minutes, whereas for the real system with combustion product gases containing moisture it was  $(251 - 60)$  minutes = 191 minutes.

Assessment of the water content and thus the saturation dew point temperature can be drawn from the maximum theoretical combustion temperature and the excess air value for combustion. Whether and to what extent air excess occurs can be determined if the maximum theoretical adiabatic combustion temperature is known. This can be obtained from a balance formula used in combustion theory [93], see Appendix D.

For the refuse, a theoretical adiabatic combustion temperature of 1760 °C can be obtained assuming stoichiometric combustion. Since such a high value has not been measured during the experiment, super-stoichiometric combustion must have taken place. Using the measured combustion temperature of 810 °C instead of the theoretical adiabatic combustion temperature, an excess air value of 2.8 is obtained, see Appendix D. This value suggests that almost two thirds of the heat energy from the combustion process is used to heat up excess air and shows that even in places with limited ventilation super-stoichiometric combustion can take place. From the excess air value, conclusions on the water content of the combustion gas and hence on the dew

point temperature can be drawn and an initial dew point temperature of 41 °C can be theoretically obtained, although this is lower than that indicated by the results of the experiment. What the experimental results suggest, i.e. the dew point temperature range of 65 °C to 85 °C, is that the dew point increases with time. This can be attributed to the effect of re-evaporation of the condensate within the lower parts of the bed with proceeding combustion. As a result of this, the water vapour content of the combustion gas increased with time and simultaneously the dew point reached the level indicated on Figure 5.5.

The range of applicability of the theoretical model was more extensively tested by comparison with the results obtained from the wood chips experiments that were undertaken until flashover occurred. The comparison of the measured temperatures with the model predictions are presented in **Figure 5.6**. The lines plotted for experimentally

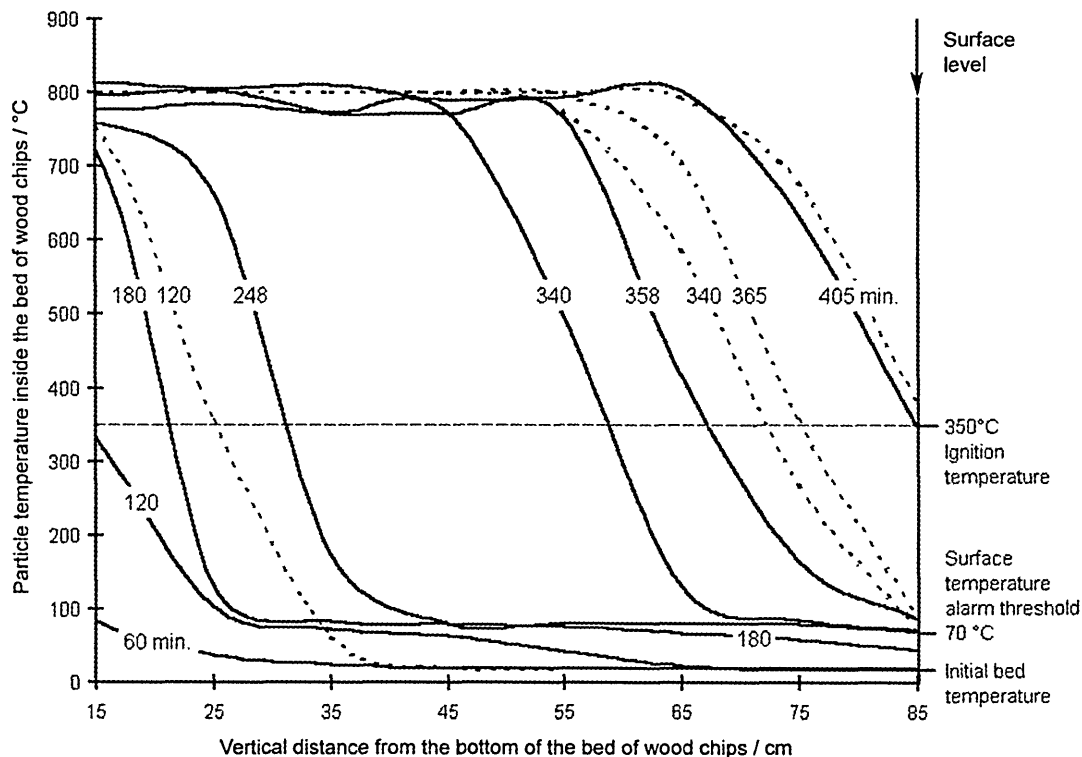


**Figure 5.6** Vertical temperature distribution above an endogenous smouldering combustion, initiated at the bottom of a 0.22 m<sup>3</sup> barrel filled with wood particles.  
**Bold curves:** measured particle temperatures along the thermocouples row  
**Dotted curves:** calculated particle temperatures

obtained data tend to be much smoother with no deviation especially at a temperature level above 100 °C, compared with those obtained for the refuse experiment in Figure 5.5. This is probably due to the more consistent particle size within the bed of wood chips, allowing more vertical flow and hence a more one-dimensional temperature field. However, the thermal effects of condensation and re-evaporation were even more distinct. The 120 minutes curve shows that the temperature inside the bed was restrained to a level of 85 °C, from 28 cm to 35 cm from the bottom of the bed, and then above this the temperature dropped further, very slowly, until the surface was reached. This 85 °C plateau is even more distinct on the 180 minutes curve. The temperature dropped with a high gradient from more than 700 °C to 85 °C within the bottom 30 cm of the bed. From there on, it stayed constant up to 60 cm before it slowly decreased to 50 °C at the surface. The condensing water vapour has released heat in the layer at 85 °C from 30 cm up to the surface during the first 180 minutes. As combustion progresses and the temperature in the upper layers rise, the condensate re-evaporates, requiring latent heat of evaporation to do so, thus providing a restraining effect on temperature rise in these layers. This can, for example, be seen on the 248 minute curve. At that time, the layer below 40 cm had a temperature of more than 100 °C, showing that all water must have returned to the vapour phase by re-evaporation, whereas the influence of condensation on the temperature development is still obvious from 45 cm up to the surface.

These phase changes involving water clearly have a great influence on the development of the temperature profile in Figure 5.6 in the layer between the fire pocket and the surface, as the zones of re-evaporation and condensation move through and finally out of the bed. In the upper layers of the bed the temperature increased faster than predicted due to the liberation of heat of condensation at temperatures below the dew point. At higher temperatures, in the layers immediately above the fire pocket, evaporation of water with the associated requirement for latent heat of evaporation, would be expected to have a restraining effect on temperature

rise. Thus, the temperature within this zone of condensation/evaporation gradually changed in the range of the dew point at about 85 °C, and was present at this level for a long time.

In the same way as for the refuse experiment, the theoretical adiabatic combustion temperature of the wood chips was calculated as 2073 °C and again an excess air value of 3 was obtained. Theoretically, the initial dew point temperature is 40 °C but in practice, this value increased rapidly to 85 °C. The relative moisture content of the combustion gas exiting the bed was measured 360 minutes after ignition. A value of 100 % relative moisture at 85 °C was obtained.

The rapidly increasing dew point temperature can be observed from **Figure 5.7**, representing the results obtained from a small scale conducted in a cylindrical bed (Ø 20 cm, height 20 cm) of wood shavings. This experiment was additionally conducted to confirm the theoretically obtained results for the initial dew point temperature and

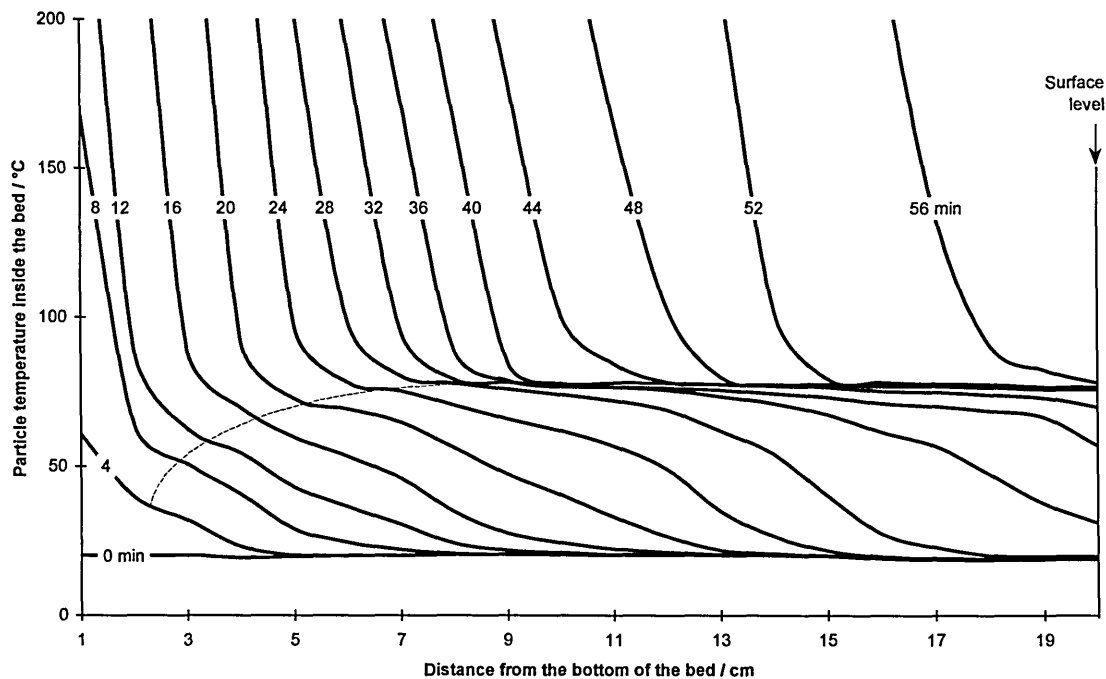


**Figure 5.7** Initial dew point temperature and rapid increase of the dew point temperature with time.  
The increase of the dew point temperature is indicated by the dotted line.

its assumed rapid increase with time. Although 20 thermocouples, vertically arranged in distances of 10 mm, and a cylindrical bed was used, the experimental design and conduction corresponded to the experiments described in section 3.3. The wood shavings had a size of 2 mm to 8 mm and a measured moisture content of 25%.

The experimental results, indicated in Figure 5.7, suggest that condensation started at a dew point temperature of approximately 40 °C after 4 minutes and reached the final dew point temperature level of approximately 80 °C after 30 minutes. This confirms both the theoretically obtained initial dew point temperature and its assumed rapid increase due to the accumulation of re-evaporated moisture in the combustion gases.

The theoretical model appears to be deficient close to the fire pocket, by predicting temperatures higher than the measured temperatures. This may be attributed to the following: The model predictions are based on a constant gas temperature of 800 °C from the very start of the calculation. In contrast, under experimental combustion conditions, about 300 minutes was needed for the fire pocket to fully develop and reach 800 °C. With increasing time, the difference between the model and experimental measurement decreased. After 358 minutes, the lowest bed temperature had exceeded the dew point temperature of 85 °C and the calculated time for a surface temperature of 85 °C was 365 minutes. This shows, that at least the calculation of the surface temperatures above the dew point temperature will be close to the measured temperatures. When the temperatures in the bed are predominately above 100 °C and all the water has returned to the vapour phase, good agreement exists between the theoretical model and experimental observation. This is demonstrated in Figure 5.6 by the good agreement between the measured and theoretically predicted value of the flashover time. It should be noted that the combustion gas is effectively a permanent gas at flashover and also that the previously mentioned deviation of the actual gas inlet temperature from the temperature used for the modelling decreases with time. This

verifies the applicability of the differential equations in the time period in which phase-changes no longer occur.

The thermal effects of water condensing mean that the surface temperature of the bed reaches an alarm threshold temperature which is detectable by IR Thermography far earlier than would be the case with a permanent gas mixture alone. The advance warning time for the presence of combustion in the wood chips experiment, using a threshold warning temperature of 70 °C, was  $(405 - 248)$  minutes = 157 minutes.

Whereas in the absence of water vapour with the combustion products composed only of permanent gases, it would in theory have been only  $(405 - 340)$  minutes = 65 minutes.

## **5.4 Applicability of IR-Thermography systems to the early detection of combustion processes inside domestic refuse beds**

Previous theoretical investigations, introduced in section 2.3, suggested that current IRT systems would not be capable of detecting the effects of endogenous combustion processes at the surface of domestic refuse beds early enough for the implementation of counter measures. The analysis of the experimental results from this investigation have confirmed this.

### **5.4.1 Required spatial resolution the early detection of a combustion process**

BRAUN and WEIDENER [7] have proposed the use of an IRT system with a spatial resolution that is able to resolve an isothermal surface area of 30 cm x 30 cm at 70 °C from the worst case distance inside a refuse bunker, which can be more than 40 metres. This has been widely supported by others [4, 5, 47, 49]. Systematic assessments as to whether this can be achieved by IRT systems already installed has not been carried out.

The proposed alarm temperature threshold of 70 °C seems to be suitable. This value is higher than the temperature reached by microbiological activity inside the bed and thus false alerts can be avoided and it is at the lower end of the dew point temperature range of the combustion gas, i.e. 65 °C to 85 °C. The results of the experiments suggest that a source of endogenous combustion deep within the bed would, theoretically, be detectable at least one hour before the combustion proceeds to the surface where flashover takes place. This time should be sufficiently long for the implementation of counter measures.

As far as the spatial resolution is concerned, a resolution of 30 cm x 30 cm is far too low. Obviously, the spatial resolution has to be improved. This was shown by both the refuse and the wood chips experiment, during which hot spots with a size of not more than 2 cm<sup>2</sup> appeared. Most IRT systems use a 320 x 240 pixel micro-bolometer

detector chip and lenses in a range of  $16^\circ \times 12^\circ$  to  $40^\circ \times 30^\circ$ . Using  $40^\circ \times 30^\circ$  lenses from a measuring distance of 40 m, the maximum measurable area, the so-called field of view (FOV), is 29.1 m x 21.4 m and the smallest theoretically resolvable area, the instantaneous field of view (IFOV), is 9.1 cm x 9.1 cm - both perpendicular to the direction of view of the IR-Camera. The IFOV represents the surface area from which all thermal radiation is received by a single IR-detector on the detector chip of the IR-camera. That even the theoretical IFOV of 9.1 cm x 9.1 cm is not sufficient can be shown by the example IR-Thermogram presented in **Figure 5.8** from the refuse experiment that exhibits a clearly defined hot spot of 2 cm<sup>2</sup> and 104.6 °C.

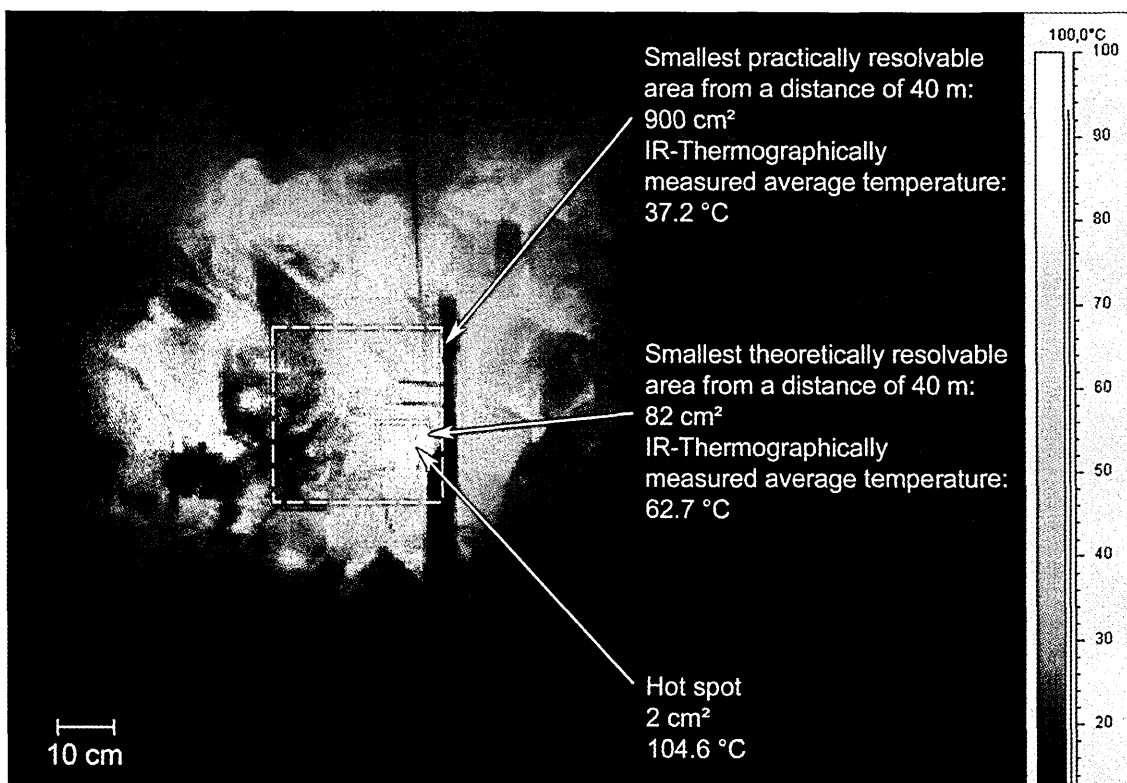


**Figure 5.8** IR-Thermogram of the refuse bed surface after 72 minutes of combustion at the bottom of the bed

For the theoretical IFOV of 9.1 cm x 9.1 cm, including the hot spot of 104.6 °C, from a measuring distance of 40 m, the IRT system would have displayed a temperature of 62.7 °C because the IRT system would not only have received the IR-radiation emitted from the hot spot but would also have received the radiation of all other particles within the IFOV. Since the remaining particles have a much lower temperature than the hot

spot and since the IRT system integrally calculates the temperature over the entire IFOV, the displayed temperature would be much lower than that of the hot spot. Taking the proposed IFOV of 30 cm x 30 cm as a basis, the integrated average temperature would be only 37.2 °C. The same conclusion, that a spatial resolution of a few square-centimetres is necessary, is supported by the wood chips experiments, **Figure 5.9**.

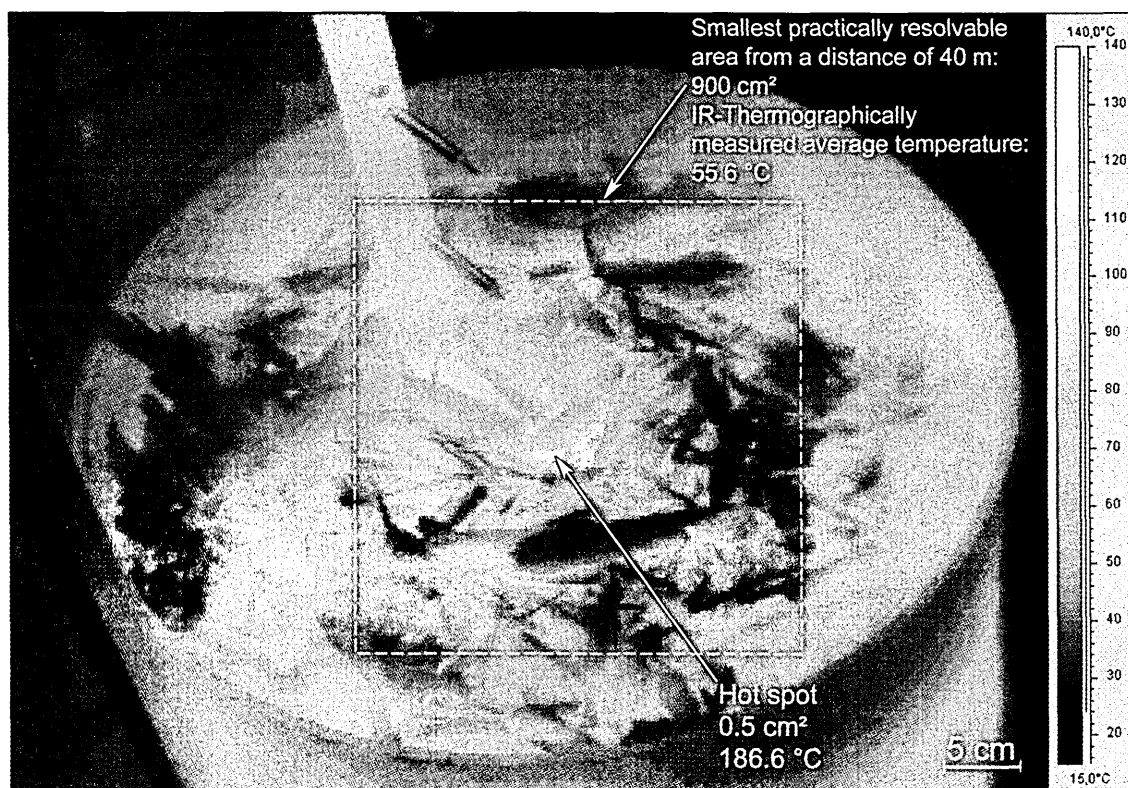


**Figure 5.9** IR-Thermogram of the wood chips surface after 390 minutes of combustion at the bottom of the bed

The earliest hot spots at the surface of a packed bed have a temperature of up to 85 °C and a size of only a few square-centimetres and steep surface temperature gradients away from them of more than 10 K/cm. Hence, the IFOV should be in a range of not more 1.0 cm x 1.0 cm and must still be achieved from a measuring distance of 40 m. To theoretically achieve this, an IRT system with a 320 x 240 pixel detector chip must use lenses of 4.6° x 3.4°, a much narrower angular resolution than current standard lenses. This value is only theoretical and implies that the surface area to be measured is perpendicular to the viewing direction of the IR-Camera, which may not be the case.

If the viewing direction is not perpendicular, the measured area increases.

Compensation for that can partly be achieved by choosing an even smaller viewing angle of  $4^\circ \times 3^\circ$ , for instance. With such a decreased viewing angle, to only a tenth of the currently suggested value, the FOV from a 40 m distance consequently decreases to 2.9 m x 2.1 m and the IFOV decreases to 0.9 cm x 0.9 cm. The effect of such a decreased IFOV on the IRT measurements is represented in **Figure 5.10** that shows that the IFOV must be much smaller than the measured object to ensure that no thermal radiation of anything other than the measured object is received by a single IR-detector of the IR-Camera. As soon as radiation from a cooler object is received, the temperature displayed by the IRT system would be too low due to the integral measurement of the temperature within the entire IFOV.

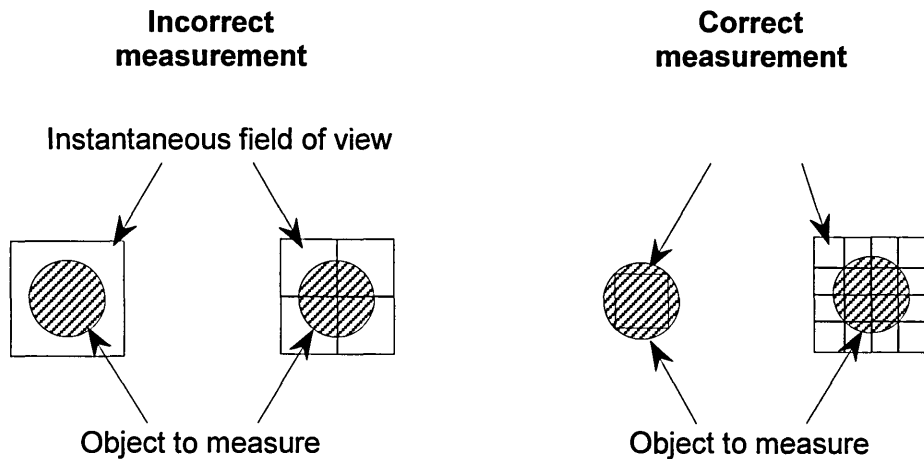


**Figure 5.10** Required spatial resolution (IFOV) for the correct measurement of objects of a specific size

For an effective early combustion detection, it has been demanded that the IRT system should scan the entire surface within less than two minutes. In currently applied systems, the surface is divided into segments, which are subsequently tracked and scanned. To do this, the IR camera is mounted onto a swivel arm on one of the long bunker walls, as shown in **Figure 5.11**, and tracks the segments in a repetitive order.

8 to 14 segments are commonly used, depending on the size of the bunker. The system has thus about 8 to 15 seconds time to monitor a segment and measure the surface temperature distribution. If the required spatial resolution is increased by a factor of ten, the number of segments consequently increases by the same magnitude and the time to track and measure decreases to 0.8 to 1.5 seconds. The swivel arm of the IR-Camera must run with shorter steps or even better continuously. Faster scanning can easily be realised because available IR-Thermography systems use detector chips that have a short response time, allowing for real-time measurements with 50 frames per second.

What is left to be implemented is a computing device that is able to cope with the data within the required short time and – even more important – telephoto lenses with viewing angles smaller than  $4^\circ \times 3^\circ$ .



**Figure 5.11** IR-Camera installations inside a refuse bunker.

Another problem arises due to the irregular nature of the refuse bunker surface, when there is a pile of refuse, behind which a hot spot can be hidden to the view of the IR-camera, as shown in **Figure 5.12**. This problem can be solved if an IRT system uses three cameras in a triangular arrangement. This increases the cost of the system

because three cameras must be installed, two of them at the bunker corners, i.e. with long measuring distances.

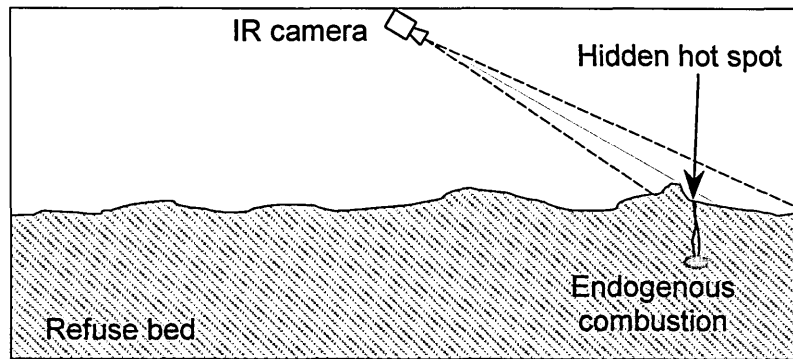


**Figure 5.12** Hot spot hidden behind a pile of refuse

#### **5.4.2 Importance of the spectral band for IR thermographic temperature measurement**

BRAUN and WEIDENER [7] have undertaken relevant laboratory experiments on the extinction, i.e. the absorption and scattering, of IR-Radiation by mist and smoke within the intervening medium. One result of these experiments, was that extinction is greater for short-wave IRT system than for long-wave IRT systems. This observation was supported by the large-scale refuse experiment in this investigation, during which both types of systems were used in conjunction with a surface contact thermometer. At surface temperatures up to 105 °C, the long-wave system achieved an accuracy of 2 K, even during the phase of mist emission, confirmed by comparative measurements using a contact thermometer. The displayed temperature values of the short-wave system were 10 K too low, due to the extinction of IR-Radiation by the intervening medium.

#### **5.4.3 Can IRT systems be applied to early detection of combustion?**

It has been shown that, due to the thermal effects of water condensing, the temperature of a hot spot at the surface of the bed reaches an alarm threshold temperature of 70 °C at least one hour before flashover takes place. Hot spots occur from the emission of hot combustion gas through channel apertures at the surface of

the bed. They have a size of only a few square-centimetres and their detection can as yet be achieved only in theory. In reality, the spatial resolution of currently available IRT systems is not sufficient, as was shown in Figure 5.8 to 5.10. The results obtained from Experiments 5 and 6 showed that, once a hot spot exceeded the dew point temperature, i.e. condensation has ceased, its temperature increased more rapidly with a simultaneous minor increase in its surface area. Due to the increasing temperature of the hot spot, the surface temperature displayed by an IRT system would also increase, even if the IFOV is larger than the hot spot. If the hot spot is not detected and the corresponding combustion is allowed to progress, the temperature of the hot spot will reach such a high level that the integral temperature of the IFOV will eventually exceed the surface temperature alarm threshold. However, the advance warning time might then become too short for the successful implementation of counter measures.

Smoke and mist, emitted from the channel apertures, is an additional problem, especially if there is so much present in the intervening medium that even long-wave IRT systems are influenced in their measurements. Traces of mist only occur as long as the bed temperature is in the range of the dew point and, although no actual technique for detection has been proposed, this detection might offer potential for early combustion detection. At higher temperature, i.e. when the condensation and re-evaporation zone has left the bed, the mist vanishes. The experiments showed that this applies to the smoke emission as well. The restriction imposed by extinction is then no longer present, but only just a very short time before flashover takes place. During the experiments this time was about five minutes, which are comparable with that observed during a real combustion in a refuse bunker fire [49].

Early detection of combustion necessitates the use of a long-wave IRT system to minimise the effects of absorption, but these systems must be extensively improved in terms of spatial resolution. This can either be achieved by IR chips using a much greater number of detectors or by the employment of telephoto lenses with a very

narrow viewing angle or zoom lenses. All of these will entail an increase in installation and maintenance cost, which will be additionally increased by the requirement of the installation of at least three IR cameras instead of one. Without these improvements, the early detection of a hot spot cannot be achieved.

## CHAPTER 6

### CONCLUSION AND RECOMMENDATIONS

### FOR FURTHER WORK

## 6 CONCLUSIONS AND RECOMMENDATIONS FOR FURTHER WORK

For the early detection of endogenous combustion processes inside packed beds of refuse, the measurement of the surface temperature distribution by IRT was proposed and a surface temperature that exceeds an alarm threshold of 70 °C was suggested to be a reliable indicator. The objective of this work was to investigate the conditions under which heat transfer takes place that leads to such a surface temperature increase. Experimentally verified results of theoretical investigations have shown that heat is predominantly transferred by the combustion gases, i.e. by convection.

Conduction and radiation do not effectively contribute. The mass flow of the combustion gas is induced by buoyancy and takes place vertically through the bed. As the combustion gas contains water vapour, this condenses when penetrating the cooler layers of the bed. The enthalpy difference caused by the phase-change influences the temperature development between the fire pocket and the surface of the bed. The condensation process is followed by the re-evaporation of the condensed moisture, requiring evaporation enthalpy of equivalent value to the previously released condensation enthalpy, as the fire pocket progresses towards the surface. Both phase-changes thus arrest the bed temperature at nearly constant values in the above defined range and in a region that is extending towards the surface of the bed. This process has a twofold effect at the surface:

1. Hot spots of less than 5 cm<sup>2</sup> and a temperature of 65 °C to 85 °C appear at the channel apertures where the combustion gas is emitted.
2. Condensing water vapour becomes visible at the channel apertures.

About one hour before flashover at the surface, condensation and re-evaporation cease and evolution of mist disappears. Thereafter, the temperatures of the hot spots increase rapidly but their increase in surface area is minimal. A few minutes before flashover, the typical situation observed during the experiments was that a hot spot of less than 10 cm<sup>2</sup> appeared at a temperature of more than 300 °C.

The task of fire prevention using IRT is the detection of the initial hot spots from very long distances using the systems which are usually installed inside the bunker. For this, the spatial resolution must be very high – ten times higher than that of the systems that are available at the moment. During the refuse experiment, a hot spot temperature of 104.6 °C was measured from a distance of five metres. If this hot spot had been measured from a typical distance of 40 m, the IRT system would have displayed a temperature of only 37.2 °C, which is far below the alarm threshold of 70 °C. During the wood chips experiment, a hot spot of 320 °C was measured just before flashover occurred. The integrally measured temperature from a distance of 40 m would have been 103.4 °C. Such a temperature would have raised the alarm, but there would not have been sufficient time left for the implementation of counter measures. The experiments have hence shown that, using the available spatial resolution, very small hot spots cannot be detected early enough and certainly not early enough for effective counter measures to be implemented.

The experimentally obtained results were used to verify a mathematical model, developed to describe the temperature development inside and at the surface of gas permeated beds. A gas that did not undergo phase-changes was assumed for the model predictions and thus the thermal effects of condensation and re-evaporation were not taken into account. These effects have been indubitably observed during the experiments and their implementation in the theoretical model would have made the model too complex rather than offering additional results. The model proved to be successful in predicting the temperature development inside the bed and, in particular, the development of the hot spots after the zone of phase-changes has left the bed. The model predicted that, once the phase-changes came to an end, it takes about one hour for the surface temperature to increase to ignition temperature. If the hot spots are not detected during the phase of condensation and re-evaporation it is, in theory, still possible to detect them early enough while their temperature increases further. The detection of a hot spot whilst its temperature increases further might be easier due to

the higher temperatures of the hot spots. Nevertheless, the experiments have shown that the size of the hot spots did not increase significantly. This emphasises the need for a high spatial resolution of the IRT system employed.

The model can also be applied to other packed beds because it allows for and adaptation of other bed and gas properties. Future applications can then focus on different beds of combustible material, such as cereal silos, plastics storages or large piles of wood.

A further recommendation of work in the field of fire prevention using IRT, is to significantly improve the spatial resolution. The experiments and also the modelling have shown that the final development from a hot spot to an open fire at the surface takes place within a few minutes. In order to detect such a hot spot early enough and supposing that its detection a few minutes before flashover will still leave sufficient time for counter measures, an IR-Thermogram of the entire surface should be obtained within less than two minutes. Due to the above mentioned improvement in spatial resolution, the field of view will decrease. To still obtain a surface scan within two minutes, this must be compensated by a rapid scanning speed. From the ergonomic point of view, the localisation of a hot spot is very difficult and can finally only be achieved by the IRT system displaying the co-ordinates of a detected hot spot in relation to the surface of the bed. Without that, it would be impossible to implement counter measures to the proper location.

During the experiments, the emission of smoke and, in particular, mist was observed for the duration of phase-changes - afterwards these emissions gradually disappeared. Although no specific technique for the detection of these emissions can be suggested, they could be used as a means of early detection of combustion processes.

# REFERENCES AND BIBLIOGRAPHY

## REFERENCES AND BIBLIOGRAPHY

---

- 1 Krause, U.; Schmidt, M.: Initiation of smouldering fires in combustible bulk materials by glowing nests and embedded hot bodies. J. Loss Prev. Proc. Ind., Vol. 10 (1997) No. 4, Elsevier 1997, pp. 237-242
- 2 Zwölfte Verordnung zur Durchführung des Bundesimmissionsschutzgesetzes (12. BImSchV), Neufassung vom 20. September 1991, (BGBl. I S. 1991)
- 3 Siebzehnte Verordnung zur Durchführung des Bundesimmissionsschutzgesetzes (17. BImSchV), Neufassung vom 20. September 1991, (BGBl. I S. 1991)
- 4 Ewert, T.: Brände in Müllbunkern erkennen. TÜ Technische Überwachung, Bd. 35 (1994), No. 10, pp. 404 - 409
- 5 Look, W.: Brände in Müllbunkern. TÜ Technische Überwachung, Bd. 36 (1995), No. 4, p. 124
- 6 LUA-Materialien No. 8, Landesumweltamt NRW: Bericht zur "Vermeidung von Bunkerbränden in Abfallverbrennungsanlagen mit Hilfe der Infrarot-Thermographie". Essen 1995
- 7 Braun, R.; Weidener, H.: The Early Detection of Fires in Waste Bunkers using Infrared-Thermography: Restrictions and Validation. VGB International Journal of Power Plant Engineering 77 (1997), No. 12
- 8 Braun, R.; Fenner, M.; Weidener, H.: Prüfkriterien zur Beurteilung unterschiedlicher IR- Thermographie-Brandfrüherkennungssysteme. VDI Seminar 43-08-02 "Brand- und Explosionsschutzmaßnahmen in Feuerungs- und Verbrennungsanlagen", Düsseldorf 15.-16.10.1998
- 9 Braun, R.; Weidener, H.: Prüfkriterien zur Beurteilung unterschiedlicher IR- Thermographie-Brandfrüherkennungssysteme. VDI Seminar 43-08-01 "Katalysatoren-, Brand-, Explosions- Schutzmaßnahmen", Düsseldorf, 13.-14.03.1997

- 
- 10 Pleß, G.: Glimmbrand in einer geschlossenen Hausmülldeponie. Brandschutz - Deutsche Feuerwehrzeitung, Heft 10/1991, Kohlhammer Stuttgart 1991
- 11 Reimann, D.O.: Konsequenzen in der Brandschutzvorsorge aufgrund eines Müllbunkerbrandes am Beispiel MHKW Bamberg. VDI Seminar 43-08-01 "Katalysatoren-, Brand-, Explosions- Schutzmaßnahmen, Düsseldorf 13.-14.03.1997
- 12 Pfeiffer, D.: Aspekte des Brandschutzes aus Sicht eines Industrieversicherers. VDI Seminar 43-08-02 "Brand-, und Explosionsschutzmaßnahmen in Feuerungs- und Verbrennungsanlagen", Düsseldorf 15.-16.10.1998
- 13 Information published by the plant authorities of Müllverbrennungsanlage Bielefeld-Herford GmbH, local newspapers and personal communications.  
[http://www.mva-bielefeld.de/content/service\\_aktuelles/service\\_pressespiegel.html](http://www.mva-bielefeld.de/content/service_aktuelles/service_pressespiegel.html)
- 14 Local newspaper article: Korzert: Brand im Müllbunker.  
<http://www.lokalseiten.de/wuppertal/2000/12/200012038.html>
- 15 Duales System Deutschland AG: DS-Documents 3<sup>rd</sup> edition: Refuse Incineration Processes in Germany. published by Der Grüne Punkt - Duales System Deutschland AG Cologne 1998
- 16 Statistisches Bundesamt: Statistisches Jahrbuch für die Bundesrepublik Deutschland und das Ausland 1993. Metzler Poeschel, Stuttgart 1996
- 17 Duales System Deutschland AG: Chronicles of Closing the Loop 1998. published by Duales System Deutschland AG, Cologne 1998
- 18 Thomé-Kozmiensky, K. J.: Die Ablagerung von Abfällen. in: Thomé-Kozmiensky, K.J.(Ed.): Deponie Ablagerung von Abfällen, EF-Verlag für Energie- und Umwelttechnik GmbH Berlin 1987, pp. 8-9.
- 19 Terms of ISO 3261 (1975): Fire Tests - Vocabulary
- 20 National Fire Protection Association: Los Angeles Fire Department Tests - Fire Detection System in Dwellings. NFPA Quarterly, 1.1963, pp. 201-215

- 
- 21 UB-Unser Brandschutz, Zeitschrift für das Brandschutzwesen: Zündquellenkatalog  
No. 1.1-1.9., Heft 7-9/91 and 5/94 - 4/95. Staatsverlag der DDR Berlin 1991-1995
- 22 Kennedy, M.: The case of the exploding haystacks: Spontaneous combustion of  
natural products in New Zealand. Australasian Biotechnology, Vol. 7, No. 2 (1997),  
pp.104-107
- 23 Demidow, P.G.; Sauschew, W.S.: Eigenschaften brennbarer Stoffe. Staatsverlag  
der DDR Berlin 1984, pp. 12-15
- 24 Rabash, D.J.; Drysdale, D.D.: Theory of Fire and Fire Processes. Fire and Materials,  
Vol. 7, No. 2, Wiley Heyden Ltd. London 1983, pp.79 - 88
- 25 Bond, J.: Sources of ignition: flammability characteristics of chemicals and products.  
Butterworth-Heinemann Oxford 1991
- 26 Demidow, P.G.; Sauschew, W.S.: Verbrennung und Eigenschaften brennbarer  
Stoffe. Staatsverlag der DDR Berlin 1980, pp. 37-51.
- 27 Worpenberg, R.: Untersuchungen zur Brandentstehung und Brandverhütung beim  
Schweißen und thermischen Trennen, insbesondere durch glühende Partikel sowie  
zur Abgrenzung von Gefahrenbereichen. Dissertation Universität Wuppertal 1989
- 28 Ladwig, T.H.: Industrial fire prevention and protection. van Nostrand Reinhold New  
York 1991
- 29 Peters, H.: Auslösung und Ausbreitung von Glimmbränden in feinteiligen  
Schüttgütern. vfdb-Zeitschrift, Heft 2/3 (1965), Altenberge
- 30 Moussa, N.A. et al.: Mechanisms of Smouldering of Cellulosic Materials.  
Proceedings of the 16<sup>th</sup> International Symposium on Combustion at the  
Massachusetts Institute of Technology, Massachusetts 15.-20.07.1976
- 31 Hedermann, D.: Stoff- und Energieumsätze bei der Ausbreitung von Schwel- und  
Glimmbränden an Probekörpern aus Cellulose. Dissertation Universität Wuppertal  
1992
- 32 Hölemann, H.: Schwel- und Glimmversuche an Baustoffen. Der Sachverständige,  
Heft 10 (1995), pp. 256-265

- 
- 33 Bowes, P.C.; Townsend, S.E.: Ignition of combustible dusts on hot surfaces. Brit. J. Appl. Phys. No. 13 (1962), pp. 105 - 114
- 34 Felgenhauer, Kohl, Neumann: Zündung brennbarer Stoffe durch heiße Flächen. UB- Unser Brandschutz, Heft 1 (1986), p. 21
- 35 Rietz, G.: Selbstentzündungsvorgänge an Schüttgütern und ihre technologische Beherrschung Teil 1. TÜ Technische Überwachung, Bd. 33 (1992) No. 11, pp. 383 - 385
- 36 Lyman, R. M.; Volkmer, J. E.: Pyrophoricity (spontaneous combustion) of Powder River Basin coals – considerations for coalbed methane development. Wyoming State Geological Survey, Coal Report CR 01-1, Laramie March 2001
- 37 Monachow, V.T.: Brandgefährlichkeit von Stoffen, Untersuchungsmethoden. Staatsverlag der DDR Berlin 1984
- 38 Hussein, H.M.: Biologische Selbsterhitzung von Heu und ihre Weiterentwicklung bis zur Selbstentzündung. Grundlagen der Kriminalistik, Band 8/1 (1972), Brandkriminalistik, pp. 359 - 375
- 39 Griffith, J.G.: Personal communications. Department of Chemistry, University of Leeds, June 1997
- 40 Kennedy, M.: Personal communications. Biochemical Engineering Manager, Industrial Research Ltd, Lower Hutt, New Zealand October 1997
- 41 Katthab et al.: Spontaneous Ignition of Oil-contaminated Cotton Fabric. Fire and Materials, Vol. 20, John Wiley & Sons Ltd. New York 1996, pp.167 - 172
- 42 Encyclopaedia of Chemical Technology, 4<sup>th</sup> edition, Volume A9, John Wiley & Sons New-York 1993, p.: 62.
- 43 UB-Unser Brandschutz, Zeitschrift für das Brandschutzwesen: Zündquellenkatalog No. 7.4, Heft 4/95, Staatsverlag der DDR Berlin
- 44 Inhülsen, D.: Biologische Selbstentzündungen. Brandschutz - Deutsche Feuerwehrzeitung, Heft 11(1994), Kohlhammer Stuttgart

- 
- 45 Hussein, H.M.: Biologische Selbsterhitzung von Heu. Handbuch der naturwissenschaftlichen Kriminalistik, Bd. 8/1 (1984), Kriminalistik Verlag Berlin
- 46 Heymer, J.E.: The entrancing flame: The facts of spontaneous combustion. Little, Brown London 1996
- 47 Schildhauer, P; Hölemann, H.: Schwelbrände in Abfallagern von Müllheizkraftwerken. VBG Kraftwerkstechnik 77 Heft 12 (1997) Essen, p. 1053
- 48 Interrogation of the crane operators of the "Müllheizkraftwerk Essen-Karnap", Germany, July 1997
- 49 Personal communication: Meeting at the Ministerium für Umwelt, Naturschutz, Landwirtschaft und Verbraucherschutz des Landes Nordrhein-Westfalen, Düsseldorf, October 2001
- 50 Siepelmeyer-Kierdorf, L.: Erkennen und Bekämpfen von Bränden in Müllbunkern. Teil 1, S+S Report, Heft 6 1996, pp. 30-33
- 51 Personal communication: Authorities of the refuse incineration plant "RZR Herten".
- 52 DIN 5496 Temperaturstrahlung, Beuth (Hrsg.), Vertrieb GmbH Berlin Köln 1973
- 53 De Witt, D. P.; Nutter, G. D. (Ed.): Theory and Practice of Radiation Thermometry. John Wiley & Son New York 1988
- 54 Chiari, J. A.; Morten, F. D.: Detectors for Thermal Imaging. Electronics Components and Applications, Vol. 4, No. 4, August 1982, pp. 242 - 252
- 55 Kruse, P. W. (Ed.): Uncooled infrared imaging arrays and systems. Acad. Press, San Diego 1997
- 56 VDI/VDE Guideline 3511 Part 4 Temperature Measurement in Industry Radiation Thermometry. VDI/VDE-Gesellschaft Meß- und Automatisierungstechnik, Fachausschuß 2.6 Technische Temperaturmessung, Beuth Verlag Berlin 1995
- 57 VDI Wärmeatlas 8. Auflage, Berechnungsblätter für den Wärmeübergang. Verein Deutscher Ingenieure VDI Gesellschaft Verfahrenstechnik und Chemieingenieurwesen (GVC), Springer, Berlin Heidelberg New-York 1997

- 
- 58 Tsotsas, E.; Martin, H.: Thermal conductivity of packed beds: A review. Chem. Eng. Process. 22 19/37
- 59 Vortmeyer, D.; Schaefer, R. J.: Equivalence of one- and two phase models for heat transfer in packed beds: One-dimensional theory. Chem. Eng. Sci. 29 (1974), p. 485
- 60 Tsotsas, E.: Über die Wärme- und Stoffübertragung in durchströmten Festbetten: Experimente, Modelle, Theorien. Fortschritt-Berichte VDI, Reihe 3, No. 223, VDI Verlag Düsseldorf 1990
- 61 Vortmeyer, D.: Packed bed thermal dispersion models and consistent sets of coefficients. Chemical Engineering Process 26 (1989), p. 263
- 62 Maxwell, J. C.: A Treatise on Electricity and Magnetism. Clarendon Press, Oxford 1873, p. 365
- 63 Deissler, R. G.; Boegli, J. S.: An investigation of effective thermal conductivities of powders in various gases. Trans. ASME, 8 (1958), pp. 1417 - 1425
- 64 Wakao, N.; Kato, K. Effective thermal conductivity of packed beds. J. Chem. Eng. Jpn. 2 (1969), 24/33
- 65 Wakao, N.; Vortmeyer, D.: Pressure dependency of effective thermal conductivity of packed beds. Chem. Eng. Sci., 26 (1971), pp. 1753 - 1765
- 66 Keller, J. B.: Conductivity of a medium containing a dense array of perfectly conducting spheres or cylinders or nonconducting cylinders. J. Appl. Phys., 34 (1963), pp. 991 - 993
- 67 Batchelor, G. K.; O'Brian, R. W.: Thermal or electrical conduction through granular material. Proc. R. Soc. London, Ser. A, 355 (1977), pp. 313 - 333
- 68 Dietz, P. W.: Effective thermal conductivity of packed beds. Ind. Eng. Chem. Fundam., 18 (1979), pp. 283 - 286
- 69 Zick, A. A.: Heat conduction through periodic arrays of spheres. Int. J. Heat Mass Transfer, 26 (1983), pp. 465 - 469
- 70 Kimura, M.: Effective thermal conductivities of packed beds. Chem. Eng. (Jpn.), 21 (1957), pp. 472 - 480

- 
- 71 Vagi, S.; Kunii, D.: Studies on effective thermal conductivity in packed beds. AIChE. J., 3 (1953), pp. 373 - 381
- 72 Masamune, S.; Smith, J. M.: Thermal conductivities of beds of spherical particles. Ind. Eng. Chem. Fundam., 2 (1963), pp. 136 - 143
- 73 Crane, R. A.; Vachon, R. I.: A prediction on the bounds on the effective thermal conductivity of granular materials. Int. J. Heat Mass Transfer, 20 (1977), pp. 711 - 723
- 74 Schumann, T. E. W.; Voss, V.: Heat flow through granular material. J. Soc. Chem. Ind., 63 (1944), pp. 337-340
- 75 Currie, J.A.: Gaseous diffusion coefficients in porous media, Br. J. Appl. Phys. 11 (1960), 314,24
- 76 Carslaw, H. S.; Jaeger, J. C.: Conduction of Heat in Solids. 2<sup>nd</sup> edition, Clarendon Press, Oxford 1959
- 77 Zehner, P.: Experimentelle und theoretische Bestimmung der effektiven Wärmeleitfähigkeit durchströmter Kugelschüttungen bei mäßigen und hohen Temperaturen. Dissertation, Karlsruhe 1972
- 78 Bauer, R.: Effektive radiale Wärmeleitfähigkeit gasdurchströmter Schüttungen mit Partikeln unterschiedlicher Form und Größenverteilung. Dissertation, Karlsruhe 1976
- 79 Schlünder, E. U. (Ed.): Heat Exchanger Design Handbook (HEDH). Sect. 2.8.1, Hemisphere, Washington DC 1986
- 80 Ridgway, K.; Tarbuck, K. J.: Voidage fluctuations in randomly-packed beds of spheres adjacent to a containing wall. Chemical Engineering Science 23 (1968), p. 1147
- 81 Krischer, O.; Kast, W.: Die wissenschaftlichen Grundlagen der Trocknungstechnik. Trocknungstechnik Erster Band, Springer, Berlin Heidelberg 1992

- 
- 82 Tsotsas, E.; Schlünder, E.-U.: Impact of particle size dispersity on thermal conductivity of packed beds: Measurement, numerical simulation, prediction. Chem. Eng. Technology. 14 (1991), 421/27
- 83 Fenner, M.; Acheson, R.; Garbett, E. S., Braun, R.: Fire prevention in refuse storage facilities using IR-Thermography. Proceedings of the 4<sup>th</sup> International Conference on Quality Reliability Maintenance, Oxford, March 2002
- 84 Fenner, M.; Acheson, R.; Garbett, E. S., Braun, R.: Heat transfer and combustion detection in refuse beds. VGB PowerTech, Issue 5 2002, VGB Verlag, Essen 2002
- 85 Euteneuer, U.: Möglichkeiten zur Früherkennung von Müllbunkerbränden - Ereignisse aus Versuchen mit Thermographiesystemen -. Aus der Tätigkeit der LIS 1989.
- 86 Baehr, H. D.; Stepahn, K.: Wärme- und Stoffübertragung. 3<sup>rd</sup> edition, , pp. 166-178, Springer, Berlin Heidelberg New-York 1998
- 87 <http://www.bpkoeln.de/produkte/datenblatt/ammoniak.htm>
- 88 Anzelius, A.: Wärmeleitung vermittelt durchströmter Medien. Zeits. F. ang. Math. u. Mech., Bd. VI, S. 291, Berlin 1926
- 89 Bateman, H.: Partial differential equations of mathematical physics. 2<sup>nd</sup> ed. p. 123, Cambridge University Press, 1959
- 90 VDI Wärmeatlas 8. Auflage, Berechnungsblätter für den Wärmeübergang. Verein Deutscher Ingenieure VDI Gesellschaft Verfahrenstechnik und Chemieingenieurwesen (GVC), Springer, Berlin Heidelberg New-York 1997, pp. Lc1 -Lc9
- 91 Gieck, R. & K.: Technische Formelsammlung. 30<sup>th</sup> edition, Gieck Verlag, Germering 1995
- 92 VDI Wärmeatlas 8. Auflage, Berechnungsblätter für den Wärmeübergang. Verein Deutscher Ingenieure VDI Gesellschaft Verfahrenstechnik und Chemieingenieurwesen (GVC), Springer, Berlin Heidelberg New-York 1997, pp. Ja1 -Ja16

---

93 Braun, R.: Brennstoffenergie. Script for the lecture "Energietechnik in der  
Entsorgung", Fachhochschule Gelsenkirchen, 2001

## A STANDARD EQUIPMENT AND CUSTOM BUILT APPARATUS

### A.1 Standard Equipment

All information concerning standard equipment was provided by the individual manufacturers of the equipment.

#### Thermocouples

**Table A.1** Specifications of the thermocouples

Manufacturer	Thermocoax		
Model	TKA 10/15/DIN	TKA 10/25/DIN	2ABI30/4000/TI/D/2AB35/6m
Type	Type K NiCr-Ni with stainless steel sheath		
Diameter	1 mm	1 mm	4 mm
Length of sensitive tip	10 mm	10 mm	10 mm
Response time with conduction convection	max. 70 ms max. 3 s	max. 70 ms max. 3 s	max. 150 ms max. 5 s
Measurement range	-200 °C to 1300 °C		
Accuracy ≤ 333 °C > 333 °C	± 2.5 K ± 0.75 %		
Length of sheath	15 cm	25 cm	400 cm

#### Platinum resistance thermometer

**Table A.2** Specifications of the Platinum resistance thermometer

Manufacturer	Heraeus
Model	PMW-EOK 100 Ohm
Type	Pt 100 precision resistance thermometer
Diameter	2 mm
Length of sensitive tip	5 mm
Measurement range	0 °C to 850 °C
Accuracy: at 0 °C at 100 °C at 420 °C	± 0.010 K ± 0.050 K ± 0.100 K

## Hewlett Packard HP 34970A Data Acquisition/Switch Unit

**Table A.3** Specifications of the Hewlett Packard HP 34970A

Channels	3 x 20
Accuracy	Type K thermocouples, range -100 °C to 600 °C: ±1.0 K 100 Ω, 1 mA current: ±0.0030 % f.d.r. + 0.0035 % f.s.r.
max. single-channel scan speed	57 measurements per second, 6 ½ digits
max. multi-channel scan speed	60 channels per second, 6 ½ digits
Thermocouple measurements	internal IST-90-software compensation, fixed or external compensation optional
Resistance measurements	4-or 2-wire resistor selectable, internal power supply; offset-compensation for 100 Ω, 1 kΩ, 10 kΩ range
Scan frequency	1 s - 30 min, increments of 0.1 s

An Intel® x86-based Laptop Computer-System with Hewlett Packard HP BenchLink Data Logger software was used for the automatic acquisition of the data acquired by the Hewlett Packard HP 34970A Data Acquisition/Switch Unit.

## Philips PM 9877K/2 Thermocouple Lineariser

**Table A.4** Specifications of the Philips PM 9877K/2 Thermocouple Lineariser

Linearisation	according to IPTS 68
Output voltage	1 mV/°C
Measuring range	-50 - +1200 °C
Overall accuracy at reference conditions	±1 °C ±0.25% of reading
Additional error over rated temperature range (cold junction error + temperature drift)	±0.05 °C ±0.02% of reading per °C deviation from T <sub>ref</sub>
Reference conditions	ambient temperature: +21 – 25 °C relative humidity 45 – 75%

## Philips PM 8262A Two Line Standard Compact Chart Recorder

**Table A.5** Specifications of the Philips PM 8262A Two Line Standard Compact Chart Recorder

Input ranges	1-2-5-10-20-50-100-200-500 mV 1-2-5-10-20-50 V
Measurement accuracy of the individual spans excluding dead band and non-linearity	1x-range: ± 0.40 % of f.s.d. 2x-range: ± 0.35 % of f.s.d. 5x-range: ± 0.25 % of f.s.d
Non-linearity	± 0.20 % of f.s.d
Dead band	≤ 0.20 % of f.s.d
Step response time	≤ 0.6 s from 5 % to 95 % f.s.d.
chart transport speeds (forward direction)	10-20-30-60-120-300 mm/min or mm/h
chart transport accuracy (forward direction)	± 1.5 mm per 20 m chart

# IR-Thermography System AVIO Compact Thermo TVS 220

Nippon Avionics AVIO 705 MK2 short-wave IR- Camera Unit

Thermal Video System Processing Unit

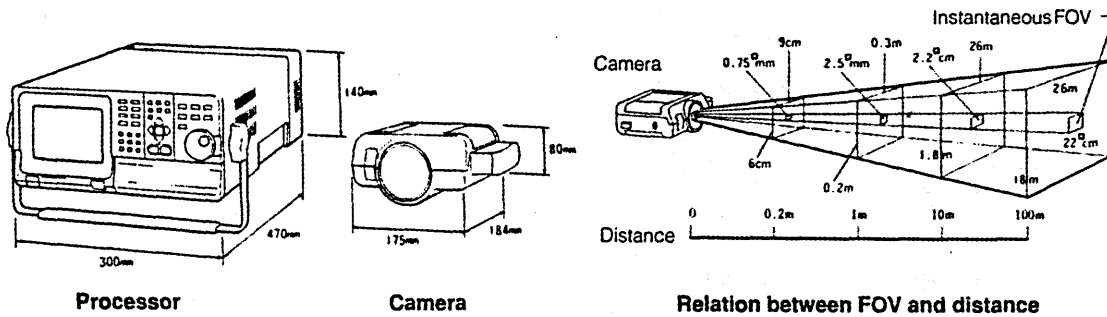


**Table A.6** Specifications of the AVIO Compact Thermo TVS 220

Field of view (FOV)	10° vertical, 15° horizontal
Measuring distance	min. 200 mm
Frames per second	30
Detector	Multi-Element Detector; Indium- Antimonit
Wavelength range	3 - 5.4 μm
Detector cooling medium	Argon-gas or optional Nitrogen-gas
Resolution	256 lines x 200 pixel
Temperature range	-40 °C to 2000 °C (absolute) -35 °C to 1600 °C (calibrated)
Minimum temperature difference	0.1 K
Sensitivity	0.01 K
Measurement accuracy	± 0.4 %
Temperature measurement	Multi-Point measurements simultaneously at up to 5 points and area measurement of a custom specified image area
Emissivity correction range	0.1 to 1.0 in increments of 0.01
Saveable thermograms	up to 40 per 1.44 MB floppy disk
Additional information	<ul style="list-style-type: none"> <li>- 2x hardware zoom</li> <li>- RS-232c interface for PC connection</li> <li>- GPIB interface</li> <li>- Remote control</li> <li>- CCD Video Camera module with video overlay</li> <li>- Mitsubishi CP 700 Video Printer</li> <li>- Sony PVM-14M4E Colour Video Monitor</li> <li>- Commodore Amiga 1081 Video Monitor</li> </ul>

## IR-Thermography System Flir ThermaCam PM 595

**Table A.7** Specifications of the Flir ThermaCam PM 595

Field of view (FOV)	24° vertical, 18° horizontal
Measuring distance	min. 500 mm
Frames per second	50
Detector	Focal Plane Array (FPA), uncooled microbolometer
Wavelength range	7.5 - 13 $\mu\text{m}$
Resolution	320 lines x 240 pixel
Temperature range	-40 °C to 500 °C optional up to 1500 °C or 2000 °C
Measurement accuracy	2 K, $\pm 2 \%$
Thermal sensitivity	0.1 K at 30 °C
Temperature measurement	Multi-Point measurements simultaneously at up to 3 points
Emissivity correction range	0.1 to 1.0 in increments of 0.01
Image Storage	High-capacity PC-Card, ATA compatible
Additional information	- 4x electronic zoom - interface for PC connection

## Fluke 52 K/J Thermometer

**Table A.8** Specification of the Fluke 52 K/J Thermometer

Temperature measurement range	Type K: -200 °C to 1370 °C Type J: -200 °C to 760 °C
Sensitivity	0.1 K
Accuracy for absolute temperature measurement (at ambient temperature 18 °C - 28 °C)	Type K: $\pm (0.1 \% \text{ f. d. r. } +0.7 \text{ K})$ Type J: $\pm (0.1 \% \text{ f. d. r. } +0.8 \text{ K})$
Accuracy for difference temperature measurement (at ambient temperature 18 °C - 28 °C)	Type K: $\pm (0.1 \% \text{ f. d. r. } +1.0 \text{ K})$ Type J: $\pm (0.1 \% \text{ f. d. r. } +1.2 \text{ K})$
Response time	1.0 s (one thermocouple connected) 1.3 s (two thermocouples connected)

## Thermocoax Heating element

**Table A.9** Specifications of the Thermocoax heating element

Electric resistance of the hot part	4.45 $\Omega$
Length of the hot part	270 mm
Maximum voltage	18 V
Maximum power consumption	72.8 W

## LIS GasVue MG-30 Laser Imaging System

The GasVue MG-30 Laser Imaging System, produced by Laser Imaging Systems, is a gas imaging system based on the Backscatter Absorption Gas Imaging (BAGI) technology, operating with a CO<sub>2</sub>-Laser that emitted radiation at 25 individual wavelengths in the range from 9.25 μm to 10.83 μm. The radiation was backscattered from a reflecting background and then received by an IRT system. Laser emission and reception of the backscattered radiation ran through the same optics, and thus the laser always pointed at the location from which the IRT system received the radiation. The functional principle of this gas visualisation system (GVS) is represented in **Figure A.1**. In the case where there is an absorbing gas plume, the laser radiation is impaired and the gas plume could be seen as a darker area on the IRT screen. Different gases absorb radiation at different wavelengths and since the laser wavelength could be triggered in the range from 9.25 μm to 10.83 μm a total of 77 gases that could be visualised. NH<sub>3</sub>-gas had to be visualised during the experimental procedures and thus, the sensitivity of the system had to be experimentally determined and a value of approximately 2 kg/year at laboratory conditions has been obtained. The GVS works in real-time mode, thus providing the possibility to detect and visualise gases online.

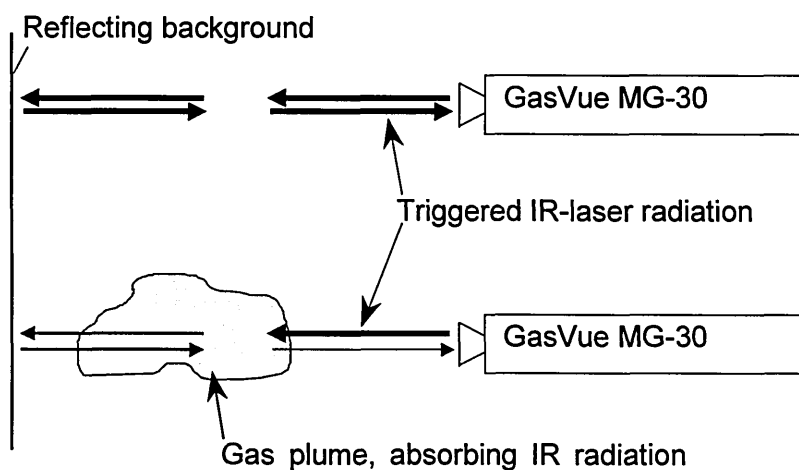


**Figure A.1** Functional principle of the GasVue gas visualisation system

## Propane Gas Burner

Standard propane gas ring burner with a maximum heat output of 20 kW.

## A.2 Custom Built Apparatus

### Electric heater powered by a built-in Thermocoax heating element

A small, electric heater was built for the small scale experiments using wood shavings. It consisted of a cylindrical shaped body with a diameter of 30 mm and a height of 10 mm. Its top consisted of a 5 mm thick copper plate and the bottom was made of 5 mm thick stainless steel. Between the two plates, the helical Thermocoax heating element was placed in such a way that the "hot" part was in between cylinders and the "cool" parts were outside. Thus, when current was applied to the heater, only the metal plates were heated up. Most of the heat was transferred through the copper top, having a higher thermal conductivity than the stainless steel bottom. To control the temperature, a Heraeus Pt 100 precision resistance thermometer was placed in a hole inside the copper top, as shown in **Figure A.2**. **Figure A.3** presents a photograph of the heater.

Heraeus PMW-EOK 100 Ohm, Pt 100 precision resistance thermometer

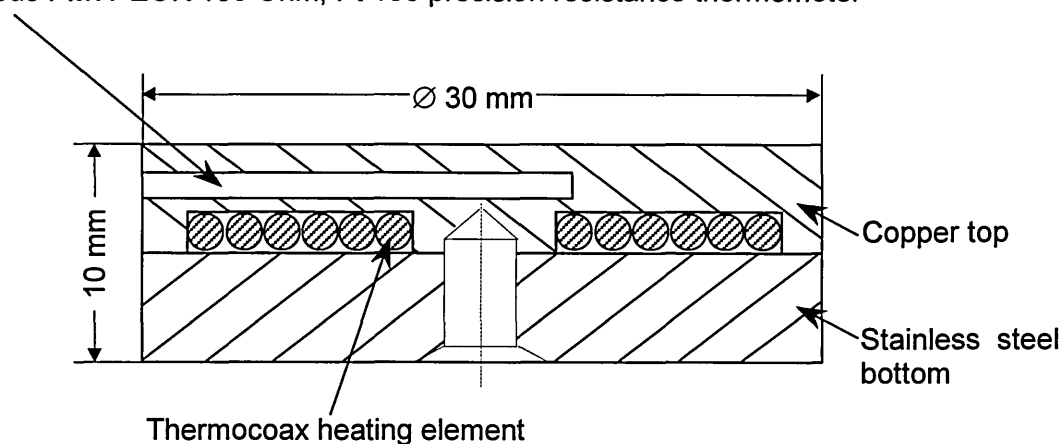


**Figure A.2** Cross-sectional schematic of the electrical heater

The electrical heating was tested with a maximum voltage of 14 V, resulting in a power consumption of 44 W. In air, a surface temperature of 698 °C was measured.

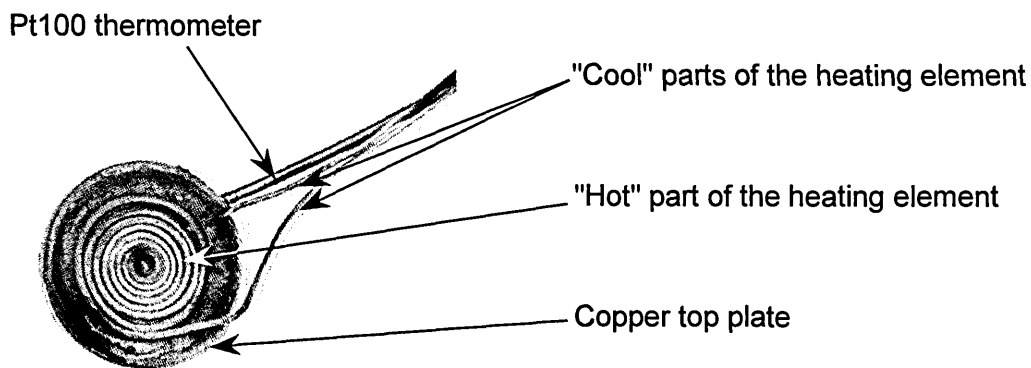


**Figure A.3** Photograph of the electric heating element with removed bottom plate. The helical "hot" part of the heating element can be seen.

### **Stainless steel beam with thermocouples**

For the experiments using the large scale bed of municipal refuse and the intermediate scale beds of wood chips, a method had to be developed for the temperature measurement in the vertical direction, in which the combustion was assumed to proceed towards the surface of the bed. The main difficulty was to achieve fixed positions for the thermocouples within the bed and to not disturb the natural distribution of the void fraction inside the bed. A 30 x 30 x 2 mm stainless steel beam with a length of 2.5 m has been used to support the 20 Thermocoax 2ABI30/4000/TI/D/2AB35/6m thermocouples, as shown in **Figure A.4**. The thermocouples were equidistantly arranged, all at 10 cm intervals, beginning at 15 cm from the bottom. All thermocouples entered the beam from the top and did therefore not disturb the refuse and wood chips bed. **Figure A.5** shows the detail of how the fixed positions of the individual thermocouples was achieved. The temperature sensitive part of the thermocouples was 10 cm away from the beam and protected against mechanical damage by stainless steel cover tubes. During Experiment 5, the beam could be welded to the bottom of the container before the refuse was filled in. During Experiment 6, the beam was attached to the barrel using screws.

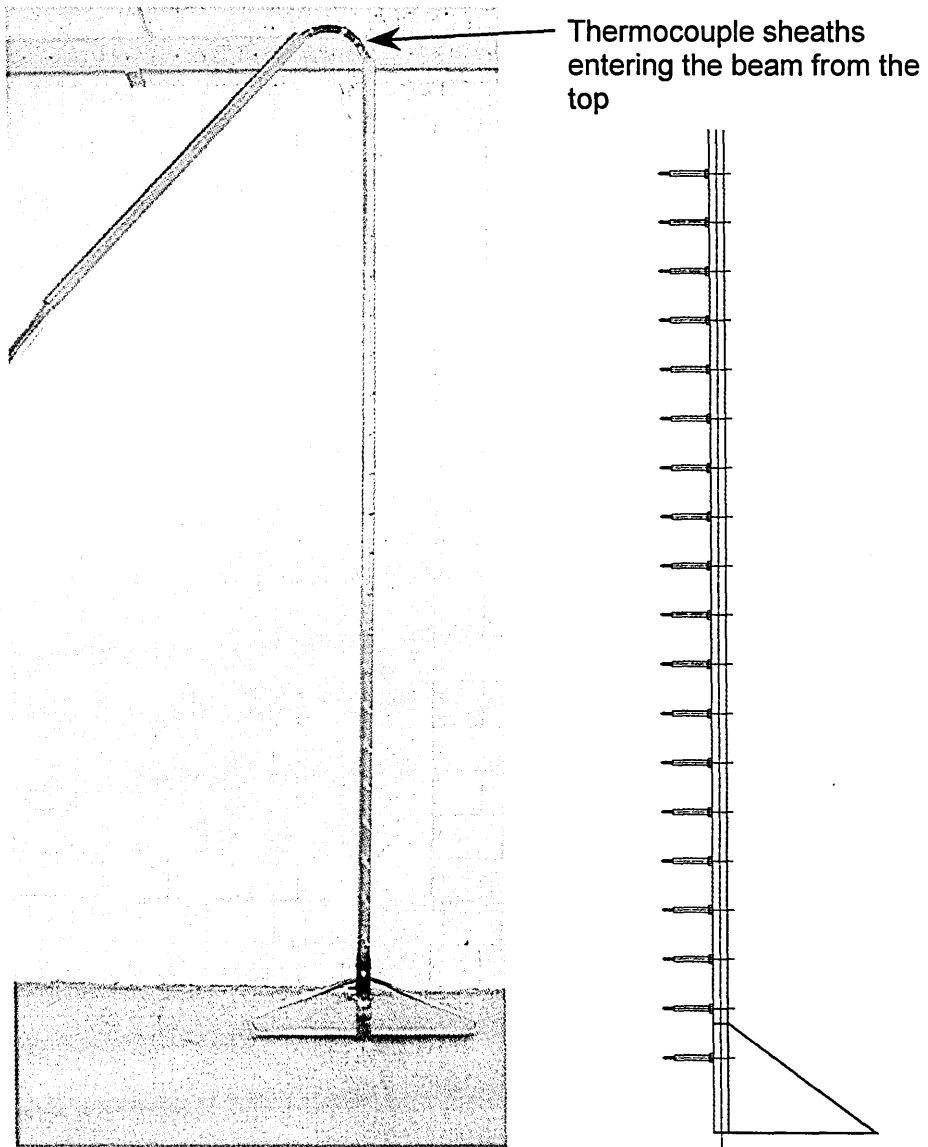


**Figure A.4** Photograph and sketch of the thermocouple support beam.  
At the top of the 2500 mm long beam, the thermocouple sheaths can be seen.

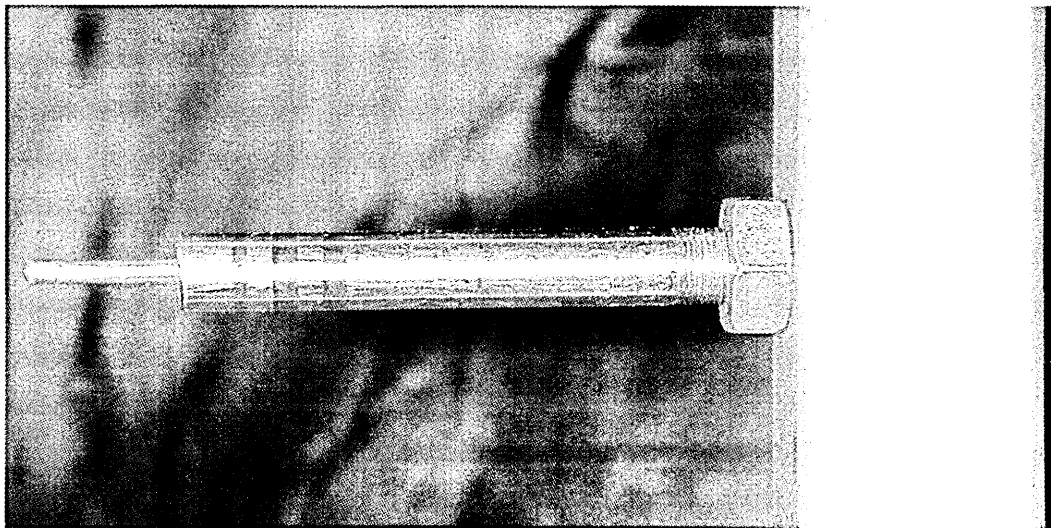
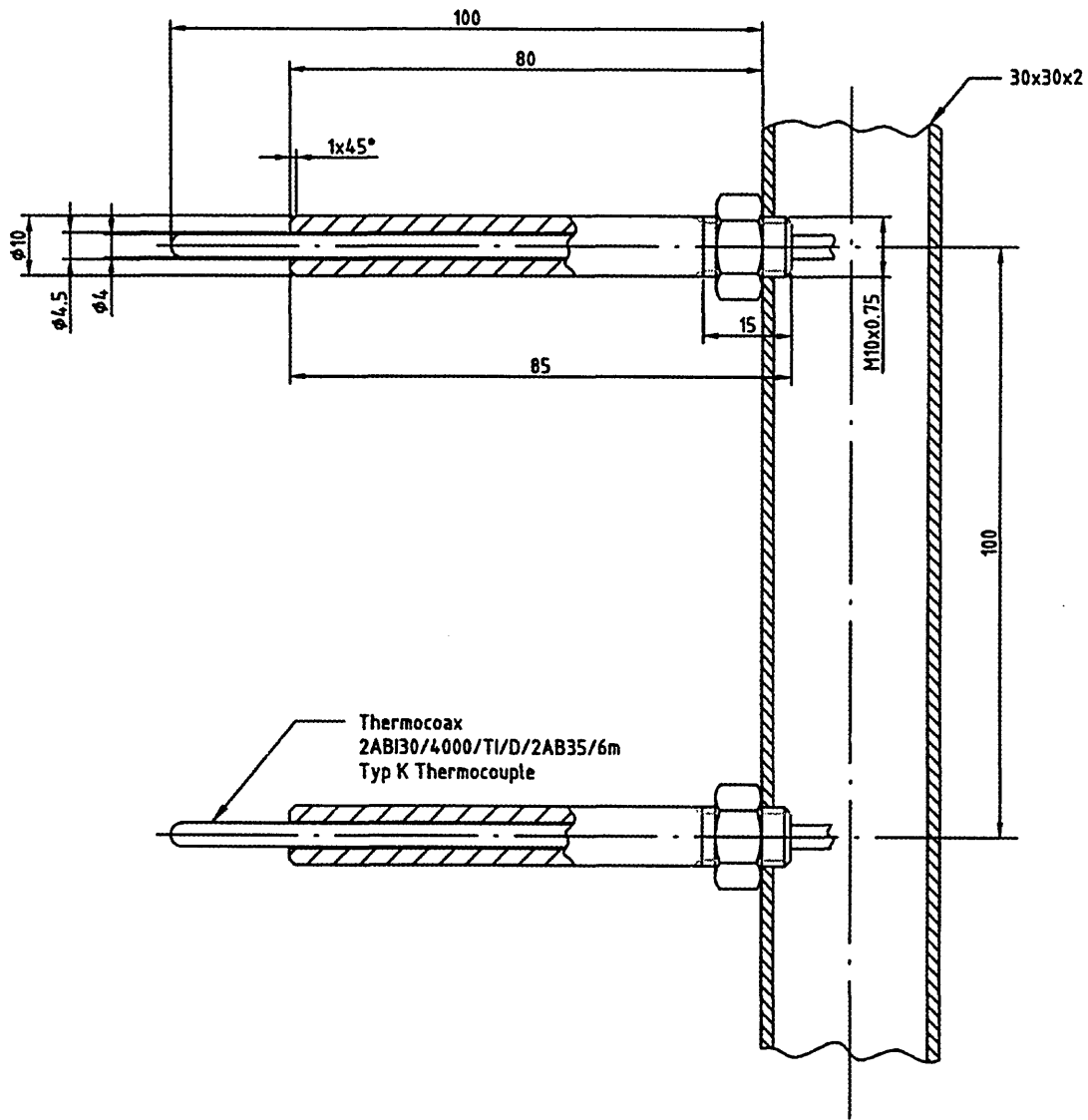


**Figure A.5** Detail sketch and photography of the thermocouple support beam. The thermocouples run through the protecting stainless steel pipe into the 30 x 30 x 2 mm beam.

## **B REPORTS ON FIRES AT GERMAN REFUSE STORAGE FACILITIES**

### **B.1 Fires at German refuse storage facilities**

#### **Refuse bunker fire at the municipal refuse incinerator Bamberg**

##### *Description*

On Friday, 7<sup>th</sup> July 1995 at 2:20 p.m., a fire emerged from inside the refuse in the storage bunker of the municipal refuse incineration plant in Bamberg, Germany [11]. Eye witnesses stated that two successive explosions had taken place before the immediately extensive fire started. The crane operator reported that the explosions took place instantly after refuse has been picked up for charging to the incineration line.

Despite the immediate fire fighting by the plant staff and the call for the public fire brigade the fire could not be controlled within two hours. The major problem was the intense smoke emission hindering effective fighting of the fire that was already spread over the entire surface. Additionally, the hydraulic systems of the delivery gates became damaged and hence not all gates could be opened for fire fighting. The closed gates had to be cut open with oxyacetylene torches and then had to be dismantled. From the open gates hydraulic oil ran onto the floor hindering the fire fighters.

Extinguishing foam has been used to fight the fire but it did not cover the surface but whirled up and flew away. After the visible fire was under control and extinguished, many smouldering fires and fire pockets became visible that partly went back to flaming combustion. Therefore, the fire brigade decided to flood the 3,000 m<sup>3</sup> bunker. For that, approximately 4,000 m<sup>3</sup> water from a near-by river was necessary. Apparently, the flooding was limited to the height of the street level and thus the bunker could not be filled up to the refuse surface level, leaving several fire pockets. Fire-watching staff were employed and finally, after two days the fire was completely extinguished.

Due to the plant being out of order, the district heating, usually powered by the plant, had to run on auxiliary oil-firing. The completely soaked refuse had to be sent to landfill sites and the plant was down for more than four weeks. The damage was approximately £ 1,500,000 [11].

### *Analysis*

At least one explosion took place at the location where the crane has picked up refuse for charging. Generally, explosions can be caused by:

- The ignition of combustible gases that may have accumulated inside the bed. The combustible gases may have been solvent vapours, methane gas from fermentation processes or pyrolysis gases from an endogenous smouldering combustion.
- A smouldering combustion underneath the surface. When the grab picked up the refuse matter this smouldering combustion might have been become exposed to more atmospheric oxygen and the temperature increased rapidly.

Refuse is highly inflammable and has a high net calorific value of about 8000 to 11000 kJ/kg [11]. Thus, the combustion spread quickly over the entire surface. The intense black smoke level was due to the high carbon content of the refuse of more than 20% by mass [11].

### **Refuse bunker fire at the municipal refuse incinerator Bielefeld**

#### *Description [13]*

On Wednesday, 20<sup>th</sup> December 2000, at approximately 03:00 the crane operator noticed white smoke inside the refuse bunker, having a maximum capacity of 10,000 tons and being loaded with approximately 3,000 tons of municipal refuse. The installed IR-Thermography system, using a surface temperature alarm threshold of 70 °C, gave alert and displayed a surface temperature of 115 °C. Three to four minutes later [49], a fire developed near the delivery locations of bulky refuse.

Since the plant's fire fighters were not able to extinguish the fire, the public and private fire brigade was called for at 03:35. When the 70 firemen arrived, the bunker was entirely filled with smoke, that extremely impaired the fire fighting. Therefore, the smoke and exhaust ventilation systems of the bunker were opened a few times during the early morning, letting the smoke exit the bunker. Since the combustion, already spread out over a surface area of 30 m<sup>2</sup>, could not be extinguished from the outside, the burning refuse was picked up with the crane grab under the command of the fire brigade, that used two mobile IRT systems to localise the smouldering combustions. The extinguishing water had already damaged the crushing machines for the bulky refuse and almost destroyed the electrical installations for the cranes. Hence, additional water was used only when further flaming combustion appeared. The smouldering refuse was charged to the incineration. After approximately 20 hours, the fire and all remaining smouldering combustions had been extinguished. The damage was £ 110,000.

### *Analysis*

The exact cause of the combustion is not known but the plant authorities assume a self-ignition process inside the refuse material, since "these processes occur from time to time" [13]. A comparable fire took place once before in 1988. Since it is not known whether or not crushed bulky refuse entered the affected area, two ways of initiation must be taken into account, i.e. self-ignition and ignition by hot material entering the bed from the crushers and being buried underneath other refuse material.

Why the IR-Thermography system gave an alert at a measured surface temperature of 115 °C instead at the set alarm threshold of 70 °C is unknown as well. It can be assumed that the smoke impaired the measurements of the system [8] or the hot spot was too small to be correctly measured before its temperature increased further. In that case, the smoke level must have been already quite intense before flashover and should have been easily detectable by the crane operator. It is not provable whether or

not the crane operator had paid the required attention to the refuse bunker all the time. If not, the installation of an automatic combustion detection system again seems advantageous, especially during the night shifts, when usually only one crane operator is present.

### **Refuse bunker fire at the municipal refuse incinerator Cronenberg**

#### *Description [14]*

On Tuesday, 5<sup>th</sup> December 2000 at 10:42 an uncontrolled combustion inside the refuse bunker of the refuse incineration plant Korzert in Cronenberg was reported to the police and fire brigade by the plant staff. After approximately 30 minutes, the fire was under control. It is assumed that the fire had been caused by either self-ignition or the delivery of burning material into the bunker. The plant has not been damaged.

#### *Analysis*

Since only very little information on the fire is available, an analysis cannot be done.

### **Refuse bunker fire at an unknown municipal refuse incinerator**

#### *Description*

The information about this fire has been provided by an insurance company which gave no information about the affected plant [12].

On Sunday, 9<sup>th</sup> August 1998 at 6:00 a.m. an explosion took place inside a 11,500 m<sup>3</sup> refuse bunker and a fire started near one of the refuse delivery locations. The fire immediately spread out over the entire refuse surface. Instantly, the crane operator switched on the automatic water sprinkling system that sprinkled water over the entire surface. As it became obvious that this would not extinguish the fire, the local fire brigade was called for. Using a mobile IRT camera, the fire brigade was able to localise the origin of the fire through the heavy smoke and fog and the fire could be extinguished. Nevertheless, the fire brigade decided to flood the entire bunker for safety reasons. The damage was £ 75,000.

### *Analysis*

The fire started near one of the refuse delivery locations, leading to the conclusion that hot material has entered the bunker from the outside, e.g. the dust cart has carried already smouldering material. When the refuse has been charged into the bunker, the higher oxygen availability might have lead to a temperature increase and to the flashover. Since there is no information about the time of the last delivery at this specific location, no conclusions can be drawn on the start-up time of the fire or on how long there might have been a smouldering combustion inside the refuse matter. Therefore, it can be assumed that there has not been a long-term process of fermentation or smouldering inside the already stored refuse. Usually, the area around the delivery locations is frequently accessed by the crane to ensure uninterrupted delivery of new refuse matter.

### **Smouldering fire at a refuse disposal site**

#### *Description*

In the winter of 1990, increased methane gas and water vapour emissions at a municipal refuse disposal site led to the assumption of a smouldering fire underneath the surface [10]. An area of approximately 10 m x 20 m was dug out by the fire brigade down to a depth of four metres. Smouldering combustion nests were found that started flaming combustion upon contact with atmospheric oxygen. At a depth of 5 metres no more smouldering was detected. The area was left open for a few days to monitor the temperatures but no further temperature increase could be detected.

#### *Analysis*

This case was an example of self-ignition due to micro-biological activity (see section 2.2.2). Influences from the outside can be excluded because the combustion started underneath the refuse surface in an area where no new refuse matter had been stored.

## **Fires at the refuse disposal site Konstanz**

### *Description No 1*

On Monday, 22<sup>nd</sup> June 1998 at 2:30, the fire brigade had been called for a fire at the refuse disposal site. 35 firemen arrived and detected an area of 250 m<sup>2</sup> of burning refuse. The combustion had spread over the surface and into the bed. Thus, the fire brigade decided to extinguish the fire with 50,000 litres of water instead of foam. At the end of the fire-fighting, the firemen were supported by the site staff that used a bulldozer to re-stack the refuse. At 6:00 the fire had been entirely extinguished.

### *Analysis*

The firemen noticed that the combustion took place at the surface and inside the bed. Since no information on the initiation of the fire can be given, it seems also possible that the combustion started inside the refuse heap instead of at its surface. From within the depth of the heap the smouldering combustion might have proceeded to the surface where flaming combustion occurred due to the rising availability of atmospheric oxygen.

### *Description No 2*

On Sunday, 22<sup>nd</sup> July 2001 around midday, the emission of black smoke from the refuse bed indicated a fire at the refuse disposal site. An area of approximately 200 m<sup>2</sup> of refuse was burning when the fire brigade arrived. Since the fire spread over the surface only, it could be extinguished using foam, as shown in **Figure B.1**.



**Figure B.1** Extinguishing of the fire at the refuse disposal site in Konstanz, Germany

*Analysis*

Since only very little information on the fire is available, an analysis cannot be done.

## **B.2 Interview with the crane operators of a municipal refuse incineration plant**

An interview with four crane operators by the author is now presented. The interview took place on July, 18<sup>th</sup> 1997 at the 'Müllheizkraftwerk Essen-Karnap', Germany.

### **Preliminary meeting – Information from the plant authorities**

On a yearly average, two to four fires occur inside the refuse bunker. Information on the causes of the fires cannot be given but based on the fact that most fires appeared near to the refuse delivery locations, it is assumed that their initiation followed the delivery of hot material to the refuse bunker. Concrete indications on fires initiated by self-ignition processes cannot be given, although it cannot be excluded.

All fires could be extinguished by the plant's fire fighting staff. The public fire brigade, that had been called for every time, just took over the co-ordination and left fire-watching staff to prevent possible new flashovers. In all cases, the smoke and exhaust ventilation systems of the bunker were closed to avoid environmental pollution. These systems would be opened only if there is no other possibility to fight the fire conventionally and if the corresponding environmental pollution could be justified.

Reliable early fire recognition systems, that must be easy to use, meet high ergonomic standards and have a high spatial resolution, are demanded. More information about the processes inside the refuse bed must be obtained to assess the available systems and, if necessary, to develop and facilitate reliable combustion detection systems.

## Interrogation of crane operators

Four crane operators were asked the same questions. The answers stated here are a combination of all individual answers.

*Q: Are there any indications that fires have been started due to biological processes?*

A: Concrete indications are impossible to give. It was observed that mist has been emitted from larger quantities of grass cuttings or other compost. The mist becomes visible approximately 48 hours after delivery, rises up to four or five metres and then dilutes to invisibility inside the bunker atmosphere. It has been observed that the plastic bags in which the grass cuttings are packed burst after a few days, due to the production of fermentation gas inside the bags.

*Q: How did the fires start?*

A: In all cases of flashover, the crane operator had picked up refuse at the location where the fire started. There has not been a single case in which the fire started at a location that had not been recently accessed by the crane grab. Most fires started with a darting flame when the oxygen availability rose due to the lifting of the refuse by the crane grab that grabs to a depth of about 2 metres. Combustible gases can also be ignited by sparks from the grab hitting the bunker wall. It cannot be determined whether these gases arise from fermentation processes or if they are, for example, solvent vapours.

*Q: Are there any indication for smouldering or pyrolysis inside the refuse?*

A: Usually, smouldering combustions inside the bed are not visible at the bed surface. In some cases light blue smoke exits the bed but cannot directly be distinguished from mist at this point. Only a visible accumulation of this light blue smoke at the underneath the ceiling lamps indicates a smouldering combustion inside the bed. In case, that there has been no detection of smoke exiting the bed so far, a meticulous examination of the bed should be done to locate the smouldering. A further smoke

source could be a fire inside the charging line of the incinerator. Usually, this fire cannot spread over to the stored refuse matter but normally it will be extinguished with water to avoid further smoke development and irritation of the crane drivers.

*Q: Are there any seasonal changes in the quantity of fires or hot spots?*

A: During the cold season the risk of fires increases because some people dispose off hot ashes or live coals to the refuse bin. Situations occurred where the refuse inside a dust cart was already ignited as the car entered the site. Therefore, a special extinguishing location for the carts has been built. The localisation of hot spots is almost impossible due to the dust load of the bunker atmosphere. On some days there are on a few metres of visibility and even the crane grab cannot be seen.

*Q: Have there been any tests of early combustion detection systems at your plant?*

A: There has not been any concrete testing so far. Measurements of the refuse have been undertaken in order to detect higher concentrations of fermentation gases like methane or carbon dioxide. No early combustion recognition system is installed at this plant.

## C SOLUTION OF THE SYSTEM OF PARTIAL DIFFERENTIAL EQUATIONS

The system of partial differential equations for the fluid and particle temperatures, respectively has been derived in section 5.2.2 and the following equations were obtained:

$$u \frac{\partial T_s}{\partial t} = k(T_F - T_P) \quad (\text{C.1})$$

$$w \left( \frac{\partial T_G}{\partial t} + C_G \frac{\partial T_G}{\partial x} \right) = k(T_S - T_G) \quad (\text{C.2})$$

Performing a variable transformation by using the dimensionless length

$$\xi = ax = \frac{k}{C_G w} x$$

and dimensionless time

$$\tau = b(C_G t - x) = \frac{k}{C_G u} (C_G t - x)$$

and with

$$\frac{\partial}{\partial t} = b C_G \frac{\partial}{\partial \tau} \quad (\text{C.3})$$

and

$$\frac{\partial}{\partial x} = a \frac{\partial}{\partial \xi} - b \frac{\partial}{\partial \tau} \quad (\text{C.4})$$

Eqn. (C.2) can be written in the form of

$$w \left( \frac{\partial T_G}{\partial t} + C_G \frac{\partial T_G}{\partial x} \right) = k(T_S - T_G)$$

$$w \left( b C_G \frac{\partial}{\partial \tau} T_G + C_G \left( a \frac{\partial}{\partial \xi} - b \frac{\partial}{\partial \tau} \right) T_G \right) = k(T_S - T_G)$$

$$w b C_G \frac{\partial}{\partial \tau} T_G - w C_G a \frac{\partial}{\partial \xi} T_G - w b C_G \frac{\partial}{\partial \tau} T_G = k(T_S - T_G)$$

$$\frac{\partial T_G}{\partial \xi} = \frac{k}{w C_G a} (T_S - T_G). \quad (\text{C.5})$$

Since

$$\frac{k}{wC_G a} = 1$$

it follows that

$$\frac{\partial T_G}{\partial \xi} = (T_S - T_G) \quad (C.6)$$

and analogously

$$\frac{\partial T_S}{\partial \tau} = (T_G - T_S). \quad (C.7)$$

Eqns. (C.6) and (C.7) give the system of differential equations with transformed variables. They imply that the quantity

$$\Delta(\xi, \tau),$$

defined by

$$\Delta(\xi, \tau) = e^{\xi + \tau} (T_G - T_S) \quad (C.8)$$

is a solution of the partial differential equation [87, 88]

$$\frac{\partial^2 \Delta}{\partial \xi \partial \tau} = \Delta. \quad (C.9)$$

The supplementary conditions that will be adopted are the constant initial temperature of the bed

$$T_S(\xi, 0) = T_{S_0} = \text{const.} \quad (C.10)$$

and the constant initial temperature of the gas from the source of combustion

$$T_G(0, \tau) = T_{G_0} = \text{const.} \quad (C.11)$$

From Eqns. (C.8), (C.9) and (C.10) it follows

$$T_S(0, \tau) = T_{G_0} - (T_{G_0} - T_{S_0})e^{-\tau},$$

$$T_G(\xi, 0) = T_{S_0} - (T_{S_0} - T_{G_0})e^{-\xi},$$

and so the supplementary conditions for the quantity

$$\Delta(\xi, \tau)$$

are

$$\Delta(\xi, 0) = \Delta(0, \tau) = T_{G_0} - T_{S_0}. \quad (C.12)$$

Eqn. (C.12) can be solved by a method of successive approximations by

$$\Delta = \Delta_0 + \Delta_1 + \Delta_2 + \dots + \Delta_{n-1} + \Delta_n,$$

where

$$\Delta_0 = T_{G_0} - T_{S_0}$$

and

$$\Delta_{n-1} = \frac{\partial^2 \Delta_n}{\partial \xi \partial \tau}.$$

This gives

$$\Delta = (T_{G_0} - T_{S_0}) I_0(2\sqrt{\xi\tau})$$

or

$$T_G - T_S = (T_{G_0} - T_{S_0}) e^{-(\xi+\tau)} I_0(2\sqrt{\xi\tau}) \quad (C.13)$$

wherein  $I_0$  is the extended Bessel function of the 1<sup>st</sup> kind and 0<sup>th</sup> order ( $n = 0$ ) in the general form of

$$I_0(x) = \sum_{k=0}^{\infty} \frac{(-1)^k \left(\frac{x}{2}\right)^{n+2k}}{k! \Gamma(n+k+1)}$$

Using the transformed variable  $s$ , it then follows that

$$T_G = T_{G_0} - (T_{G_0} - T_{S_0}) e^{-b(C_G t - x)} \int_0^{ax} e^{-s} I_0(2\sqrt{b(C_G t - x)s}) ds \quad (C.14)$$

and analogously

$$T_S = T_{S_0} + (T_{G_0} - T_{S_0}) e^{-ax} \int_0^{b(C_G t - x)} e^{-s} I_0(2\sqrt{axs}) ds. \quad (C.15)$$

These are the solutions of the initial differential equations and can generally be used for the modelling. Tests have shown that the expressions  $e^{-b(C_G t - x)}$  and  $e^{-ax}$  cause problems when being computed. This is due to computer programs being unable to calculate discrete results for  $e^{-307}$  and lower, but setting these results equal to zero.

Therefore, the calculations came to an end before reasonable results could be obtained. Consequently, Eqns. (C.14) and (C.15) must be simplified for computing.

Introducing a factor  $\Delta_G$

$$\Delta_G = e^{-b(C_G t - x)} \int_0^{ax} e^{-s} I_0(2\sqrt{b(C_G t - x)s}) ds, \quad (C.16)$$

the fluid temperature  $T_G$  can be expressed by

$$T_G = T_{G_0} - (T_{G_0} - T_{S_0}) \Delta_G. \quad (C.17)$$

Further substitution in the form of

$$\sigma = 2\sqrt{b(C_G t - x)}\sqrt{s} \quad (C.18)$$

is introduced. The first derivation of Eqn. (C.18) is

$$\frac{d\sigma}{ds} = 2\sqrt{b(C_G t - x)} \frac{1}{2\sqrt{s}}$$

and can be written as

$$ds = \frac{\sqrt{s}}{\sqrt{b(C_G t - x)}} d\sigma = \frac{\sigma}{2b(C_G t - x)} d\sigma. \quad (C.19)$$

Integration of Eqn. (C.19) gives

$$s = \frac{\sigma^2}{4b(C_G t - x)}. \quad (C.20)$$

Inserting Eqn. (C.18) in Eqn (C.20) gives

$$\sigma(0) = 0$$

$$\sigma(ax) = 2\sqrt{b(C_G t - x)}\sqrt{ax} = 2\sqrt{b(C_G t - x)ax}$$

$$\Delta_G = e^{-b(C_G t - x)} \int_0^{2\sqrt{b(C_G t - x)ax}} e^{-\frac{\sigma^2}{4b(C_G t - x)}} I_0(\sigma) \frac{\sigma}{2\sqrt{b(C_G t - x)}} d\sigma \quad (C.21)$$

$$\Delta_G = \frac{e^{-b(C_G t - x)}}{2\sqrt{b(C_G t - x)}} \int_0^{2\sqrt{b(C_G t - x)ax}} e^{-\frac{\sigma^2}{4b(C_G t - x)}} \sigma I_0(\sigma) d\sigma \quad (C.22)$$

Introducing the abbreviations

$$\mu = \sqrt{b(C_G t - x)} \quad (C.23)$$

and

$$\nu = \sqrt{ax} , \quad (C.24)$$

$\Delta_G$  can be expressed by

$$\Delta_G = 2 \frac{e^{-\mu}}{(2\mu)^2} \int_0^{2\mu\nu} e^{-\frac{\sigma^2}{(2\mu)^2}} \sigma I_0(\sigma) d\sigma . \quad (C.25)$$

Inserting Eqn. (C.25) in Eqn. (C.17) finally gives

$$T_G(x, t) = T_{G_0} - (T_{G_0} - T_{S_0}) 2 \frac{e^{-\mu}}{(2\mu)^2} \int_0^{2\mu\nu} e^{-\frac{\sigma^2}{(2\mu)^2}} \sigma I_0(\sigma) d\sigma \quad (C.26)$$

and analogously

$$T_S(x, t) = T_{S_0} + (T_{G_0} - T_{S_0}) 2 \frac{e^{-\nu}}{(2\nu)^2} \int_0^{2\mu\nu} e^{-\frac{\sigma^2}{(2\nu)^2}} \sigma I_0(\sigma) d\sigma . \quad (C.27)$$

The problem of high negative exponents of the e-function still remains and thus, for computing purposes, the Bessel function  $I_0(\sigma)$  will be substituted by an approximation in the form of

$$I_0(\sigma) = \frac{e^\sigma}{\sqrt{2\pi\sigma}} . \quad (C.28)$$

Inserting in (C.16) gives

$$\begin{aligned} \Delta_{G_{asympt.}} &= 2 \frac{e^{-\mu}}{(2\mu)^2} \int_0^{2\mu\nu} e^{-\frac{\sigma^2}{(2\mu)^2}} \sigma \frac{e^\sigma}{\sqrt{2\pi\sigma}} d\sigma \\ \Delta_{G_{asympt.}} &= \frac{2}{(2\mu)^2} \int_0^{2\mu\nu} \frac{1}{\sqrt{2\pi}} \frac{e^{-\frac{\sigma^2}{(4\mu)^2} + \sigma - \mu^2}}{\sqrt{\sigma^{-1}}} d\sigma \\ \Delta_{G_{asympt.}} &= \frac{2}{\sqrt{2\pi}(2\mu)^2} \int_0^{2\mu\nu} \frac{e^{-\frac{\sigma^2}{(4\mu)^2} + \sigma - \mu^2}}{\sqrt{\sigma^{-1}}} d\sigma \end{aligned} \quad (C.29)$$

and finally by inserting Eqn. (C.29) in Eqn. (C.17)

$$T_{G_{asympt.}}(x,t) = T_{G_0} - (T_{G_0} - T_{S_0}) \frac{2}{\sqrt{2\pi}(2\mu)^2} \int_0^{2\mu\nu} \frac{e^{-\frac{\sigma^2}{(4\mu)^2 + \sigma} - \mu^2}}{\sqrt{\sigma}^{-1}} d\sigma . \quad (C.30)$$

Analogously the particle temperature can be derived from

$$T_{S_{asympt.}}(x,t) = T_{S_0} + (T_{G_0} - T_{S_0}) \frac{2}{\sqrt{2\pi}(2\nu)^2} \int_0^{2\mu\nu} \frac{e^{-\frac{\sigma^2}{(4\nu)^2 + \sigma} - \nu^2}}{\sqrt{\sigma}^{-1}} d\sigma . \quad (C.31)$$

Eqns. (C.30) and (C.31) describe the fluid and particle temperatures both in time and location. When  $t \rightarrow \infty$ , the right hand side of (C.30) becomes 0. This means  $T_G(x, \infty) = T_S(x, \infty)$ . From (C.31) it can be seen that if  $t \rightarrow \infty$ ,  $T_G$  converges to  $T_{G_0}$  and consequently it follows that  $T_G(x, \infty) = T_S(x, \infty) = T_{G_0}$ . Computing these solutions does no longer bear the previously described problem and even though the model has been simplified, the solution has an accuracy of more than 99 % compared to the non simplified version when time values are greater than 1000 seconds. Figure 5.2 displays the qualitative solution of the simplified model equations.

## D COMBUSTION TEMPERATURE, EXCESS AIR AND DEW POINT

The maximum theoretical adiabatic combustion temperature can be obtained from a balance formula used in combustion theory from reference [91].

$$\dot{m}_F H_{u,F} + \dot{m}_F h_F + \dot{m}_{Air} h_{Air} = \dot{m}_E h_E + \dot{m}_A h_A + \dot{m}_R H_{u,R} + \dot{m}_R h_R \quad (D.1)$$

wherein  $\dot{m}$  is the mass flow rate of a fuel,  $H_u$  the net calorific value and  $h$  the mass specific enthalpy. The subscripts refer to:  $F$  fuel at ambient temperature  $\vartheta_{amb}$ ,  $Air$  air at  $\vartheta_{amb}$ ,  $E$  exhaust gas at adiabatic combustion temperature  $\vartheta_{ad}$ ,  $A$  ashes at  $\vartheta_{ad}$  and  $R$  residues at  $\vartheta_{ad}$ . Divided by  $\dot{m}$ , Eqn. (D.1) can be written in the form of

$$H_{u,F} + h_F + \frac{\dot{m}_{Air}}{\dot{m}_F} h_{Air} = \frac{\dot{m}_E}{\dot{m}_F} h_E + \frac{\dot{m}_A}{\dot{m}_F} h_A + \frac{\dot{m}_R}{\dot{m}_F} H_{u,R} + \frac{\dot{m}_R}{\dot{m}_F} h_R. \quad (D.2)$$

With [91]

$$h_F = c_{p,F} \Big|_{0^\circ\text{C}}^{\vartheta_{amb}} \vartheta_{amb}$$

$$\frac{\dot{m}_{Air}}{\dot{m}_F} = \lambda L_{min,n} \rho_{Air,n}$$

$$h_{Air} = c_{p,Air} \Big|_{0^\circ\text{C}}^{\vartheta_{amb}} \vartheta_{amb}$$

$$\frac{\dot{m}_E}{\dot{m}_F} = 1 + \lambda L_{min,n} \rho_{Air,n}$$

$$h_E = c_{p,E} \Big|_{0^\circ\text{C}}^{\vartheta_{ad}} \vartheta_{ad}$$

$$\frac{\dot{m}_A}{\dot{m}_F} = 0.35$$

$$h_A = c_{p,A} \Big|_{0^\circ\text{C}}^{\vartheta_{ad}} \vartheta_{ad}$$

$$h_R = c_{p,R} \Big|_{0^\circ\text{C}}^{\vartheta_{ad}} \vartheta_{ad}$$

it follows that

$$\begin{aligned}
 H_{u,F} + c_{p,F} \int_{0^\circ\text{C}}^{\vartheta_{amb}} \vartheta_{amb} + \lambda L_{min,n} \rho_{Air,n} c_{p,Air} \int_{0^\circ\text{C}}^{\vartheta_{amb}} \vartheta_{amb} &= \\
 &= \left(1 + \lambda L_{min,n} \rho_{Air,n}\right) c_{p,E} \int_{0^\circ\text{C}}^{\vartheta_{ad}} \vartheta_{ad} + \frac{\dot{m}_R}{\dot{m}_F} H_{u,R} + \frac{\dot{m}_R}{\dot{m}_F} c_{p,R} \int_{0^\circ\text{C}}^{\vartheta_{ad}} \vartheta_{ad} + \frac{\dot{m}_F}{\dot{m}_A} c_{p,A} \int_{0^\circ\text{C}}^{\vartheta_{ad}} \vartheta_{ad}
 \end{aligned}$$

wherein  $L_{min,n}$  is the minimum amount of air required for stoichometric combustion,

$\rho_{Air,n}$  is the density of air at 0 °C and  $\lambda$  denotes the excess air value. With a given or

estimated value of  $\lambda$ ,  $\vartheta_{ad}$  then can be derived from

$$\vartheta_{ad} = \frac{H_{u,F} - \frac{\dot{m}_R}{\dot{m}_F} H_{u,R} + \lambda L_{min,n} \rho_{Air,n} c_{p,Air} \int_{0^\circ\text{C}}^{\vartheta_{amb}} \vartheta_{amb} + c_{p,F} \int_{0^\circ\text{C}}^{\vartheta_{amb}} \vartheta_{amb}}{\frac{\dot{m}_R}{\dot{m}_F} c_{p,R} \int_{0^\circ\text{C}}^{\vartheta_{ad}} \vartheta_{ad} + \left(1 + \lambda L_{min,n} \rho_{Air,n}\right) c_{p,E} \int_{0^\circ\text{C}}^{\vartheta_{ad}} \vartheta_{ad} + \frac{\dot{m}_F}{\dot{m}_A} c_{p,A} \int_{0^\circ\text{C}}^{\vartheta_{ad}} \vartheta_{ad}}, \quad (\text{D.3})$$

or  $\lambda$  can be calculated if  $\vartheta_{ad}$  is known, using

$$\lambda = \frac{\frac{\dot{m}_R}{\dot{m}_F} \left( H_{u,R} + c_{p,R} \int_{0^\circ\text{C}}^{\vartheta_{ad}} \vartheta_{ad} \right) - H_{u,F} - c_{p,F} \int_{0^\circ\text{C}}^{\vartheta_{amb}} \vartheta_{amb} + c_{p,R} \int_{0^\circ\text{C}}^{\vartheta_{ad}} \vartheta_{ad} + \frac{\dot{m}_F}{\dot{m}_A} c_{p,A} \int_{0^\circ\text{C}}^{\vartheta_{ad}} \vartheta_{ad}}{L_{min,n} \rho_{Air,n} \left( c_{p,Air} \int_{0^\circ\text{C}}^{\vartheta_{amb}} \vartheta_{amb} - c_{p,E} \int_{0^\circ\text{C}}^{\vartheta_{ad}} \vartheta_{ad} \right)} \quad (\text{D.4})$$

The minimum amount of air required for stoichometric combustion can be calculated from

$$L_{min,n} = 8.877 \cdot c + 26.44 \cdot h + 3.325 \cdot s - 3.332 \cdot o, \quad (\text{D.5})$$

using the mass fractions of the individual elements as listed in Table 5.3.

Using data from **Table D.1** for Eqn. (D.3) and assuming stoichometric combustion, a theoretical adiabatic combustion temperature of 1760 °C can be obtained for the refuse and a value of 2073 °C can be obtained for the wood chips. Since such high values have not been measured during the experiments, super-stoichometric combustion must

have taken place. Using the measured combustion temperature of 810 °C for the refuse and 800 °C for the wood chips instead of the theoretical adiabatic combustion temperature, an excess air value of 2.8 for the refuse combustion and a value of 3 for the wood combustion can be obtained from Eqn. (D.4).

**Table D.1** Properties for the calculation of the theoretic adiabatic combustion temperature  $\vartheta_{ad}$  and excess air value  $\lambda$  of domestic refuse and wood chips

	Domestic refuse	Wood chips
$\frac{\dot{m}_R}{\dot{m}_F}$ a)	0.08	0.08
$\frac{\dot{m}_A}{\dot{m}_F}$	0.35	0.003
$C_{p,A} \Big _{0^\circ\text{C}}^{\vartheta_{ad}}$	1.0 kJ/(kg K)	1.0 kJ/(kg K)
$H_{u,R}$ b)	2015 kJ/kg	11000 kJ/kg
$H_{u,F}$ c)	8060 kJ/kg	13500 kJ/kg
$C_{p,F} \Big _{0^\circ\text{C}}^{\vartheta_{amb}}$ d)	1.92 kJ/(kg K)	1.76 kJ/(kg K)
$L_{min,n}$ e)	2.22 m <sup>3</sup> /kg <sub>Fuel</sub>	3.64 m <sup>3</sup> /kg <sub>Fuel</sub>
$C_{p,Air} \Big _{0^\circ\text{C}}^{\vartheta_{amb}}$ f)	1.01 kJ/(kg K)	1.01 kJ/(kg K)
$\rho_{Air,n}$ f)	1.275 kg/m <sup>3</sup>	1.275 kg/m <sup>3</sup>
$C_{p,E} \Big _{0^\circ\text{C}}^{\vartheta_{ad}}$ g)	1.08 kJ/(kg K)	1.08 kJ/(kg K)
$C_{p,R} \Big _{0^\circ\text{C}}^{\vartheta_{ad}}$ h)	0.84 kJ/(kg K)	0.84 kJ/(kg K)
$\vartheta_{amb}$ b)	20 °C	20 °C
$\vartheta_{ad}$ b)	810 °C	800 °C

- a) Estimated values
- b) Measured value
- c) Taken from Table 5.3
- d) Value for 20 °C used for refuse and wood
- e) Calculated using Eqn. (D.5) [91]
- f) Taken from reference [57]
- g) Arithmetic mean value for air from 0 °C to 800 °C

With the formulas given in reference [91] and with the excess air values of 2.8 and 3, respectively, the volumetric water content of the combustion gases can be calculated. For the refuse combustion gas, a volumetric water content of 8.2% can be calculated and the volumetric water content of the wood chips combustion gas is 7.4 %. A dew point temperature of 41 °C for the refuse combustion gas and of 40 °C for the wood combustion gas is obtained.

Braun, R.; Fenner, M.; Weidener, H.:

Prüfkriterien zur Beurteilung unterschiedlicher IR- Thermographie-  
Brandfrüherkennungssysteme.

VDI Seminar 43-08-02 "Brand- und Explosionsschutzmaßnahmen in  
Feuerungs- und Verbrennungsanlagen"

Düsseldorf, Germany, 15<sup>th</sup> –16<sup>th</sup> October 1998

# **Prüfkriterien zur Beurteilung unterschiedlicher IR-Thermographie-Brandfrüherkennungssysteme**

**Prof. Dr.-Ing. Rainer Braun  
Dipl.-Ing. Markus Fenner  
Dipl.-Ing. Hubertus Weidener**

**Institut für rationelle Energieverwendung  
und  
Labor für Energietechnik in der Entsorgung**

**Fachhochschule Gelsenkirchen**

**VDI Bildungswerk  
Seminar 43-08-02  
15.-16. Oktober 1998  
Düsseldorf**

**Brand- und Explosionsschutzmaßnahmen  
in Feuerungs- und Verbrennungsanlagen**

# 1 Erforderliche Brandschutzfunktionen und erwartete Darstellung mit Hilfe verfügbarer Thermographiesysteme

Das Lagern inhomogener Restmüllgemenge birgt die Gefahr der Brandentstehung. Entsprechende sicherheitstechnische Vorkehrungen sind deshalb unerlässlich, vor allem für die umfangreiche Zwischenlagerung in den Müllbunkern großer Anlagen der thermischen Restmüllverwertung. Im Sinne der Störfallverordnung, der 12. BImSchV, ist hier Sorge zu tragen, daß eine Brandentstehung durch geeignete Maßnahmen von vornherein verhindert oder durch eine sehr weitgehende Früherkennung so beherrscht wird, daß die Auswirkung unbedeutend gering bleibt. Diese Brandschutzverpflichtung kann die Leistungsfähigkeit des Betriebspersonals, selbst wenn es sich um höchste Aufmerksamkeit bemüht, deutlich überfordern, so daß es geboten ist, zu dessen Unterstützung automatisch wirkende Sicherheitseinrichtungen einzusetzen. Auch die sogenannte Abfallverbrennungsverordnung, die 17. BImSchV, zielt in diese Richtung, indem sie emissionsbezogen fordert, Müllbunker zum Zwecke der Früherkennung von Bränden mit einer automatischen Brandüberwachung auszurüsten.

Als eine den genannten Verordnungen entsprechende technische Maßnahme ist die Anwendung der Infrarot-Strahlungsthermometrie vorgeschlagen worden. Von dieser wird erwartet, daß sie neben der Brandfrüherkennung, wenn erforderlich, als zusätzliche Brandschutzfunktion auch eine effektive Brandbekämpfung ermöglicht [1, 2].

Mit Hilfe der Strahlungsthermometrie kann die von der Oberfläche des gelagerten Abfalls ausgehende Infrarotstrahlung erfaßt und damit die Temperatur der Oberfläche berührungsfrei und aus großer Distanz ermittelt werden [3,4]. Ziel ist es, durch die Feststellung örtlich erhöhter Temperaturwerte frühzeitig Schwelvorgänge sowie Brand- und Glutnester, d.h. den möglichen Beginn einer Brandentstehung, zu erkennen. Man mißt damit jedoch keinesfalls in die Abfall-schüttung hinein. Was deren Inneres betrifft, so ist man vielmehr auf einen Wärme- und Stofftransport angewiesen, der dazu führt, daß auch verborgene Schwel- oder Glimmbrandnester die Temperaturverteilung auf der Oberfläche ausreichend prägen, [1, 2]. Diese Beeinflussung der Verteilung der Oberflächentemperatur wird natürlich durch die zufällige Art der überdeckenden Schüttung und durch deren Mächtigkeit bestimmt. Wie tiefgehend die Detektion eines Schwel- oder Glimmbrandnestes gelingt, hängt aber in jedem Fall von dem Vermögen der Strahlungsthermometrie ab, die Temperaturverteilung aufzulösen. Dabei ist neben der thermischen Auflösung insbesondere die geometrische Auflösung entscheidend, das heißt die Fähigkeit, auch sehr kleine erwärmte Mündungsflächen von Wärmetransportkanälen aufzuspüren [2]. Da solche erhitzten Flächenelemente immer Bestandteil eines größeren Temperaturfeldes sind, das nur in Form eines Thermogrammes, d.h. durch die gleichzeitige Aufnahme einer großen Zahl von Meßpunkten erfaßt werden kann, ist es zweckmäßig, die Strahlungsthermometrie in Form einer Infrarot-Thermographie anzuwenden.

Die Technik der Infrarot-Thermographie ist seit langem verfügbar [3, 4]. Sie arbeitet mit einem Bandstrahlungs-pyrometer, d.h. mit einem Sensor, dessen Empfindlichkeit sich auf einen kleinen Teil des Infrarotbereichs des elektromagnetischen Spektrums beschränkt. Dieser Spektralbereich wird der Meßaufgabe angepaßt, wobei die zu berücksichtigende Temperatur des strahlenden Meßobjektes und die spektrale Durchlässigkeit des Zwischenmediums ausschlaggebend sind. Von Vorteil ist, daß durch die Wahl eines Spektralbereiches außerhalb des sichtbaren Lichtes die vom Meßobjekt ausgehende elektromagnetische Strahlung relativ ungestört empfangen werden kann. Damit läßt sich neben der Brandfrüherkennung grundsätzlich auch die zweite Brandschutzfunktion darstellen, die Unterstützung der Brandbekämpfung.

Für die Müllbunker-Thermographie kommen zwei alternative IR-Spektralbereiche in Betracht, ein "kurzwelliger" zwischen den Wellenlängen 2 und 5  $\mu\text{m}$  und ein "langwelliger" zwischen den Wellenlängen 8 und 12  $\mu\text{m}$ . Die bisherigen Realisierungen dieser Bereiche unterscheiden sich durch die jeweils eingesetzte Sensorkühlung. Im kurzwelligen Bereich ist bereits eine Betriebstemperatur, die nur 100 K unterhalb der Umgebungstemperatur liegt, ausreichend. Diese kann mit einer einfachen, wartungsarmen thermoelektrischen Kühleinrichtung aufrechterhalten werden, was relativ kostengünstige Systemlösungen erlaubt. Ein entsprechendes System ist erstmalig 1995 in einem Müllbunker installiert worden [5]. Wegen der knappen Kühlung des Sensors reicht dessen Empfindlichkeit nicht aus, um bei Umgebungstemperatur, also bei einem relativ niedrigen Temperaturniveau der Abfallschüttung, das Meßfeld thermisch so weit aufzulösen, daß eine Orientierung im Sinn der räumlichen Zuordnung der Meßobjekte möglich ist. Zur Überwindung dieses Defizites wird im Spektralbereich zwischen 0,4 bis 2  $\mu\text{m}$  mit Hilfe einer CCD-Kamera zusätzlich ein Videobild aufgenommen, das dem Thermogramm als Hintergrundbild beigelegt wird, eine Maßnahme, die allerdings im Brandfall durch Rauch und Wasserdampf stark beeinträchtigt ist.

Im alternativen, langwelligen Spektralbereich sind die hier bisher eingesetzten IR-Sensoren in der Regel deutlich ausgedehnter gekühlt worden. Man hat eine Betriebstemperatur aufrechterhalten, die 215 K unterhalb der Umgebungstemperatur liegt. Soll dies ausreichend praxistauglich durchgeführt werden, so ist die Verwendung eines relativ aufwendigen Stirling-Mikrokühlers erforderlich, dessen Standzeit zudem auf ca. 8600 h begrenzt ist, was im Vergleich zum thermoelektrisch gekühlten System zu höheren Systemkosten führt, deren Gegenwert allerdings das erzielbare hervorragende Auflösungsvermögen bildet. Das langwellige System ist bereits in mehreren großen Müllbunkern realisiert worden. Die erste Installation erfolgte 1991 [6]. **Bild 1** zeigt ein Beispiel der produzierten sogenannten Graustufen-Thermogramme. Es belegt, daß die erzielte thermische Auflösung bereits auf dem Niveau der Umgebungstemperatur so gut ist, daß die erforderliche räumliche Orientierung ohne weitere Hilfe sichergestellt werden kann.

Seit einigen Monaten stehen für die thermographische Brandfrüherkennung auch solche Systeme zur Verfügung, die, obwohl sie im langwelligen Spektralbereich arbeiten, dennoch ohne die sonst übliche, aufwendige Kühlung betrieben werden können. Es wird ein sogenannter Mikrobolometer-Array-Detektor verwendet, der das Thermogramm mit Hilfe einer sehr großen Zahl einzelner IR-Sensoren erzeugt. Da die in konventionellen Scanner-Systemen erforderlichen Schwingspiegelmechanismen und Chopper entfallen und da die nur geringfügige Kühlung in einfacher Weise thermoelektrisch erfolgen kann, ergeben sich grundsätzlich sehr wartungsarme und kostengünstige Lösungen. Die Leistungsfähigkeit solcher als radiometrische Temperaturmeßtechnik angebotenen Systeme soll erstmalig an den Brennstoffschüttungen großer Müllverbrennungsanlagen unter Beweis gestellt werden. Hierüber werden die nachfolgenden Seminarbeiträge berichten.

Da die Verfügbarkeit der Thermographietechnik bereits zu ersten Anwendungen in großen Restmüllbunkern veranlaßt hat, stellt sich die Frage, ob die Brandschutzziele ausreichend sicher erreicht werden. Es ist insbesondere zu klären, welche Restriktionen beherrscht werden müssen und welche Prüfkriterien anzuwenden sind, um die Wirksamkeit ausgeführter thermographischer Brandfrüherkennungssysteme zu beurteilen. Mit diesen Fragen sollen sich die folgenden Ausführungen unter besonderer Beachtung der alternative nutzbaren Spektralbereiche auseinandersetzen.

## 2 Auswirkung der zu berücksichtigenden Restriktionen

### 2.1 Unsicherheit der Vorgabe des Emissionsgrades des Abfallgemenges

Das als Strahlungsthermometer arbeitende Thermographiesystem schließt aus dem empfangenen und meßtechnisch bewerteten Strahlungsfluß, der von einem Meßobjekt ausgeht, auf dessen Temperatur. Dies gelingt allerdings nur dann, wenn bekannt und dem Strahlungsthermometer vorgegeben ist, mit welchem Emissionsgrad  $\epsilon$  das Meßobjekt Strahlung aussendet. Es stellt sich die Frage, bis zu welcher Fehlergrenze Abweichungen der gemessenen Temperaturwerte toleriert werden müssen, weil die unterschiedlichen Emissionsgrade der Komponenten des Abfallgemenges unbekannt sind, bzw. nicht differenziert berücksichtigt werden.

Bild 2 zeigt ein Thermogramm, das an einer Zusammenstellung ausgewählter Abfallgegenstände aufgenommen worden ist. Alle Objekte lagen auf einem horizontalen, 80 °C temperierten, schwarz lackierten Untergrund. Man erkennt eine Vielzahl unterschiedlicher Temperaturniveaus. Diese Unterschiede sind teilweise tatsächlich vorhanden, was sich mit Miniatur-Thermoelementen, die als Berührungsthermometer die Oberflächentemperatur erfassen, feststellen läßt. Die Ursache ist der unterschiedliche Wärmetransport, der sicherlich auch für die Verhältnisse an der Oberfläche einer Abfallschüttung charakteristisch ist. Ein großer Teil der in den Thermogrammen angezeigten Temperaturunterschiede ist jedoch nur scheinbar, also tatsächlich nicht vorhanden. Hier ist die Ursache die Vielfalt der vorhandenen Emissionsgrade, ein Umstand der näher untersucht worden ist.

Mit Hilfe mehrerer mit Emissionsgradstellern ausgerüsteter Bandstrahlungs-pyrometer und Thermographiesysteme sind die Emissionsgrade zahlreicher Abfallgegenstände ermittelt worden. Zu diesem Zweck war lediglich deren Oberflächentemperatur zu messen, was allerdings bei Schüttungen aus Humus, Sand oder Staub mit beachtlichen Schwierigkeiten verbunden ist. Zu deren Überwindung mußte mit Hilfe von Thermoelementen der innerhalb der jeweiligen Schüttungsschicht vorhandene Temperaturabfall aufgenommen werden, um daraus durch Extrapolation auf die Oberflächentemperatur zu schließen. Mit der auf diesem Weg gleichzeitig zu bestimmenden Wärmeleitfähigkeit der Staubschüttung konnte dann auch die Oberflächentemperatur dünn eingestaubter Abfallstoffe berechnet werden.

Es ist schließlich auch der Einfluß des gewählten Emissionsgrades auf die vom Thermographiesystem angezeigten Temperaturwerte ermittelt worden, und zwar für beide interessierenden Spektralbereiche. **Bild 3** betrifft das Beispiel Gips. Die folgenden Aussagen lassen sich daraus ableiten. Eine 10 % umfassende Abweichung des eingestellten  $\epsilon$ -Wertes vom wahren Wert führt in beiden Spektralbereichen gleichermaßen zu Temperaturabweichungen, die 2 K nicht überschreiten. Es wird allerdings auch die Gefahr, größeren  $\epsilon$ -Abweichungen zu unterliegen, deutlich. Immerhin unterscheiden sich die in den unterschiedlichen Spektralbereichen festgestellten Emissionsgrade um mehr als 10 %. Hätte man im kurzwelligen Bereich nicht  $\epsilon = 0,63$ , sondern den für den langwelligen Bereich geltenden Wert 0,89 benutzt, so hätte sich eine Temperaturanzeige ergeben, die 8 K zu niedrig ist.

**Tafel 1** gibt eine Übersicht über die insgesamt ermittelten Emissionsgrade, die im übrigen bevorzugt bei der als Alarmtemperatur in Frage kommende Temperatur von 70 °C aufgenommen worden sind. Es wird deutlich, daß die Emissionsgrade im langwelligen Bereich durchgängig größer sind als im kurzwelligen Bereich. Die sehr krassen Unterschiede, wie derjenige beim lackbeschichteten Konservendosendeckel, sind jedoch eher selten und insofern nicht typisch, als sie das Oberflächenbild z.B. einer Hausmüllschüttung nicht wesentlich prä-

gen. Hier sind Stoffe wie Humus, Sand und vor allem Staub maßgebender. Diese aber weisen in beiden Spektralbereichen einen nahezu gleichen, hohen Emissionsgrad auf. Insbesondere ist festzustellen, daß bereits eine dünne Staubschicht von 0,3 mm Dicke unabhängig vom Untergrund zu einem hohen Emissionsgrad zwischen 0,86 und 1 führt.

## 2.2 Störungen durch reflektierte Fremdstrahlung

Als sehr unangenehm und deshalb entsprechend kritisch einzuschätzen gilt die Gefahr der Auslösung eines Fehlalarms. Diese besteht in Form von Fremdstrahlung, die durch Reflexion zum Thermographiesystem gelangen kann. Ziel von Laborexperimenten war es, diese möglichen Reflexionen zu quantifizieren. Die dabei unter praxisferner "Mühewaltung" durch Reflexionen erzielbaren Störungen der wahren Temperaturverteilung waren in jedem Fall gering. So konnte mit Hilfe einer Müllbunkerleuchte und einer bezüglich des Müllbunkerbetriebes ungewöhnlich wirksamen Reflexionsebene, die sich auf Umgebungstemperaturniveau befand, im Thermogramm des benutzten kurzwelligen Systems ein Signal bewirkt werden, das als alarmauslösendes überhitztes Meßobjekt einzuschätzen ist, **Bild 4**; es zeigte sich aber auch, daß diese Störung mit wachsender Strahlungstrecke, die in diesem Fall von der Leuchte über die Reflexionsebene zum Sensor des Thermographiesystems führt, deutlich abnimmt. Offensichtlich ist dies eine Folge der begrenzten geometrischen Auflösung des Temperaturfeldes, ein Effekt, der in **Bild 5** erläutert wird. Er bedeutet, daß eine Fläche einheitlicher Temperatur vor einem niedriger temperierten Hintergrund erst oberhalb einer Mindestgröße ausreichend genau erfaßt wird. Bei einem zu kleinen Meßobjekt wird Hintergrundstrahlung miterfaßt, was zu einer erheblichen Abweichung des angezeigten Temperaturwertes führen kann [7]. Ausschlaggebend ist - dies läßt sich experimentell sehr einfach belegen - die Meßdistanz: Bei der Vergrößerung einer geradlinigen Entfernung zwischen Meßobjekt und IR-Sensor wächst die Temperaturabweichung sehr stark an, bis schließlich das Meßobjekt nicht mehr zu erkennen ist. Das bedeutet, daß die potentiell von reflektierter Fremdstrahlung ausgehende Gefahr durch eine unerwünschte Schwäche des Thermographiesystems deutlich gemildert wird.

In einem abschließenden, weiteren Experiment ist die Auswirkung einer kleinen Infrarot-Strahlungsquelle, die etwa einer glimmenden Zigarette vor einem auf 20 °C temperierten Hintergrund entspricht, untersucht worden, **Bild 6**. Die Temperatur dieser Strahlungsquelle von 500 °C ist durch ein aus 4 m Entfernung aufgenommenes Thermogramm sowohl im kurzwelligen als auch im langwelligen Spektralbereich erfaßt worden: Im Spektralbereich 3,0 bis 5,3 µm ergab sich 279 °C und im Spektralbereich 8 bis 14 µm 74 °C. In beiden Fällen war die geometrische Auflösung der Thermographie gleichermaßen unzureichend. Der kleinste auflösbare Meßfleck war größer als das Meßobjekt, d.h. das Meßergebnis war ein integraler Temperaturwert, der sowohl das hochtemperierte Meßobjekt als auch den niedrigtemperierten Hintergrund erfaßt. Die aus dem Meßfleck empfangene Strahlungsleistung war somit bei beiden Thermographiesystemen geringer als diejenige, welche aus einem gleichmäßig auf 500 °C temperierten Meßfleck zu empfangen wäre. Daß dabei die Meßwertabweichung im langwelligen Spektralbereich deutlich größer ausfällt als im kurzwelligen Spektralbereich, ist eine Folge der unterschiedlichen Temperaturkontraste. Eine Erläuterung liefert **Bild 7**. Hier werden die in den benutzten Spektralbereichen von einem Schwarzen Strahler in Abhängigkeit von der Temperatur abgegebenen Strahlungsleistungen als Flächen dargestellt und verglichen. Die Gegenüberstellung der schraffierten Flächen macht deutlich, daß die Strahlungsleistung einer Potenzfunktion folgend progressiv mit der Strahlertemperatur ansteigt und daß dieser progressive Anstieg im kurzwelligen Spektralbereich wesentlich ausgeprägter erfolgt. Während z.B. bei den Temperaturen 20 °C und 70 °C die jeweiligen Verhältnisse der Strahlungsleistungen in beiden Spektralbereichen klein und nahezu gleich sind, ergeben sich bei der Kombination der Temperaturen

20 °C und 500 °C sehr unterschiedliche Flächenverhältnisse. Dabei erreicht das Verhältnis im kurzwelligeren Bereich den sehr hohen Wert von 565.

Daß der Temperaturkontrast bei hohen Temperaturen deutlich unterschiedlich ausfällt, bedeutet, daß eine Reduzierung der vom IR-Meßsystem empfangenen Strahlungsleistung im kurzwelligen Spektralbereich zu einer geringeren Temperaturabweichung führt als im langwelligen Spektralbereich. Dies ist ein beachtlicher Vorteil der kurzwelligen Meßsysteme, der zur Folge haben kann, daß bei einer unzureichenden geometrischen Auflösung die Meßabweichung tolerierbar klein bleibt. Was allerdings die Reflexion der von einem hochtemperierten Störstrahler ausgehenden Fremdstrahlung betrifft, so kann sich die im kurzwelligen Spektralbereich als Folge des günstigen Temperaturkontrastes gegebene, ausgeprägte Empfindlichkeit als deutlicher Nachteil erweisen.

### 2.3 Extinktion der Meßstrahlung im Zwischenmedium

Der wesentliche Vorteil der Infrarot-Strahlungsthermometrie ist, daß die Temperatur berührungsfrei ermittelt wird. Dies ist möglich, weil die zwischen dem Meßobjekt und dem Infrarot-Sensor ausgetauschte Strahlung als Meßsignal genutzt werden kann. Voraussetzung ist jedoch, daß die Strahlungsdichte durch das Zwischenmedium nicht unzulässig geschwächt wird. Eine solche, Extinktion genannte Schwächung ergibt sich, wenn absorbierende und streuende Komponenten das Transmissionsvermögen des Zwischenmediums einschränken. In der Müllbunkeratmosphäre kommen Wasserdampf, Kohlendioxid und Aerosole, insbesondere Staub, Wasserdampf und Rauch, in Betracht, deren Wirkung von der Konzentration und der Länge der belasteten Strahlungstrecke abhängt.

Der durch Kohlendioxid und Wasserdampf verursachten Absorption trägt die praktische Strahlungsthermometrie durch die Wahl eines geeigneten Spektralbereiches - ein sogenanntes atmosphärisches Fenster - Rechnung. Bei Temperaturen  $< 200^{\circ}\text{C}$  eignet sich hierfür der Spektralbereich 8 bis 12  $\mu\text{m}$  nahezu uneingeschränkt [4, 5]. Im alternativen Spektralbereich 2 bis 5  $\mu\text{m}$  dagegen ist eine Schwächung der spektralen Strahlungsdichte zu berücksichtigen [4, 5]. Das kann durch rechnerische Eliminierung der distanzabhängigen Absorption immer dann erfolgen, wenn die  $\text{CO}_2$ - und  $\text{H}_2\text{O}$ - Konzentrationen konstant und bekannt sind [4]. Es ist in diesem Fall auch möglich, die Absorption des Zwischenmediums durch eine Senkung des dem Strahlungsthermometer vorzugebenden Emissionsgrades des Meßobjektes zu kompensieren. Bezüglich eines Brandfalles sind diese Maßnahmen jedoch wegen der hohen und unbekannt, in der Müllbunkeratmosphäre vorhandenen  $\text{H}_2\text{O}$ - und  $\text{CO}_2$ - Konzentrationen in Frage zu stellen.

Was die für den Müllbunkerbetrieb besonders relevante Extinktion durch Staub betrifft, so sind beide Spektralbereiche gleichermaßen betroffen. Dies belegt ein mit **Bild 8** erläutertes Experiment, das an einer künstlich erzeugten Wirbelschicht aus feinem Müllbunkerstaub durchgeführt worden ist. Der hier benutzte "Schwarze Strahler" von 70 °C bewirkt wegen der Schwächung der Strahlungsdichte ein Signal, das rund 20 K zu niedrig ist. Ähnliche Beobachtungen sind auch vor Ort, d.h. im Müllbunker selbst, mehrfach gemacht worden. Ein typisches Ergebnis ist, daß das zufällige Auftreten einer Staubwolke geringer Konzentration auf einer 20 m langen Strahlungstrecke den angezeigten Temperaturwert eines Thermographiesystems unabhängig vom benutzten Spektralbereich um bis zu 15 K absenkt. Dies ist auch in Betracht zu ziehen, wenn wegen der Unsicherheit absoluter Temperaturwerte zur Unterstützung der Aussage die zeitliche Veränderung der Temperatur im Rahmen einer Temperatur-Trendanalyse erfaßt wird. Diese Meßstrategie kann zusätzlich zur thermographischen Brandfrüherkennung

beitragen, muß aber ebenfalls die zufällige Auswirkung von Staubwolken berücksichtigen, denn es ist durchaus möglich, daß die Temperatur an der Oberfläche der Abfallschüttung kurzfristig steigt, während die Temperaturanzeige des Thermographiesystems wegen einer zunehmenden Staubbelastung des Zwischenmediums sinkt.

Tritt ein Brandfall ein, so wird der Raum oberhalb der Schüttung durch Verbrennungsgase, insbesondere  $H_2O$  und  $CO_2$ , sowie durch Rauchaerosole, insbesondere Rußpartikel und Wasserdampf, belastet. Das grundsätzliche Vermögen der IR-Meßtechnik, die dann undurchsichtige Atmosphäre zumindest teilweise so zu durchdringen, daß wesentliche Komponenten wie die Wände, die Konturen der Schüttung, der Krangreifer, das Löschmittel und der Brandherd erkennbar werden, ist natürlich eine willkommene Funktion. Die Frage in welchem Spektralbereich diese Unterstützung der Brandbekämpfung besser gelingt, war Gegenstand einer experimentell gestützten vergleichenden Beurteilung [10]. Deren Ergebnis ist:

- Der bei hohem Temperaturniveau im kurzwelligen Spektralbereich gegebene sehr günstige Temperaturkontrast reicht nicht aus, um die hier vorhandene Extinktion der IR-Strahlung zu kompensieren.
- Die Extinktion wird nicht nur durch Absorption, insbesondere an gasförmigem  $H_2O$  und  $CO_2$ , sondern auch durch Streuung der IR-Strahlung an den Aerosolen Wasserdampf und Rauchpartikel bewirkt.
- Im kurzwelligen Spektralbereich ist die Extinktion, auch bei hohen Temperaturen, deutlich ausgeprägter als im langwelligen Spektralbereich.
- Der Beitrag der langwelligen IR-Thermographie zur Brandbekämpfung im Müllbunker ist deutlich effizienter als derjenige der kurzwelligen IR-Thermographie.

#### 2.4 Begrenzung des Wärmetransportes in der Abfallschüttung

Da sich Brände auch aus im Inneren der Abfallschüttung vorhandenen Schwelbrand- oder Glimmbrandnestern entwickeln können, ist es eine wesentliche Aufgabe der Brandfrüherkennung, die an der Schüttungsoberfläche auftretenden Hinweise rechtzeitig zu erfassen. Ein sehr sicherer Hinweis ist in jedem Fall der Anstieg der Oberflächentemperatur und damit ein thermographisch meßbares Signal. Dieses kommt aber nur dann zustande, wenn ein ausreichender Wärmetransport vorhanden ist, das heißt, wenn die wärmedämmende Wirkung der das Schwel- oder Glimmnest überdeckenden Abfallschicht nicht zu groß ist. Experimentelle Untersuchungen belegen, daß der durch Wärmeleitung bewirkte Wärmetransport nahezu wirkungslos ist und deshalb die Temperatur selbst in dünnen Schichten so weit abfällt, daß im Temperaturfeld an der Oberfläche keine Spuren mehr zu erkennen sind. Eine deutliche Beeinflussung des Oberflächentemperaturfeldes ergibt sich erst dann, wenn Konvektion als zusätzlicher Transportmechanismus auftritt, das heißt, wenn Wärme durch Luft, Wasserdampf und gasförmige Verbrennungs- oder Pyrolyseprodukte transportiert wird, die an die Oberfläche diffundieren.

Der in **Bild 9** beschriebene Brandversuch betrifft ein durch Autooxidation entstandenes endogenes Brandnest, das sich bis zum Oberflächenbrand ausdehnt. Man erkennt, daß wegen des großen Temperaturgradienten, der als Folge des Wärmetransportwiderstandes  $12 \text{ K/cm}$  und mehr beträgt, die Oberflächentemperatur zunächst weitgehend unbeeinflusst bleibt, daß diese dann jedoch mit der Ausdehnung des Brandnestes ansteigt und man schließlich mit der Wahrnehmung von  $70 \text{ °C}$  an der Oberfläche über eine Alarmschwelle verfügt, die 40 Minuten vor dem Beginn des Oberflächenbrandes erreicht wird.

Mit **Bild 10** wird ein weiteres Experiment beschrieben, das mit einem elektrischen Heizkörper und verschiedenen Sägemehlschüttungen unterschiedlicher Porosität durchgeführt worden ist. Die Porosität  $\psi$  ist als relatives Lückenvolumen definiert. Der Wert  $\psi = 0,83$  entspricht in gu-

ter Näherung dem 1993 in Deutschland registrierten Mittelwert des in den Abfallbehältern gesammelten Hausmülls. Der in einem Müllbunker gelagerte Restmüll weist niedrigere, bis etwa  $\psi = 0,5$  reichende Werte auf. Es zeigt sich im Experiment, daß der überdeckte Heizkörper erst dann die Temperatur an der Oberfläche der Schüttung gut erkennbar beeinflusst, wenn die Heizkörpertemperatur bis auf ca. 350 °C erhöht wird. Bei dieser Temperatur wird eine Verbrennungsreaktion und damit auch ein Wärme transportierender Stoffstrom ausgelöst, dessen Wirkung offensichtlich mit steigender Porosität größer wird.

Die Wirkung des Stofftransportes läßt sich mit einem weiteren Experiment bestätigen, welches mit nichtbrennbaren hochporösen Glaswollschichten ( $\psi \approx 1$ ) durchgeführt worden ist. Aus **Bild 11**, welches die meßtechnisch ermittelten Ergebnisse wiedergibt, erkennt man, daß immer dann, wenn anstelle des auf 450 °C temperierten elektrischen Heizkörpers schwelendes Sägemehl der gleichen Temperatur die überdeckte Wärmequelle bildet, wegen des konvektiven Wärmetransportes die Oberflächentemperatur deutlich stärker beeinflusst wird.

Die Auswertung des in Bild 11 beschriebenen Experimentes bietet schließlich eine weitere, sehr wichtige Aussage:

An der Oberfläche der porösen Schicht trifft man ausgeprägte Temperaturgradienten an. In einem Flächenelement von nur 4 cm<sup>2</sup> unterschieden sich die im Experiment festgestellten Maximalwerte der Oberflächentemperatur um bis zu 8 K von dem jeweils geltenden Mittelwert. Dies weist darauf hin, daß zur Erkennung örtlicher Maximaltemperaturen eine hohe geometrische Auflösung des Temperaturfeldes erforderlich ist.

### 3 Überprüfung der Wirksamkeit installierter Thermographiesysteme

#### 3.1 Definition einer Prüfplatte

Die Wichtigkeit der Schutzziele, derentwegen das Thermographiesystem beim Betrieb eines Müllbunkers angewendet wird, veranlaßt, die notwendige Überprüfung der tatsächlich erreichten Wirksamkeit mit besonderer Sorgfalt durchzuführen. Wegen der Komplexität des zu installierenden Systems einerseits, und wegen der Unzumutbarkeit einer an den Anwender gerichteten Forderung nach extensivem Detailwissen andererseits, ist es sinnvoll, diese Aufgabe möglichst ganzheitlich zu lösen. In diesem Sinne ist es zweckmäßig, sich eines Prüfkörpers zu bedienen, mit welchem bei einer ersten Validierung oder bei den sich wiederholenden sicherheitstechnischen Prüfungen ein erhitzter Bereich im Müllbunker simuliert wird und die Funktionserfüllung des Gesamtsystems nachgewiesen werden kann. Nachdem in [1 und 2] der Einsatz eines derartigen Prüfkörpers bereits empfohlen worden ist, stellt sich hier abschließend die Frage nach dessen Gestaltung.

Geht man davon aus, daß die Hauptfunktion des Thermographiesystems darin besteht, das auf der Oberfläche der Abfallschüttung vorhandene Temperaturfeld zu erfassen, so ist es konsequent, die Prüfung mit Hilfe eines definiert temperierten Flächenelementes vorzunehmen, welches als Bestandteil der Oberfläche plaziert wird. Es ist somit eine Prüfplatte und nicht etwa ein räumliches Gebilde, wie es in [11] diskutiert wird, erforderlich. Verwendet man eine Kugel, einen Zylinder oder einen Kubus, so werden Flächenrichtungen außerhalb derjenigen der Schüttungsoberfläche angeboten. Es entsteht eine "Positionsleuchte", die zu leicht zu erkennen ist und deshalb nicht die notwendige Prüfstrengung aufweist. Diesbezüglich ist im übrigen auch bei der Prüfplatte darauf zu achten, daß deren Positionierung zum Zwecke der Absicherung des Prüfergebnisses möglichst ungünstig erfolgt, d.h. mit möglichst ungünstiger Distanz und Blickrichtung. Eine entsprechende quadratische Prüfplatte ist entwickelt und erprobt worden

[12]. Sie wird elektrisch beheizt, und die Temperatur der weitgehend isothermen Oberfläche wird mit einem kalibrierten elektrischen Widerstandsthermometer erfaßt. Der Emissionsgrad beträgt 0,96 im langwelligen und 0,93 im kurzwelligen Spektralbereich. Es lassen sich beliebig wählbar sowohl konstante Temperaturen als auch Aufheizraten einstellen, letzteres zum Zwecke der Überprüfung von Trendanalysen.

### 3.2 Prüfungsbeispiele

Mit Hilfe der beschriebenen Prüfplatte sind in neun großen Müllbunkeranlagen die dort bereits fest installierten Thermographiesysteme überprüft worden. Es handelte sich um vier verschiedene Systeme, ein langwelliges und drei kurzwellige. **Tafel 2** gibt ein Beispiel der ermittelten Prüfergebnisse wieder. Es betrifft das langwellige System, dessen Sensor mit einem Sterling-Mikrokühler gekühlt wird [6].

Das für eine Systembewertung deutlich wichtigste Kriterium ist die geometrische Auflösung des zu erfassenden Temperaturfeldes. Zusätzlich ist aber auch die Prüfung wichtig, ob sich Alarmschwellen sicher darstellen lassen, das heißt, ob das Thermogramm ausreichend genau an die Temperaturskala angebunden ist. Zu diesen Prüfkriterienkombinationen werden in [1] Erwartungen mitgeteilt, daß unter realen Bedingungen, d.h. bei ausreichend großem Blickfeld und ausreichend großer überwindener Meßdistanz die Temperatur eines isothermen Meßobjektes, dessen Oberfläche 5 cm x 10 cm beträgt, mit einer Fehlergrenze von 5 K an der Oberfläche der Abfallschüttung detektiert wird, so daß bei Erreichen eines vorgegebenen Schwellenwertes - es wird 70 °C empfohlen - der erforderliche Alarm ausgelöst werden kann. Bei Vorversuchen, die unter Laborbedingungen durchgeführt wurden, ergab sich, daß keines der derzeit verfügbaren Systeme einer solchen Qualitätsanforderung entsprechen kann. Diese ist jedoch weitgehend willkürlich gestellt, so daß eine Reduzierung nicht zugleich eine Mißachtung des Schutzzieles bedeuten muß. Unter Berücksichtigung des technisch Machbaren könnte man deshalb als kleinsten aufzulösenden Meßfleck die Fläche von 30 cm x 30 cm wählen und eine Fehlergrenze von 5 K bei der Temperaturbestimmung festlegen. Der solchermaßen reduzierten Vorgabe konnte das in **Tafel 2** beurteilte System entsprechen, dies auch bei einer großen Meßdistanz und bei einem sehr großen, durch die Blickwinkel 30° und 40° gekennzeichneten Blickfeld.

Ausschlaggebend für eine vergleichende Beurteilung sollte nicht die absolute, sondern die vielmehr die relative geometrische Auflösung sein, d.h. das Verhältnis der kleinsten detektierbaren Meßfläche  $A$  zum gesamten Blickfeld FOV. Diesbezüglich zeigte sich, daß das hier angeführte Beispiel unter allen untersuchten Systemen die deutlich höchste Qualität aufwies.

## Literatur

- [1] Katzer, H. und von Borries, W.: Frühzeitige Erkennung von Brandentwicklungen im Abfallbunker. VGB Kraftwerkstechnik 74 (1994) H. 10, S. 873 - 874
- [2] von Borries, W. und Katzer, H.: Vermeidung von Bunkerbränden in Abfallverbrennungsanlagen mit Hilfe der Infrarot-Thermographie. Materialien Nr. 8, Essen: Landesumweltamt Nordrhein-Westfalen (Hrsg.) 1995
- [3] VDI/VDE -Gesellschaft für Meß- und Automatisierungstechnik (Hrsg.): Technische Temperaturmessung, Strahlungsthermometrie. VDI/VDE-Richtlinie 3511, Blatt 4, Berlin: Beuth Verlag 1995
- [4] Walther, L. und Gerber, D.: Infrarotmeßtechnik. 2. Aufl. Berlin: VEB Verlag Technik 1983
- [5] Kaiser, P.: IR-Thermographie in Müllbunkern mit kurzwelligen Kameras. Abfallwirtschafts Journal (1996), H. 4, S. 34-38
- [6] Ewert, T.: Brände in Müllbunkern erkennen. TÜ 35 (1994) Nr. 10 S. 404 - 409
- [7] Bücher, R.: Infrarotsichtgeräte und Wärmebildkameras. Brandschutz/Deutsche Feuerwehr-Zeitung (1992) Nr. 8 S. 514 - 521
- [8] Breuckmann, B.: Bildverarbeitung und optische Meßtechnik in der industriellen Praxis. München: Franzis-Verlag 1993
- [9] Baehr, H. D. und Stephan, K.: Wärme- und Stoffübertragung. Berlin: Springer 1994
- [10] Braun, R. und Weidener, H.: Experimentell gestützte vergleichende Beurteilung der alternativen Verwendung der langwelligen oder der kurzwelligen IR-Thermographie zur Unterstützung der Brandbekämpfung in Restmüllbunkern. Bericht über eine im Auftrag der Von Roll Umwelttechnik AG durchgeführte Untersuchung. FH Gelsenkirchen Okt. 1997
- [11] Brand, B.: Erfahrungen aus Abnahmeversuchen an Müllbunker-Überwachungssystemen mittels IR-Kamera. VGB Kraftwerkstechnik 78 (1998), H. 1, S. 64-70
- [12] Braun, R. und Weidener, H.: Früherkennung von Bunkerbränden mit Hilfe der IR-Thermographie - Restriktionen und Validierung. VGB Kraftwerkstechnik 77 (1997), H. 12, S. 1047-1052



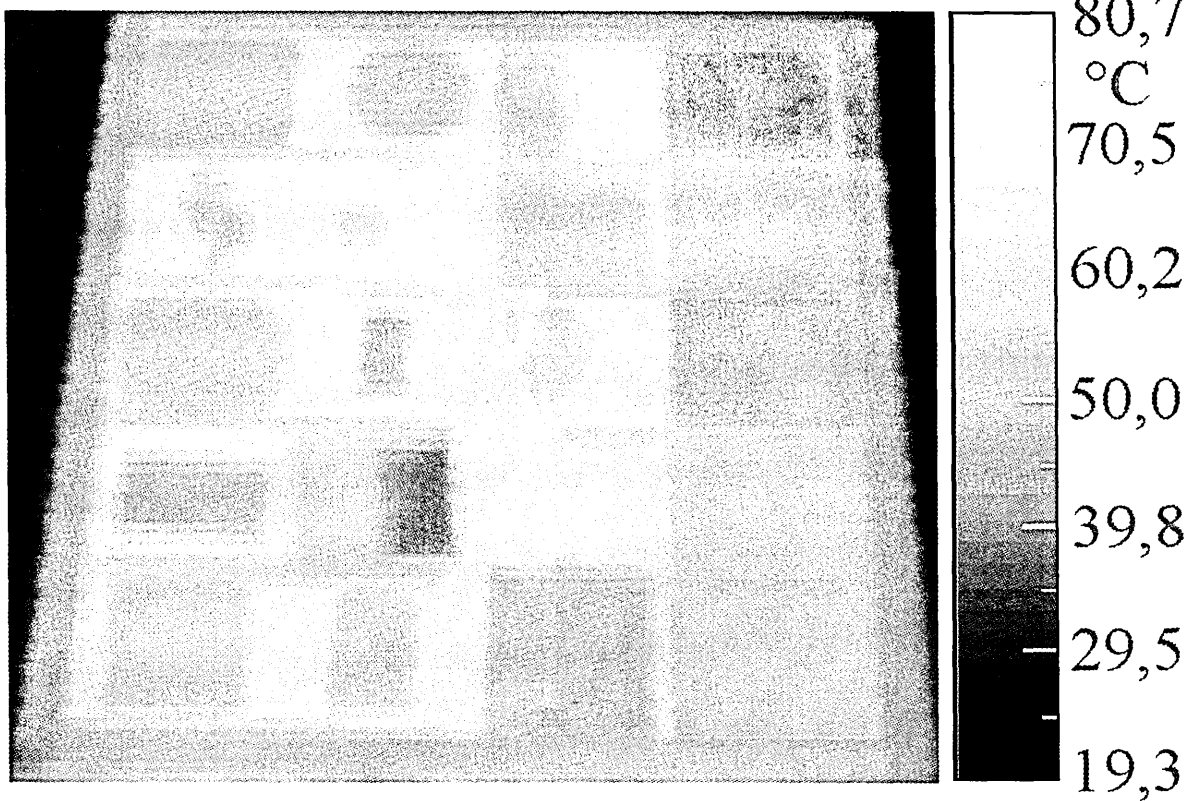
**Bild 1.** Graustufen-Thermogramm der Schüttungsfläche eines Hausmüllbunkers einschließlich der Abkippstellen;

System:

IMUS, Hörotron GmbH, Elmshorn;

IR-Meßtechnik:

740/760 Radiometer Inframetrics, Spektralbereich 8 - 12  $\mu\text{m}$



<b>Teppichboden</b> Polyamidfaser  $t_0 = 69,4 \text{ } ^\circ\text{C}$	<b>Konservendosen- deckel</b> weißlackiert mit Lack auf Wasserbasis  $t_0 = 71,9 \text{ } ^\circ\text{C}$	<b>blauer Müllsack</b> PE-LD, auf blankem Al- und auf geschwärztem Untergrund  $t_0 = 72,9 \text{ } ^\circ\text{C}$	<b>Müllbunkerstaub</b> aus dem Bereich des oberen Bunkerrandes $s \approx 5 \text{ mm}$
<b>PU-Schaum</b> grobe Struktur  $t_0 = 60,4 \text{ } ^\circ\text{C}$	<b>Hart-PVC</b> grau  $t_0 = 60,4 \text{ } ^\circ\text{C}$	<b>weißes Papier</b> Cellulose, $80 \text{ g/m}^2$  $t_0 = 71,9 \text{ } ^\circ\text{C}$	<b>Humus</b> entnommen aus Gartenabfällen $s \approx 5 \text{ mm}$
<b>Gips</b> weiß  $t_0 = 69,4 \text{ } ^\circ\text{C}$	<b>Al-Platte</b> oxidiert  $t_0 = 67,3 \text{ } ^\circ\text{C}$	<b>Karton</b> farbig  $t_0 = 68,5 \text{ } ^\circ\text{C}$	<b>Sägemehl</b> grobe Struktur $s \approx 5 \text{ mm}$
<b>Verbundverpackung</b> 75% Cellulose 5% Al-Folie 20% PE-Folie $t_0 = 73,7 \text{ } ^\circ\text{C}$	<b>Weißblech</b> hochglänzend, zur Hälfte eingestaubt  $t_0 = 73,8$	<b>PE-HD-Folie</b>  $t_0 = 69,9 \text{ } ^\circ\text{C}$	<b>Reinsand</b> 0,1-0,5 mm Körnung $s \approx 5 \text{ mm}$
<b>Keramik-Fliese</b> hellgraue Oberfläche  $t_0 = 71,1 \text{ } ^\circ\text{C}$	<b>Blei-Platte</b> oxidiert  $t_0 = 73,1 \text{ } ^\circ\text{C}$	<b>Polyätherschaum</b> Polsterschaumstoff  $t_0 = 48,0 \text{ } ^\circ\text{C}$	<b>Sepeolith-Mineral</b> Katzenstreu $s \approx 5 \text{ mm}$

**Bild 2.** Graustufen-Thermogramm ausgewählter Komponenten des Abfallgemenges; den horizontalen Untergrund bildet eine auf  $80 \text{ } ^\circ\text{C}$  temperierte schwarze Platte; Spektralbereich  $3,0$  bis  $5,3 \text{ } \mu\text{m}$  (Avio, TVS 2000 Nippon Avionics),  $t_0$  gibt die mit Miniatur-Thermoelementen gemessene Oberflächentemperatur an

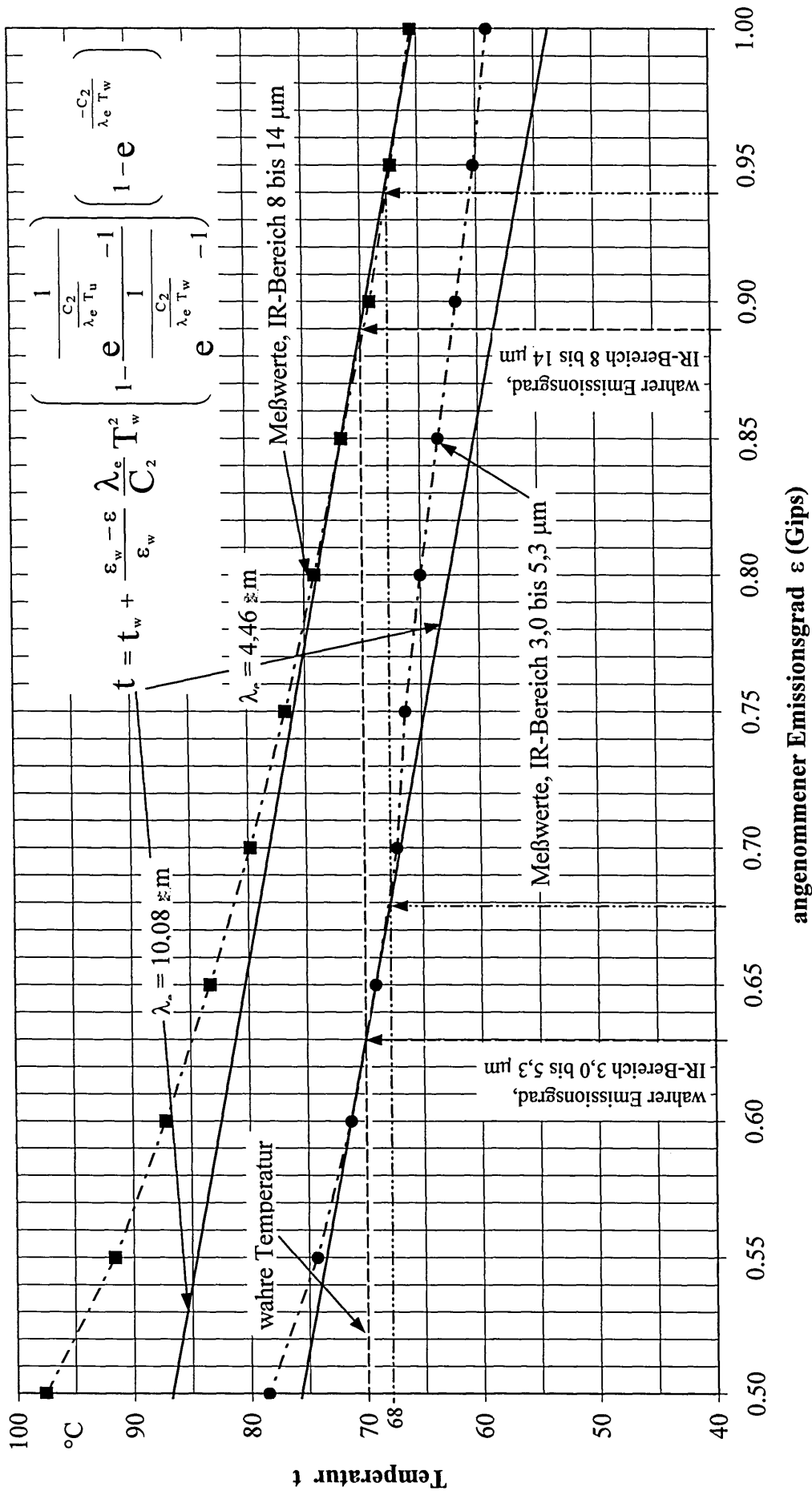


**Bild 3.** In den Wellenlängenbereichen 3,0 bis 5,3 μm (●) und 8 bis 14 μm (■) gemessene, bzw. nach [3] berechnete Abhängigkeit der Temperatur t vom angenommenen Emissionsgrad ε für Gips

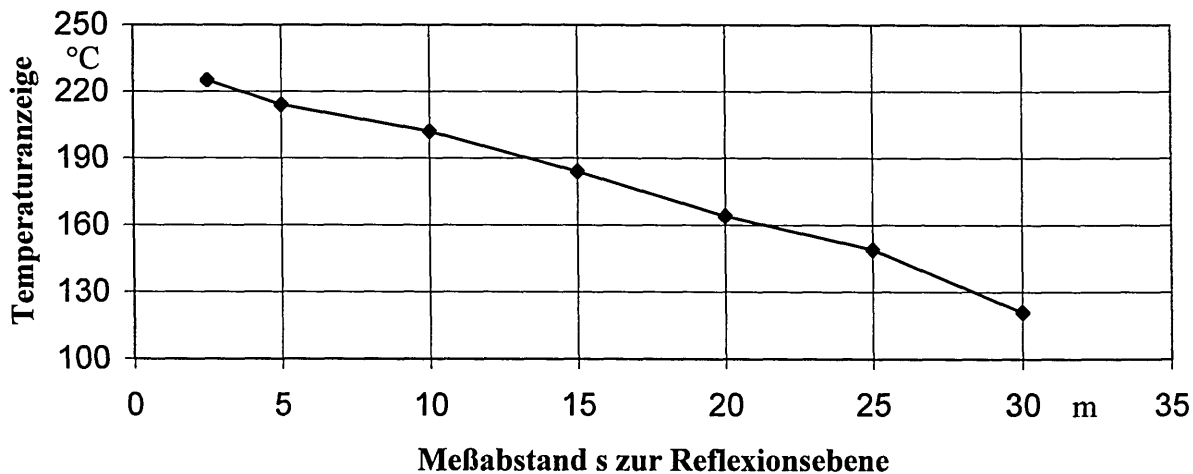
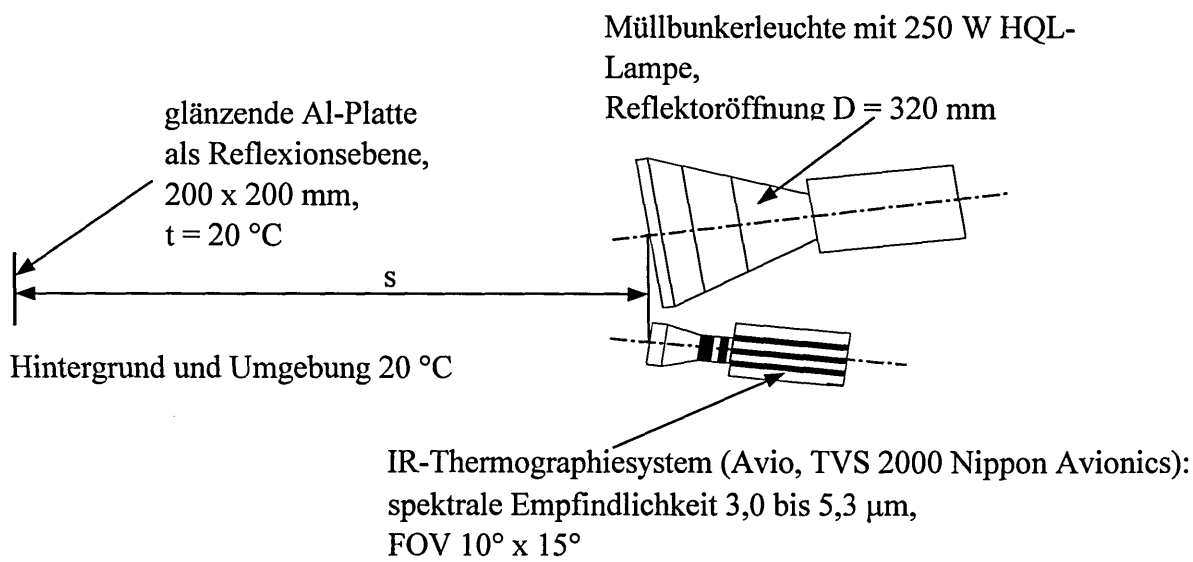


**Bild 4.** Experimentelle Ermittlung des distanzabhängigen Einflusses einer reflektierten Störstrahlung

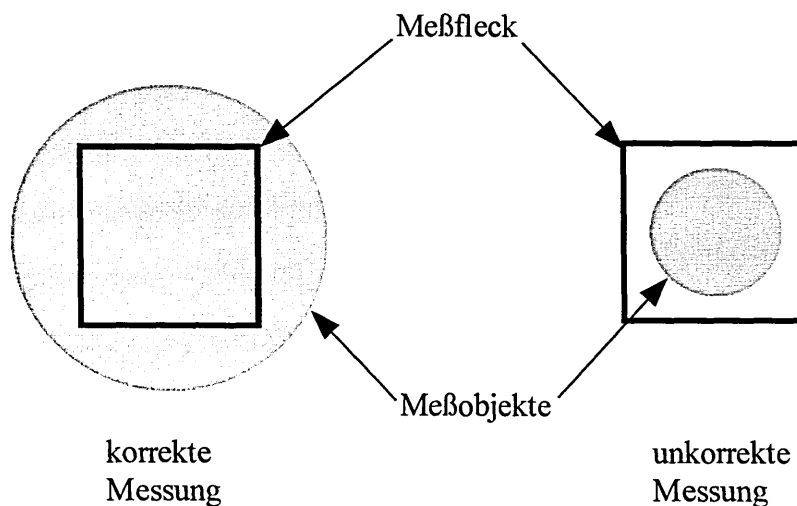


**Bild 5.** Mögliche systematische Abweichung des gemessenen vom wahren Temperaturwert als Folge einer nicht ausreichenden geometrischen Auflösung [8]

Schwarzer Strahler Emissionsgrad  $\epsilon \approx 1$   
Durchmesser 30 mm, 500 °C

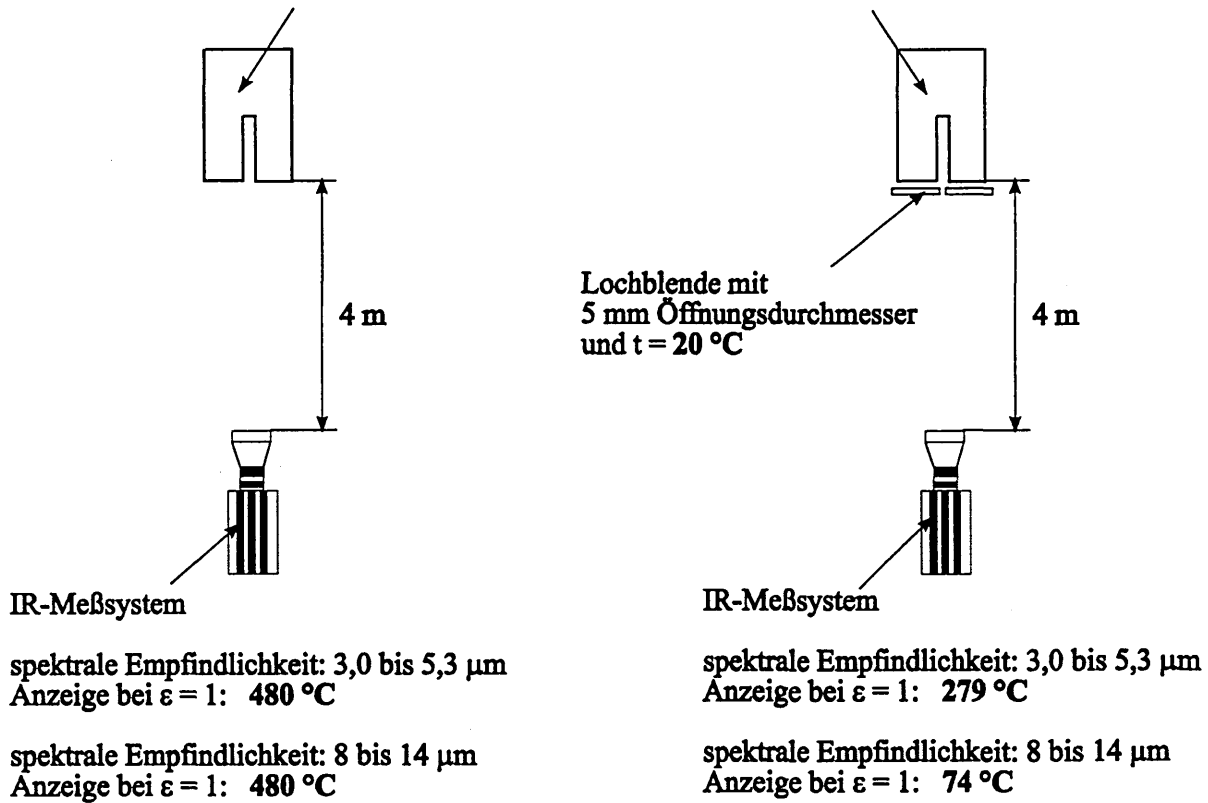
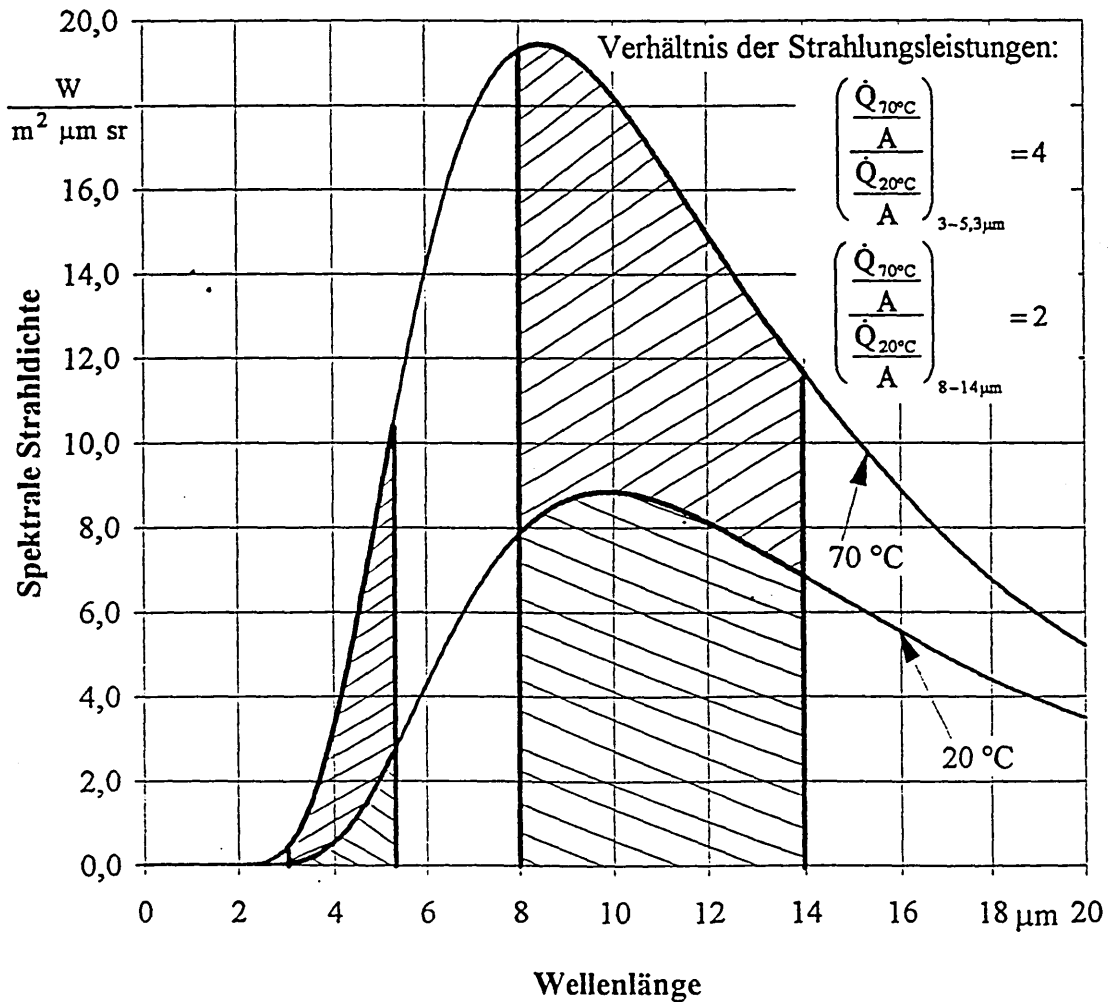
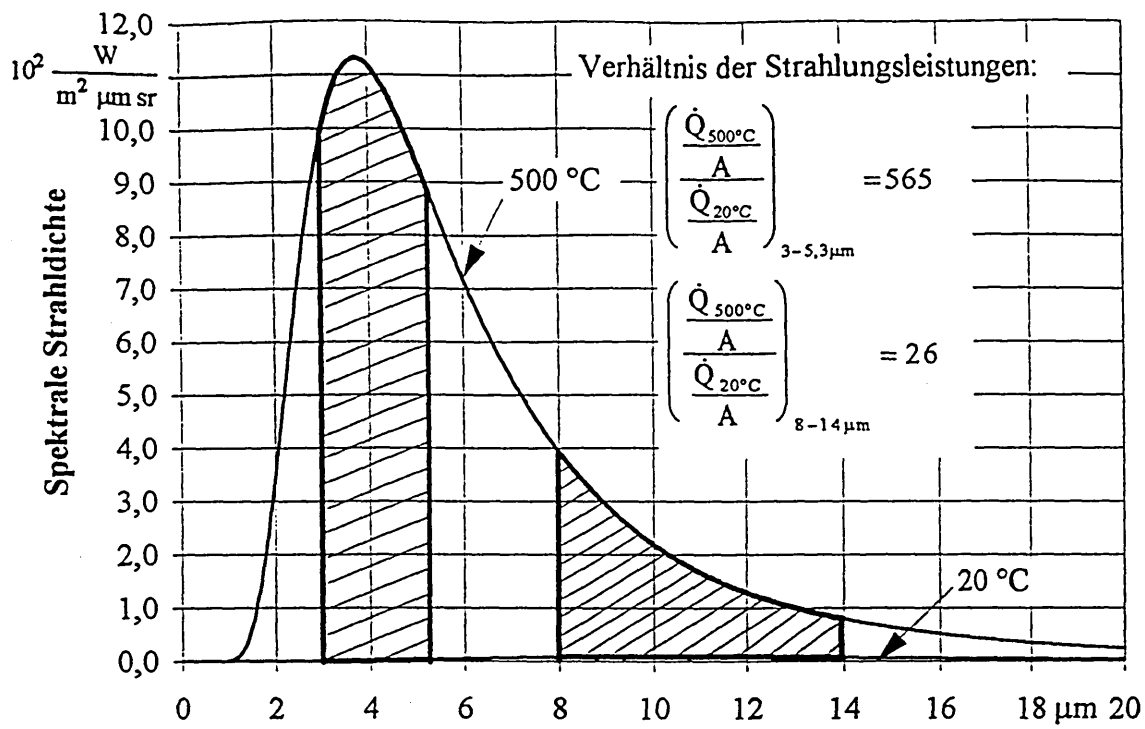
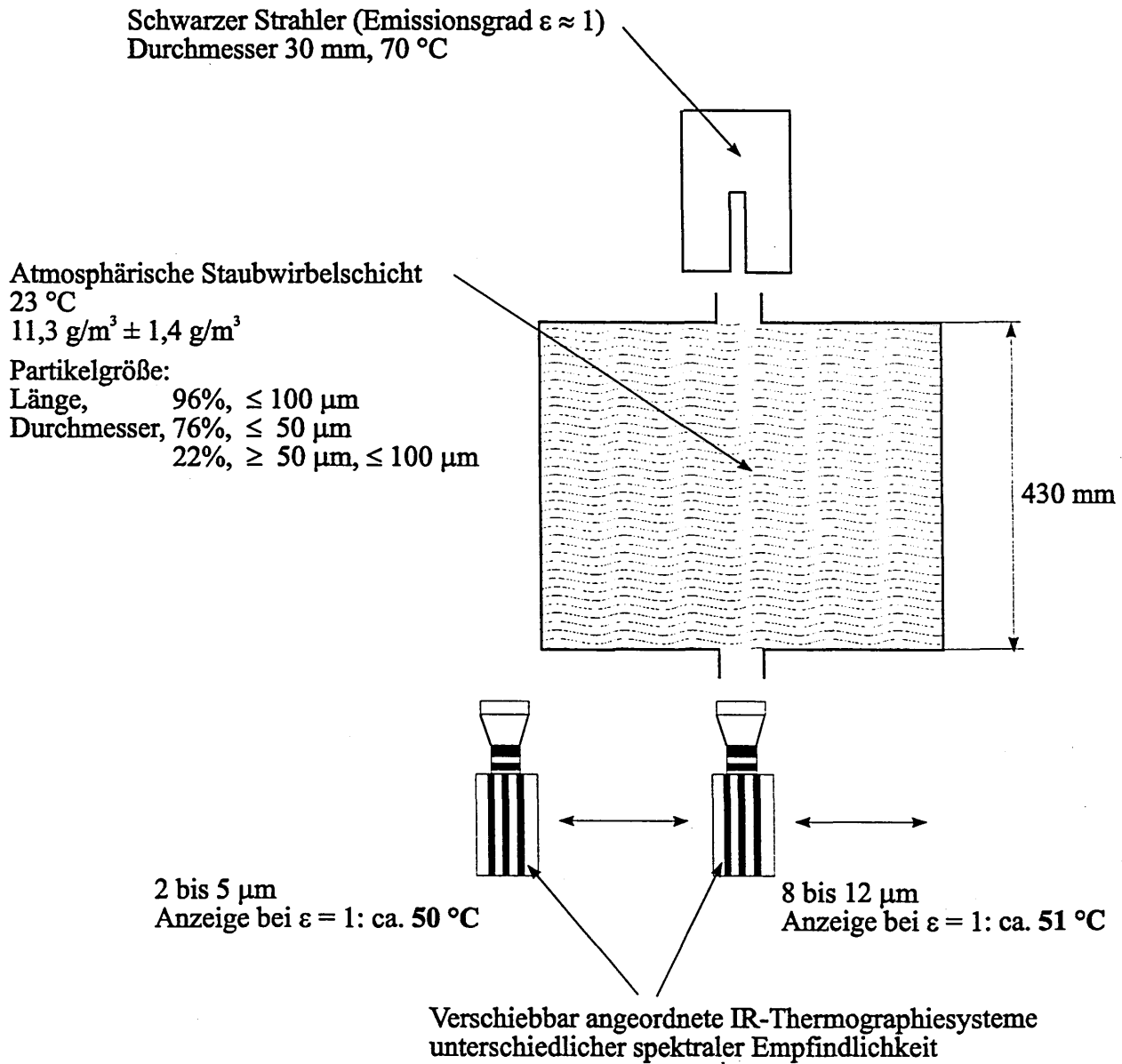


Bild 6. Auswirkung eines "Störfleckes" von 500 °C innerhalb eines deutlich größeren Meßfleckes von 20 °C auf die Temperaturanzeige unterschiedlicher Bandstrahlungs-pyrometer



**Bild 7.** Spektrale Strahllichte eines Schwarzen Körpers bei verschiedenen Temperaturen [9]; die schraffierten Flächen betreffen die von den zwei zu vergleichenden Bandstrahlungspyrometern (3 bis 5,3  $\mu\text{m}$  und 8 bis 14  $\mu\text{m}$ ) jeweils empfangenen Strahlungsleistungen



**Bild 8.** Experimentelle Ermittlung der durch Absorption der IR-Strahlung in aufgewirbelten Müllbunkerstaub bewirkten Abweichung des angezeigten Temperaturwertes vom wahren Wert.  
Spektrale Empfindlichkeit der benutzten IR-Thermographiesysteme:  
2 bis 5 µm (Agema IS THV 900 SW/TE) und 8 bis 12 µm (Agema IS THV 900 LW/ST)

Schüttung:  
Sägespäne 2 mm bis 4 mm  
 $\psi = 0,83$

Schüttungskern:  
Sägespäne 0,5 mm bis 1 mm  
 $\psi = 0,64$   
getränkt mit Leinöl

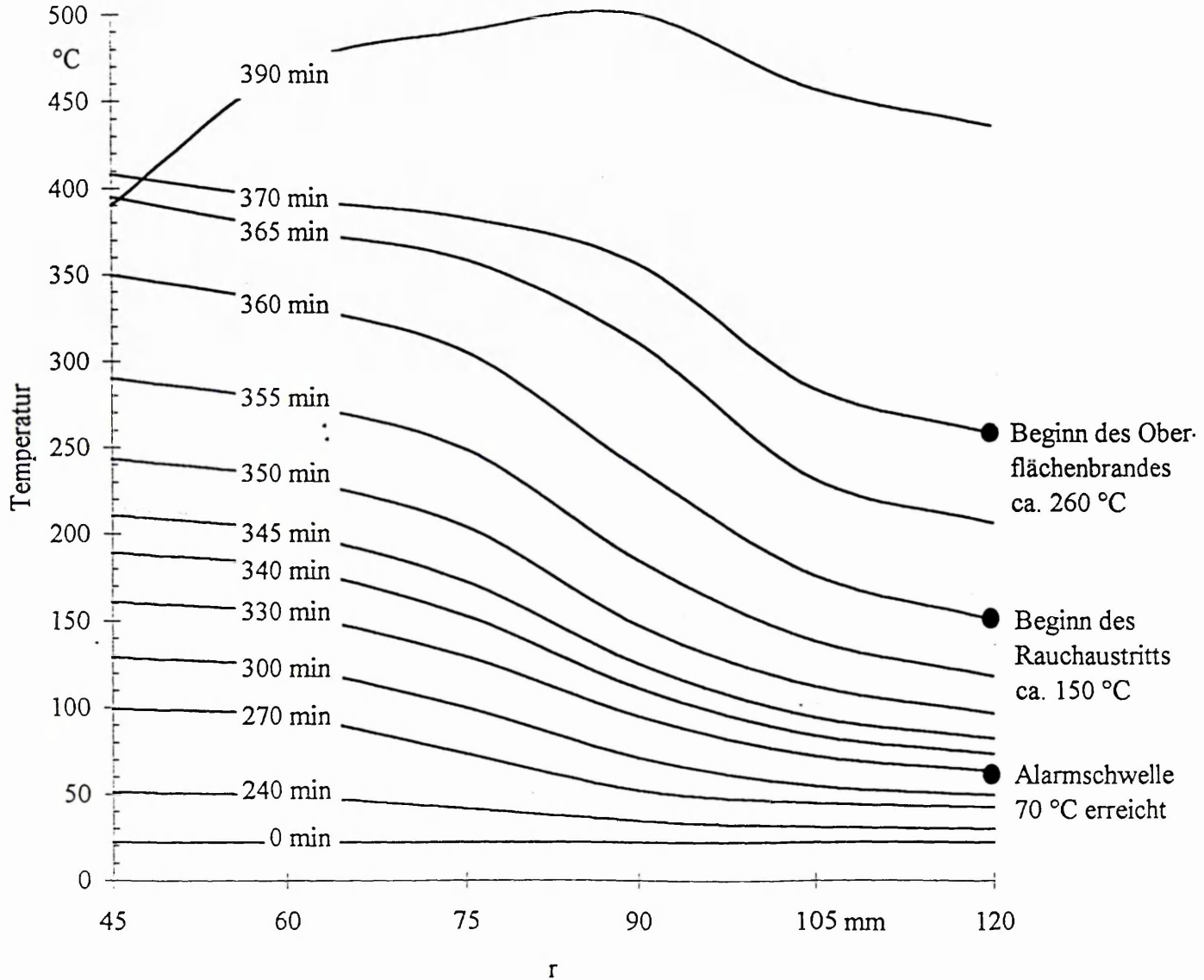
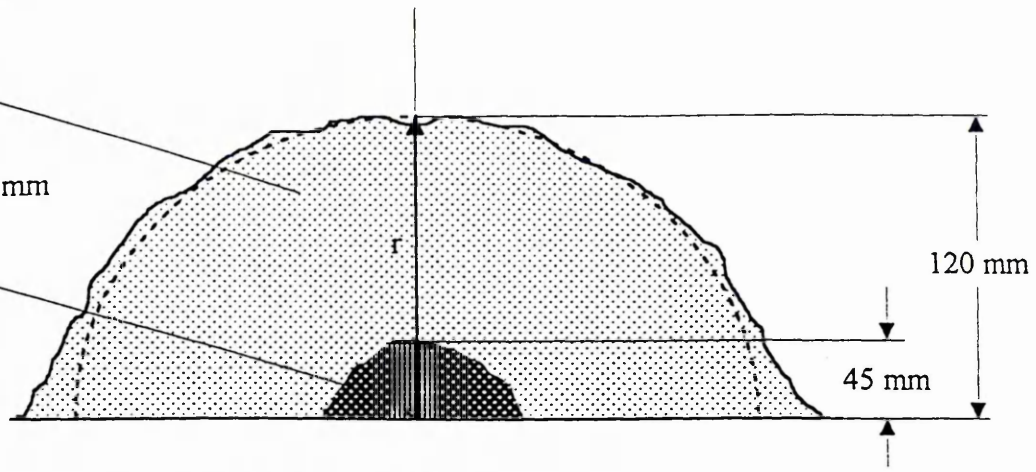


**Bild 9.** Gemessene zeitliche Änderungen der Temperatur an der Oberfläche und innerhalb einer halbkugelförmigen Sägemehlschüttung (längs r) mit endogenem Selbstentzündungsvorgang im Schüttungskern

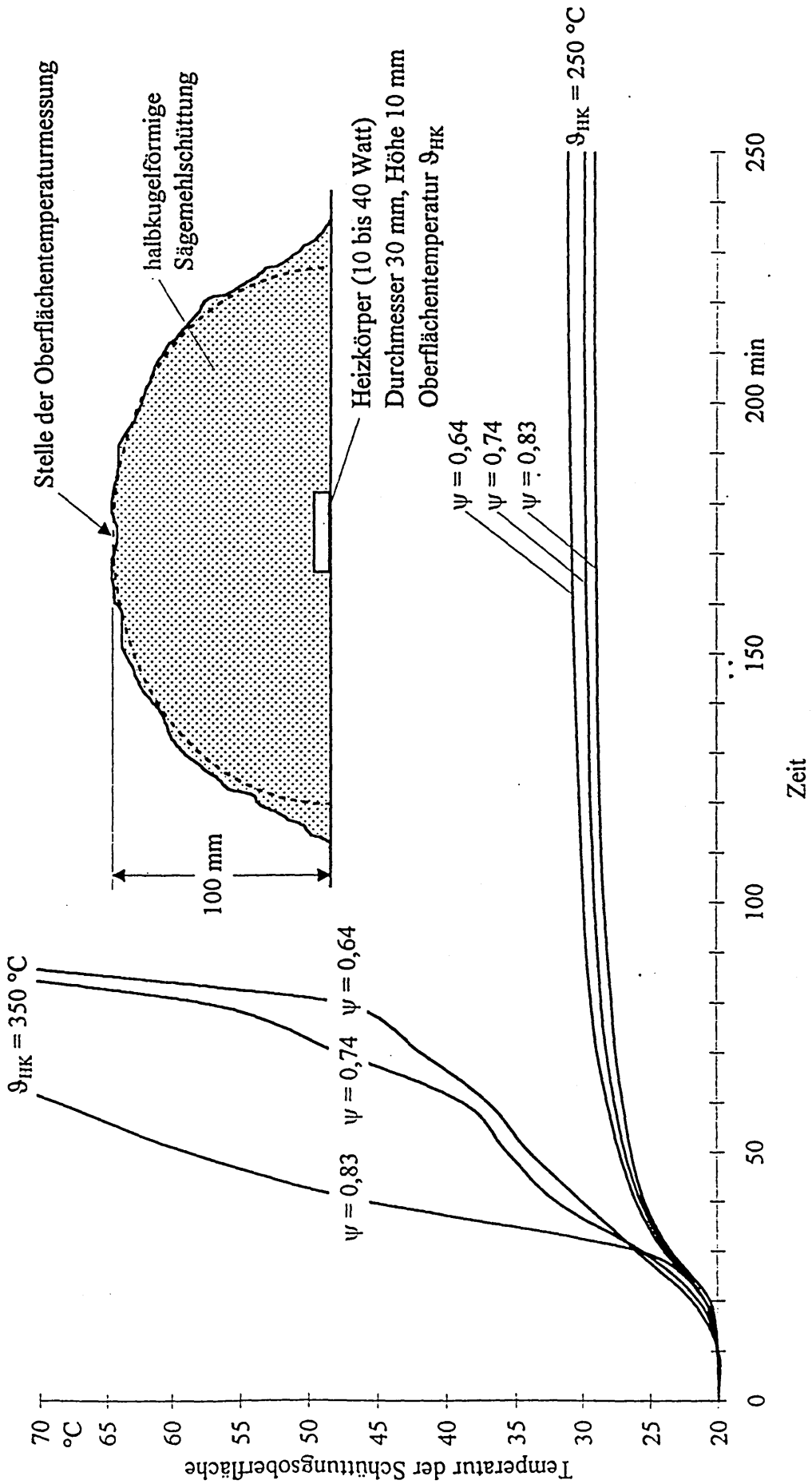
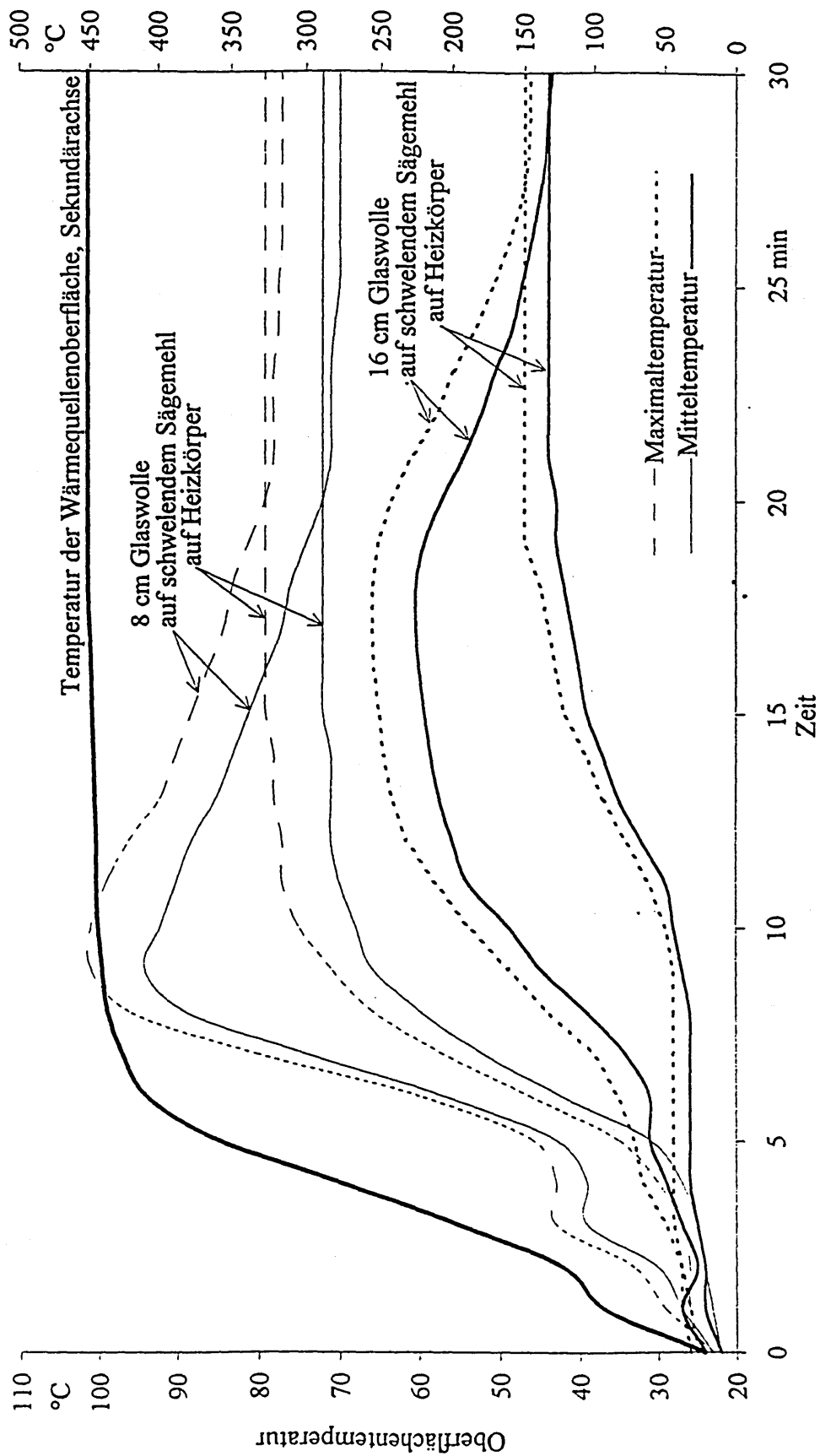


Bild 10. Gemessene zeitliche Änderungen der Oberflächentemperatur von Sägemehlschüttungen unterschiedlicher Porosität  $\psi$ , die einen elektrischen Heizkörper bedecken, dessen Temperatur nach 10 Minuten Aufheizzeit den konstanten Wert  $\vartheta_{HK}$  aufweist (Umgebungstemperatur 20 °C)



**Bild 10.** Gemessene zeitliche Änderung der Temperatur in einem repräsentativen,  $4 \text{ cm}^2$  großen Flächensegment der Oberfläche zweier verschieden dicker Glaswollschichten (feine Glaswolle, Porosität  $\psi \approx 1$ ), die eine Wärmequelle bedecken; die Wärmequelle wird durch schwelendes Sägemehl, bzw. durch einen elektrischen Heizkörper gebildet

**Tafel 1.** Ermittelte Emissionsgrade ausgewählter Komponenten des Abfallgemenges

<b>Abfallstoff</b>	<b>Oberflächentemperatur</b> °C	<b>Emissionsgrad <math>\epsilon</math></b> Wellenlängenbereich 3,0 $\mu\text{m}$ bis 5,3 $\mu\text{m}$	<b>Emissionsgrad <math>\epsilon</math></b> Wellenlängenbereich 8 $\mu\text{m}$ bis 14 $\mu\text{m}$
gelbe PE-HD Folie, 0,1 mm, auf geschwärztem Untergrund von 80 °C	69,9 <sup>1)</sup>	1,00	1,00
blaue PE-LD Folie, 0,1 mm, auf geschwärztem Untergrund von 80 °C	72,9 <sup>1)</sup>	0,91	0,95
blaue PE-LD Folie, 0,1 mm, auf blankem Al-Untergrund von 80 °C	72,9 <sup>1)</sup>	0,48	0,61
Hart PVC, grau	60,4 <sup>1)</sup>	0,99	0,99
weißes Papier auf geschwärztem Untergrund von 80 °C	71,9 <sup>1)</sup>	0,73	0,92
farbiger Karton auf geschwärztem Untergrund von 80 °C	68,5 <sup>1)</sup>	0,69	0,88
Gips	69,4 <sup>1)</sup>	0,63	0,89
Keramik-Fliese	71,1 <sup>1)</sup>	0,64	0,79
Konservendendeckel, hellgrau lackiert	71,9 <sup>1)</sup>	0,38	0,77
Weißblech, glänzend	73,8 <sup>1)</sup>	0,14	0,18
glatte Al-Platte, oxidiert	67,3 <sup>1)</sup>	0,30	0,35
Blei-Platte, oxidiert	73,1 <sup>1)</sup>	0,53	0,67
Sand, 0,1-0,5 mm Körnung	22,0 <sup>2)</sup>	0,96	0,93
Sepeolith (Katzenstreu)	22,0 <sup>2)</sup>	0,97	0,97
Humus, trocken	22,0 <sup>2)</sup>	0,95	0,96
Humus, feucht	22,0 <sup>2)</sup>	0,97	0,97
Müllbunkerstaub <sup>4)</sup>	22,0 <sup>2)</sup>	0,92 <sup>5)</sup>	0,94 <sup>5)</sup>
glattgestrichene Staub- schichten auf Al-Platte <sup>4)</sup>			
0,0 mm	22,0 <sup>2)</sup>	0,30	0,35
0,3 mm	22,0 <sup>2)</sup>	0,91	0,93
0,5 mm	22,0 <sup>2)</sup>	0,91	0,93
1,0 mm	22,0 <sup>2)</sup>	0,91	0,93
Sand, 0,1-0,5 mm Körnung	70,1 <sup>3)</sup>	0,92	0,98
Sepeolith (Katzenstreu)	74,8 <sup>3)</sup>	1,00	1,00
Humus, trocken	71,7 <sup>3)</sup>	1,00	1,00
Humus, feucht	60,5 <sup>3)</sup>	0,86	0,92
Müllbunkerstaub <sup>4)</sup>	69,3 <sup>3)</sup>	0,86	1,00

1) gemessen mit kalibrierten Miniatur-Mantelthermoelementen

2) bei Umgebungstemperatur,  $\epsilon$ -Bestimmung über einen Hintergrund von 150 °C nach [3]

3) Aufnahme des Temperaturverlaufs in der Schüttung mit 4 eingebrachten Miniatur-Mantelthermoelementen; Ermittlung der Oberflächentemperatur durch lineare Extrapolation

4) feine Struktur, aus dem Bereich des oberen Bunkerrandes

5) bestätigt mit Hilfe einer spektralen Vermessung des diffusen Reflexionsvermögens

**Tafel 2.** Überprüfung eines verfügbaren Thermographiesystems an einer definierten ebenen Prüfplattenoberfläche

Thermographiesystem	langwelliger Spektralbereich 8 bis 12 mm Detektorkühlung $DT \approx 215$ K unterhalb Umgebungstemperatur mit Stirling-Mikrokühler  Bildaufbau: 25 Hz Bildfrequenz	
Prüfort	Labor	Müllbunker
Prüfkörper: Emissionsgrad	$\varepsilon = 0,96$	$\varepsilon = 0,93$ (mit dünner Staubschicht)
Fläche Oberflächentemperatur <sup>1)</sup>	$A = 5 \text{ cm} \times 10 \text{ cm}$ $70,0 \text{ }^\circ\text{C}$	$A = 30 \text{ cm} \times 30 \text{ cm}$ $64,0 \text{ }^\circ\text{C}$
Meßdistanz	$d = 7 \text{ m}$	$d = 47,4 \text{ m}$
Zwischenmedium	weitgehend staubfreie, trockene Luft	Staub oder Wasser nicht wahrnehmbar
eingestellter Emissionsgrad	$\varepsilon = 0,92$ <sup>2)</sup>	$\varepsilon = 0,93$ <sup>3)</sup>
gewählter Temperatur-Meßbereich	$-19 \text{ }^\circ\text{C}$ bis $81 \text{ }^\circ\text{C}$	$-19 \text{ }^\circ\text{C}$ bis $81 \text{ }^\circ\text{C}$
Blickfeld: Blickwinkel (Öffnungswinkel) Blickfeldgröße FOV bei d	$30^\circ \times 40^\circ$ $3,8 \text{ m} \times 5,1 \text{ m}$	$30^\circ \times 40^\circ$ $25,4 \text{ m} \times 34,5 \text{ m}$
Winkel zwischen der Blickrichtung und der Flächennormalen des Prüfkörpers	$0^\circ$	$58^\circ$
Abweichung der ermittelten von der wahren Temperatur	5,0 K	15,2 K
relative geometrische Auflösung $A/\text{FOV}$ bei Tolerierung der Abweichung	$0,26 \cdot 10^{-3}$	$0,10 \cdot 10^{-3}$

1) erfaßt mit einer kalibrierten Pt 100-Meßeinrichtung bei einer Fehlergrenze von  $\pm 0,5$  K

2) mit dem Thermographiesystem bei einer Probemessung aus sehr kleiner Meßdistanz für die Richtung der Flächennormalen festgestellt

3) zur Erfassung des Thermogrammes der gesamten Oberfläche der Müllschüttung gewählter konstanter Wert

Fenner, M.; Braun, R.; Acheson, R.; Garbett, E. S.:

Fire prevention in refuse storage facilities using IR-Thermography.

Proceedings of the 4<sup>th</sup> International Conference on Quality,

Reliability, and Maintenance

St. Edmund Hall University of Oxford, UK, March 2002, Professional

Engineering Publishing Limited, London UK 2002

# Fire prevention in refuse storage facilities using IR-Thermography

**M FENNER**

School of Engineering, Sheffield Hallam University, UK and EnergielInstitut, University of Applied Sciences Gelsenkirchen, Germany

**R BRAUN**

EnergielInstitut, University of Applied Sciences Gelsenkirchen, Germany

**R ACHESON and E GARBETT**

School of Engineering, Sheffield Hallam University, UK

## ABSTRACT

Combustion arising from an endogenous source of ignition in domestic refuse is analysed in terms of the associated heat and mass transfer processes. The potential use of IR-Thermography for the early detection of such fires is discussed.

## 1 INTRODUCTION

Following a number of disastrous fires in the storage bunkers of municipal refuse incineration plants in Germany, legislation has been introduced requiring the installation of automatic combustion detection systems (1). It has been proposed that such systems should use IR-Thermography for the measurement of the surface temperature of the refuse bed. It is believed that a source of endogenous combustion deep within the refuse, would be detectable from the surface temperature distribution (2), thus giving the possibility for automatic warning of a potential fire by using an appropriate alarm threshold surface temperature (3). As yet, not all plants are equipped with such systems and of the more than twenty existing plants that are, installations and operating practices are not standardised. This situation has arisen because opinion varies as to the effectiveness of such systems and how best to apply and interpret the results they give. Additionally, quantitative understanding of the effect of an endogenous combustion source on the surface temperature distribution of the refuse bed, has until now not been investigated. This paper presents the results of an experimental investigation carried out to analyse the heat and mass transfer processes inside refuse and similar particulate beds. A mathematical model has been developed to simulate the processes taking place and, verified by experimental procedures, predict the temperature distribution inside and at the surface of a refuse bed. The results obtained have been used to assess the effectiveness of IR-Thermography for early combustion detection systems.

## 2 MODELLING APPROACH AND EXPERIMENTAL PROCEDURES

Theoretical analysis and the results of small-scale experiments (4) have shown that heat and mass transfer from smouldering fires inside refuse beds can be mathematically modelled using the following simplifying assumptions:

- (a) Heat is predominantly transferred by the gaseous combustion products and hence conduction can be neglected.
- (b) The properties of the particles and gaseous phase are constant and the latter does not undergo a phase change.

(c) The gas flow is driven by buoyancy almost vertically through random channels arising from the voids inside the bed such that heat transfer can be considered to be one-dimensional.

The corresponding partial differential equations, derived from an energy balance in a volume element of the bed, have been solved analytically and the solution presented as the dotted lines in Figures 1 and 2, superimposed on the results of experimental measurements. The mathematical predictions have been experimentally verified by initiating local endogenous combustion at the bottom centre of a 2.0 m x 2.3 m x 6.5 m bed of typical refuse and measuring the temperature distribution inside and at the surface of the bed. A row of twenty thermocouples was placed at the centre of the bed for temperature measurements in the direction in which the combustion proceeds, i.e. vertically upwards. For comparison, the surface temperature distribution was measured using two IR-Thermography systems: one measuring in the spectral range 2 to 4  $\mu\text{m}$  and the other in the spectral range 7.5 to 13  $\mu\text{m}$ . During the experiment, the longer wavelength system proved to be more reliable, being less sensitive to the effects of absorption of IR-radiation from the intermediate medium (3). After 72 minutes, the experiment was aborted, due to heavy smoke emission, when combustion had proceeded to within approximately 120 cm of the surface of the bed. A second experiment was undertaken with a bed of wood chips that could be combusted until flashover occurred, without the problem of harmful smoke being generated. A barrel ( $\varnothing$  58 cm x 85 cm) was filled with wood chips  $\leq$  100mm. Such a bed has nearly the same porosity and particle density as refuse and can thus be used as a substitute in terms of heat transfer parameters.

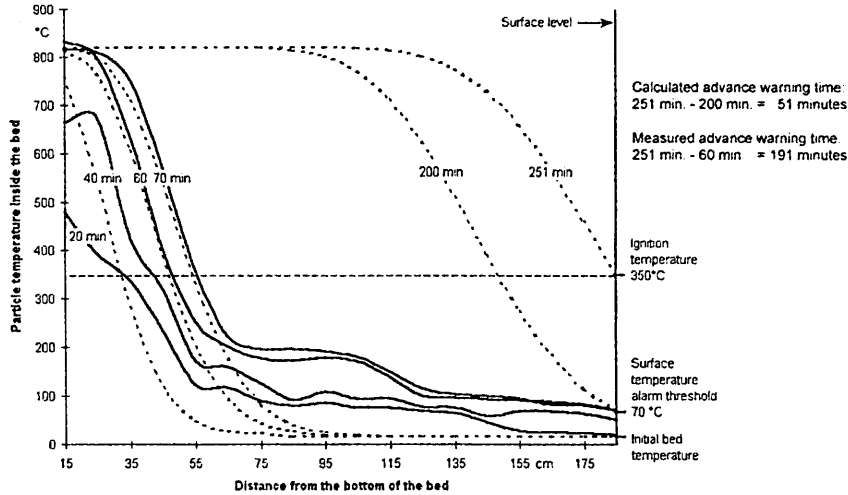
### 3 RESULTS

Figure 1 shows that there is good agreement between measured and predicted results at higher temperatures, but less so at lower temperatures, especially below 100 °C. In this zone, the measured temperatures are clearly higher than the calculated values. This must in part be attributed to the non one-dimensional conditions assumed in the model, compared with the real situation inside a heterogeneous refuse bed, together with the effect of condensation of the water content of the combustion product gases in the cooler part of the bed. The latent heat of condensation clearly influences the development of the temperature profile in Figure 1 in the layer between the fire pocket and the surface. These conclusions are further supported by the results obtained from the much longer second experiment conducted in a bed of wood chips, presented in Figure 2. When temperatures in the bed are predominately above 100 °C and all the water has returned to the vapour phase, good agreement exists between the theoretical model and experimental observation. This is demonstrated in Figure 2 for the second experiment by the good agreement between the measured and theoretically predicted value of the flashover time.

The thermal effects of water condensing mean that the surface temperature of the bed reaches an alarm threshold temperature which is detectable by IR Thermography far earlier than would be the case with a permanent gas mixture alone. The advance warning time for the presence of combustion in the refuse experiment, using a threshold warning temperature of 70 °C, was 191 minutes. Whereas in the absence of water vapour with the combustion products composed only of permanent gases, it would in theory have been only 51 minutes. Similar conclusions apply for the wood particle experiment: 157 minutes warning in the actual experiment, compared with a theoretical value of 65 minutes in the absence of water vapour.

The IR thermogram presented in Figure 3, taken after 72 minutes combustion, exhibits a clearly defined hot spot on the surface of the refuse bed, with an indicated temperature of

104.6 °C and steep surface temperature gradients away from it of more than 10 °C/cm. The primary hot spot is positioned immediately above the fire pocket, confirming the assumption made in the theoretical model that the flow of combustion product gases is vertical. Minor deviations from vertical flow, suggested by the secondary peaks in Figure 3, may occur due to the heterogeneous composition and the widely differing particle sizes of the refuse.



**Figure 1** Temperature distribution vertically above the endogenous smouldering combustion at the bottom of a 30 m<sup>3</sup> municipal refuse bed, versus time. Bold curves: measured particle temperatures along the thermocouples row; Dotted curves: calculated particle temperatures.

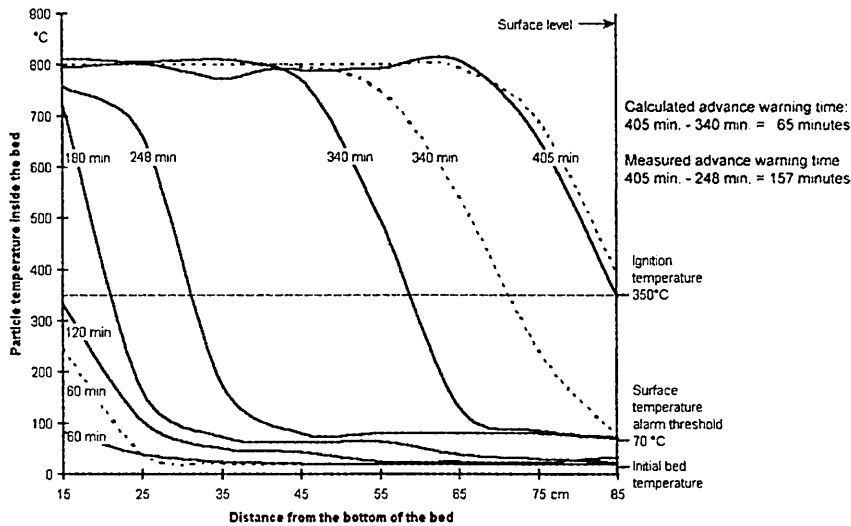


**Figure 2** Temperature distribution vertically above the endogenous smouldering combustion at the bottom of a 0.22 m<sup>3</sup> wood particles bed, versus time. Bold curves: measured particle temperatures along the thermocouples row; Dotted curves: calculated particle temperatures.

#### 4. DISCUSSION

The potential benefits of early combustion detection are derived from the time available between the first appearance of a hot spot at the surface whose temperature is above the selected alarm threshold, usually 70 °C, and the ignition temperature. This time is vital for the early implementation of counter measures. Current standard IR-Thermography systems have a 320 x 240 pixels micro-bolometer detector chip and use 30° x 40° lenses. Their smallest theoretical resolvable area from a measuring distance of 40 m, which is typical for their use in refuse bunkers, is 9.1 cm x 9.1 cm. For the data shown in Figure 3, the integrated average temperature for this area would be 62.7 °C and thus below an alarm threshold of 70 °C, even though the maximum observed temperature was 104.6 °C. To be effective, an IR-Thermography system with a very high geometrical resolution is required. This could be achieved by either employing a more sensitive detector chip with a greater number of pixels or by using a telephoto lens. With current detector chips, a telephoto lens must have a viewing angle of approximately 3° x 4° to successfully detect a small hot spot. This represents an extremely small area that can be observed by the IR-Thermography system. To cover the entire area of a refuse bed would require a single thermal imaging device to rapidly scan the surface about every two minutes [2].

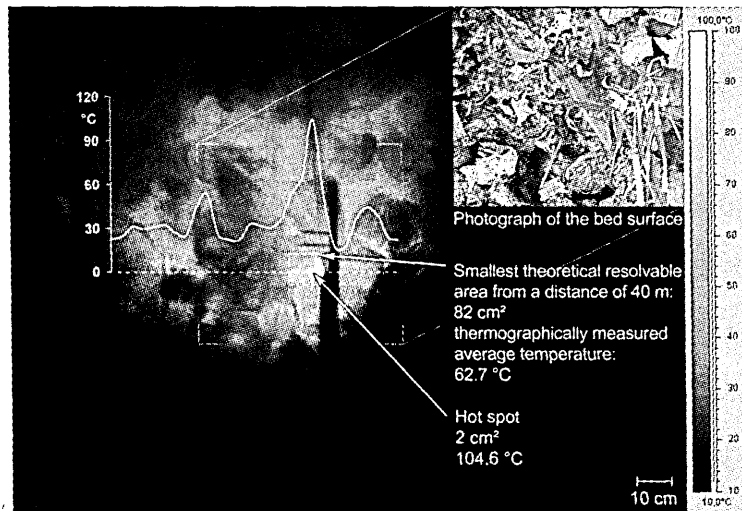


**Figure 3** IR-Thermogram, spectral range 7.5 to 13  $\mu\text{m}$ , of the refuse surface, emissivity 0.95, 72 minutes after ignition

#### REFERENCES

- (1) Siebzehnte Verordnung zur Durchführung des Bundesimmissionsschutzgesetzes (17. BImSchV), Neufassung vom 20. September 1991, (BGBl. I S. 1991)
- (2) LUA-Materialien No. 8, Landesumweltamt NRW: Bericht zur "Vermeidung von Bunkerbränden in Abfallverbrennungsanlagen mit Hilfe der Infrarot-Thermographie". Essen 1995
- (3) Braun, R.; Weidener, H.: The Early Detection of Fires in Waste Bunkers using Infrared-Thermography: Restrictions and Validation. VGB International Journal of Power Plant Engineering 77 (1997), No. 12
- (4) Fenner, M.: Model studies of heat and mass transfer in heterogeneous particulate beds. Ph.D. Thesis, Sheffield Hallam University, in preparation

Fenner, M.; Braun, R.; Acheson, R.; Garbett, E. S.:

Heat Transfer and Detection of Endogenous Combustion in a  
Refuse Bed.

VGB PowerTech, Volume 82/2002, VGB Verlag, Essen 2002

# Heat Transfer and Detection of Endogenous Combustion in a Refuse Bed

## Kurzfassung

### Wärmetransport und Brandfrüherkennung in Hausmüllschüttung

Endogene Schmelbrände in Hausmüllschüttungen beeinflussen deren Oberflächentemperatur. Das wird nahezu vollständig durch konvektiven, von den Verbrennungsgasen verursachten Wärmetransport bewirkt. Der Transportmechanismus Wärmeleitung ist unbedeutend. Theoretische Untersuchungsergebnisse, die experimentell verifiziert wurden, belegen dies.

Der Gasmassenstrom wird durch Auftrieb erzeugt und fließt innerhalb der Schüttung durch kleine, von den Lückenvolumina gebildete Kanäle. Aus dem im Brennstoff enthaltenen Wasser und Wasserstoff resultiert ein entsprechendes Partialvolumen an Wasserdampf im Verbrennungsgas. Bei der Abkühlung in den höher gelegenen Schichten erreicht dieser Wasserdampf den Sättigungszustand und kondensiert. Dieser Aggregatzustand des Wassers bleibt so lange erhalten, bis der sich ausdehnende Brandherd für eine Rückverdampfung sorgt. Die dabei freigesetzte Kondensationsenthalpie und die später aufgenommene Verdampfungsenthalpie bewirken in den Schichten oberhalb des Brandherdes ein weitgehend gleichmäßiges Temperaturniveau, das sehr langsam, d. h. in einem Zeitraum von mehr als zwei Stunden, von 65 auf 85 °C ansteigt. In dieser Zeit resultieren an der Oberfläche kleinste Oberflächenerwärmungen, so genannte „hot spots“ und Spuren von Wasserdampf. Letztere bieten sicherlich ein Potential zur Brandfrüherkennung. Eine konkrete Messtechnik ist allerdings noch nicht vorgeschlagen worden. Was die hot spots betrifft, so ist die IR-Thermographie sicherlich ein geeignetes Hilfsmittel zur Brandfrüherkennung.

Die hot spots haben bis circa 45 Minuten vor Ausbruch eines Oberflächenbrandes eine Temperatur von maximal 85 °C und, bedingt durch die kleinen Öffnungen der Strömungskanäle, eine Fläche von nicht mehr als 10 cm<sup>2</sup>. Um diese kleinen hot spots über die geforderte Distanz hinweg zuverlässig detektieren zu können, muss ein zur Brandfrüherkennung eingesetztes IR-Thermographiesystem eine sehr hohe geometrische Auflösung bieten. Wird diese Grundanforderung erfüllt und wird die Alarmschwellentemperatur im Bereich des vorherrschenden Wasserdampftaupunktes zwischen 65 und 85 °C gewählt, so bietet sich die Möglichkeit, einen endogenen Brandherd bis zu zwei Stunden vor Durchbruch an die Oberfläche zu detektieren.

Etwa ein Stunde vor Brandausbruch kommt wegen der hohen Schüttungstemperaturen keine Kondensation mehr zustande und die Verdampfung trocknet die Schüttung, so dass die Nebelspuren weitgehend verschwinden. Die Temperatur der hot spots steigt dann schnell an, dies allerdings ohne deutliche Zunahme der Ausdehnung. In den Experimenten zeigte sich als typische Endsituation, wenige Minuten vor Brandausbruch, z. B. ein erwärmter Oberflächenbereich von 20 cm<sup>2</sup> mit einer thermographisch gemessenen Mitteltemperatur von 103,4 °C, der einen 2 cm<sup>2</sup> großen hot spot von 320 °C enthielt. Diese Schlussphase läßt keine verwertbare Möglichkeit zur Brandfrüherkennung und damit zur Ergreifung geeigneter Gegenmaßnahmen zu.

## Introduction

Following a number of disastrous fires in the storage bunkers of municipal refuse incineration plants [1], legislation requiring the installation of automatic combustion detection systems was introduced in Germany in 1991 [2]. It has been proposed that such systems should use IR-thermography (IRT) for the measurement of the surface temperature of the refuse bed. It has also been suggested that a source of endogenous combustion deep within the refuse would be detectable from the surface temperature distribution [3], thereby providing the means for automatic warning of a potential fire using an appropriate alarm threshold surface temperature [4].

As yet, not all plants in Germany are equipped with such systems, but of the more than twenty existing plants that are, the equipment used and their installation and operating practices are not yet standardized. This situation has arisen because opinion varies as to the effectiveness of such systems and how best to apply and interpret their results. Additionally, quantitative understand-

ing of the effect of an endogenous combustion source on the surface temperature distribution of the refuse bed has, until now, not been investigated.

This paper presents the results of an experimental investigation carried out to analyse the heat and mass transfer processes inside refuse and similar particulate beds. A mathematical model has been developed to simulate the processes taking place. The model, verified by experiment, predicts the temperature distribution inside and at the surface of a refuse bed. The results have been used to assess the effectiveness of IRT for early combustion detection systems.

## Model Approach

Theoretical and experimental analysis [5] have shown that heat and mass transfer from smouldering fires inside refuse beds can be modelled using the following simplifying assumptions:

- Heat is predominantly transferred by the gaseous combustion products and hence conduction and radiation can be neglected.
- The properties of the particles and gaseous phase are constant and the latter does not undergo a phase change.
- The gas flow is driven by buoyancy almost vertically through random channels arising from the voids inside the bed such that heat transfer can be considered to be one-dimensional.

Consideration of an energy balance for a volume element of a particulate bed above the combustion results in the following partial differential equations.

For the solid particles:

$$(1 - \psi) \rho_S c_{pS} \frac{\partial T_S}{\partial t} = \alpha_{aS} (T_G - T_S) \quad (1)$$

For the gaseous phase:

$$-\psi \rho_G c_{pG} \frac{\partial T_G}{\partial t} - \frac{\dot{m}_G c_{pG}}{A \psi} \frac{\partial T_G}{\partial x} = \alpha_{aS} (T_G - T_S) \quad (2)$$

Nomenclature:

$T_G, T_S$	temperature of the gaseous phase and solid particles, respectively
$\psi$	void fraction

## Authors

Dipl.-Ing. M. Fenner

School of Engineering, Sheffield Hallam University, Sheffield/United Kingdom and EnergielInstitut, Fachhochschule Gelsenkirchen, Gelsenkirchen/Germany.

Professor Dr.-Ing. R. Braun

EnergielInstitut, Fachhochschule Gelsenkirchen, Gelsenkirchen/Germany.

Dr. R. Acheson

School of Engineering, Sheffield Hallam University/Sheffield/United Kingdom.

Dr. E. S. Garbett

School of Engineering, Sheffield Hallam University/Sheffield/United Kingdom.

$\rho_G, \rho_S$	density of the gaseous phase and solid particles, respectively
$c_p$	specific heat capacity
$\alpha$	convective heat transfer coefficient gas phase to particle
$a_S$	particle surface per unit volume
$\dot{m}_g$	gaseous mass flow rate
$A$	cross-sectional area of the bed
$t$	time
$x$	vertical distance through the bed

The boundary conditions can be derived [5] from the assumptions of constant gas inlet temperature  $T_G(0,t) = T_{G_0}$  and constant initial solid temperature  $T_S(x,0) = T_{S_0}$ . Equations (1) and (2) have been analytically solved by variable transformation and have been further simplified for computing purposes by substitution to obtain the following relationships:

For the solid particles:

$$T_S(x,t) = T_{S_0} + (T_{G_0} - T_{S_0}) \frac{2}{\sqrt{2\pi(2\nu)^2}} \int_0^{2\mu\nu} e^{-\frac{\sigma^2}{(4\nu)^2} + \sigma - \nu^2} \frac{d\sigma}{\sqrt{\sigma}} \quad (3)$$

For the gaseous phase:

$$T_G(x,t) = T_{G_0} - (T_{G_0} - T_{S_0}) \frac{2}{\sqrt{2\pi(2\mu)^2}} \int_0^{2\mu\nu} e^{-\frac{\sigma^2}{(4\mu)^2} + \sigma - \mu^2} \frac{d\sigma}{\sqrt{\sigma}} \quad (4)$$

Therein, the parameters to be varied are given by

$$\nu = \sqrt{\frac{\alpha \cdot a_S}{c_G \cdot \psi \cdot \rho_G \cdot c_{pG}}} \cdot x \text{ and } \mu = \sqrt{\frac{\alpha \cdot a_S}{c_G \cdot (1-\psi) \cdot \rho_S \cdot c_{pS}}} \cdot (c_G \cdot t - x)$$

and  $\sigma$  is the integration variable.

Substitution of appropriate values for the properties of typical municipal refuse [5] into the model equations (3) and (4) produces the curves presented in Figure 1 that shows how the temperature profile of the solid particles throughout the height of the bed above the heat source changes as a function of time. The curves identified for time 't' and 't + Δt' correspond respectively to the first appearance at the surface of the bed of a hot spot, whose temperature is above a selected alarm threshold and to the point at which ignition occurs. The potential for early combustion detection and the implementation of countermeasures is thus represented by the time Δt. It is desirable that Δt should be as large as is practicably possible to permit the early introduction of countermeasures either to extinguish the combustion inside the bed, if necessary by digging out the affected area, or at least to prevent flashover using an extinguishing agent. The IRT systems employed on many refuse plants in Germany common-

ly employ a surface temperature alarm threshold of 70 °C [3, 4]. This is considered to be the lowest reasonable temperature that will avoid false alarms caused by heat generated by microbiological processes.

### Experimental Procedure

To test the validity of the proposed mathematical model two experiments have been undertaken. These involved monitoring the temperature distribution inside and at the surface of a bed of combustible particulate material after initiating a localized source of endogenous combustion at the base of the bed.

A row of 20 thermocouples, mounted on a stainless steel beam to fix their vertical position, was placed at the centre of the bed, directly above the source of combustion. Since the thermocouples themselves act as particles in terms of heat transfer, the measured temperatures can be considered as particle temperatures and not as fluid temperatures. The surface temperature distribution of the bed was monitored using two IRT systems, one measuring in the spectral range 2 to 4 μm and the other in the spectral range 7.5 to 13 μm. During the experiment, the longer wave length system proved to be more reliable, being less sensitive to the effects of absorption of IR-radiation by airborne particles [6].

For the first experiment, a batch of typical German municipal refuse [5], was used as the bed material in a 2.0 × 2.3 × 6.5 m, 30 m<sup>3</sup> container, as shown in Figure 2. The bed was locally ignited by the introduction of a propane gas burner flame through small holes in the bottom of the container, directly below the row of thermocouples. The flame was turned off immediately after ignition of the refuse had been achieved. The experiment was aborted after 72 minutes, due to

heavy smoke emission, when combustion had proceeded to within approximately 120 cm below the surface of the bed.

Since the first experiment had to be terminated before the desired flashover could be achieved, a second experiment was undertaken with a bed of wood particles that could be combusted until flashover occurred without the problem of harmful smoke being generated. A 0.22 m<sup>3</sup> (Ø 58 cm, height 85 cm) barrel (Figure 3), was filled with a sieved fraction (100 mm mesh) of particles. Such a bed has almost the same porosity and particle density as refuse [5] and can thus be used as a substitute in terms of heat transfer parameters. Once ignited, smouldering endogenous combustion was allowed to proceed until ignition occurred at the surface of the bed allowing observation of heat transfer processes inside the bed, the development of the surface temperature distribution, and the way in which the flashover occurred.

### Comparison of the Predicted with the Experimental Results

The results of the experiment using municipal refuse are presented in Figure 4, as

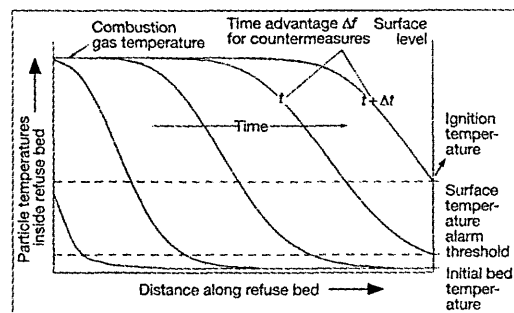


Figure 1. Qualitative solution of the partial differential equations for the particle temperature inside a bed with typical municipal refuse subjected to an endogenous smouldering combustion at the bottom. Permanent combustion gas without phase change and constant particle and fluid properties are assumed.

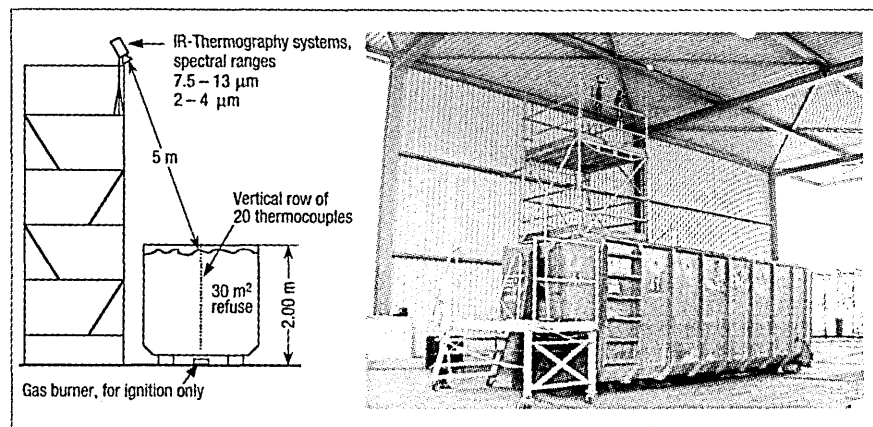


Figure 2. Set-up of the large-scale municipal refuse experiment.

plots of the temperature distribution inside the bed after various time intervals from first ignition. The results of the theoretical model are superimposed as broken lines for comparison.

Figure 4 shows that there is good agreement between measured and predicted results at higher temperatures, but less so at temperatures below 200 °C. In this zone, the measured temperatures are clearly higher than the calculated values. This must in part be attributed to the particular heterogeneous refuse bed because different combustion gas flow channels become available with the proceeding of the combustion towards the surface. From the experimental results, a dew point temperature range of 65 °C to 85 °C

was obtained and hence, the temperature differences below 85 °C must be attributed to the effect of condensation of the water content of the combustion product gases in the cooler part of the bed. On condensing, water vapour releases latent heat, which produces a local heating effect in the upper layers of the bed and which has not been included in the model.

The magnitude of the heat release is given by the difference between the gross calorific value and the net calorific value of the refuse. Deriving these values from an average elementary analysis of municipal refuse, see Table 1, the difference 1050 kJ/kg, which is 13 % of the net calorific value. This additional 13 % of heat is released within the

cooler part of the bed and, due to the large local heat transfer coefficients during condensation of about 6000 W/(m<sup>2</sup> K), arrests the temperature drop throughout the bed. As combustion progresses and the temperature in the upper layers rises, the condensate re-evaporates, requiring latent heat of evaporation to do so, thus providing a restraining effect on temperature rise in these layers. These phase changes clearly have a great influence on the development of the temperature profile in Figure 4 in the layer between the fire pocket and the surface. From 40 minutes after first ignition up to the abortion of the experiment after 72 minutes, the lowest bed temperature gradually changes in the range of the increasing dew point, i.e. 65 °C to 85 °C.

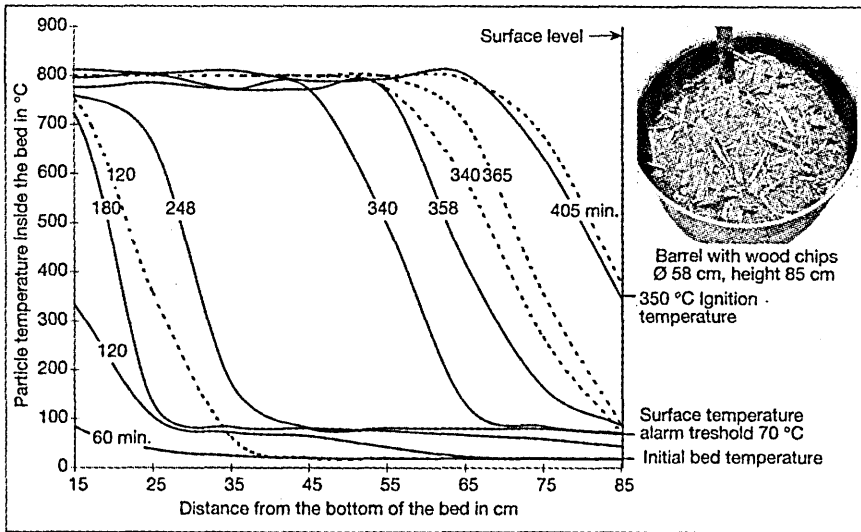


Figure 3. Temperature distribution, measured by thermocouples, in time vertically above the self-preserving endogenous smouldering combustion at the bottom of a 0.22 m<sup>3</sup> barrel filled with wood chips.  
**Bold curves:** measured particle temperatures along the thermocouples row  
**Dotted curves:** calculated particle temperatures

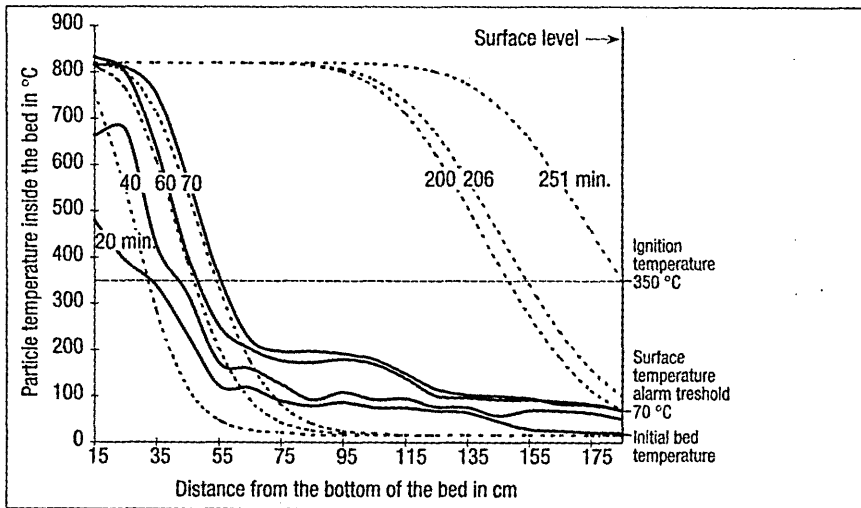


Figure 4. Temperature distribution, measured by thermocouples, in time vertically above the self-preserving endogenous smouldering combustion at the bottom of a 30 m<sup>3</sup> municipal refuse bed.  
**Bold curves:** measured particle temperatures along the thermocouples row  
**Dotted curves:** calculated particle temperatures

If the experiment had been allowed to progress the temperature profile throughout the bed would eventually be sufficiently high that no liquid water would remain. Heat transfer would therefore be between the solid refuse and what was effectively a permanent gas, which is the basis for the theoretical model. The results for the model and experiment should thus converge under these conditions at a surface temperature level above 85 °C. The results from the theoretical model, indicated on Figure 4, suggest that this condition would have occurred after about 206 minutes and that ignition flashover at the surface would have occurred after about 251 minutes.

The thermal effects of water condensing mean that the surface temperature of the bed reaches an alarm threshold temperature that is detectable by IRT far earlier than would be the case with a permanent gas mixture alone. In addition, since not all water vapour condenses, traces of mist exit the bed, being a potential indicator of a combustion. The results presented in Figure 4 indicate that the advance warning time for the presence of combustion in the refuse experiment, using a threshold warning temperature of 70 °C, was about 251 minutes – 60 minutes = 191 minutes. Whereas in the absence of water vapour with the combustion products composed of permanent gases only, it would in theory have been 251 minutes – 200 minutes = 51 minutes.

Table 1. Elementary analysis and calorific values of municipal refuse [7].

	% by mass	
Carbon	22	
Oxygen	8	
Hydrogen	2	
Ash	35	
Water	25	
Net calorific value		8060 kJ/kg
Gross calorific value		9110 kJ/kg

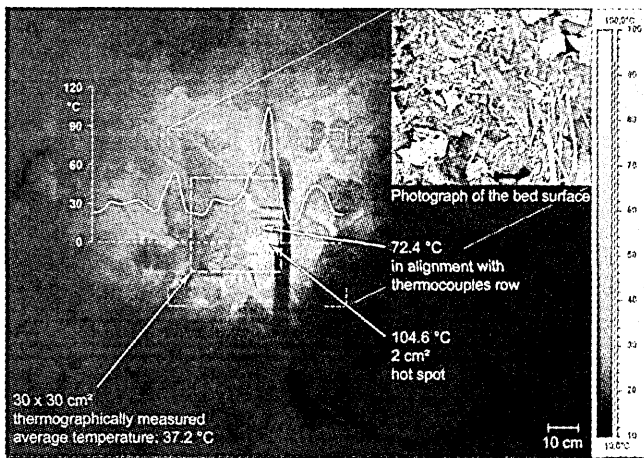


Figure 5. IR-Thermogram, spectral range 7.5 to 13  $\mu\text{m}$ , of the refuse surface, emissivity 0.95, 72 minutes after ignition, showing a single, very small hot spot. The temperature profile along the dotted line shows surface temperature gradients of more than 10 K/cm.

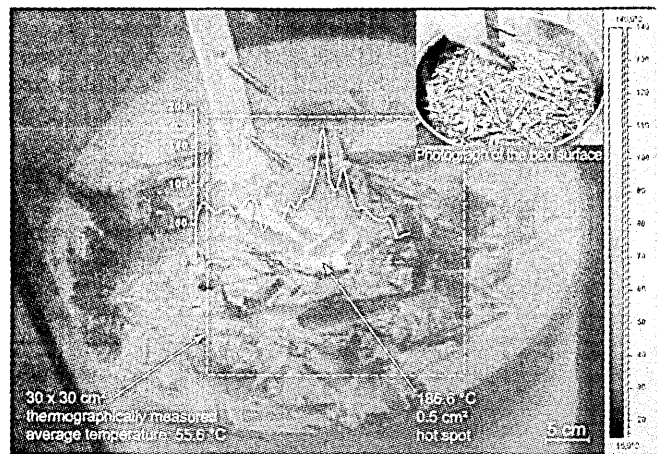


Figure 6. IR-Thermogram, spectral range 7.5 to 13  $\mu\text{m}$ , of the wood chip surface, emissivity 0.95, 390 minutes after ignition, showing a single, very small hot spot. The temperature profile along the dotted line shows surface temperature gradients of more than 10 K/cm.

Basically, the same applies to the results of the experiment using wood chips that are presented in Figure 3. At the beginning, the calculated temperatures are higher than the measured temperatures, which must be attributed to the following: The model calculations are based on a constant gas temperature of 810 °C from the very start of the combustion. In contrast, the experimental combustion needed about 200 minutes to fully develop and reach 800 °C. With increasing time, the difference between model and measurement decreases. After 358 minutes, the lowest bed temperature has exceeded the dew point temperature of 85 °C and the calculated time for a surface temperature of 86 °C is 365 minutes. This shows that at least the calculation of the surface temperatures above the dew point temperature is reasonably close to the measured temperatures.

The prediction of the time of flashover agrees with the experimental values. It should be noted that the combustion gas is a permanent gas at flashover and also that the previously mentioned deviation of the actual gas inlet temperature from the temperature used for the modelling decreases with time. This verifies the applicability of the differential equations in the time period in which phase-changes no longer occur. Although the flashover is correctly predicted by the model, the initial attainment of the surface temperature alarm threshold is not, due to the condensation and re-evaporation effects. In reality the non-permanent gas gives an advance warning time that is approximately 108 minutes longer than the model would predict for a permanent gas. This means, the modelled temperature distribution gives the worst case scenario in terms of advance warning time. Nevertheless, the model prediction shows an advance warning time of approximately 45 minutes, which would be sufficient for the

implementation of appropriate countermeasures.

Figure 5 shows a thermogram of the refuse surface taken 72 minutes after combustion started. This exhibits a clearly defined hot spot on the surface of the refuse bed with an indicated temperature of 104.6 °C and steep surface temperature gradients away from it of more than 10 K/cm. The primary hot spot is positioned immediately above the fire pocket, confirming the assumption made in the theoretical model that the flow of combustion product gases is vertical. Minor deviations from vertical flow, suggested by the secondary peaks in Figure 5, may occur due to the heterogeneous composition and the widely differing particle sizes of the refuse.

Braun and Weidener [4] have considered the use of an IRT system with a geometric resolution that is able to resolve an isothermal area of down to 30 cm  $\times$  30 cm. For the data presented in Figure 5, the integrated average temperature of an area of this size including the hot spot, would be only 37.2 °C. This is far below any reasonable alarm threshold and demonstrates the need for an IRT system with a much higher geometrical resolution. This is again emphasized in Figure 6, which displays an IR-Thermogram of the wood particle bed surface 390 minutes after ignition. A 0.5 cm<sup>2</sup> hot spot is evident directly above the smouldering fire pocket. Compared to the refuse experiment, the lack of the deviation of the hot spot is due to the more consistent particle size of the wood. The temperature gradients have the same high values.

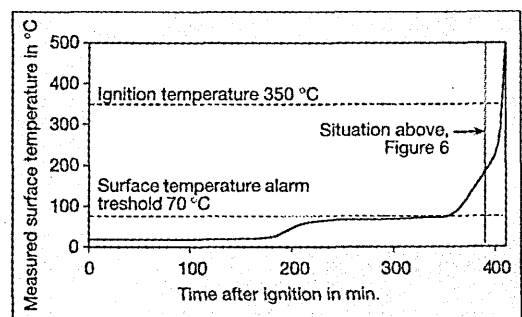


Figure 7. Maximum IR-measured surface temperature of the wood particles bed versus time. Condensation and re-evaporation keep the surface temperature in a range of 60 °C to 85 °C for about 180 minutes before the temperature increases rapidly and the flashover occurs.

Figure 7 shows the measured maximum surface temperature of the wood particles bed versus time. As the wood particles have got a more consistent particle size, the influence of condensation and re-evaporation on the surface temperature distribution can be even better observed. Observing Figure 7, it can again be suggested, that the phase-changes keep the surface in the dew point temperature range, i.e. 60 °C to 85 °C, for about 150 minutes. About 60 minutes before the flashover, condensation has ceased and re-evaporation begins to dry the bed. At the end of this process, the temperature of the hot spot at the surface increases rapidly together with a simultaneous increase in their surface area. The latter is not rapid and thus, the hot spot does not extend over a large surface area. The experiments show a maximum hot spot area of 20 cm<sup>2</sup> with a thermographically measured average temperature of 103.4 °C, within which occurs a 2 cm<sup>2</sup> hot spot at approximately 320 °C about three minutes before flashover occurred.

### Summary

Experimentally verified theoretical results suggest that heat from endogenous combustion processes in refuse beds is predominantly transferred by the combustion gas, i.e. by convection. The mass flow is driven almost vertically by buoyancy through small random channels which result from the void fraction. Due to the hydrogen and the moisture content of the refuse, the combustion gas contains water vapour. Thus, condensate drops out in the cooler layer and clearly influences the temperature between the fire pocket and the surface. In these layers the temperature gradually changes in the range of the increasing dew point, i.e. 65 °C to 85 °C, and is present at this level for more than two hours before the condensate is re-evaporated as the fire pocket extends. These condensation and re-evaporation processes result in traces of early hot spots and mist at the surface which exits the refuse bed and becomes progressively more apparent. The hot spots can be used for the early combustion detection and, although no actual technique for detecting the traces of mist has been proposed, their detection might offer a potential in early combustion detection as well.

Whilst condensation and re-evaporation occurs, the hot spots are in a temperature range up to 85 °C and due to the very small channel apertures they have a maximum size of not more than 10 cm<sup>2</sup>. Therefore, an IRT system must have a very high geometrical resolution to detect these very small hot spots over the required distance and if the surface temperature alarm threshold is chosen in the above range of the dew point, an alarm is possible more than two hours before the flashover.

About one hour before the flashover, condensation no longer occurs and re-evaporation begins to dry the bed. Thereafter, the temperatures of the hot spots at the surface increase rapidly together with a simultaneous minor increase in their surface area. A few minutes before the flashover, a maximum hot spot area of 20 cm<sup>2</sup> with a thermographically measured average temperature of 103.4 °C has been detected, within which occurs a 2 cm<sup>2</sup> hot spot at approximately 320 °C. This final development is too rapid to offer any further potential for early combustion detection.

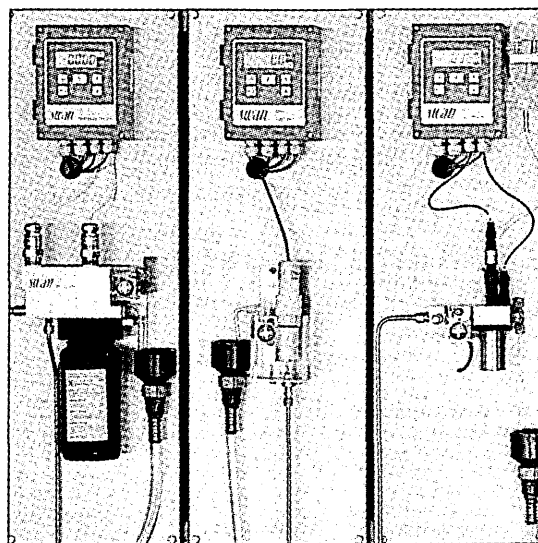
### References

- [1] Reimann, D. O.: Konsequenzen in der Brandschutzvorsorge aufgrund eines Müllbunkerbrandes am Beispiel MHKW Bamberg. VDI Seminar 43-08-01 „Katalysatoren-, Brand-, Explosionsschutzmaßnahmen“. Düsseldorf 13. – 14.03.1997.
- [2] Siebzehnte Verordnung zur Durchführung des Bundesimmissionsschutzgesetzes (17. BImSchV), Neufassung vom 20. September 1991 (BGBl. I S. 1991).
- [3] LUA-Materialien No. 8, Landesumweltamt NRW: Bericht zur „Vermeidung von Bunkerbränden in Abfallverbrennungsanlagen mit Hilfe der Infrarot-Thermographie“. Essen 1995.
- [4] Braun, R., und Weidener, H.: The Early Detection of Fires in Waste Bunkers using Infrared-Thermography: Restrictions and Validation. VGB International Journal of Power Plant Engineering 77 (1997), No. 12.
- [5] Fenner, M.: Model studies of heat and mass transfer inside heterogeneous particulate beds. Ph.D. Thesis, Sheffield Hallam University, in preparation.
- [6] Braun, R.; Fenner, M.; Weidener, H.: Prüfkriterien zur Beurteilung unterschiedlicher IR-Thermographie-Brandfrüherkennungssysteme. VDI Seminar 43-08-02 „Brand- und Explosionsschutzmaßnahmen in Feuerungs- und Verbrennungsanlagen“, Düsseldorf 15. – 16. 10. 1998.
- [7] Reimann, D.O., und Hämmerli, H.: Verbrennungstechnik für Abfälle in Theorie und Praxis. Schriftenreihe: Umweltschutz, Bamberg 1995.

*swan*  
ANALYTICAL INSTRUMENTS

### Complete Instrument Panel for Feedwater Analysis

Includes Specific Conductivity, Acid (Cation) Conductivity, Dissolved Oxygen and pH measurements.



#### Each Analyzer with

- Two Signal Outputs 4 .. 20 mA
- Two Limit Switches
- Alarm Relay
- Flow Measurement with Alarm

Factory tested • Easy to service • Low maintenance

SWAN sets the standard

*swan*  
ANALYTICAL INSTRUMENTS

SWAN ANALYTISCHE INSTRUMENTE AG · CH-8616 RIEDIKON  
Phone ++41 1 943 63 00  
FAX ++41 1 943 63 01  
www.swan.ch  
E-Mail: swan@swan.ch